Modelling heterotypic cell interactions in the context of Barrett's Oesophagus progression



Carlos Ruiz Puig

Somerville College

University of Oxford

A thesis submitted for the degree of

Doctor of Philosophy

Hillary 2020

Abstract

Oesophageal adenocarcinoma originates in the gastroesophageal junction and has a poor prognosis. Barrett's oesophagus is a common, innocuous condition occurring prior to most adenocarcinoma cases. This lesion is frequent in patients suffering from gastroduodenal reflux and involves columnar cells replacing a segment of the squamous lining of the distal oesophagus. High variability in the length of the segment exists between individuals and typically patients with longer lesions have an increased risk of developing adenocarcinoma. However, the pathways promoting this replacement and determining its final length are unknown. In this thesis, I investigate models to study this phenomenon *in vitro*.

In the first part of this thesis, I describe a system that I developed to study interactions between epithelial cell populations and apply it to combinations of cells which are crucial for Barrett's oesophagus progression. My findings indicate that squamous and early Barrett's oesophagus derived cells form stable junctions and that reflux-like epidermal growth factor concentrations can disrupt this stability.

In part two, I adapt existing 3D culture methods to study heterotypic junctions *in vitro*. Combining oil bath and plastic printing techniques, I have constructed rings with organoid epithelial lining. I demonstrate as well that it is possible to control the ring's size via the addition of fibroblasts into the collagen. Through addition of a divider, I was able to recapitulate heterotypic junctions between organoid populations and, by making the moulds higher, I show that it is possible to generate tube structures using the same technique. Additionally, I demonstrate that using fibroblast gradients in the tubes can control their shape. Building upon the contractibility of the fibroblasts, I also show that adaptors can be fixed at the ends of the tubes to control flow through it. Using this system, I am able to coat the tube's lumen with epithelia and infect the cells with pathogens to recapitulate a more natural infection.

Lastly, I generated an endoscopic mucosal resection biobank for microdissection with the samples being annotated with the assistance of pathologists. I then validated this system by micro-dissecting three candidate patients.

Acknowledgements

First, I would like to thanks my supervisors Professors Xin Lu and Jens Rittscher for giving me the opportunity and the support to do this project. I am very thankful as well for the funding received from the Ludwig Institute for Cancer Research during the duration of the Thesis.

Next, I would like to thank Felix Zhou, Ludo Buti, Linna Zhou and Andrew Roth who taught me or complemented the skills needed to do the different parts of this Dphil project.

I would also like to thank the friends who helped me both in the lab and with the writing of the thesis, Thomas Leissing, Aitor Serres Armero , Marsha Wallace and Derek Leske. I want to thank as well the medical doctors that annotated the histology sections during this project: Professor Robert Goldin, Professor Viktor H. Koelzer and Dr Lai Mun Wang.

At the bench-side, Stefanie Zentelis, Dennis Sängberg, Richard Owen, Mike White, James Chan, Xiao Qin, Jingyi Ma, Liz Slee, Tom Carroll, Brittany Jacobs and others were always great help during wet-lab and social hours alike.

I am equally grateful for the support of the excellent technical and administrative team in the Ludwig including Richard Lisle, Mark Shipman, Veronica Counsell, Indrika Ratnayaka, Alex Royer and a long list of colleagues.

From other parts of the Ludwig institute I need to thanks Diogo Dias, Erica de Zan, Giovanni Stracquadanio, Linxin Li, Laura Mosteo, Yurena Vivas among others.

Finally, I would like to thank the people supporting me from back in Spain, including my parents Eugenio Maria Ruiz-Martinez and Maria Isabel Puig Povedano, my sister Elena Carmen Ruiz Puig, grandparents Josep Puig Freixes and Isabel Povedano Marín and my close friends Marc Segarra Mondejar, Raquel Garcia Vernet, Marina Ramiro Pareta, Temístocles and Sergio Plana García.

To all of them I apologise for not being able to write a more personal thanks commenting shared anecdotes. Otherwise, the acknowledgment section might extend beyond the thesis content. I just want you to know that without each one of you my time in Oxford would have been less successful, exciting and worthy of remembrance.

Publications

- Zhou FY & Ruiz-Puig C, Owen RP, White MJ, Rittscher J, Lu X. Motion Sensing Superpixels (MOSES): A systematic framework to quantify and discover cellular motion phenotypes. Elife. 2019 Feb 26;8.
- Zhou L, Ruiz-Puig C, Jacobs BA, Han X, Lisle R, Bayley H, Lu X. Bioengineered Gastrointestinal Tissues with Fibroblast-Induced Shapes. Adv. Funct. Mater. 2020 Nov 2007514.
- Buti L, Ruiz-Puig C, Sangberg D, Leissing T, Brewer CR, Owen RP , Sgromo B, Royer C, Ebner D, and Lu X. CagA–ASPP2 complex mediates loss of cell polarity and favors H. pylori colonization of human gastric organoids. PNAS. 2020 Feb 117 (5) 2645-2655.
- Owen RP, White MJ, Severson DT, Braden B, Bailey A, Goldin R, Wang LM, Ruiz-Puig C, Maynard ND, Green A, Piazza P, Buck D, Middleton MR, Ponting CP, Schuster-Boeckler B, Lu X. Single cell RNA-seq reveals profound transcriptional similarity between Barrett's oesophagus and oesophageal submucosal glands. Nat Commun. 2018 Oct 15;9(1):4261.
- Zhou FY , Ruiz-Puig C, Owen RP, White MJ, Rittscher J, Lu X. Characterization of Biological Motion Using Motion Sensing Superpixels. Bio-protocol. 2019 Sep 9; 18.
- Zhou FY & Ruiz-Puig C, Owen RP, White MJ, Rittscher J, Lu X. Motion Sensing Superpixels (MOSES): A systematic framework to quantify and discover cellular motion phenotypes. Biorxiv. 2018 Jan.

Declaration

All the material presented in this thesis is the result of my own work, except where specifically indicated here and in the corresponding sections:

1. In chapter 3, the coding and development of MOSES as well as the statistical analysis and graphical representation of my wet lab work results was carried out by Dr Felix Y. Zhou.

2. In chapter 4, Dr Linna Zhou contributed equally to technology design, model printing and discussion. Richard Lisle took care of mould design optimization and final printing.

3. In chapter 5, the original idea for combining microdissection with proteomics in oesophageal samples as well as securing partial funding of the project was done by Dr Richard P. Owen.

Contributions by the aforementioned colleagues are indicated in the text of the thesis at the relevant points. None of the work presented in this thesis has been accepted or submitted for any degree, diploma or certificate or other qualification in this University or elsewhere.

Carlos Ruiz-Puig, 2020

Contents

List of Figures **xiii**

List of Abbreviations **xvi**

1 Introduction **1**

1.1 Summary . . . 2
1.2 The upper gastrointestinal tract . . . 3
1.2.1 The oesophagus . . . 4
1.2.2 The stomach . . . 6
1.2.3 The duodenum . . . 8
1.2.4 Heterotypic epithelial junctions . . . 9
1.3 Oesophageal Adenocarcinoma . . . 10
1.3.1 Epidemiology . . . 10
1.3.2 Diagnosis . . . 11
1.3.3 Staging . . . 12
1.3.4 Survival . . . 13
1.3.5 Treatment . . . 13
1.3.6 New treatment strategies . . . 14
1.3.7 Preventive surveillance . . . 15
1.4 Barrett's Oesophagus . . . 15
1.4.1 The Barrett's oesophagus epithelium . . . 17
1.4.2 The origins of Barrett's oesophagus . . . 17
1.4.3 Barrett's oesophagus progression to adenocarcinoma . . . 19
1.4.4 Clinical implications of Barrett's oesophagus segment length 20
1.4.5 Length of Barrett's oesophagus and progression to cancer . . 20
1.4.6 Barrett's oesophagus length and clonality . . . 22
1.4.7 The establishment of Barrett's oesophagus length . . . 23
1.5 Gastroesophageal reflux disease . . . 25
1.5.1 Definition . . . 25
1.5.2 Components of gastric origin . . . 25
1.5.3 Components of hepatic origin . . . 27
1.5.4 Components of pancreatic origin . . . 28

1.5.5 Components of duodenal origin 29
1.6 Epidermal growth factor 29
1.6.1 The EGFR signalling pathway 29
1.6.2 The epidermal growth factor in gastrointestinal homeostasis 30
1.6.3 EGF levels in the upper gastrointestinal tract 32
1.6.4 EGF gradient and intestinal metaplasia at the distal oesophagus 34
1.7 Hypothesis 34
1.8 Thesis aims 36

2 Materials and Methods **37**
2.1 Materials 38
2.1.1 Cell lines 38
2.1.2 Reagents 38
2.1.3 Antibodies and plasmids 41
2.1.4 Other 41
2.1.5 Software 41
2.2 Methods 41
2.2.1 Cell culture 41
2.2.2 Organoid media preparation 42
2.2.3 Conditioned media production 43
2.2.4 Assessing conditioned media batch quality 44
2.2.5 Growing organoids from biopsies 46
2.2.6 Splitting organoids 46
2.2.7 Freezing Cell lines for storage 47
2.2.8 Mycoplasma testing and cell line authentication 47
2.2.9 Fluorescent labelling 47
2.2.10 Heterotypic junction Co-culture assay 47
2.2.11 Time-lapse Image acquisition 48
2.2.12 Studying cell heterotypic monolayers using MOSES 48
2.2.13 Immunofluorescence staining for heterotypic junctions 49
2.2.14 Deparaffination and hydration of paraffin embedded sections 49
2.2.15 Immunofluorescence staining of formalin fixed, paraffin embedded sections 49
2.2.16 Cell counting with convolutional neural newtworks 50
2.2.17 Migration-independent cell counting in videos 50
2.2.18 Predicting cell density using dye fluorescence intensity . . . 51
2.2.19 Producing the lipid-oil mix for the oil bath 51
2.2.20 Preparing collagen for 3D collagen ring or tube casting . . . 51
2.2.21 Making Clevers' collagen rings 51

2.2.22 Designing and 3D printing plastic moulds 52
2.2.23 Casting collagen rings 52
2.2.24 Casting collagen tubes 53
2.2.25 Adding adapters to the tubes 53
2.2.26 Constructing adapter caps 53
2.2.27 Coating the collagen tubes with cells 54
2.2.28 Preparing *Helicobacter pylori* selective agar plates 54
2.2.29 Culturing *Helicobacter pylori* in plates 54
2.2.30 Liquid culture of *Helicobacter pylori* in Brucella broth media 54
2.2.31 Infecting inner tube monolayers using *Helicobacter pylori* . . 55
2.2.32 3D sample processing 55
2.2.33 Haematoxylin and eosin staining 56
2.2.34 IHC staining 56
2.2.35 Liquid culture of *Helicobacter pylori* in Brucella broth media 57
2.2.36 Infecting inner tube monolayers using *Helicobacter pylori* . . 57
2.2.37 Slide scanning and analysis 57
2.2.38 Sectioning samples for tissue microdissection 57
2.2.39 Methyl green staining 58
2.2.40 Tissue micro-dissection 58

3 Designing a 2D model of the SCJ to study Barrett's oesophagus segment growth 59
3.1 Research aim 60
3.2 Chapter summary 60
3.3 Introduction 62
3.3.1 Choosing the stages of progression to model 63
3.3.2 Cell line selection 64
3.3.3 Plating adjacent cell populations 65
3.3.4 Labelling cells for co-culture experiments 66
3.3.5 Computational extraction of metrics from cell interaction videos 68
3.3.6 MOSES analysis 70
3.4 Results 74
3.4.1 Experimental design 74
3.4.2 Oesophageal squamous and Barrett's oesophagus cells form a stable junction *In vitro* in the absence of EGF 74
3.4.3 Serum free medium prevents collective cell behaviour in our model 75
3.4.4 Gastric adenocarcinoma cell line behaviour differs from OAC cell lines 79

3.4.5 The use of fluorescent dyes changes cell behaviour under serum conditions but is not colour specific. 80
3.4.6 High EGF concentrations can disrupt the squamous-columnar junction stability and increase the columnar segment length *In vitro* 82
3.4.7 Columnar invasion of the squamous lining *In vitro* is not determined by cell proliferation 85
3.4.8 Inhibition of EGFR using lapatinib prevents the invasion of BO and OAC derived cell lines *In vitro* 86
3.4.9 Deoxycholic acid does not produce the same effects as EGF presence in the medium 86
3.5 Discussion 88
3.5.1 The combinations selected produce three different interaction phenotypes 88
3.5.2 *In vitro* results with *In vivo* EGF concentrations suggests EGF in reflux can influence BO length 90
3.5.3 Migration and not proliferation may drive segment expansion *In vitro* 92
3.5.4 EGFR inhibition might be producing cell toxicity 93
3.5.5 Deoxycholic acid is not able to disrupt the junction at neutral pH 94
3.5.6 A simple 2D model consisting of only epithelial cells may be insufficient to test the reflux effect on BO segment growth . 96

4 Using 3D printing techniques to generate a 3D models of heterotypic junctions in the gastrointestinal tract 99
4.1 Research aim 100
4.2 Chapter summary 101
4.3 Introduction 102
4.3.1 Animal models 102
4.3.2 Organotypic culture 105
4.3.3 Organoids 106
4.3.4 Organoids use in co-culture methods 108
4.3.5 Organ-on-a-chip and microfabrication 109
4.4 Heterotypic junctions using organoids 110
4.4.1 Printing organic structures with organoid cells 111
4.4.2 Nanoprinting of droplets in an oil-lipid bath 113
4.5 Model required characteristics 114
4.6 Contributions 115

4.7 Results . . . 115
4.7.1 Adapting available organotypic culture systems to generate a differentiated SCJ *In vitro* . . . 115
4.7.2 Organoid nanoprinting using an oil bath . . . 116
4.7.3 Using a 3D printed mould and bigger droplets to enhance organoid fusion . . . 116
4.7.4 Adding fibroblasts changes the extracellular matrix and controls the ring shape . . . 120
4.7.5 Fibroblast mediated contraction of the ring is concentration-dependent . . . 121
4.7.6 Fibroblast concentration define collagen fibre density and fibroblast location . . . 121
4.7.7 Forming heterotypic junctions in the ring using a divider. . . 122
4.7.8 Using larger moulds to form large tubular collagen scaffolds 125
4.7.9 The collagen tube shape can be altered by using different fibroblasts concentrations in each tube segment . . . 125
4.7.10 Using fibroblast contraction at the tube's edges to attach plastic adapters . . . 126
4.7.11 Populating the tube's lumen with epithelial cells using adapters 127
4.7.12 Infecting tubes with gastric epithelial lining in the lumen . . 128
4.7.13 The tube's collagen walls stop the diffusion of both medium and air . . . 130
4.8 Discussion . . . 131
4.8.1 Drawbacks of using organotypic culture for heterotypic junctions 131
4.8.2 An improved ring collagen method replicates histological accurate epithelium . . . 131
4.8.3 Fibroblasts contraction as a tool for tissue engineering . . . 133
4.8.4 Controlling droplet fusion and heterotypic junctions 134
4.8.5 Printing self-shaping tubular structures . . . 135
4.8.6 Controlling flow allows for both populating and infection of the tube lumen . . . 136
4.8.7 Properties of collagen walls . . . 137
4.8.8 Future directions . . . 137
4.9 Conclusion . . . 145

5 Combining microdissection and proteomics to study Barrett's oesophagus progression 147
5.1 Research aim . . . 148
5.2 Introduction . . . 149

5.2.1 Barrett's Oesophagus to OAC progression occurs in a complex environment . . . 149
5.2.2 Techniques to study complex microenvironments driving Barrett's oesophagus at a cellular subtype level . . . 150
5.2.3 Advantages of working with proteins . . . 153
5.2.4 Using microdissection and proteomics to study Barrett's oesophagus . . . 154
5.3 Experimental design . . . 155
5.4 Contributions . . . 156
5.5 Results . . . 157
5.5.1 Patient case selection pipeline . . . 157
5.5.2 Sectioning FFPE blocks pattern . . . 158
5.5.3 Sample annotation . . . 158
5.5.4 Sample selection and microdissection . . . 161
5.6 Discussion . . . 162
5.6.1 Mounting thinner sections on microdissection slides . . . 163
5.6.2 Use of biopsies in place of paraffin blocks . . . 168
5.6.3 Using results to study pathologists lack of consensus . . . 168

6 Conclusions **170**
6.1 Conclusion . . . 171
6.1.1 Designing a model of the interaction between squamous and BO cell populations . . . 171
6.1.2 EGF can disrupt the stability between squamous and oesophageal cell types and promote columnar segment growth *in vitro* . . . 172
6.1.3 EGF activates BO segment growth is not proliferation dependant *in vitro* . . . 175
6.1.4 The use of a divider can generate 3D models of the squamous-columnar junction in organotypic models . . . 177
6.1.5 Combining oil-lipid bath with 3D printed moulds improves existing technique to fuse epithelial organoids . . . 177
6.1.6 Control over the cell populations of each ring segment to form heterotypic junctions . . . 178
6.1.7 Fibroblasts populations contract the collagen scaffold in a concentration dependant manner . . . 178
6.1.8 Production of longer tubular structures and shaping them using fibroblast concentrations . . . 179
6.1.9 Adapters allow the control over the contents in the tube's lumen enabling lining of the internal wall with epithelial cells 180

6.1.10 The collagen wall is impermeable enabling future use into microfluidic circuits 180
6.1.11 Design of future xenografting experiments in mice models . . 182
6.1.12 Microdissection and proteomics analysis approach 184

References **188**

List of Figures

1.1 **The upper gastrointestinal tract** 4
1.2 **The structure of the oesophagus wall and its different layers** 5
1.3 **Haematoxylin and eosin staining of an oesophageal section** 6
1.4 **The structure of the gastric wall and its different layers** . . 7
1.5 **The structure of the duodenum wall and its different layers** 9
1.6 **Oesophageal cancer subtypes and place of origin** 10
1.7 **Oesophageal adenocarcinoma incidence worldwide** 11
1.8 **Oesophageal adenocarcinoma TNM staging** 12
1.9 **Oesophageal adenocarcinoma ten-year survival improvement** 13
1.10 **Oesophageal adenocarcinoma treatment decision tree** 14
1.11 **Oesophageal adenocarcinoma new treatment inhibitors** . . . 15
1.12 **New treatments costs compared with conventional chemotherapy** 16
1.13 **Barrett's oesophagus origin candidates** 19
1.14 **Barrett's oesophagus progression to adenocarcinoma** 21
1.15 **Barrett's oesophagus length stratification** 22
1.16 **Barrett's oesophagus clonal expansion** 24
1.17 **Effect of low pH reflux on the squamous epithelium** 27
1.18 **EGFR signalling** 31
1.19 **EGF concentration across the upper GIT** 33
1.20 **EGF gradient formation at the distal oesophagus** 35

2.1 **Well layout for luciferase conditioned media testing** 45

3.1 **Celltracker dyes** 67
3.2 **Possible population interactions types** 69
3.3 **Summary of MOSES analysis** 72
3.4 **Uses of MOSES analysis in *In vitro* models** 73
3.5 **Summary of video number per condition** 74
3.6 **EPC2 and CP-A form a stable junction *In vitro*** 76
3.7 **MOSES analysis of the three combination in our model** . . 77
3.8 **Serum free medium prevents collective behaviour** 79
3.9 **Gastric adenocarcinoma cell line and EPC2 co-culture** . . . 80

3.10 **Studying dye toxicity across the cell combinations** 81
3.11 **MOSES mesh analysis of EGF titration** 83
3.12 **MOSES metrics analysis of EGF titration** 84
3.13 **Calculating cell proliferation using a CNN** 85
3.14 **Cell proliferation prediction through dye decay** 87
3.15 **Lapatinib and Deoxycholic acid effect on junction stability** 88
3.16 **Alternatives to EGF activating convergent pathways** 95
3.17 **Model limitations and proposed solutions** 98

4.1 **Animal models for Barrett's oesophagus** 104
4.2 **Oesophagojejunostomy in rodent** 105
4.3 **Organoids use in co-culture methods** 111
4.4 **Hans Clevers' method to fuse organoids in collagen rings** . 112
4.5 **Nanoprinting using an oil-lipid bath** 114
4.6 **Organotypic models of the heterotypic junction** 117
4.7 **Dissociating organoid into cells for nanoprinting** 118
4.8 **Combining plastic 3D printing and oil-lipid baths** 119
4.9 **Collagen ring method comparison** 120
4.10 **Fibroblasts ring contraction is concentration dependant** . . 122
4.11 **Fibroblasts contraction changes collagen fibre packing** . . . 123
4.12 **Heterotypic junction formation using a divider** 124
4.13 **Heterotypic junction immunofluorescense staining** 124
4.14 **Experimental design to form tubular collagen structures** . . 126
4.15 **Self-shaping tubular structures** 127
4.16 **Adapter and cap variations** 128
4.17 **Populating and infecting the tubes lumen** 129
4.18 **Collagen wall impermeability** 130
4.19 **Summary of future directions** 139
4.20 **Using nanoprinting to increase complexity** 144

5.1 **Steps during tissue microdissection** 153
5.2 **Pipeline of sample selection for microdissection** 157
5.3 **Block processing protocol** 159
5.4 **Example of histology annotations for microdissection** 160
5.5 **Annotation table for selected** 161
5.6 **Block MS17-821-A2 annotations** 162
5.7 **Block MS17-821-A2 microdissection** 163
5.8 **Block MS17-2698-A2 annotations** 164
5.9 **Block MS17-2698-A2 microdissection** 165
5.10 **Block MS17-15410-B2 annotations** 166

5.11 **Block MS17-15410-B2 microdissection** 167

6.1 **Low pH effect on EGF production in the BO segment** . . . 173
6.2 **Human biopsies to study EGF in BO expansion** 174
6.3 **Adapting the 2D model to a screening platform** 176
6.4 **Organoid use in combination with the tube model** 183
6.5 ***in vivo* experiments with mice** 185
6.6 **Sequential biopsy microdisection and MS analysis** 187

List of Abbreviations

2D . . . . . Two-dimensional

3D . . . . . Three-dimensional

ABS . . . . . Acrylonitrile butadiene styrene

APS . . . . . Ammonium peroxide sulphate

ATCC . . . . . American Type Culture Collection

BO . . . . . Barrett's Oesophagus

BSA . . . . . Bovine serum albumin

CAF . . . . . Cancer associated fibroblasts

CDX . . . . . Caudal type homeobox

CIV . . . . . Cell Image Velocimetry

CK . . . . . Cytokeratin

CNN . . . . . Convolutional neural network

CyTOF . . . . Cytometry by time of flight

DCA . . . . . Deoxycholic acid

DMEM . . . . Dulbecco's Modified Eagle Medium

DNA . . . . . Deoxyribonucleic acid

ECM . . . . . Extracellular matrix

EDTA . . . . . Ethylene diamine tetra acetic acid

EGF . . . . . Epidermal growth factor

EGFR/ERBB1 Epidermal growth factor receptor

EGFRi . . . . Epidermal growth factor receptor inhibitor

EMR . . . . . Endoscopic mucosal resection

FACS . . . . . Fluorescence activated cell sorting

FBS . . . . . Foetal bovine serum

FFPE . . . . . Formalin-Fixed Paraffin-Embedded

FGFR . . . . . Fibroblast growth factor receptor

GIT . . . . . Gastroinstetinal tract

GOJ . . . . . Gastroesophageal junction

GORD . . . . Gastroesophageal reflux disease

GST . . . . . Glutathione-S-transferase

H&E . . . . . hematoxylin & eosin

HEPES . . . . 4-(2-hydroxyethyl)-1-piperazineethanesulfonic acid

HER2/ERBB2 Human epidermal growth factor receptor 2

HFF . . . . . Human Fetal Fibroblast

HGD . . . . . High-grade dysplasia

IF . . . . . Immunofluorescence

IHC . . . . . Immunohistochemistry

IL . . . . . Interleukin

IM . . . . . Intestinal metaplasia

JNK . . . . . c-Jun N-terminal kinase

KSFM . . . . . Keratinocyte serum free medium

LGD . . . . . Low-grade dysplasia

MAPK . . . . Mitogen activated protein kinase

MET/HGFR . Hepatocyte growth factor receptor

MOSES . . . . Motion sensing superpixels

MS . . . . . Mass spectrometry

MSD . . . . . Mean square displacement

NGS . . . . . Normal goat serum

NSAID . . . . Nonsteroidal anti-inflammatory drugs

OAC . . . . . Oesophageal adenocarcinoma

OSCC . . . . . Oesophageal squamous cell carcinoma

OSG . . . . . oesophageal submucosal glands

PALM . . . . . Photoactivated localization microscopy

PBS . . . . . Phosphate buffered saline

PEN . . . . . Polyethylene naphthalate

Pen/Stre . . . Penicillin/streptomycin

PIV . . . . . Particle Image Velocimetry
PPI . . . . . Proton pump inhibitor
RNA . . . . . Ribonucleic acid
RNA-seq . . . RNA sequencing
RPMI . . . . . Roswell Park Memorial Institute
RTK . . . . . Receptor tyrosine kinase
SCJ . . . . . Squamous-columnar junction
scRNA-seq . . Single cell RNA sequencing
t/T . . . . . Time
TAMs . . . . . Tumor associated macrophages
TOF . . . . . Time of flight
Treg . . . . . T-regulatory cells
UK . . . . . United Kingdom
USA . . . . . United States of America
VEGF . . . . . Vascular endothelial growth factor
VEGFR . . . . Vascular endothelial growth factor receptor

Symbols and Units

α . . . . . Alpha
β . . . . . Beta
^{o}**C** . . . . . Degree centigrade
g . . . . . Gram
h . . . . . Hour
L . . . . . Litre
m . . . . . 10^{-3}
u . . . . . 10^{-6}
n . . . . . 10^{-9}
M . . . . . Molar
min . . . . . Minutes
O/N . . . . . Overnight
RT . . . . . Room temperature
sec . . . . . Second

1 Introduction

Contents

1.1 Summary 2
1.2 The upper gastrointestinal tract 3
1.2.1 The oesophagus 4
1.2.2 The stomach 6
1.2.3 The duodenum 8
1.2.4 Heterotypic epithelial junctions 9
1.3 Oesophageal Adenocarcinoma 10
1.3.1 Epidemiology 10
1.3.2 Diagnosis 11
1.3.3 Staging 12
1.3.4 Survival 13
1.3.5 Treatment 13
1.3.6 New treatment strategies 14
1.3.7 Preventive surveillance 15
1.4 Barrett's Oesophagus 15
1.4.1 The Barrett's oesophagus epithelium 17
1.4.2 The origins of Barrett's oesophagus 17
1.4.3 Barrett's oesophagus progression to adenocarcinoma . . 19
1.4.4 Clinical implications of Barrett's oesophagus segment length 20
1.4.5 Length of Barrett's oesophagus and progression to cancer 20
1.4.6 Barrett's oesophagus length and clonality 22
1.4.7 The establishment of Barrett's oesophagus length 23
1.5 Gastroesophageal reflux disease 25
1.5.1 Definition 25
1.5.2 Components of gastric origin 25
1.5.3 Components of hepatic origin 27
1.5.4 Components of pancreatic origin 28
1.5.5 Components of duodenal origin 29

1.6 Epidermal growth factor 29
1.6.1 The EGFR signalling pathway 29
1.6.2 The epidermal growth factor in gastrointestinal homeostasis 30
1.6.3 EGF levels in the upper gastrointestinal tract 32
1.6.4 EGF gradient and intestinal metaplasia at the distal oesophagus 34
1.7 Hypothesis 34
1.8 Thesis aims 36

1.1 Summary

Oesophageal adenocarcinoma is a cancer subtype of the upper gastrointestinal tract originating at the gastroesophageal junction. Because of its location, the diagnosis is often late, and mortality rates are high.

A sedentary lifestyle defines most of its risk factors. As a result, its incidence had been increasing in the developed world during the past decades. In recent years, the incidence has plateaued. Yet, developing countries adopting a westernised lifestyle might develop similar trends.

Even with the onset of new treatments, a good prognosis still relies on early detection. To achieve this, research has focused on a precursor lesion: Barrett's oesophagus. However, this condition is common and seldom progresses into cancer, and surveillance is in most cases unnecessary. As a result, national healthcare services would benefit from a better stratification of the patients at risk, helping them reduce unnecessary costs.

In Barrett's oesophagus, columnar cells replace the squamous epithelium in the distal oesophagus. Although described decades ago, Barrett's oesophagus is not well understood. Controversies exist over its cell of origin, evolution to adenocarcinoma and treatment. Other progression stages like the mechanisms that enable the original cells to colonise the lower oesophagus are unknown. Understanding how Barrett's oesophagus achieves its final length, a risk factor for oesophageal adenocarcinoma,

could have clinical implications. The compounds present in gastroduodenal reflux, a risk factor for Barrett's oesophagus, are the best candidates to promote Barrett's oesophagus segment growth. Recent studies have focused on bile acids because of their DNA damaging and ROS producing properties. Other elements present in the reflux like the epidermal growth factor have received less attention. This growth factor also has the potential to regulate the final length of the lesion.

This introduction describes the upper gastrointestinal tract. In it, each organ has a layered structure lined with an epithelium with its own differentiation pathways. It continues with oesophageal adenocarcinoma, its epidemiology, treatment and prognosis, then describes Barrett's oesophagus origin, evolution and risk factors focusing in segment length. It continues discussing the different reflux compounds that might explain differences in Barrett's oesophagus length. Finally, the epidermal growth factor in the reflux and its influence in segment length is discussed.

1.2 The upper gastrointestinal tract

The upper gastrointestinal tract is the segment of gastrointestinal tract (GIT) derived from the embryonic foregut. This comprises the mouth, pharynx, oesophagus, stomach and duodenum. The lower oesophageal sphincter controls passage from the oesophagus to the stomach. The pyloric sphincter regulates flow from the stomach into the duodenum. (Figure 1.1). This thesis is limited to the events that occur in the gastroesophageal and gastroduodenal junctions. As a result, the organs investigated are the oesophagus, the stomach and the duodenum.

The upper gastrointestinal tract comprises a sequence of specialised organs sharing a lumen. Epithelial cells are found lining the skin and organs of its internal passageways [1]. Each organ has unique epithelial cell populations adapted to their specific role. Where the epithelium from different organs meet, a heterotypic junction is formed. For instance, in the squamous-columnar junction the squamous lining of the oesophagus meets the columnar epithelium of the stomach (Figure 1.1).

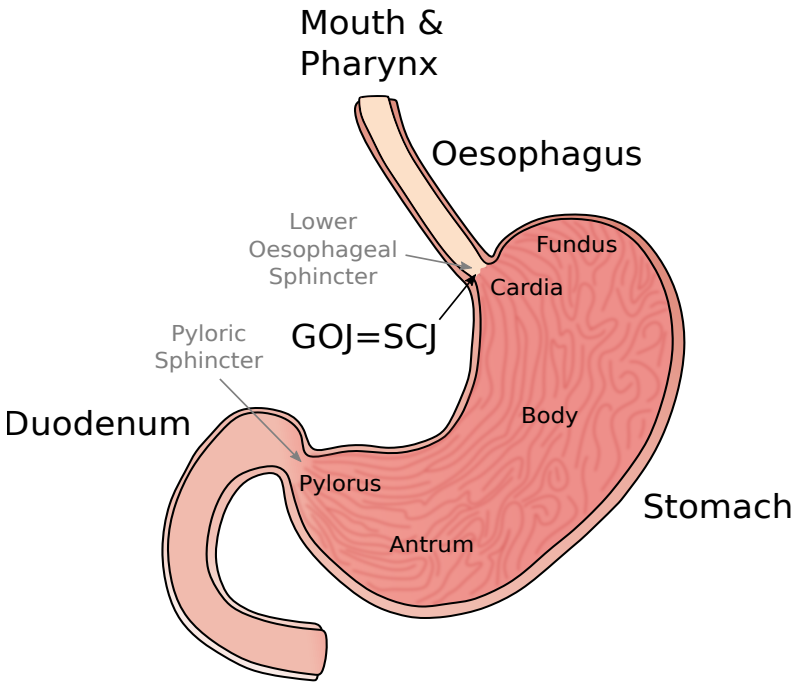

Figure 1.1: The upper gastrointestinal tract Anatomy of the upper gastrointestinal tract, extending from the mouth to the duodenum. In the gastroesophageal junction (GOJ) the squamous epithelium of the oesophagus meets with the columnar lining of the stomach forming the squamous-columnar junction (SCJ).

1.2.1 The oesophagus

The oesophagus is a tubular organ about 25 cm long. It connects the pharynx with the uppermost side of the stomach. The oesophageal wall is comprised of fibro-muscular structure, which generates peristaltic movement, and together with gravity, allows food transfer through the oesophagus to the stomach. The oesophageal wall has the following layers: mucosa, submucosa, muscularis propria with traversal fibres, muscularis propria with longitudinal fibres and adventitia. The oesophageal mucosa is further subdivided in the epithelium, the basement membrane and the muscularis mucosa (Figure 1.2).

The oesophageal epithelium

The oesophagus and the trachea originate in the fourth week of development from a common structure. The foetal oesophagus is comprised of a 3-4 cell thick columnar lining. Between week 14-16 of development, a new squamous epithelium replaces

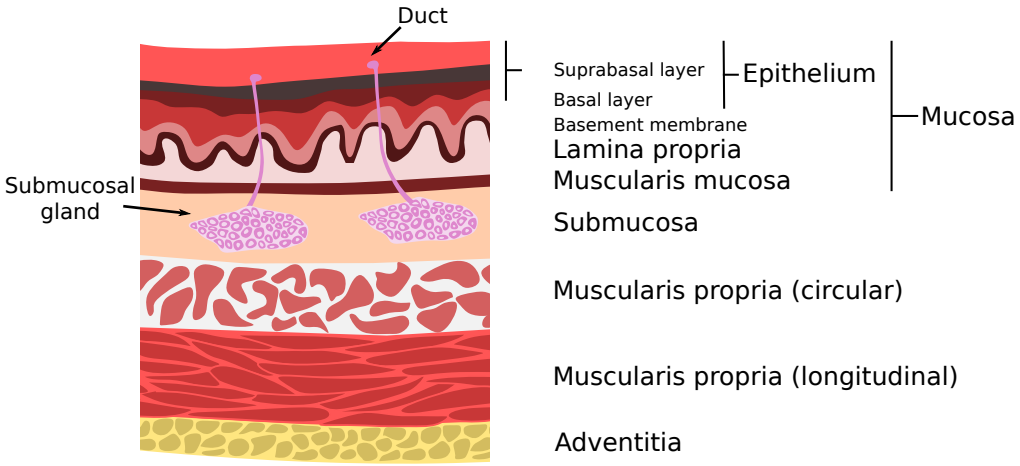

Figure 1.2: The oesophagus wall and its different layers Diagaram of a cross-section of the oesophgeal wall with its different layers. The mucosa is formed by a multilayered non-keratinized squamous epithelium with different stages of differentation. The oesophageal glands in the submucosa form ducts extending to the lumen through the squamous epithelium.

the columnar lining [2]. The signalling pathways leading to this process and how this transition occurs are not well understood.

The adult oesophagus presents a non-keratinized, stratified epithelial lining approximately 25 cells wide. It comprises a proliferative basal layer and a suprabasal layer. The suprabasal layer presents a differentiation gradient, with the terminally differentiated cells found at the interphase with the lumen. The epithelial homeostasis occurs through balanced proliferation, migration and shedding into the lumen [3]. Unlike rodents, in humans the suprabasal layer of the epithelium is not keratinized. The human mucosa is thus more susceptible to thermal, abrasive and low pH injuries [4].

The oesophageal submucosal glands

The oesophageal submucosa contains a population of epithelial cells organized into glands. The oesophageal submucosal glands (OSG) have two parts: first, the acini in the submucosal connective tissue which are made of cuboidal epithelial cells and second, the ducts extending from these acini into the lumen (Figure 1.2). The ducts transition from cuboidal to squamous epithelium towards the luminal surface

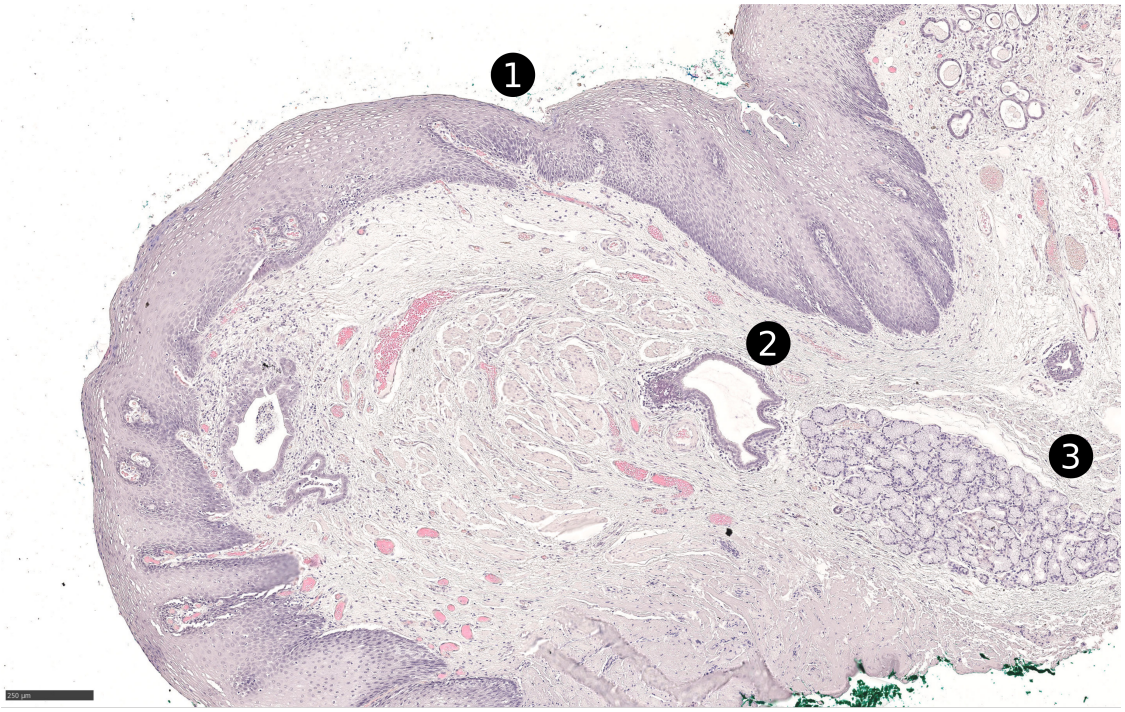

Figure 1.3: Haematoxylin and eosin staining of an oesophageal section 1) Healthy squamous epithelia of the oesophagus. 2) oesophageal submucosal gland duct and 3) oesophageal submucosal gland acini. scalebar: 250um

where the secretions of the glands are released. This location might allow subtances transiting the oesophagus to influence ductal cells (Figure 1.3) [5].

The origin of OSG is unknown. The OSG might arise from ingrowths salivary gland or squamous papillae [6]. Another theory proposes it originates of residual columnar epithelium remaining after embryogenesis [7]. The presence of OSG varies between 4 and 50% depending on the individual. Further, the OSG present an unequal distribution across the oesophagus. The OSG are more common at the proximal and distal ends of the oesophagus [8]. The glands secrete mucus, bicarbonate, epithermal growth factor (EGF) and prostaglandins. These compounds help protect and repair the epithelium [9].

1.2.2 The stomach

The stomach is a dilated tubular organ located between the oesophagus and the duodenum, it subdivides into cardia, fundus, body (or corpus), antrum and pylorus (Figure 1.1). The wall of the stomach presents almost the same layered structure

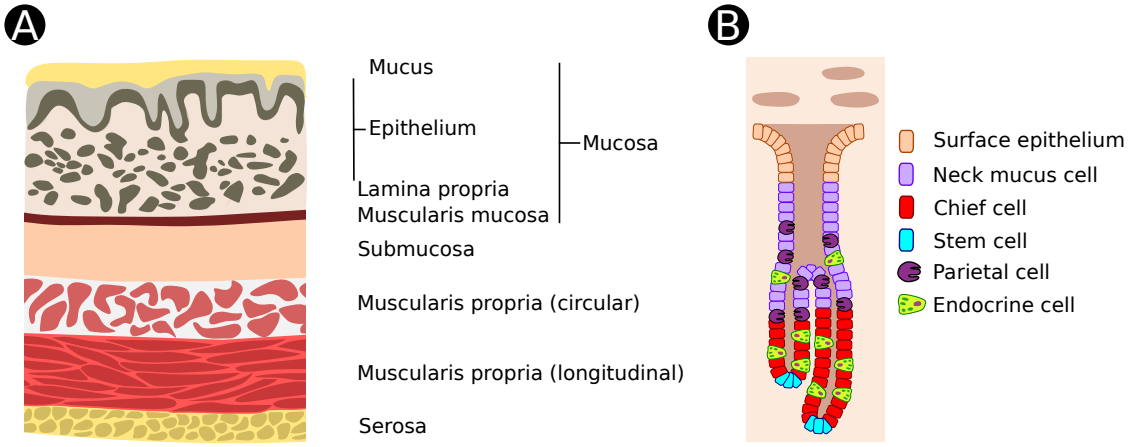

Figure 1.4: The gastric wall and its different layers A) Diagaram of a cross-section of the gastric wall with its different layers. B) Detail of the epithelium formed by gastric pits with cells differentiated into specialized subtypes.

as the oesophagus, the exception being a thicker tunica serosa which replaces the adventitia (Figure 1.4 A). The stomach performs the chemical digestion of food using enzymes and hydrochloric acid. The lower oesophageal and pyloric sphincters control the flow in and out of the stomach.

The gastric epithelium

The stomach epithelium consists of a columnar monolayer arranged in glandular structures. The gland cellular populations vary across the stomach. The epithelium in the corpus gives the stomach most of its functionality. The glands in the corpus have five distinct differentiated cell populations. The surface and neck mucous cells localize at the top of the gland and secrete protective mucus. The parietal cells at the neck release hydrochloric acid and other factors to the lumen. The chief cells populate the bottom of the glands releasing digestive enzymes. The glands also contain populations of stem cells, Tuft cells and endocrine cells (Figure 1.4 B).

The cardia and pylorus specialize in preventing damage from materials transiting the stomach, thus most of their epithelial cell population consists of mucous-secreting cells. At the base of the glands, there are the progenitor cells in charge of self-renewal [10]. These cells are positive for the columnar stem cell marker LGR5 [11].

1.2.3 The duodenum

The duodenum is the first segment of the small intestine. Unlike the rest of the small intestine, it develops from the foregut. This organ functions as a semipermeable barrier incorporating nutrients and water into the blood. The duodenum is also the meeting point of several organ secretions helping digestion. The wall of the duodenum presents the same layers as the stomach (Figure 1.5 A). The duodenum consists of 4 parts connecting the gastric pylorus with the jejunum. Remarkably, the major duodenal papilla forms at the union of the pancreatic duct and common bile duct and joins with the second part, known as "D2" or vertical segment, connects to the major duodenal papilla. The pancreatic duct connects the pancreas with the duodenum and secretes the pancreatic juice into the duodenum. This alkaline mix contains enzymes helping to digest lipids, proteins and sugars.

The common bile duct forms at the union of two ducts: first, the common hepatic duct, connecting it to the liver, and second, the cystic duct extending from the gallbladder. The bile synthesized in the liver transits to the gallbladder where it gets concentrated. After eating, the levels of the cholecystokinin hormone increase which contracts the gallbladder and relaxes the hepatopancreatic sphincter releasing the bile. The bile emulsifies the lipids circulating through the duodenum forming micelles. The formation of micelles has two functions: Micelles help digest the lipids in them by exposing them to pancreatic lipases and also help absorb fat-soluble vitamins including retinoic acid, D, E and K.

The duodenal epithelium

The duodenal epithelium acts as a barrier to insults from the stomach and the common bile duct. Additionally, it further digests transiting materials and absorbs nutrients and water. The columnar lining of the duodenum is organized in villiform structures which increase the surface area with its contents, aiding the duodenal function (Figure 1.5).

The duodenal mucosa cells divide into the secretory and absorptive lineages consisting of enterocytes. The enterocytes polarize towards the lumen presenting a

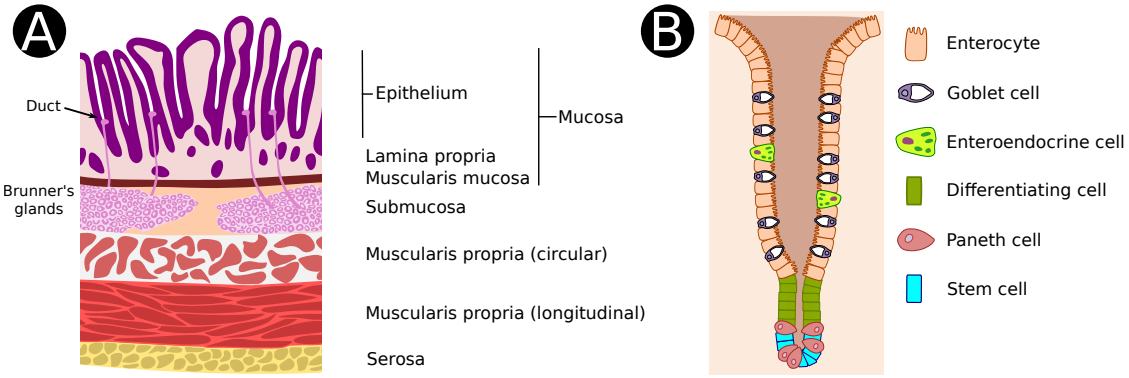

Figure 1.5: The duodenum wall and its different layers A) Diagram of a cross-section of the duodenal wall with its different layers. B) Detail of the cell populations in the duodenal villi.

structure called microvilli which enables absorption by increasing the surface area with the lumen contents. The secretory lineage further divides into the mucus-secreting and hormone-releasing lineages, the former consisting of goblet cells and the latter of Paneth and enterocrine cells (Figure 1.5 B).

Brunner's glands

The duodenum above the hepatopancreatic sphincter presents structures known as Brunner's glands. These structures are more abundant next to the stomach [12]. As in the oesophagus, these submucosal glands have a cuboidal epithelial lining.

Interestingly, Brunner's glands present similarities with oesophageal submucosal glands. First, the glands originate from mucosal ingrowths in weeks 14 to 16 [13]. Second, Owen et al. showed that both gland types share molecular markers like MUC6 and trefoil factors [14] . Finally, they also secrete mucus bicarbonate and epidermal growth factor into the lumen. These compounds aid enzymatic reactions, prevent low pH mucosal damage and lubricate the duodenum [15].

1.2.4 Heterotypic epithelial junctions

In the upper gastrointestinal tract, the different epithelia of each organ meet forming heterotypic junctions. These junctions in the GIT and other organs are hotspots for metaplasia and malignancy [16] , [17] , [18], highlighting the potential for Oesophageal adenocarcinoma malignancy.

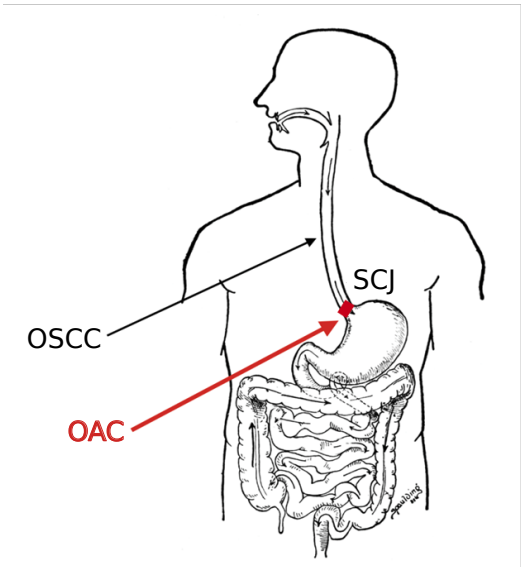

Figure 1.6: Oesophageal cancer subtypes and place of origin Anatomic location of the two oesophageal cancer subtypes.

1.3 Oesophageal Adenocarcinoma

Oesophageal cancer causes a sixth of the cancer-related deaths worldwide [19]. The two distinct subtypes are oesophageal squamous cell carcinoma (OSCC) and the oesophageal adenocarcinoma (OAC) (Figure 1.6), each subtype being epidemiologically and pathologically distinct. The OSCC develops from the squamous epithelium of the oesophagus. OAC evolves from columnar metaplastic cells located in the gastroesophageal junction.

1.3.1 Epidemiology

OAC caused a fifth of the 456.000 oesophageal cancer-related deaths worldwide in 2012. While the global incidence of OSCC declines, OAC incidence increased in the last decades in developed countries [20] ,[21], [22],[23]. As a result, OAC incidence has surpassed OSCC's in several nations. An example is the United Kingdom, with the highest OAC incidence per capita. [24]. As sedentary lifestyle related obesity influence OAC incidence, the trends could replicate in developing countries (Figure 1.7).

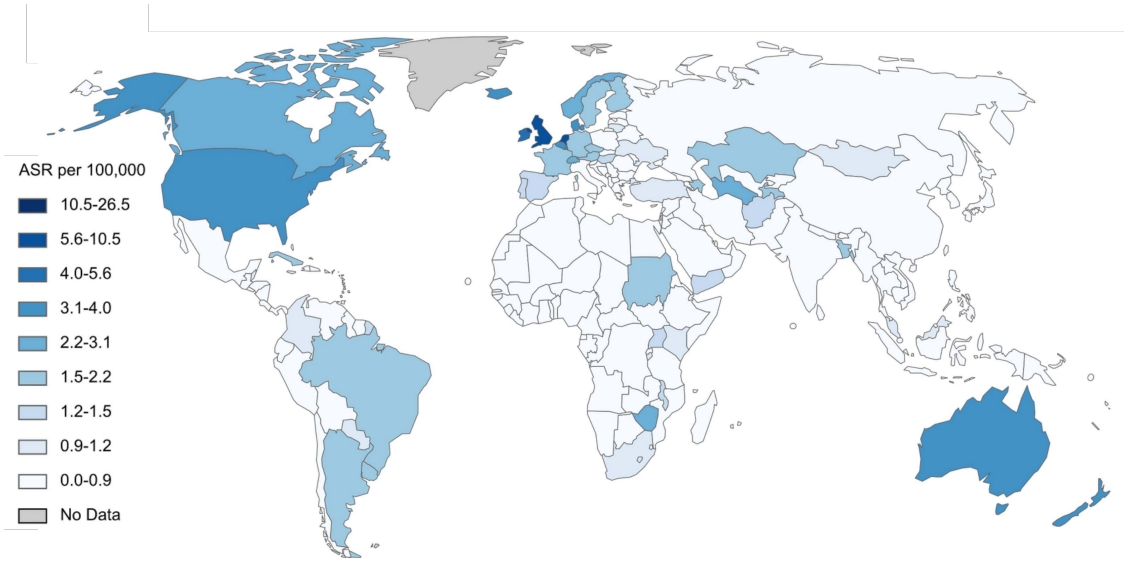

Figure 1.7: Oesophageal adenocarcinoma incidence worldwide The incidence of OAC is higher in the western world with the United Kingdom having the highest incidence worldwide. Adapted from [32]

Gender and age are the two other main epidemiological risk factors for OAC. Males are six times more likely to develop OAC than females [25]. The risk also increases in individuals older than 60 years [23].

1.3.2 Diagnosis

The expansile nature of the oesophagus complicates early diagnosis. With obstructions appearing in late stages, patients are often diagnosed through two symptoms: Involuntary and progressive weight loss and difficulty and pain when swallowing. Patients with those symptoms are likely to have already locally advanced cancer. The local lymphatic drainage connects to the thoracic duct and the mediastinal, gastric and coeliac nodes. This facilitates distant metastases to vital organs [26], [27]. As a result, most cases of cancer have already invaded lymph nodes or metastasized to other organs when diagnosed. In the UK patients, the first diagnosis includes lymph or distant metastases in 70-80% of the cases [28]. Late detection prevents patients from benefiting of curative therapy and increases recurrence risk [29], [30] , [31].

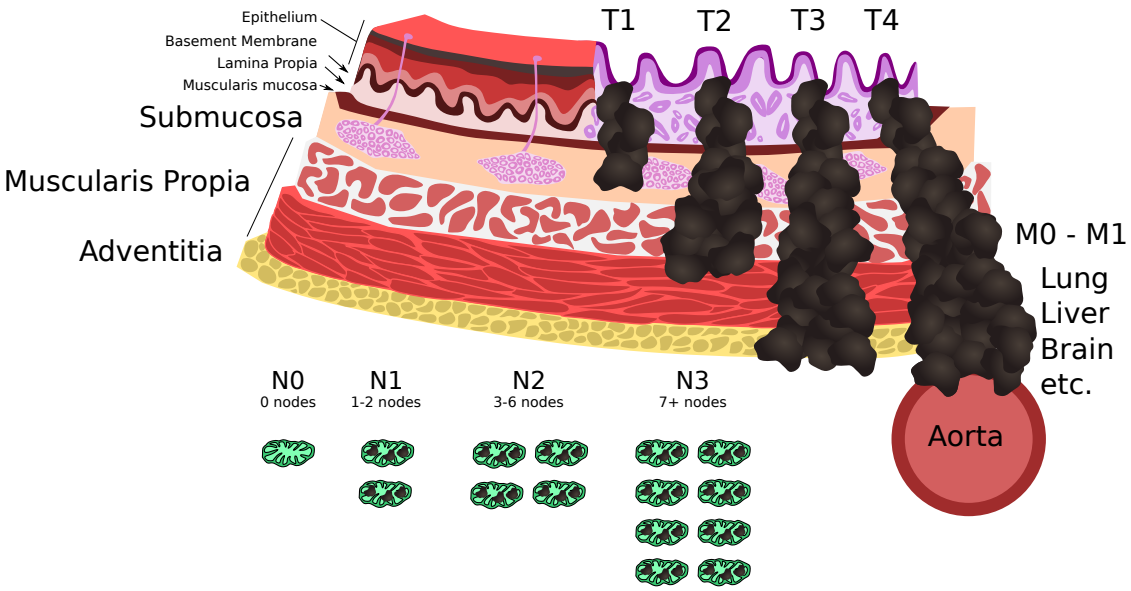

Figure 1.8: Oesophageal adenocarcinoma TNM staging Cartoon summary of TNM staging.

1.3.3 Staging

The OAC staging uses the Tumour-Node-Metastasis (TMN) classification (Figure 1.8). This classification describes the stage using three letters: T, N and M.

T indicates how deep into the oesophagus wall the tumour has invaded. T1a labels cancers confined in the mucosa. T1b indicates that the tumor has affected the submucosal layer. T2 labels cancers confined to the muscularis propria. T3 is used when the cancer has invaded the adventitia. Finally, T4 states invasion to neighbouring structures.

N refers to the number of lymph nodes affected by metastases. N0 for no nodes affected, N1 for 1-2, N2 for 3-4 and N3 when there are 7 or more.

Finally, M indicates whether there are (M1) or not (M0) metastases to distant organs [33].

Even when affecting the oesophagus, when found also 2 cm below the gastroesophageal junction, the cancer is considered to be a gastric cancer [34].

Staging is the major factor determining both treatment and survival of OAC patients.

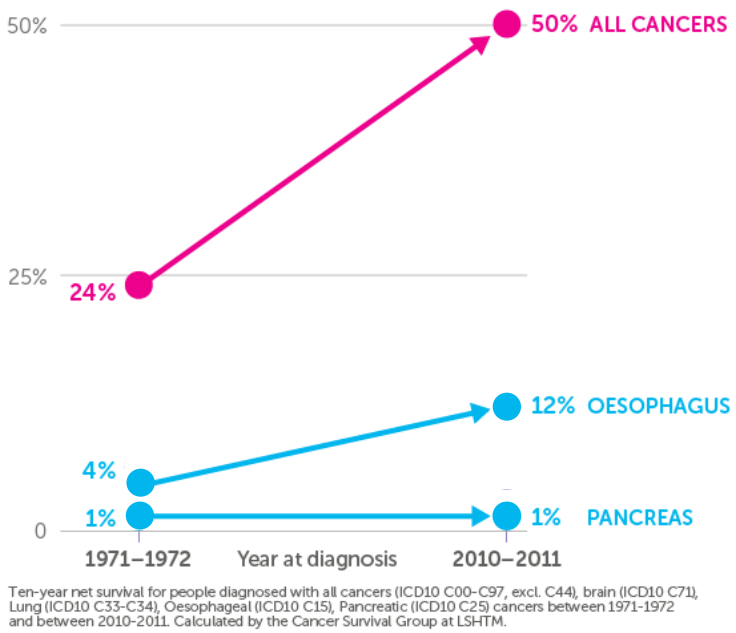

Figure 1.9: Oesophageal adenocarcinoma ten-year survival improvement Summary of the 10-year survival improvement in the UK in the last four decades. Adapted from [37]

1.3.4 Survival

5-year survival rates for all OAC cases varies across countries. In the United Kingdom they were up to 15.1% during the years 2010 - 2011 [35]. Survival was higher in the United States, with a 19% 5-year survival between 2008-2014.

Staging is the main 5-year survival predictor. In the United States, it is 45% for localized (T1-T2), 24% for regional (T3-T4) and as low as 5% when the tumour has distant metastases (M1) [36].

Unlike other cancer types, survival rates for OAC have improved little. For instance, 10-year survival in the UK has only improved from 5% to 12.3% in the last 40 years. This 7% increase in survival rates is significantly lower than the mean 25% seen in the overall cancer patients (Figure 1.9).

1.3.5 Treatment

Endoscopic mucosal resection (EMR) for tumours confined to the mucosa (T1a) [38] and oesophageal resection is used when extending into the submucosa (T1b and T2). Tumours limited to the oesophageal wall (T3) or the adjacent regions

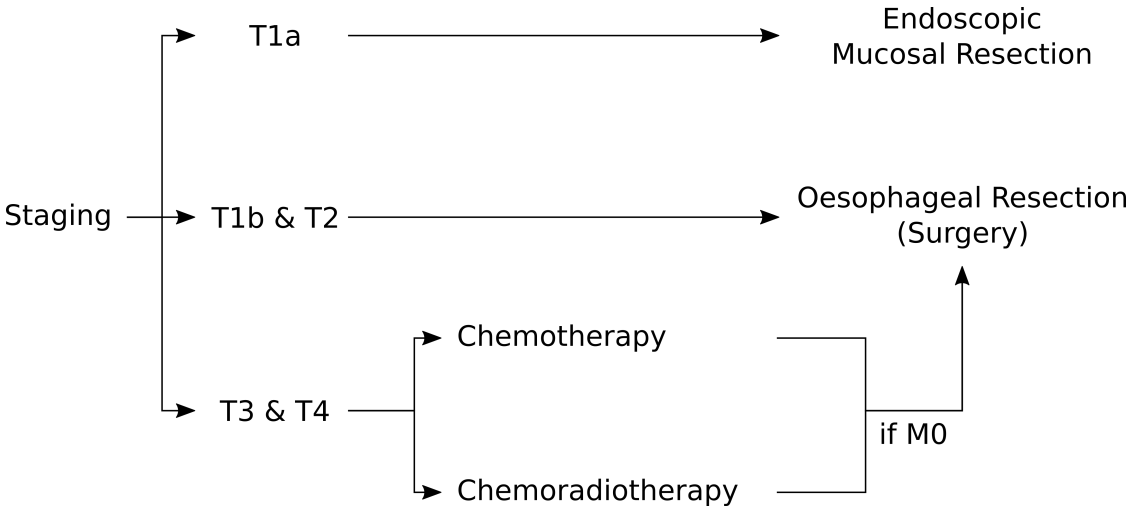

Figure 1.10: Oesophageal adenocarcinoma treatment decision tree Decision tree for oesophageal cancer treatment of patients after staging.

(T4, N1-3), are treated with chemotherapy or chemoradiotherapy followed by surgery. Palliative care chemotherapy or chemoradiotherapy are used in cases with distant metastases (M1) in which surgery would reduce their quality of life without increasing survival (Figure 1.10) [39].

1.3.6 New treatment strategies

The limited success of current treatments has promoted research in new curative strategies. Previous efforts have centred around developing inhibitors for key signalling pathways. The transmembrane proteins Receptor Tyrosine Kinases (RTK) have received special attention as they are usually mutated or overexpressed in OAC cancer. The RTK inhibitors tested include: EGFR [40], [41], [42], MET [43], [44], FGFR ([45], VEGFR ([46], [47] and HER2. Among these, the HER2 trastuzumab inhibitor is the only drug developed to date that improves patient survival [48].

Recent clinical trials have changed to an immunotherapy strategy, targeting cells to boost immune response. The most frequently used type of immunotherapy are monoclonal antibodies that act as check-point blockade inhibitors. These antibodies block the receptor interactions that silence T-cell death signalling.

Monoclonal antibodies tested in OAC include: PD1 (Nivolumab, [49] and CTLA4 (Ipilimumab, [50] presented by T-lymphocyte and PDL1 (Durvalumab, Ludwig-2015

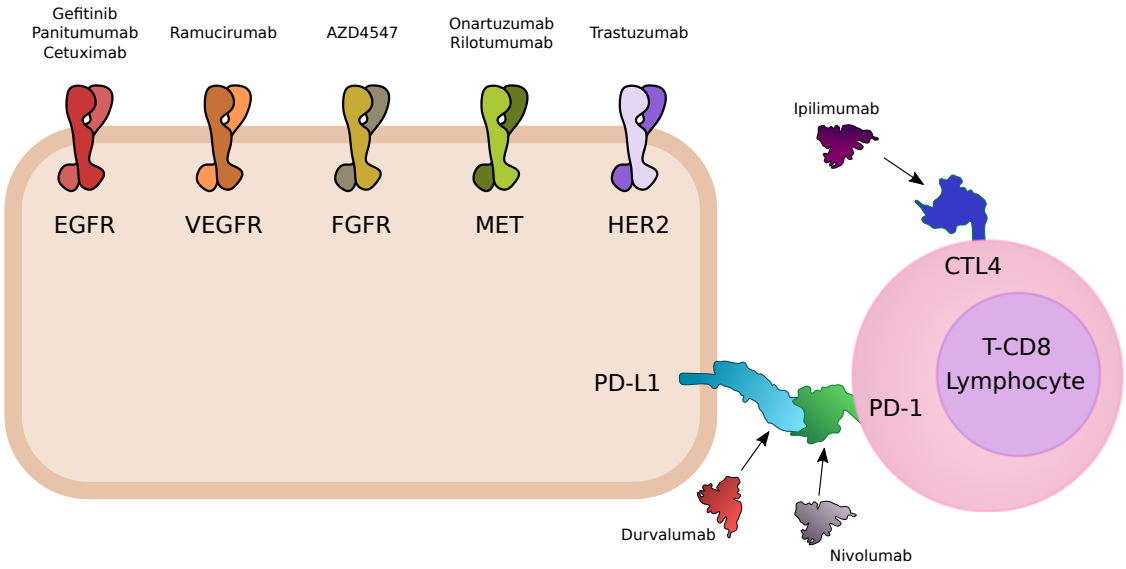

Figure 1.11: Oesophageal adenocarcinoma new treatment inhibitors Inhibitors used as new treatments against oesophageal adenocarcinoma targeting Receptor tyrosine kinases and Check point blockade receptors.

clinical trial) on the tumour cell surface. Other immunotherapy emerging strategies are cancer vaccines and adoptive T-cell transfer (Figure 1.11).

1.3.7 Preventive surveillance

Most of these new treatment strategies are still under clinical trial. Moreover, the cost of these treatments is higher than conventional treatments (Figure 1.12). Indeed, the new treatment complements the conventional ones meaning their costs stack, thus the most cost-effective approach continues to be early detection and surveillance [51],[52].

As previously stated, OAC is usually diagnosed late. In the clinic, preventive surveillance relies on monitoring patients with Barrett's Oesophagus (BO). Barrett's oesophagus is a precursor lesion preceding most OAC cases. This population is 50 times more likely to develop OAC during their lifetime [53].

1.4 Barrett's Oesophagus

The Z-line is the point where the oesophagus and the stomach meet. In healthy individuals, the transition between squamous and columnar epithelia also happens

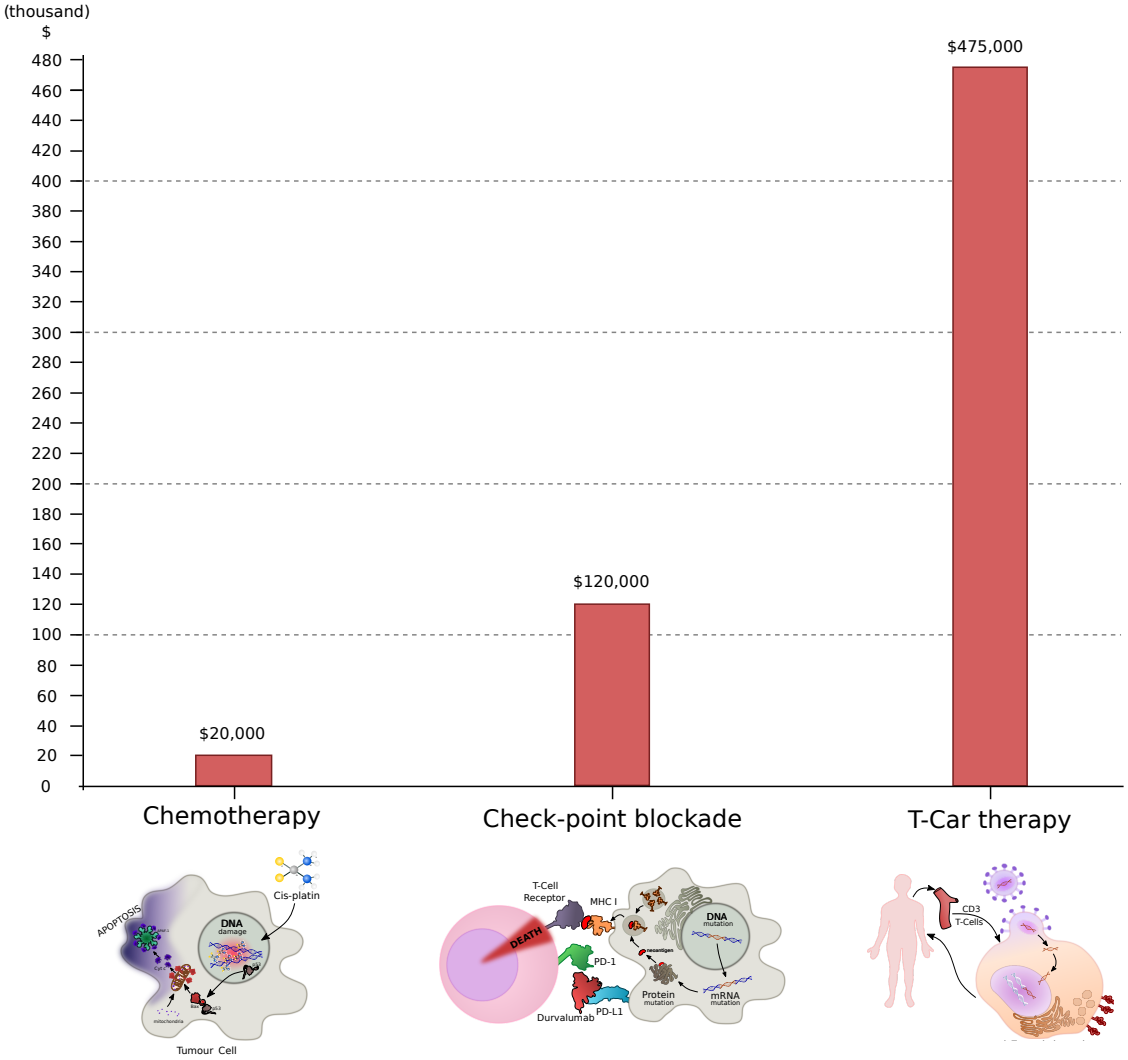

Figure 1.12: New treatments costs compared with conventional chemotherapy Bar plot comparing the costs of chemotherapy treatment with new treatment being developed.

there. The point where this transition happens is the squamous-columnar junction. In Barrett's oesophagus, columnar cells replace the squamous lining of the distal oesophagus. As a result the squamous-columnar junction displaces proximally. The BO length is the distance between the Z-line and the new squamous-columnar junction. In the United States, the presence of goblet cells is a required requisite for BO diagnosis. This epithelium, with goblet cells, resembles the duodenal epithelium and is thus called intestinal metaplasia [54].

1.4.1 The Barrett's oesophagus epithelium

The Barrett's oesophagus epithelium is organized in glands. This epithelium contains cell populations found in other organs. Besides goblet cells, Paneth cells, also found in the intestine, can be present. Acid-producing enteroendocrine cells normally found in the stomach are also common. Rarer cell population from the pancreas and other organs can also be present. Both histopathological and single-cell RNA-seq analysis have been used to find these populations [14] ,[55] , [56].

1.4.2 The origins of Barrett's oesophagus

The BO epithelium is heterogeneous. The presence of cell types also present in other organs makes it difficult to clarify their origin. Currently, the source of BO first cells is still a controversial topic. Here we describe the competing theories.

Gastric migration

In 1950, BO is first described. The authors theorize it is a result of a hiatal hernia or stricture. This stricture pushing the gastric epithelium into the distal oesophagus [57]. This was later replaced by a theory suggesting gastric epithelium migration is the origin [58], [59] , [60]. However, this theory was still unable to explain the presence of goblet cells in cases with IM [61], [62]. Better knowledge of the differentiation processes led to new theories. An elegant experiment with mice by Quante et al. showed that overexpression of the cytokine IL-1Beta can generate IM in cardia cells. This suggest that gastric migration and transdifferentiation might be originating the BO epithelium in humans [63].

Squamous transdifferentiation and transcomittment

According to the transdifferentiation and the transcomittment hypothesis, BO arises from the original squamous epithelia. The difference between the two being the need for a dedifferentiation step [64], [65]. Previous *in vitro* observations using squamous cells support these theories. For example, the inhibition of Notch signalling triggers the production of columnar markers. Both notch inhibitors and compounds in

the refluxate can replicate this effect [66], [67]. This includes columnar keratins, intestinal markers like CDX2 and mucus [68]. It can also downregulate squamous markers and generate hyperplasia [69].

Immune cell progenitor origin

This theory suggests that immune cell progenitors under inflammation can generate columnar epithelium *in vivo*. To study the contribution of immune cells to Barrett's metaplasia, Sarosi et al [70] transplanted male bone marrow into female rats. To mimic gastroesophageal reflux, the scientist joined the rat's oesophagus with the jejunum. The oesophagojejunostomy resulted in intestinal metaplasia appearing in the oesophagus. Interestingly, some of the metaplastic cells had Y chromosomes, the only source for these chromosomes being cells produced by the male bone marrow. Surprisingly, not all the columnar cells present in the oesophagus had Y chromosomes.

Junctional progenitor cell recruitment

Although squamous islands can exist inside Barrett's oesophagus, all BO segments extend from the squamous-columnar junction. This theory supports a residual stem cell population in the junction as the origin of BO. Wang et al. found a population of columnar cells present only in the junction. This population had both squamous markers like p63 and columnar like keratin 7. Then they damaged the neighbouring squamous epithelium using an inducible keratin 6 promoter. After the neighbouring squamous population disappeared, the residual population was able to colonize a segment of the oesophagus [71]. Recently, Jiang et al. detected another population of p63+, CK5+,CK7+ cells at the junction. This population could be grown *in vitro* as organoids. After stimulation with CDX2, the cells differentiated into intestine-like epithelium [72].

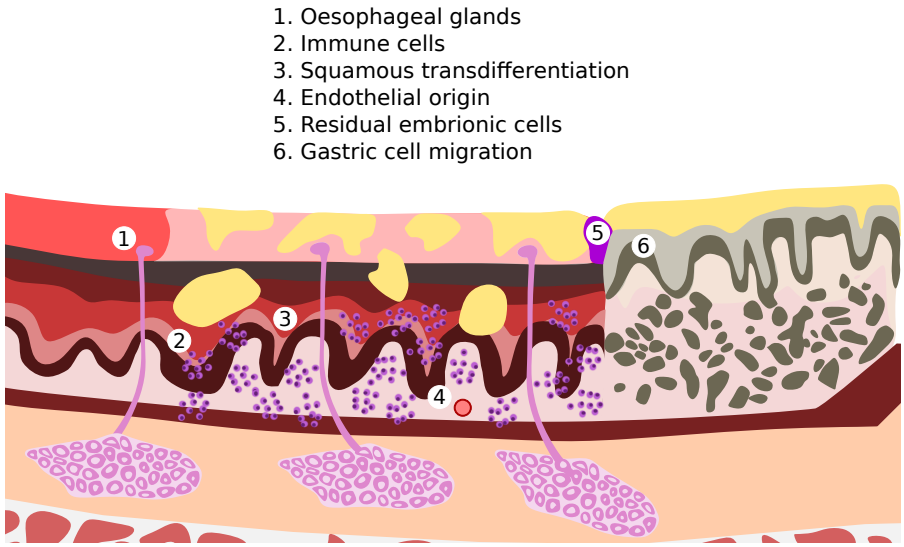

Figure 1.13: Barrett's oesophagus origin candidates Cartoon summary of the existing hypothesis for the Barrett's oesophagus cell of origin.

Oesophageal submucosal gland origin

This theory suggests cells from the oesophageal submucosal glands are the origin of BO. As previously described, the OSG presence is higher next to the squamous-columnar junction. Also, the OSG are more abundant in BO segments [8], [73]. Interestingly, Leedham et al. tracked a p16 (CDK2A) mutation from OSG to the BO epithelia [74]. Furthermore, our lab conducted a single-cell sequencing study in squamous and BO epithelium. The study showed cells in the healthy oesophagus with a BO expression signature. Immunohistochemistry staining using common markers showed that the cells came from the OSG [14]. As mentioned before, the oesophageal submucosal glands originate from residual stem cells. It is possible that the K7+/p63+ population described at the junction could also be at the luminal end of the OSG.

A summary of all the possible origins can be found in (Figure 1.13)

1.4.3 Barrett's oesophagus progression to adenocarcinoma

Around 2-5% of the western population will have BO at some point in their lives. Barrett's oesophagus metaplasia is asymptomatic. Thus, its clinical relevance derives from its potential to progress into OAC [18]. The yearly chance of progression to

OAC varies between 0.12% and 0.65% depending on the study [75] , [76]. Although not required, the presence of goblet cells increases the chance of progressing to OAC [77] , [78].

Transition to OAC happens following a dysplastic stepwise transition, the steps being low-grade and high-grade dysplasia followed by adenocarcinoma. Individuals with low-grade dysplasia have a 1.4% yearly chance of developing OAC. [78]. The chances increase further with high-grade dysplasia and can reach 4% if the HGD segment is localized or 40% if it's diffuse (Figure 1.14) [79].

1.4.4 Clinical implications of Barrett's oesophagus segment length

Barrett's oesophagus is asymptomatic. Early diagnosis for BO relies on assessing individuals that present risk factors. In the UK, the guidelines recommend endoscopic screening for patients satisfying two criteria. First, the patient needs to have gastric reflux oesophagitis (GORD). Second, they need to match at least three of the fours risk factors: [54]. Having an age over 50 years, male sex [83], white ethnicity and, obesity [84], [85], [86]. A lower threshold can apply to patients with a family history of BO or OAC. The present guidelines only recommend endoscopy to assess the presence of BO. New methods are being developed to simplify the diagnosis, both reducing costs and inconveniences to the patients. Examples of these are capsule endoscopy or the use of a cytosponge [87], [88], [89].

1.4.5 Length of Barrett's oesophagus and progression to cancer

The length of Barrett's oesophagus varies between individuals. BO is stratified into three categories based on segment length: ultra-short-segment (length is < 1 cm above the Z-line), short-segment (lengths 1-3 cm) and long-segment BO (>3 cm).

Long-segment BO is 7.3 times more likely to develop into OAC yearly (0.22%/year) than short-segment. Compared with ultra-short-segment the chances are 22 times higher [90]. Studies supporting length as a predictor for progression are abundant in the literature [91], [92], [93], [94]. Avidan et al. studied the increase in progression

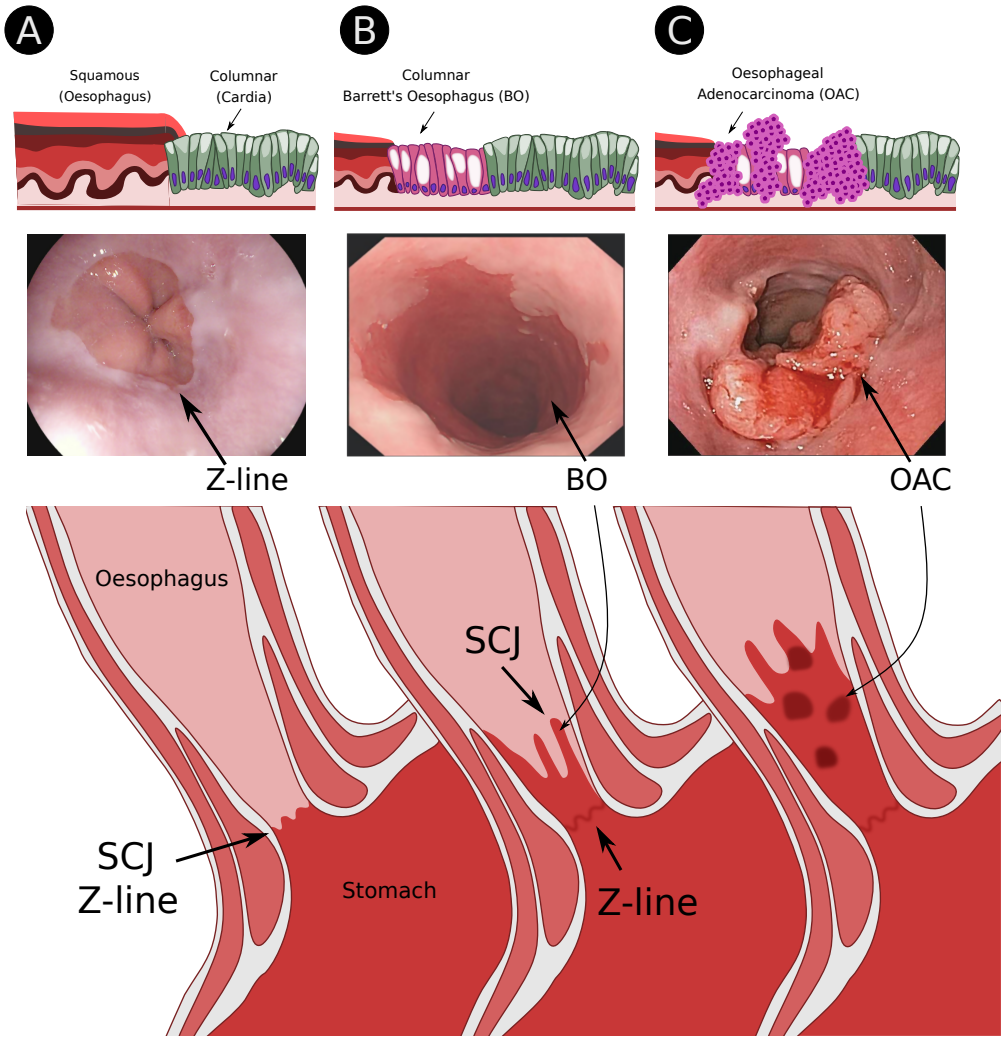

Figure 1.14: Barrett's oesophagus progression to adenocarcinoma Different stages of the squamous-columnar junction (SCJ) during Barrett's oesophagus to oesophageal adenocarcinoma progression. A) SCJ between the squamous epithelium of the oesophagus and the columnar lining of the stomach. This junction happens in the Z-line or gastroesophageal junction (Endoscopy image from [80]). B) Junction between Barrett's oesophagus (BO) cells and the squamous epithelium of the oesophagus (endoscopy image from [81]). C) Oesophageal adenocarcinoma arising from BO in the distal oesophagus (endoscopy image from [32]). Lower panel inspired by progression cartoon from [82].

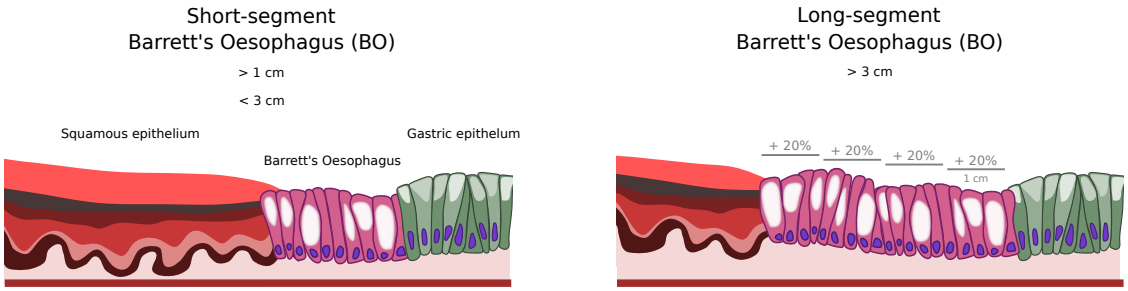

Figure 1.15: Barrett's oesophagus length stratification Barrett's oesophagus can be classified in short and long-segment BO depending on whether the length is shorter or longer than 3 cm. The longer the Barrett's oesophagus segment the higher the chances of developing oesophageal adenocarcinoma. Each additional centimetre increasing by almost 20% the chance of developing high-grade dysplasia or OAC.

to OAC for each extra centimetre of BO, each extra centimetre increasing the conversion to either high-grade dysplasia or OAC by almost 20% [95].

The last update of the guidelines for both the UK [54] and Australia [96] reflects the importance this risk factor. Patients are now stratified between short-segment and long-segment. Endoscopic screenings for long-segment are conducted every 2-3 years instead of 3-5 (Figure 1.15).

1.4.6 Barrett's oesophagus length and clonality

An explanation for the effect of segment length on progression to OAC might be the clonal nature of BO. Before becoming dysplastic, BO epithelium is already highly mutated. With areas of the BO segment presenting distinct mutations. Each one of these different areas is a clone. These mutations, like the reported in OSG, might be present even before a BO segment appears [74], [65].

These clones compete with each other for space and resources. The clones with certain mutations will be able to outcompete their neighbours and grow. This expansion increases the cell population with those mutations. A larger number of clonal cells increases the chance of new mutations arising in one of them. Accumulating mutations, a clonal population can progress to low-grade, high-grade and finally OAC [97], [98], [65], [99].

Simplistically, longer BO segments have more cells. The chance to mutate is the same for each cell. As a result, longer BO segments are likely to have more

mutations, the higher mutation load generating more diverse clonal populations. Long-segment BO are thus more likely to generate malignant clone populations. However, publications exist claiming that clones do not appear or expand at a high rate. Under these conditions, the Darwinian selection of malignant clones would not happen. The original mutations of the clone would determine its success [100].

BO clonal studies taking sequential biopsies both proximal to distal and transversely exist. These studies mutations are more likely shared between biopsies aligning in the proximal-distal axis, meaning clones have an elongated shape [98], [97]. This suggests clonal expansion is directional. Clones expand more easily towards the proximal oesophagus than across its circumference. Clones thus grow faster replacing the squamous epithelium than competing with each other (Figure 1.16).

1.4.7 The establishment of Barrett's oesophagus length

A large study with 3600 patients suggests that the final BO length is established before its diagnosis. The study also shows that length does not vary afterwards. BO final length is thus established fast and this new SCJ kept stable over time [101]. Meta-analysis of smaller studies replicate these findings, with partial segment shortening only seldom reported in the longest BO cases [102], [103], [104]. This suggests two options: the existence of a signalling pathway with constant intensity kept through time or a single signalling time-point resulting in a new squamous-columnar junction that remains stable indefinitely.

Segment length is a known predictor of malignancy. However, the mechanisms explaining these length differences are not well understood. As mentioned before, the presence of reflux is the main risk factor for BO. With the depth of the oesophagus reached during the reflux episodes varying across patients. As such, segment length variation might correlate with reflux reach into the proximal oesophagus. Under that hypothesis, one or more of the reflux components should be determining BO growth proximally.

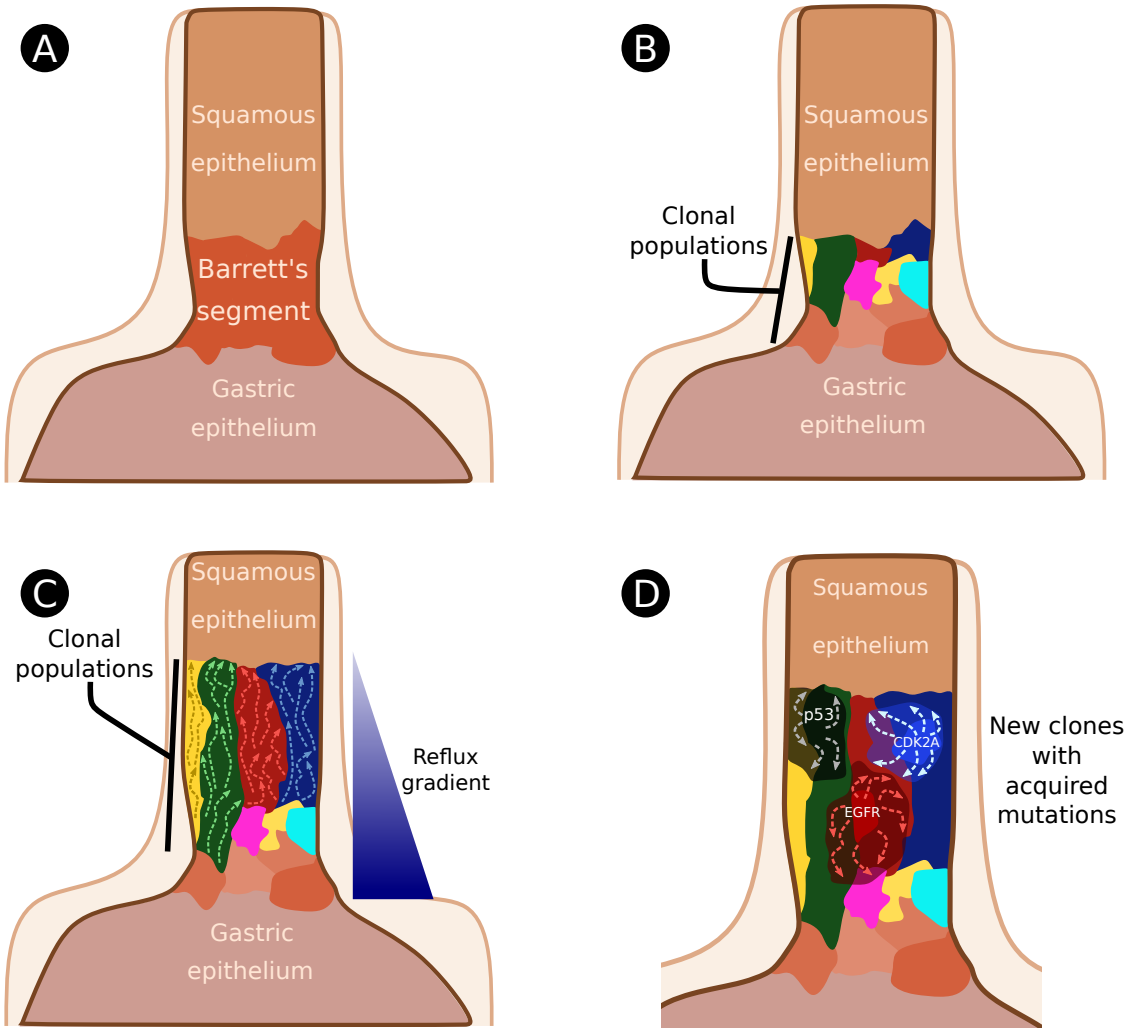

Figure 1.16: Barrett's oesophagus clonal expansion A) The Barrett's oesophagus segment extends from the gastroesophageal junction to the proximal oesophagus. B) Across the segment several BO clonal populations are found. C) During reflux episodes a gradient is formed allowing the clones in the boundary with the squamous epithelium to grow. It may be that outcompeting the squamous epithelium is easier than invading another adjacent clone, explaining their elongated shape. D) Cells in the clones can acquire new mutations stochastically, making mutations being more common in clones with more cells. The new clones harbouring mutations are able to outcompete their neighbours and grow. Repeating this process, the clones might acquire mutations that make them malignant and become OAC.

1.5 Gastroesophageal reflux disease

1.5.1 Definition

There is no international consensus defining gastroesophageal reflux disease. The disease is diagnosed through the manifestation of a continuum of symptoms [105]. A working definition of GORD is: " A condition that develops when the reflux of stomach contents causes troublesome symptoms and/or complications" [106]. The reflux can also contain contents from the duodenum, the most studied example being bile acids. GORD can damage the oesophageal mucosa and cause oesophagitis [86]. The incidence of GORD in the UK is high, affecting 4.5% of the population [107]. As mentioned before, GORD is a prerequisite to screen for BO using endoscopy [54]. The direct link between reflux and OAC progression brought attention to the components in reflux driving BO and its progression to OAC.

1.5.2 Components of gastric origin

The stomach connects to the distal end of the oesophagus. As such, most contents during refluxate come from it. Gastric fluids contain both hormones and acidic secretion. Gastric hormones correlate both with higher and lower BO incidence. For instance, high levels of ghrelin increasing BO incidence while high leptin levels decrease it [108], [109]. Hormone levels change with food intake and obesity [110], [111], therefore these effects might only be due to a correlation with other risk factors.

The effect of hydrochloric acid on BO onset is better studied [112]. Hydrochloric acid production lowers the pH of the gastric contents. This secretion can bring the acidity as low as pH 1. Reflux episodes generate a pH gradient in the oesophagus, with the pH being lowest next to the stomach [113]. This acidity is the main cause of mucosal damage during reflux [114]. Interestingly, low pH also generates hyperproliferative behaviour in the BO lining [115], [116]. The combination of squamous mucosa damage and BO proliferation could explain the final length of the BO segment. The observation that acid exposure correlates with longer BO segments

supports this hypothesis [117], [118]. However, low pH correlates with the presence of the other reflux components, therefore, these findings are only correlative.

Acid reflux effect on healthy squamous epithelium

Although reflux causes damage to the mucosa, it does not remove the squamous cell lining completely. The consequences of exposure to the contents of reflux are the following:

- Disruption of the cell-cell junctions in the squamous epithelium making it more sensitive to external insults [119].
- Damage induced by exposure to low pH. This damage leads to inflammation that causes immune cell infiltration in the mucosa [120].
- Hyperplasia of the basal layer. The proliferative layer at the bottom of the epithelium doubles in response to low pH [121],[122]. Interestingly, the basal hyperproliferative behavior indicates that there are still cell layers present after the reflux episodes. This remaining cell population supports the idea of squamous transdifferentiation being of BO origin. Yet, for all the other BO origin hypotheses, a mechanism to replace this cell population by the columnar lining must exist.

A summary of the effects reflux episodes have in the squamous epithelium can be found in Figure 1.17.

Drug treatment of reflux acidity

Non-steroidal anti-inflammatory drugs (NSAIDs) and proton pump inhibitors (PPI) can reduce reflux acidity. Indeed, reports of therapy with nonsteroidal anti-inflammatory drugs (NSAIDs) reducing BO length exist [123], [124]. Unfortunately, the biggest PPI trial with >2500 patients is incomplete. The trial recorded initial but not final BO length [125].

Evidence of the effect of pH on BO colonization exists in BO mucosal ablation experiments, wherein 54.3% of the patients treated with PPI do not have recurrent

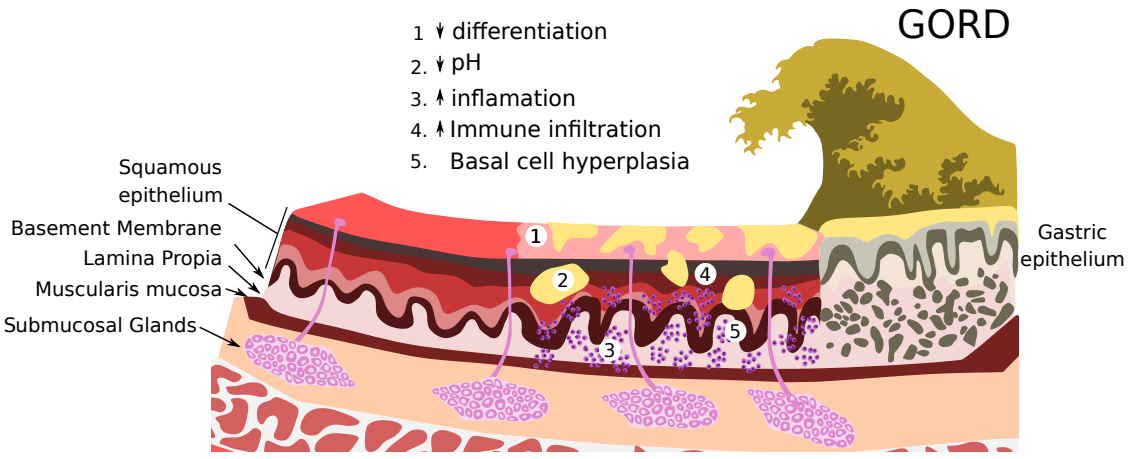

Figure 1.17: Effect of low pH reflux on the squamous epithelium Cartoon summary of the effects of reflux episodes on the healthy squamous epithelium.

BO segments. This is likely derived from a complete ablation of the original epithelium. However, the remaining patients have partial recurrence [126]. The effect of PPI suggests that residual BO epithelium benefits from low pH to expand.

1.5.3 Components of hepatic origin

Bile acids

GORD can carry components present in the duodenum. These compounds in the duodenum might be secretions from the liver or pancreas. For instance, one of the most studied components of the reflux is bile secreted from the liver.

Bile is an alkaline, lipid rich aqueous solution produced in the liver. 95% of its volume is water. The rest are bile acids (67%), phospholipids (22%), proteins (4.5%), cholesterol (4%) and bilirubin (0.3%) [127]. Bile acids can be further subdivided in primary and secondary. There are two primary bile acids, cholic acid and chenodeoxycholic acid. The latter is derived from cholesterol through multistep pathways [128], [129]. The liver cells can further modify them by adding either taurine or glycine [130]. After secretion, the enzyme 7- dehydroxylase can transform them into secondary bile acids. This enzyme is present in the intestinal microbiota bacteria. It can convert cholic acid into deoxycholic and chenodeoxycholic into lithocholic acid [131]. Tertiary acids are also formed after

further bacterial modifications. A process known as enterohepatic circulation recycles these bile acids. [132]

Bile acids have been linked to carcinogenesis. Deoxycholic acid was described as a carcinogenic in 1940 [133],and further evidence has accumulated since [134]. BO patients have higher concentrations of bile acids in the oesophageal mucosa [135]. Other studies show a relationship between secondary bile acids and BO and OAC. The most studied is deoxycholic acid. These act by generating free oxygen radicals and DNA damage [135], [136], [137], [138], [139], [140]. Interestingly, bile acids in low pH solubilize better. This synergistic effect increases damage to the squamous oesophageal lining [64], [135].

Retinoic acid

One of the functions of bile acids is to emulsion vitamins, which allows the intestine to better absorb them. Reflux episodes can drive both vitamins and bile acids into the oesophagus. Retinoic acid, derived from vitamin A, has been studied in the context of BO. In mice, retinoic acid increased oesophageal mucosa proliferation in response to damage [141]. In humans, this induced proliferation is likely to also affect OSG and stem cells. Higher proliferation compared to squamous cells might also explain BO expansion. Experiments with human biopsies, show that retinoic acid can generate BO segments replacing the squamous lining [142]. Interestingly, this only happened in a fraction of the biopsies. The presence of OSG could be a possible explanation, unfortunately, the studies lacked histological analysis from the biopsies before treatment.

A less studied component of the bile is bilirubin. With studies showing a correlation between high bilirubin levels and BO [143].

1.5.4 Components of pancreatic origin

The pancreas secretes enzymes into the duodenum to aid food digestion. Trypsin is a secreted protease which helps with protein digestion. Due to the lack of

mucus, trypsin could damage the squamous epithelium. Experiments with rats show trypsin derived mucosal damage *in vivo* [144].

Two of the most studied pancreatic secretions are insulin and glucagon. This interest derives from their role in diabetes. Interestingly, high levels of insulin correlate with Barrett's oesophagus [109], [145]. Type II diabetes patients, under insulin intake treatment presented a similar trend, even after correcting for obesity [146].

1.5.5 Components of duodenal origin

The duodenum is the meeting point between ingested organic matter and most digestive enzymes. The duodenum also releases its own substances to its lumen. The Brunner's glands generate most of these secretions, including mucus, bicarbonate and epidermal growth factor. These substances help maintain and repair tissue homeostasis. Bicarbonate helps buffer the low pH from secretions moving in from the stomach [147], [148]. Brunner glands also produce large quantities of epidermal growth factor (EGF) [15], [149], [6], [150], [151]. As a result, EGF is present at a high concentration in the duodenal lumen. As bile acids, EGF is likely to be present also in the reflux. Considering this, it is surprising that the effect of EGF present in the reflux on BO has not been well studied.

1.6 Epidermal growth factor

The epidermal growth factor is a 53 amino acid residues long protein [152]. EGF was first described in the urine and named urogastrone. [153], [154]. EGF activates the eponymous receptor EGFR (Epidermal growth factor receptor). EGFR is part of the Receptor Tyrosine Kinase (RTK) family [155].

1.6.1 The EGFR signalling pathway

Receptor tyrosine kinases (RTKs) control a wide range of complex biological functions. These functions include cell growth, motility, differentiation, and metabolism. EGFR (ERBB1) belongs to the ERBB family of RTK. Also in this

family are HER2 (ERBB2), ERBB3 and ERBB4. The receptors are found as dimers in the cells, either as homodimers or heterodimers (Figure 1.18 A).

EGFR activation promotes cell motility, proliferation and survival through three main signalling pathways (Figure 1.18 B) [156]. A third mechanism for migration is only described in some cell types. In mammary gland cells, EGFR activation promotes focal point dissociation and the extension of new lamedipolium. Combined, this process promotes cell migration (Figure 1.18 C) [157], [156].

Interestingly, components of the refluxate like bile acids [158], [159] and retinoic acid [160] can activate EGFR. EGFR activation also increases the more dysplastic a BO segment becomes [161]. In OAC, Both EGFR (ERBB1) and HER2 (ERBB2) have constitutively activating mutations in 15% and 32% of their cases [162]. Taken together, this publication suggests a competitive advantage for clones having active EGFR, allowing these clones to outcompete neighbours and mutate until they turn malignant. Thus it is possible that in earlier stages, EGFR activation could help BO clones outcompete the squamous epithelium.

1.6.2 The epidermal growth factor in gastrointestinal homeostasis

EGF is a key growth factor for the maintenance of the epithelial mucosa. In humans, EGF prevents apoptosis and increases proliferation of intestinal stem cells and keratinocytes [163], [164]. EGF also increases migration both in tumour and healthy cells types [165], [166], [167], [168]. EGF helps wound healing of damaged mucosa by combining both proliferation and migration [169]. This property is used in the clinic to treat wounds and acid-derived ulcers in the GIT [170], [171], [172].

Besides promoting repair, EGF can inhibit the secretion of acid by parietal cells. In mice, acid secretion halves when supplemented by 20 ng/ml EGF [173], [174]. This effect is reproducible in other mammals including guinea pigs, rats and rabbits [175], [176], [177].

An elegant experiment in humans shows EGF levels increase in response to low luminal pH. In it, pentagastrin is used to treat healthy volunteers. Pentagastrin is a

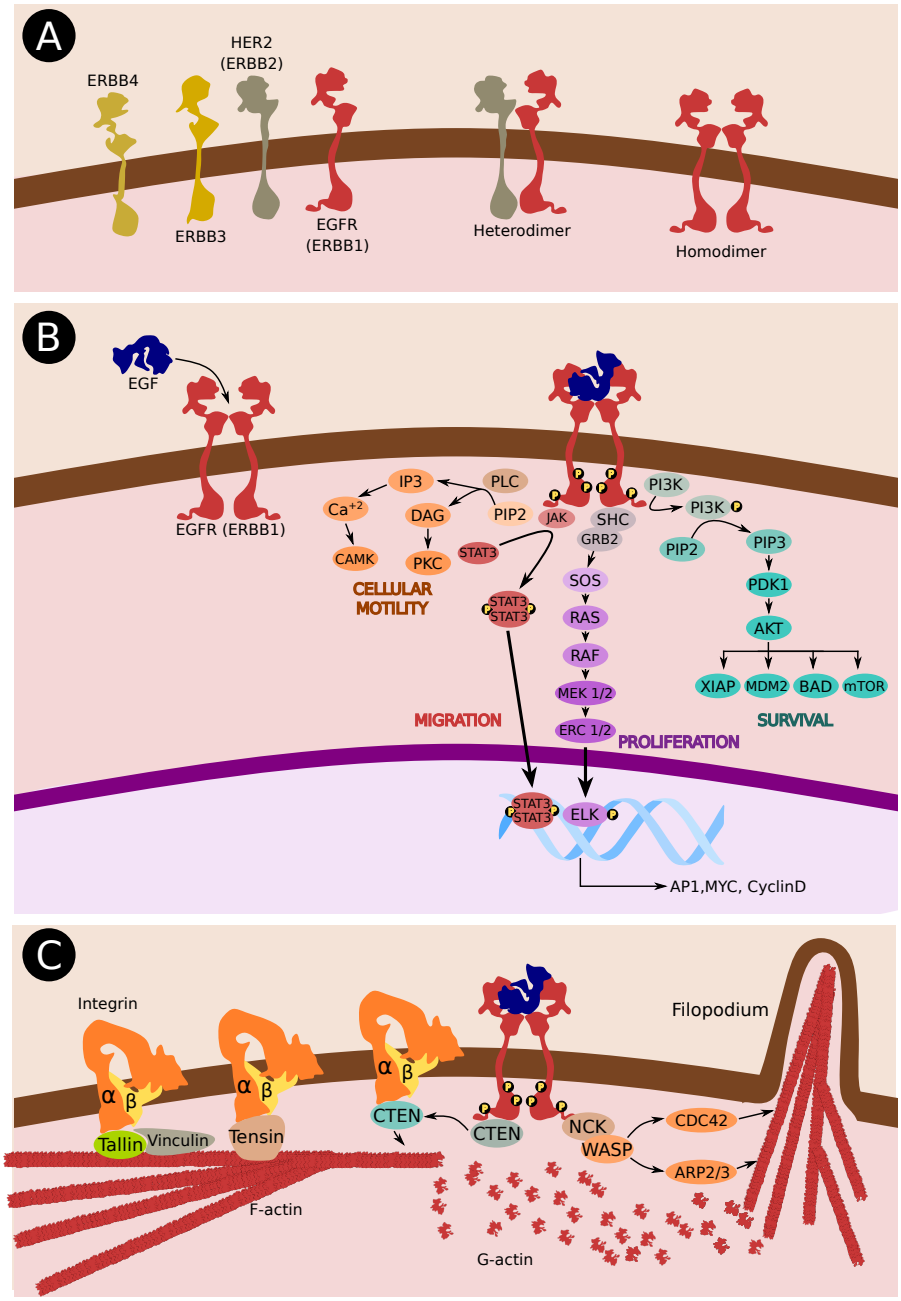

Figure 1.18: EGFR signalling A) EGFR (ERBB1) forms part of the ERBB family together with HER2, ERBB3 and ERBB4. These proteins form homotypic and heterotypic dimers. B) Signalling cascades of EGFR. EGF is the ligand of EGFR. When active, EGFR self-phosphorylates its cytoplasmic domain activating several signalling cascades promoting proliferation, migration and survival of the cell. C) In some cell types, e.g. mammary glands, EGFR promotes focal adhesion dissociation and formation of filopodium. Firstly, EGFR activation replaces tallin, vinculin, and tensin for CTEN, solubilising the f-actin into g-actin. Then, EGFR activates WASP through NCK. WASP then increases ARP2/3 and CDC42 activity forming filopodium and promoting migration.

gastric synthetic substitute for increasing hydrochloric acid production. Volunteers treated with pentagastrin increased duodenal EGF concentration by 33% [178]. Later publications confirmed the compensation mechanism [179], [180]. This mechanism works by cleaving pepsinogen into pepsin at low pH. The pepsin generated promotes EGF production. EGF then lowers the pH by inhibiting hydrochloric acid production [149].

Taken together, EGF levels in the GIT works as a compensation mechanism in response to low pH. EGF keeps homeostasis by inhibiting acid production and increasing cell migration and proliferation. This compensation mechanism could trigger GORD episodes. This would increase EGF secretion from OSG, BO epithelium and duodenal Brunner's glands.

1.6.3 EGF levels in the upper gastrointestinal tract

In 1962, Stanley Cohen discovered the submaxillary salivary glands secreted EGF in mice [181]. Currently, several sources of EGF in the human upper GIT are known. The main ones are the salivary glands, the OSG, Brunner's glands and the liver. These glandular structures vary in abundance and EGF secretion rates. As a result, EGF levels across the upper GIT vary (Figure 1.19). Reported EGF concentrations in the human upper GIT are [178], [149]:

- 2.7 ng/mL in the saliva
- 2 ng/mL in the oesophagus
- 0.42 ng/mL in the stomach
- 0.3 ng/mL in the liver
- 8.5 ng/mL in the pancreatic juice
- 21 ng/mL in the duodenal lumen

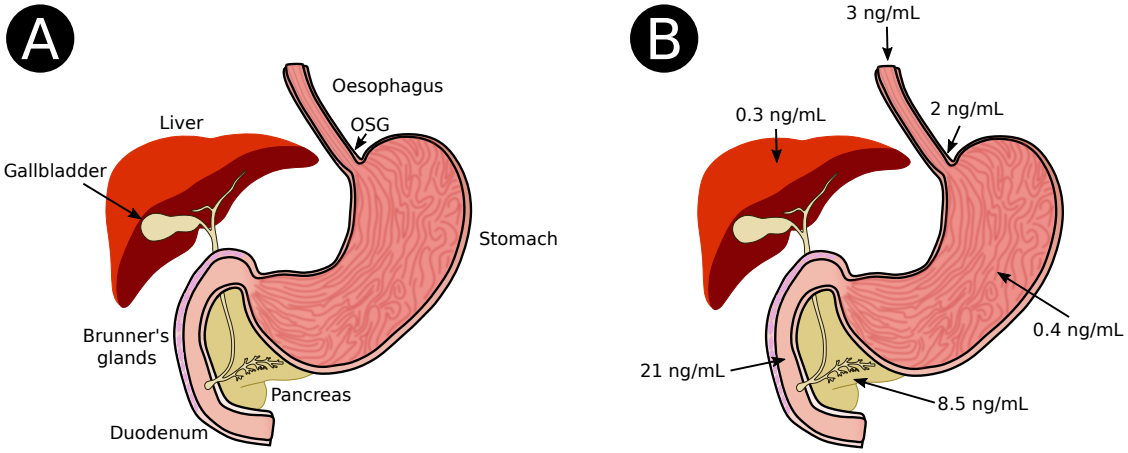

Figure 1.19: EGF concentration across the upper GIT A) Anatomy of the different organs contributing to reflux juice composition. B) EGF concentrations across the upper gastrointestinal tract.

Interestingly, EGF concentrations are highest in the duodenum, being ten times higher than in the oesophageal lumen. This is likely caused by the Brunner's gland pancreatic secretions and response to low luminal pH. Gastric pH is lower in some patients suffering from GORD [182]. Because EGF levels increase at lower pH, it is likely GORD patients present even higher EGF concentration.

Reflux episodes can carry compounds from the duodenal lumen into the distal oesophagus. With a study reporting correlation between duodenal and oesophageal concentrations of trypsin and bile acids [183]. Thus, EGF concentration in the oesophagus is likely to increase during reflux episodes. In the distal oesophagus, EGF presence should correlate with bile acid concentration and low pH. In additions, during reflux epidodes, EGF levels should increase through secretions from OSG and BO segment in response to low pH.

Low pH increases proliferation in the Brunner's glands making them hyperplastic [184]. This phenomenon also occurs in low pH induced gastrointestinal ulcers [185], [186]. These cell populations share markers with the submucosal glands and secrete EGF, and like BO, present a pyloric-like gland lining [187]. OSG shares both structure and function with Brunner's glands. It is thus possible that a hyperproliferative response also happens in OSG or BO. The hyperproliferative

epithelium could then outcompete the squamous lining and become larger. As low pH increases EGF levels, this behaviour might lead to an EGF mediated reaction.

1.6.4 EGF gradient and intestinal metaplasia at the distal oesophagus

An evidence of the existence of an EGF gradient in the distal oesophagus comes from the presence of goblet cells in intestinal metaplasia. Studies on BO and duodenal epithelium show EGFR activation producing goblet cell differentiation [188], [189], [190]. The presence of EGF in the reflux could activate EGFR and generate goblet cells *in vivo*. The EGF in the reflux should form a higher gradient at the GOJ. As a result, goblet cells should be more abundant next to the stomach. However, reports confirm that more goblet cells are present at the proximal BO [61]. This could be explained by a second gradient involving low pH. This pH gradient would prevent the formation of goblet cells, favouring a gastric mucus release of cell types instead. Goblet cells would then form closer to the proximal end of the Bo segment, where the pH is less acidic but the EGF levels are still high enough to promote goblet differentiation. This phenomenon could explain why inflammation is lower next to the gastroesophageal junction as gastric mucus releasing cell types would prevent acid related damage better than the intestinal goblet cells. (Figure 1.20) [191].

1.7 Hypothesis

An EGF gradient generated by reflux promotes BO colonization of the distal oesophagus determining its final length.

In short, this hypothesis rests on four pieces of evidence.

- 1) Low pH promotes EGF production in submucosal glands by a compensatory mechanism. In the duodenum, Brunner's glands use this mechanism to generate high EGF concentrations (Figure 1.20 A).

- 2) Reflux episodes carry substances from the duodenal lumen to the distal oesophagus. A well-known example being bile acids. Thus, it is likely that

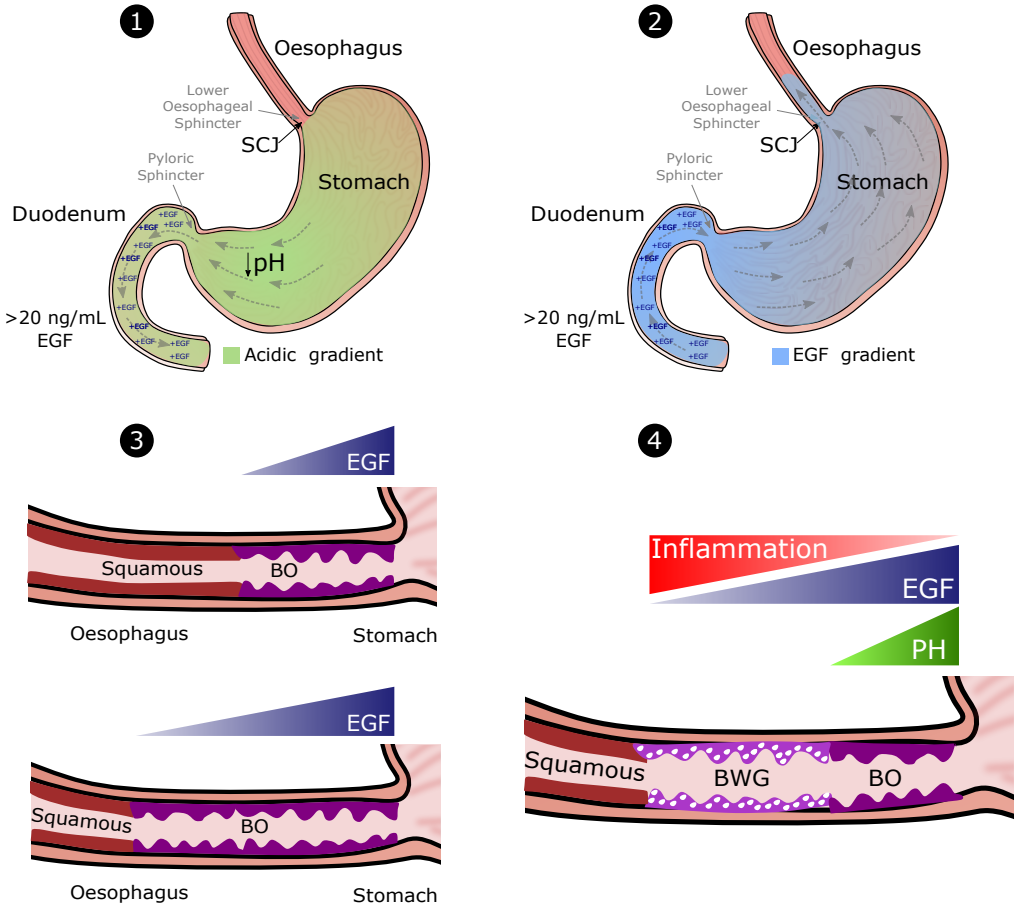

Figure 1.20: EGF gradient formation at the distal oesophagusA) Low pH in the gastric juice entering into the duodenum promotes generation of EGF as a compensation mechanism. B) EGF is carried from the duodenum to the distal oesophagus during reflux episodes. C) EGF promotes invasion of the squamous epithelium by BO cell populations. Longer gradients generate longer BO segments. D) EGF and pH gradients can also explain the reason goblet cells and the inflammation are higher proximally.

EGF is brought during reflux episodes to the distal oesophagus as well (Figure 1.20 B).

- 3) Reflux generates gradients in the oesophagus. The deeper into the oesophagus the reflux enters, the longer the gradient will be. EGF promotes cell migration and proliferation. Barrett's oesophagus might be more sensitive to EGFR activation than squamous cells. This enables replacement of the squamous lining while the EGF concentration is high. Thus longer gradients of EGF will generate longer segments of Barrett's oesophagus (Figure 1.20 C).

- 4) A double gradient of EGF and pH could could also explain the higher presence of goblet cells proximally. The low pH would prevent the appearance of goblet cells next to the stomach. Once the pH gradient diminishes, the EGF levels in the proximal end of the BO segment would increase the presence of goblet cells in that region (Figure 1.20 D).

1.8 Thesis aims

Establish 2D and 3D experimental platforms that model the cellular behaviours observed in Barrett's oesophagus expansion and progression to Oesophageal adenocarcinoma in the context of reflux episodes with high EGF levels.

2
Materials and Methods

Contents

2.1 Materials 38
2.1.1 Cell lines 38
2.1.2 Reagents 38
2.1.3 Antibodies and plasmids 41
2.1.4 Other 41
2.1.5 Software 41
2.2 Methods 41
2.2.1 Cell culture 41
2.2.2 Organoid media preparation 42
2.2.3 Conditioned media production 43
2.2.4 Assessing conditioned media batch quality 44
2.2.5 Growing organoids from biopsies 46
2.2.6 Splitting organoids 46
2.2.7 Freezing Cell lines for storage 47
2.2.8 Mycoplasma testing and cell line authentication 47
2.2.9 Fluorescent labelling 47
2.2.10 Heterotypic junction Co-culture assay 47
2.2.11 Time-lapse Image acquisition 48
2.2.12 Studying cell heterotypic monolayers using MOSES . . 48
2.2.13 Immunofluorescence staining for heterotypic junctions . 49
2.2.14 Deparaffination and hydration of paraffin embedded sections 49
2.2.15 Immunofluorescence staining of formalin fixed, paraffin embedded sections 49
2.2.16 Cell counting with convolutional neural newtworks . . . 50
2.2.17 Migration-independent cell counting in videos 50
2.2.18 Predicting cell density using dye fluorescence intensity . 51
2.2.19 Producing the lipid-oil mix for the oil bath 51
2.2.20 Preparing collagen for 3D collagen ring or tube casting . 51

2.2.21 Making Clevers' collagen rings 51
2.2.22 Designing and 3D printing plastic moulds 52
2.2.23 Casting collagen rings 52
2.2.24 Casting collagen tubes 53
2.2.25 Adding adapters to the tubes 53
2.2.26 Constructing adapter caps 53
2.2.27 Coating the collagen tubes with cells 54
2.2.28 Preparing *Helicobacter pylori* selective agar plates . . . 54
2.2.29 Culturing *Helicobacter pylori* in plates 54
2.2.30 Liquid culture of *Helicobacter pylori* in Brucella broth media 54
2.2.31 Infecting inner tube monolayers using *Helicobacter pylori* 55
2.2.32 3D sample processing 55
2.2.33 Haematoxylin and eosin staining 56
2.2.34 IHC staining 56
2.2.35 Liquid culture of *Helicobacter pylori* in Brucella broth media 57
2.2.36 Infecting inner tube monolayers using *Helicobacter pylori* 57
2.2.37 Slide scanning and analysis 57
2.2.38 Sectioning samples for tissue microdissection 57
2.2.39 Methyl green staining 58
2.2.40 Tissue micro-dissection 58

2.1 Materials

2.1.1 Cell lines

Type	Designation	Source	Identifiers
Cell line (H.sapiens	EPC2-hTert	Prof. Hiroshi Nakagawa	-
Cell line (H.sapiens)	CP-A	ATCC	ATCC:CRL-4027 / RRID:CVCLC451
Cell line (H.sapiens)	OE33	ECACC	ECACC:96070808/RRID:CVCL0471
Cell line (H.sapiens)	AGS	ATCC	ATCC:CRL-1739;RRID:CVCL0139
Cell line (H.sapiens)	CACO-2	Laboratory stock	ATCC: HTB-37/RRID:CVCL0025
Cell line (M.musculus)	L Wnt-3A	ATCC	ATCC: CRL-2647/RRID:CVCL0635
Cell line (H.sapiens)	Hek293t R-spondin 1-Fc	Laboratory stock	
Cell line (H.sapiens)	Hek293t Noggin	Laboratory stock	
Cell line (H.sapiens)	Hek293t luciferase reporter	Laboratory stock	
Cell line (H.sapiens)	HFF	Laboratory stock	
Organoid (H.sapiens)	Duodenum Organoid (id: 2662)	From biopsy	
Organoid (H.sapiens)	Gastric Organoid (id: 2954)	From biopsy	
Bacteria (*Helicobacter pylori*)	*H. pylori*, G27 strain	Laboratory stock	

2.1.2 Reagents

Reagent	Source	Catalogue number	Stock preparation
KSFM	Gibco	17005042	
Trypsin	Gibco	25200056	
Soy Trypsin Inhibitor from Glycine max	Sigma-Aldritch	T9128-1G	dilute 0.1 g in 400 mL PBS
DMEM high glucose GlutaMAX	Gibco	10566016	
Advanced DMEM/F-12	Gibco	12634028	
RPMI 1640 media	Gibco	21875Ð034	
Human recombinant EGF	Gibco	PHG0313	
Celltracker Orange (CMRA) 50 ug	Life Technologies	C34551	diluted in 10 uL DMSO for 10 mM stock
Celltracker Green (CMFDA) 50 ug	Life Technologies	C7025	diluted in 11 uL DMSO for 10 mM stock
Celltracker DeepRed 15 ug	Life Technologies	C34565	diluted in 21.5 uL DMSO for 10 mM stock
Image-iTx Signal Enhancer	Thermo Fisher	I36933	
Antibody diluent background reducing	Agilent Dako	S3022	
Antibody dilutent	Agilent Dako	S0809	
Fluoromount-G	SouthernBiotech	0100Ð01	
DAPI (1 mg/ml)	Thermo Fisher	62248	1:1000 dilution
1 M NaOH			
Tris			
EDTA			
Tween-20			
10x Tris-EDTA + Tween buffer (ph 9)	Made in the lab		12.1 g Tris + 3.7g EDTA + 0.5 mL Tween in 1L water
Triton-X			
DPBS (10X) no calcium no magnesium	Gibco	14200075	
Undecane	Sigma-Aldritch	B3051	
1-2-diphytanoyl-sn-glycero-3-phosphocholine	Avanti Polar Lipids	850356P-25mg	
hexadecane	Sigma-Aldritch	H6703-100ML	
Silicone oil AR 20	Sigma-Aldritch	10836-100ML	
Collagen type I rat tail 100 mg	Corning	354249	
Matrigel	Corning	354234	
Commercial R-spondin 20mg	Peprotech	120-38	dilute in 800 uL H20 0.1% BSA
Commercial Noggin 5 ug	Peprotech	120-10C	dilute in 1mL H20 0.1% BSA
Commercial Wnt3A 10 ug	Peprotech	120-17	dilute in 200 uL H20 0.1% BSA
EGF 100 ug	ThermoFisher	PHG0311	dilute in 2 mL H20 0.1% BSA
Gastrin 1 mg	Sigma-Aldritch	G9145	dilute in 4.7 mL/ PBS 1% BSA aliquot 1:10 afterwards
Nicotinamide	Sigma-Aldritch	N0636-500G	0.244 G in 2mL H2O
A83-01	Sigma-Aldritch	SML0788-25MG	dilute 10 mG in 475 uL DMSO
SB202190 5 mg	Sigma-Aldritch	S7067-5MG	dilute in 1.3594 mL/ DMSO
FGF-10 25 mg	Peprotech	100-26	dilute in 125 uL Sodium Phosphate ph 7.4
N2 Supplement (100x)	Gibco	17502001	
B27 Supplement (50x) Serum Free	Gibco	17504001	
N-acetyl-l-cysteine 5G	Sigma-Aldritch	A9165	dilute 0.81595 g in 10 mL H20
Y-27632 (Rock inhibitor) 5 mG	Sigma-Aldritch	SCM075	dilute in 15.64 mL H2O
CHIR99021 (GSK3 inhibitor) 5 mG	Sigma-Aldritch	SML1046-5MG	dilute in 3.59 mL DMSO
16% Formaldehyde (w/v) Methanol-free	Thermo Fisher	28908	dilute 1:4 in PBS keep up to a week in 4 C
100 u/mL penicillin 100 g/mL streptomycin	Gibco	15140122	
Antibiotic Antimycotic Solution (100)	Sigma-Aldritch	A5955-100ML	
2 mM L-glutamine	Gibco	25030	
foetal bovine serum (FBS)	Biosera	FB-1370/500	
Haematoxylin			
Eosin			
Alcoholic acid			
Scott's water			
HistoClear National Diagnostics	Thermo Fisher	12358637	
MycoAlertPLUS Mycoplasma Detection Kit	Lonza	LT07-705	
ProLong Gold Antifade Mountant	Life Technologies Ltd	P36930	
Lapatinib	Sigma-Aldritch	SML2259	
HistoGel Specimen Processing Gel	Thermo Fisher	HG-4000-012	
Deoxycholic acid (DCA)	Sigma-Aldritch	30960-25G	
Opti-MEM[a] I Reduced Serum media	Gibco	31985-062	
HEPES	Sigma-Aldritch	H3375	Diluted to 1 M concentration in water
G-418 (Neomycin)	Sigma-Aldritch	108321-42-2	
Zeocin	Gibco	R25001	
VectaMount Permanent Mounting media	Vectorlabs	H-5000	
Normal Goat Serum (NGS)			
Ethanol	Sigma-Aldritch	34852	
Methanol	Sigma-Aldritch	322415-2L	
Trypsin-EDTA (0.05%) phenol red	Gibco	25300054	
TrypLE Express Enzyme (1X) phenol red	Gibco	12605028	
30% H2O2 Solution		31642	
Citrate Buffer			
VECTASTAIN Elite ABC HRP Reagent	Vectorlabs	PK-7100	
DAB Peroxidase (HRP) Substrate Kit	Vectorlabs	SK-4100	
Brucella media	Sigma-Aldritch	B3051	
H. pylori selective supplement (DENT)	Oxoid	SR0147	
Vancomycin	Sigma-Aldritch	1404-93-9	
Trimethoprim	Sigma-Aldritch	T7883	
Cefsulodin	Sigma-Aldritch	52152-93-9	
Amphotericin B	Sigma-Aldritch	A2942-50ML	
0.1 M Sodium Acetate buffer ph 4.2	Sigma-Aldritch	236500-500 g	1.36 g in 100mL water adjust with acetic acid
Methyl Green (ethyl violet free)	Sigma-Aldritch	323829-5G	0.5 g diluted in 100 mL
0.5 % solution			sodium acetate buffer

2.1.3 Antibodies and plasmids

Reagent	Source	Catalogue number	Dilution
Goat polyclonal anti-mouse AlexaÊFluor 488	Thermo Fisher	A-11001	1:400
Phalloidin Alexa Fluor 647	Thermo Fisher	A22287	1:400
Mouse monoclonal anti E-cadherin	Becton Dickinson U.K Ltd.	610181	1:400
Villin-1 (R814) Antibody	Cell Signaling	2369S	1:100
Anti-Mucin 5AC [CLH2]	Abcam	ab77576	1:100
Anti-Collagen type I	Cell Signaling	39952S	1:800
Anti-ASPP2	Santa Cruz Biotechnology	sc-135818	1:500
Anti-CagA	Santa Cruz Biotechnology	sc-25766	1:500
Anti-citokeratin 8	Santa Cruz Biotechnology	sc-8020	1:200
Biotynilated goat anti-mouse	Vector Laboratories	BA-2020	1:250
Biotynilated goat anti-rabbit	Vector Laboratories	BA-1000	1:250
Plasmid renilla reporter vector (50 ng/uL)			

2.1.4 Other

Reagent	Source	Catalogue number
Polysine Microscope Adhesion Slides	Thermo Fisher	P4981
25 culture-inserts 2-well for self-insertion	Ibidi	80209
Alvetex 12-well insert	ReproCell	AVP005-12
µ-Slide 8 Well	Ibidi	80826
Ultimaker 2+ 3D printer and 3D printing plastic (ABS)	Ultimaker	
MembraneSlide 1.0 PEN (D)	Zeiss	415190-9041-000
Big AdhesiveCap 500 opaque for microdissection	Zeiss	415190-9201-000

2.1.5 Software

Software	Source
Cura	ultimaker.com/software/ultimaker-cura
Metamorph	www.moleculardevices.com/products/cellular-imaging-systems /acquisition-and-analysis-software/metamorph-microscopy
NDP.view2	/www.hamamatsu.com/us/en/product/type/U12388-01/index.html
Fiji ImageJ (TrackMate Plugin)	imagej.net/Fiji || RRID:SCR$_0$02285
Motion Sensing Superpixels (MOSES)	elifesciences.org/articles/40162
Superpixels	www.biorxiv.org/content/10.1101/248104v1

2.2 Methods

2.2.1 Cell culture

EPC2 (from Prof. Hiroshi Nakagawa, University of Pennsylvania, Perelman School of Medicine, Department of Gastroenterology, USA) and CP-A (ATCC) cells were grown in full KSFM (Thermo Fisher), AGS (ATCC), CACO-2(ATCC) and OE33

(ECACC) in full RPMI with 10% FBS (v/v), 5 mL Pen/Strep and 5 mL glutamine. Both were supplemented with glutamine and Penicillin streptomycin at 37°C and 5% CO2 until 80% confluent. To passage EPC2 and CP-A, cells were resuspended after trypsinization for 5 min with PBS supplemented with soybean trypsin inhibitor (0.25 g/L) to prevent cell death prior to resuspension in KSFM. Other cell lines were resuspended after trypsinization for 5 min with PBS. Cell were then centrifuged down and split according to division rates.

2.2.2 Organoid media preparation

1 mL of organoid media was prepared by mixing its components as indicated in the following table:

Component	uL/mL	10 mL	Concentration
R-spondin 1 conditioned media	20% volume	20% volume	batch dependent
Noggin conditioned media	20% volume	20% volume	batch dependent
Wnt3A conditioned media	50% volume	50% volume	batch dependent
N2 supplement (100x)	10 uL	100 uL	1x
B27 supplement (50x)	20 uL	200 uL	1x
Epidermal growth factor	1 uL	10 uL	50 nG/mL
Gastrin	1 uL	10 uL	10 nM
Nicotinammide	10 uL	100 uL	10 mM
A83-01	0.12 uL	1.2 uL	500 nM
SB202190	1 uL	10 uL	10 uM
FGF-10	1 uL	10 uL	100 nG/mL
N-acetyl-l-cysteine	2 uL	20 uL	500 uM
Y-27632 (Rock inhibitor)	1 uL	10 uL	10 uM
CHIR99021 (GSK3-Beta inhibitor)	1 uL	10 uL	3 uM
Penicillin and Streptomycin	10 uL	100 uL	

The rock inhibitor (Y-27632) and the GSK3-beta inhibitor (CHIR99021) were added for new organoids or first passage after thawing. When commercial Wnt, R-spondin 1 or noggin was used, the volume up to 1 mL was replaced with full advanced DMEM. media was then filtered using a 0.2 um filter.

The stock aliquots for the different components were prepared as indicated in the following table:

Component	Weight	Dilution
Epidermal growth factor	100uG	2mL H2O 0.1% BSA
Gastrin	1 mG	4.7 mL PBS 1% BSA followed by 1:10 dilution
Nicotinammide	0.244 G	2 mL H2O
A83-01	10 mG	475 uL/DMSO
SB202190	5 mG	1.3594 mL/DMSO
FGF-10	25 mG	125 uL SodiumPhosphate pH 7.4
N-acetyl-l-cysteine	0.8159 G	10 mL H2O
Y-27632 (Rock inhibitor)	50 mG	15.64 mL H2O
CHIR99021 (GSK3-Beta)	5 mG	3.59 mL DMSO

2.2.3 Conditioned media production

Wnt3A conditioned media

L Wnt-3A cell were thawed into a T175 flask with 25 mL of media containing: DMEM with 5% FBS , 1% L-Glutamine, 2 uL mL of 1M HEPES and 0.4 mg/mL G-418 (Neomycin, 0.01 g for 25 mL). Note: Use of advanced DMEM makes cells produce less WNT3A. Once confluent (3 days) cells were split 1:3 using the same media. Once confluent, the three flasks were split into 16 T175 flasks. One of the flasks was left with neomycin and frozen dawn after confluency. The other 15 flasks were kept with 25 mL DMEM with 5% FBS , 1% L-Glutamine and 2 uL mL of HEPES during 5 days. Then, the media is collected and centrifuged to remove dead cells. After filtering, the media is kept at 4 oC. The flasks were refilled again with 25 mL of media. After 2 extra the collection process was repeated. Both batches are mixed together, and 10 mL aliquots were kept at -80 oC in 15 mL tubes.

R-spondin conditioned media

The protocol is the same as for Wnt3A conditioned media with the following exceptions: Cells used are Hek293t cells transfected with C-terminal fc tagged R-spondin 1. The media used was Advanced DMEM-F12 with 5% FBS, 1% L-Glutamine, 2 ul/ml 1 M Hepes and 3 ul/ml Zeocin (for a final concentration of 0.3 mg/ml). Instead of collecting 25 ml of media after 5 days and 25 ml more at day 7; 50 mL of media without zeocin was added and then collected after 7 days.

Noggin conditioned media

Noggin conditional media was made as described in "Making R-spondin 1 conditional media" but instead of zeocin, puromycin was used as selection drug at a final concentration of 10 mg/mL (1ul/ml of the stock solution).

2.2.4 Assessing conditioned media batch quality

Wnt3A and R-spondin 1 activity can vary between batches. Each batch was tested using HEK293t cells with a WNT3A promoter luciferase reporter. R-spondin 1 was also tested using this cell line because it can also activate the Wnt3A reporter.

Plating luciferase reporter cells

After collecting the first batch of media after 5 days, Wnt3A reporter HEK293t cells were thawed into a T75 containing DMEM media with 10% FBS, 1% L-glutamine and 0.4 mg/mL G-418 (Neomycin). Once confluent, cells were resuspended in 19 mL of media. Of the 19 mL, 500 ul were plated into each well of a 24 well plate. The 7 mL left were frozen downas stock.

Hek293t reporter cells transfection with a control Renilla vector

Before testing the conditioned media all the wells but the negative control were transfected with a renilla vector constitutively active. This acts as cell number reporter and was used to normalize the luciferase activity. The renilla vector needed to be transfected into a total of 21 wells. Transfection solution for a total of 22 wells was made to ensure there was enough volume. Two tubes were prepared: The first containing 550 uL of Opti-MEM and 4.4 uL of Renilla vector stock solution. This concentration was calculated with this formula:

$$4.4uL = 22wells * \frac{25ul}{1well} * \frac{0.4\frac{nG}{uL} \quad desired \quad concentration}{50\frac{nG}{uL} \quad stock \quad concentration}$$

The second containing 550 ul Opti-MEM and 33 ul lipofectamine 2000. The lipofectamine volume was calculated with this formula:

$$33uL = 22wells * \frac{1.5uL}{1well}$$

The tubes were then left at RT for 5 min to allow lipofectamine micelles to form. After the 5 minutes, contents from both tubes were mixed. Care was taken not to touch the walls of the 1.5 mL tube as this would sisrupt the micelles. The mix was left at RT for 15 min. 50 ul of the mix were then added drop-wise in each one of the 21 wells. After 5 hours Wnt3A conditional media was tested as indicated in "Testing Wnt3A conditional media".

Testing Wnt3A or R-spondin 1 conditioned media

To test the conditional media, the cells prepared ha the media replaced by DMEM with 5%FBS, 1% L-Glutamine, and 2 uL/mL 1M HEPES with the percentage of conditional media indicated in the following figure:

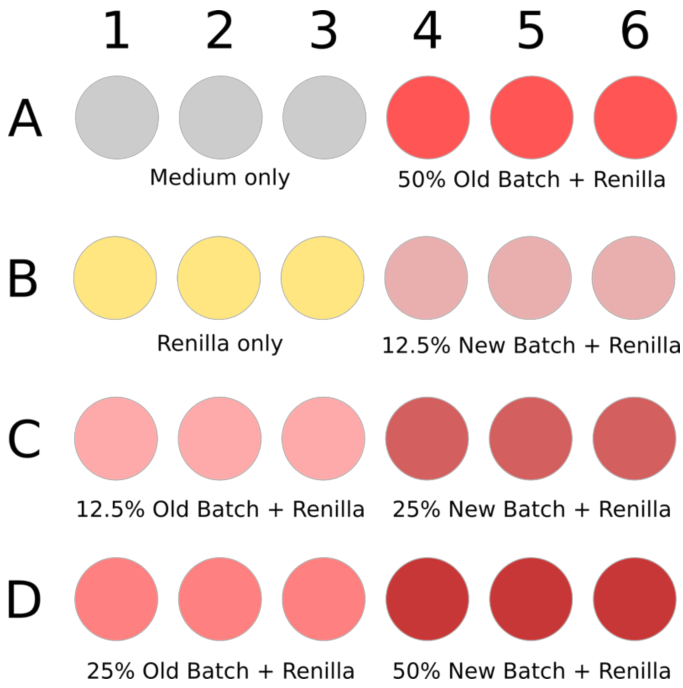

Figure 2.1: Well layout for luciferase conditioned media testing

Cells are left O/N in the incubator at 37 C, 5% CO2. Next day, cells were washed with PBS. Care needed to be taken not to detach the cells. PBS was then removed by inverting the plate on top of the sink. Next, the plate was put inverted at -80 C. From here, samples were treated using the dual-luciferase reporter assay from Promega. The kit's protocol can be found at [192].

2.2.5 Growing organoids from biopsies

Biopsies taken from Endoscopy in the John Radcliffe Hospital were kept on ice in Advanced DMEM-F12 with 1% glutamine, 2 ul/mL HEPES (1M) and 1% Pen/Strep prior to processing. The biopsies were cut into small pieces using scissors before being pelleted and washed with cold PBS twice. Then, the biopsies were washed with PBS + 5 mM EDTA, centrifuged down, resuspended again in PBS + 5 mM EDTA and left in a roller at 4 C for 15 minutes. Samples were then washed twice with PBS and incubated in TriplE at 37 C, 5% CO2 for 30 minutes. The samples were then pelleted using a microcentrifuge and, after removing the TryplE, washed twice more with PBS. After the washes, samples were pipetted vigorously up and down to dissociate the chunks of tissue. Occasionally, tissue pieces were too big, and the pipette tip was cut to make the hole bigger. After letting the bigger tissue pieces settle down, the supernatant was transferred into a new microcentrifuge tube. The contents were then pelleted down, and the supernatant discarded. The pellet was then resuspended in the amount of Matrigel required according to pellet size and distributed in 50 ul drops into 24 well plate's wells. After 5 minutes incubation at 37 C and 5% CO2, 500 ul of organoid media with Pen/Strep, Antibiotic Antimycotic Solution, Rock inhibitor and GSK3 inhibitor was added in each well. Once in culture, the media was replaced by normal organoid media with antibiotics every other day.

2.2.6 Splitting organoids

Organoids were split when they reached a considerable size. This happened usually after 7 days in culture. First, the Matrigel containing the organoids was resuspended in ice cold PBS into a microcentrifuge tube. The organoids are then pelleted using a microcentrifuge and the PBS removed. If the organoids were to be used in an experiment, 3 ice cold PBS washes would follow to prevent residual Matrigel from sticking on the organoids. After pelleting the organoids, they were resuspended again in TryplE and incubated at RT for 5 minutes. The organoids were then pelleted again and resuspended in 120 ul of Matrigel for each original organoid well and pipetted up and down to dissociate the organoids in it. Before the Matrigel

warmed up, the tube contents were distributed in 40 uL drops in a 24 well plate. The plate was then incubated for 10 minutes at 37 oC, 5% CO2. Once the Matrigel gelated, 500 ul of organoid media was added to each well.

2.2.7 Freezing Cell lines for storage

Cells were resuspended at a concentration of 10^6 cells/ml with 90% FBS +10% DMSO freezing media following centrifugation and stored at 80 C before passing to liquid nitrogen storage. Organoids were resuspended using ice-cold PBS.Then centrifuged down and stored using the same freezing media as cell lines.

2.2.8 Mycoplasma testing and cell line authentication

All cell lines were tested monthly for mycoplasma infection using MycoAlert PLUS Mycoplasma Detection Kit at the Ludwig Cancer Institute, Oxford. All cell lines but CACO-2 and HFF, were authenticated by Eurofins.

2.2.9 Fluorescent labelling

Cells were labelled using Celltracker Green CMFDA and Celltracker Orange CMRA dyes (Life Technologies) according to their protocol. Two different concentrations 2.5 µM and 10 µM were used. The lower concentration still permits tracking but has fewer toxicity concerns. (! The red and orange dye have different molecular weights, the material section explains how to make 10 mM stock solution.) Briefly, one million cells were pelleted in a 15 mL tube. The cells were then resuspended in their usual culture media without serum. with the desired dye concentration and incubated 45 min at 37 oC. Then, cells were pelleted and washed with serum free media and incubated for 30 min at 37 C. Finally, cells were pelleted and resuspended in the desired media for the experiment.

2.2.10 Heterotypic junction Co-culture assay

In 70 µL of culture media, 70,000 labelled cells were seeded into each side of a cell culture insert (Ibidi) in one well of a 24-well plate. After 12 h, inserts were

removed and the well washed three times with PBS to remove non-attached cells before adding the desired media (KSFM or 1:1 mixture of KSFM:RPMI +5% FBS for filming. For the perturbations, in this thesis EGF, was also added to the media at the stated concentrations.

2.2.11 Time-lapse Image acquisition

The different conditions were filmed on a Nikon microscope for 96 or 144 h at a frequency of 1 image per hour. 2x and 4x objectives were used. The microscope filter wavelengths used to visualise the red and green dyes were 546 nm and 488 nm, respectively. The Nikon microscope was controlled using the Metamorph software. Images were then processed into videos using ImageJ.

2.2.12 Studying cell heterotypic monolayers using MOSES

MOtion SEnsing Superpixels (MOSES) was developed and used by Dr. Felix Yuran Zhou to study the behaviour of the cell populations in our "temporary divider Co-culture assay" experiments. A description of the software development, metrics and usage can be found in:

- Zhou et al. Bio Protocols 2019: Most detailed protocol on MOSES use.
- Zhou & Ruiz-Puig et al. ELife 2019
- Zhou & Ruiz-Puig et al. Biorxiv 2018

The code , under a Ludwig non-commercial, academic license, is stored in the following github repository: https://github.com/fyz11/MOSES where it is updated and maintained or in https://github.com/elifesciences-publications/MOSES for an archived copy.

2.2.13 Immunofluorescence staining for heterotypic junctions

The heterotypic junction Co-culture assay was made in 8 Well µ-Slides with optical bottom. Samples were washed twice with PBS and fixed with 4% formaldehyde for 15 min. The samples were then washed twice and permeabilised with 0.1% Triton-X for 15 min. Samples were blocked with image-iT Fx signal enhancer for 1 h before incubation with primary antibody overnight in Agilent Dako Antibody Diluent with Background Reducing at 4°C. Following 3 washes of 10 min in PBS, samples were incubated for 2 h in the dark the desired secondary antibodies adding Alexa Fluor 647 Phalloidin if required, both at a 1:400 dilution, and DAPI (1 mg/mL) at 1:1000 dilution. All of these components were diluted in Agilent Dako Antibody diluent. Finally, samples were washed three times with PBS and mounted using 200 uL of Fluoromount-G. 5 uL Prolong Gold Antifade mountant was used for samples on slides.

2.2.14 Deparaffination and hydration of paraffin embedded sections

First, sample slides were baked at 60 oC for 1 hour to prevent detachment. Then, the slides went through a deparaffination and hydration process consisting in submerging the rack with the samples in solvents following these steps: 2 x 5 min in Histoclear 2 x 3 min in 100% ethanol 1 x 1 min in 90% ethanol 1 x 1 min in 70% ethanol 1 x 4 min in miliQ H2O

2.2.15 Immunofluorescence staining of formalin fixed, paraffin embedded sections

After following the steps in "Deparaffination and hydration of paraffin embedded sections", the rack with the samples was then boiled in 1x Tris-EDTA+Tween buffer (prewarmed for 10 min in the microwave) for 10 min. Using a wax-pen the area around the sample was sealed. The slide were then introduced into a humidifier.

From here the steps were the same as in "Immunofluorescence staining", starting with the 0.1% Triton-X permeabilization step.

2.2.16 Cell counting with convolutional neural newtworks

A convolutional neural network (CNN) was used to automatically count cells in DAPI-stained nuclei confocal images. It trains a model that will convert any input image to a dot image in which sum of all its intensities equals the number of cells present. This CNN is based in the one published in Xie et al, 2016 and is explained in detail in our MOSES publication(Zhou & Ruiz-Puig et.al eLife 2019).The program was run by Dr. Felix Yuran Zhou and the manual annotation made by Carlos Ruiz-Puig. Briefly, for the DAPI stained images, training data was generated by randomly sampling 200 patches of 256x256 pixels among all our 4096x4096 pixels images. The patches were then annotated by adding a dot at the centre of each DAPI stained nucleus. From each one of these patches, 50 smaller 64x64 patches were randomly generated, giving a total of 10,000. 30% of those were used to train the model using a mean absolute error (MAE) loss and the other 70% to test the results. Image X shows the difference between using mean absolute deviation between manually annotated 256x256 patches and CNN counted ones. The counts were then assigned to one cell line or another by converting the green and orange fluorescent channels into two binary masks and filtering out the counts with them.

2.2.17 Migration-independent cell counting in videos

The same CNN described in "Cell counting with CNN" was used to count cells in videos, this time using annotations for the green and orange channel. In this case binary mask needed to be calculated prior to the patch selection as it was moving in each time-point. 100 patches of 64x64 pixels were then randomly selected in each time-point and fluorescent mask to obtain an average density. The proliferation rate was then calculated by comparing the average cell density over time. To ensure there the dye used was not biasing our results, a third count using the phase contrast channel was done subsetting again the areas using the fluorescent channel masks.

2.2.18 Predicting cell density using dye fluorescence intensity

This second approach to count cell densities was used consisting in comparing fluorescence intensity decay through the video frames. The most frequent (modal) intensity for each frame and each channel was used and then fitted into a linear gradient. We used the absolute value of this linear gradient as a proxy for proliferation coefficient.

2.2.19 Producing the lipid-oil mix for the oil bath

1,2-diphytanoyl-sn-glycero-3-phosphocholine at 0.2–0.5 mg/ml was used in all the experiments. Diluted in "oil", a 1:1 (v/v) mixture of hexadecane and silicone oil AR 20.

2.2.20 Preparing collagen for 3D collagen ring or tube casting

Keep all components and the mix on ice during all the process. First, we filter the three components needed for collagen gelation: collagen type I from rat tail, 1 M NaOH and 10X PBS to ensure they are sterile using a 0.2 um filter. To produce 1mg/mL collagen, 300 uL of collagen type I are mixed with 593 uL of organoid media, 41 uL of 10X PBS , followed by 5.5 uL of 1M NaOH. After mixing well the contents should change from yellow (acidic pH) to pink (neutral pH).

2.2.21 Making Clevers' collagen rings

Wells were coated with FBS for 30 min at RT to prevent collagen attachment to the plastic. After removing the FBS, 200 uL collagen, with two confluent wells of pelleted organoids resuspended in it if required, are pipetted into the side of the wells forming a ring. The ring is left for 20 min in the incubator at 37 oC and 5% CO2 to gelate. After incubation, rings are washed twice with PBS. If the collagen contained organoids, 600 uL of organoid media was added after the last wash. If no organoids were added, 600 uL of complete DMEM (10% FBS + Pen/Strep + Glutamine) was added after the last wash. media was changed daily after this step.

2.2.22 Designing and 3D printing plastic moulds

Moulds were designed using the Fusion 360 software and then rendered for printing using the Cura software. Finally the mould were printed using ABS plastic using an Ultimaker 2+ 3D printer.

2.2.23 Casting collagen rings

Moulds and mould dividers were sterilized by submerging them into pure ethanol, then let air-dry under the hood. 900 uL of lipid-oil were added to each one of the wells in a 24 well plate needed. The mould, with the divider if doing half-half rings, is then submerged into the lipid-oil making sure it touches the bottom of the well. Organoids (two confluent 24 wells of organoids per ring) and/or fibroblast/immune cells were resuspended in the collagen ready for for gelation (see "Preparing collagen for 3D collagen ring or tube casting") when required. After resuspending the required cells in it, a total of 200 uL of the collagen-cell mix was added in small drops into the mould. When doing half-half rings, each half was filled with the desired mix making sure the drops cover also the sides of the divider. The droplets are then left to settle down for 10 min. If a divider was used, it was removed once the 10 min were over. Once the droplets settled down, part of the lipid-oil bath was removed being careful to not disturb the droplets. The lipid-oil removed in this step was recycled after filtering it. Once the sobrant lipid-oil was removed, 1 mL of Undecane is added to further dilute the concentration of lipid in the oil to ensure droplet-droplet fusion. The plate containing the samples was then put in the incubator at 37 oC, 5% CO2 for 20 min to promote the gelation of the collagen. Following the gelation, the lipid-oil + Undecane mix was removed and switched carefully for 1 miL PBS. The mould was then removed followed by two 1 mL PBS washes to remove residual oil. If the collagen contained organoids, 600 uL of organoid media was added after the last wash. If no organoids were added, 600 uL of complete DMEM (10% FBS + Pen/Strep + Glutamine) was added after the last wash. media was changed daily after this step.

2.2.24 Casting collagen tubes

As “Casting collagen rings” with the following differences Longer moulds of 3 cm or 10 cm length were used after sterilizing them with ethanol. As container for the mould, a 15 mL tube conical bottom was cut until the cylindrical part, including the cap, had the desired length of either 3 or 10 cm. The mould was then introduced into the cylindrical tube making sure the base was flat on the cap. After the mould is introduced, the tube was filled completely with lipid-oil solution. The tube is filled then drop by drop using the desired fibroblast concentration diluted in them. After each 2 mL the droplets were allowed to settle for 5 min. For tubes with a gradient of mixed fibroblast, different collagen-fibroblast mixes were prepared and added consecutively letting the droplets settle after each mix. Once the tube mould was full, the tube is covered with a 15 mL tube cap and put into the incubator at 37 oC, 5% CO2 for 20 min to gelate its contents. After gelation is complete, the mould is removed from the 15 mL tube horizontally, preventing the contents to leak out, and put into a cell culture dish filled with PBS. The contents were then released from the mould by carefully flowing PBS from one side of the tube. Once the collagen tube was released, PBS was flowed inside to separate the collagen that might be stuck together. The PBS was then changed three times and replaced by full DMEM media.

2.2.25 Adding adapters to the tubes

The adapters for the tube’s ends were added, using forceps. This was done immediately after the tube was cast to allow for collagen contraction to secure it in place.

2.2.26 Constructing adapter caps

Caps to prevent cell flow through the tube adapters were built by removing the membrane of a 0.2 um cell strainer and pushing it wrapped to the bottom of a 200 uL pippete tip. Once the membrane could not be pushed further, the tip was cut using scissors leaving the narrow end and the wrapped membrane together.

2.2.27 Coating the collagen tubes with cells

One of the ends of the tube was shut permanently by making a knot around the collagen with a previously sterilized string. The other end of the tube ended in an adapter. Holding the adapter end outside the media, 100 ul of media with a total of 10 million cells in it was added to the tube interior. After adding the cells, the adapter was closed using the adapter cap. The plate is then left inside the incubator at 37 oC, 5% CO2. To prevent having a more densely populated monolayer of cells in one side of the tub due to gravity, the tube was rotated once after 3 hours. The next day the adaptor cap was removed, and the inside of the tube washed with prewarm full DMEM. media is then changed twice to remove residual cells outside the tube.

2.2.28 Preparing *Helicobacter pylori* selective agar plates

39 grams of Columbia Blood Agar Base were diluted in 1 litre ddH2O and autoclaved. Before it gelates, add 70 ml of lysed horse blood with 10 mg of *Helicobacter pylori* Selective Supplement (DENT), 5 mg of Vancomycin, 5 mg of Trimethoprim, 5 mg of Cefsulodin and 5 mg of Amphotericin B. After mixing all together, the solution was aseptically distributed into petri dishes and kept at 4 oC.

2.2.29 Culturing *Helicobacter pylori* in plates

An *H. pylori* aliquot was thawed at RT , added as a drop on top of the blood agar plate and grown in 5% CO2 at 37 oC. The bacteria plates were split by using an inoculation loop and streaking them into a new plate.

2.2.30 Liquid culture of *Helicobacter pylori* in Brucella broth media

Bacteria were grown by resuspending them from a blood agar plate in Brucella broth media supplemented with 10% FBS and 10 mg of *Helicobacter pylori* Selective Supplement (DENT) in a 50 mL falcon tube partially closed. The tube was then cultured in microaerophile conditions inside a 37 oC incubator shaking at 190 rpm. The next day, bacteria can be frozen down as aliquots or used to infect cells.

2.2.31 Infecting inner tube monolayers using *Helicobacter pylori*

A collagen tube was populated with an AGS cell monolayer as described in "Coating the collagen tubes with cells". Pen/Strep was not used in the media during the process to prevent killing the bacteria. After growing the *H. pylori* overnight in Brucella media, 109 bacteria were centrifuged down at 3000 rpm for 5 minutes and resuspended in 100 ul full DMEM. The cap at the end of the tube was removed, the adapter hold up with forceps and the bacteria introduced in it before closing it again with the same cap. *H. pylori* was left in the tube for 7 hours in a 37 oC, 5% CO2 incubator. The cap was then removed, and the inside of the tube washed with warm DMEM. After the washes, the sample was ready for processing.

2.2.32 3D sample processing

Samples were washed twice with PBS and then fixed with 4% formaldehyde either at 4 oC overnight or 30 min at 37 oC. Organoids are pelleted and fixed only for 15 min instead. If the sample cannot be processed next morning, formaldehyde was changed by 70% ethanol. Fragile samples (rings, Organotypic 3D culture on membrane) and organoids were embedded using Histogel, previously melted using a microwave in a beaker full of water. Care must be taken to keep rings in the same horizontal plane to get full sections when cutting slides.

The samples were put into a tissue cassette and then processed O/N using the tissue processor. The next morning, the cassettes were left to warm in a hot paraffin bath for 10 min and then embedded into paraffin blocks. Samples grown on membranes or tubes were split in half and embedded in two different paraffin blocks. Unless otherwise stated 4 um section were cut from the block using a microtome. After letting the sections unwrap on a 37 oC water bath for a minute, two sections are put on a previously labelled slide. Samples are then dried on a slide oven at 37 oC and packed into slide boxes.

2.2.33 Haematoxylin and eosin staining

After following the steps in "Deparaffination and hydration of paraffin embedded sections", the rack with the samples was stained going through the following steps: 1 x 5 min haematoxylin + 2 min wash in running H2O 1 dip in acidic alcohol + 2 min wash in running H2O 1 x 30 seconds in Scot's water + 2 min wash in running H2O 1 x 5 min in eosin + 1 min wash in running H2O 1 x 30 seconds in 70% ethanol 1 x 30 seconds in 90% ethanol 1 x 1 minute in 100% ethanol 1 x 2 minutes in 100% ethanol 2 x 5 minutes in histoclear Finally, slides were mounted using vectamount and left to dry overnight.

2.2.34 IHC staining

After following the steps in "Deparaffination and hydration of paraffin embedded sections", endogenous peroxidases were inactivated by incubating them in 3% (v/v) H2O2 diluted in methanol (with 30% H2O2 stock, 50 ml H2O2 in 450 ml methanol) for 15 min. Antigen retrieval was then done by boiling the sample for 10 minutes in already boiling citrate buffer. Slides were left to cool down and put into a humidifier after removing the citrate buffer carefully. The area around the sample was sealed using a wax pen and the samples were blocked with PBS with 10% NGS. Following the blocking step, the sections were incubated overnight with the primary antibody diluted PBS in 5% NGS. Next day, slides were washed 3 times with PBS for 5 minutes and incubated with the secondary biotinylated antibody for 1 hour in the dark at RT. Slides were then washed three times with PBS and incubated in VECTASTAIN Elite ABC HRP Reagent for 15 minutes at room temperature before being washed again 3 times for 5 minutes with PBS. Sections were then incubated between 3 and 10 minutes with HRP solution (DAB substrate kit, 2.5 ml ddH2O, 1 drop of H2O2 solution, 1 drop of buffer and 2 drops of DAB). To stop the reaction, samples were then dipped in ddH2O. Once the reaction was stopped, samples were counterstained in haematoxylin for 12 seconds and dipped in water again to refor 5 minutes in 90% ethanol, followed by 5 minutes in 100%

ethanol and 2 times in histoclear for 5 minutes. Finally, slides were mounted with vectamount and left to dry overnight.

2.2.35 Liquid culture of *Helicobacter pylori* in Brucella broth media

Bacteria were grown by resuspending them from a blood agar plate in Brucella broth media supplemented with 10% FBS and 10 mg of *Helicobacter pylori* Selective Supplement (DENT) in a 50 mL falcon tube partially closed. The tube was then cultured in microaerophile conditions inside a 37 C incubator shaking at 190 rpm. The next day, bacteria can be frozen down as aliquots or used to infect cells.

2.2.36 Infecting inner tube monolayers using *Helicobacter pylori*

A collagen tube was populated with an AGS cell monolayer as described in "Coating the collagen tubes with cells". Pen/Strep was not used in the media during the process to prevent killing the bacteria. After growing the *H. pylori* overnight in Brucella media, 109 bacteria were centrifuged down at 3000 rpm for 5 minutes and resuspended in 100 ul full DMEM. The cap at the end of the tube was removed, the adapter hold up with forceps and the bacteria introduced in it before closing it again with the same cap. *H. pylori* was left in the tube for 7 hours in a 37 oC, 5% CO2 incubator. The cap was then removed, and the inside of the tube washed with warm DMEM. After the washes, the sample was ready for processing.

2.2.37 Slide scanning and analysis

Slides were scanned using a Hamamatsu automated slide scanner, the output files were analysed using NDP.view2.

2.2.38 Sectioning samples for tissue microdissection

14 slides were cut from each Oesophageal mucosal resection block. The two first sections were cut at 4 um on polylysine coated slides and the next two at 10 um thickness on Zeiss MembraneSlide 1.0 PEN (D) used for microdissection. The

microdissection slides need to be activated previosuly by incubating under UV light during 30 min.

This alternation continues until 8 polylysine coated 4 um slides and 6 PEN membrane coated 10 um thickness slides were obtained. Slide number 6 was then stained using the H&E protocol described before and annotated by three pathologists. The rest of the 4 um slides were stored for future use.

2.2.39 Methyl green staining

To have enough contract to distinguish the different histological features of the tissue we were microdissecting a counterstain using methyl green is needed. All the 10 um sections were counterstained with methyl green as follows: Slides were rehydrated as indicated in "Deparaffination and hydration of paraffin embedded sections". Then dipped into methyl green (0.5% w/v solution) and washed in water to remove excess of dye. Finally, the slides were backed during 1 hour at 37oC.

2.2.40 Tissue micro-dissection

The desired areas were cut using the PALM microscope in the Wellcome Trust building and the Nanozoom software. The cap was changed for each tissue type and the tissue collected from the all the slides of that block before changing tubes and desired target. The sticky end of the tube might get clogged when to much tissue is introduced into it. To prevent this, the tube is closed carefully and centrifuged down using a bench microcentrifuge. After the micro-dissection is complete, samples are stored at -20 degrees.

3

Designing a 2D model of the SCJ to study Barrett's oesophagus segment growth

Contents

3.1 Research aim 60
3.2 Chapter summary 60
3.3 Introduction 62
3.3.1 Choosing the stages of progression to model 63
3.3.2 Cell line selection 64
3.3.3 Plating adjacent cell populations 65
3.3.4 Labelling cells for co-culture experiments 66
3.3.5 Computational extraction of metrics from cell interaction videos 68
3.3.6 MOSES analysis 70
3.4 Results 74
3.4.1 Experimental design 74
3.4.2 Oesophageal squamous and Barrett's oesophagus cells form a stable junction *In vitro* in the absence of EGF . 74
3.4.3 Serum free medium prevents collective cell behaviour in our model 75
3.4.4 Gastric adenocarcinoma cell line behaviour differs from OAC cell lines 79
3.4.5 The use of fluorescent dyes changes cell behaviour under serum conditions but is not colour specific. 80
3.4.6 High EGF concentrations can disrupt the squamous-columnar junction stability and increase the columnar segment length *In vitro* 82
3.4.7 Columnar invasion of the squamous lining *In vitro* is not determined by cell proliferation 85

3.4.8 Inhibition of EGFR using lapatinib prevents the invasion of BO and OAC derived cell lines *In vitro* 86
3.4.9 Deoxycholic acid does not produce the same effects as EGF presence in the medium 86
3.5 Discussion 88
3.5.1 The combinations selected produce three different interaction phenotypes 88
3.5.2 *In vitro* results with *In vivo* EGF concentrations suggests EGF in reflux can influence BO length 90
3.5.3 Migration and not proliferation may drive segment expansion *In vitro* 92
3.5.4 EGFR inhibition might be producing cell toxicity 93
3.5.5 Deoxycholic acid is not able to disrupt the junction at neutral pH 94
3.5.6 A simple 2D model consisting of only epithelial cells may be insufficient to test the reflux effect on BO segment growth 96

3.1 Research aim

As previously suggested in the introduction, the epidermal growth factor present in gastrointestinal reflux episodes could form a gradient in the distal oesophagus and thereby promote Barrett's oesophagus colonization. *In vitro* models to study the interaction between squamous cells and the columnar cells of Barrett's oesophagus in the squamous-columnar junction and test this hypothesis are not available. This chapter's aim is to generate an *in vitro* model to study these interactions. Once the model is established, the next objective is to test the hypothesis suggesting that the epidermal growth factor in the reflux might promote Barrett's oesophagus colonization of the distal oesophagus.

3.2 Chapter summary

This chapter describes the prerequisites for development of a 2D model of the squamous-columnar junction formed by two distinct cell types, namely Barrett's oesophagus and the normal squamous lining of the oesophagus. In order to study

the interaction of the two cell monolayers representing the junction between BO and the squamous epithelium, cells must be plated in such a format that they form a defined line of contact. This requires control over the plating process to make two adjacent epithelial monolayers. Furthermore, the different cell types need to be labelled distinctively in order to record and study their interactions over time. Finally, analysis of the recorded interactions must then be fast, objective and reproducible to properly compare the conditions.

Following the listed prerequisites, the experimental design and implementation of a model fulfilling these conditions is discussed. In brief, the cells were labelled using fluorescent dyes and then plated using a divider to keep the populations adjacent but unmixed. Once the populations are plated adjacently, the interactions are recorded, and the footage analysed using computer vision techniques.

This experimental design was then used to investigate three stages of oesophageal adenocarcinoma progression *In vitro*. These stages were the interaction of healthy squamous epithelium with either squamous epithelium, Barrett's oesophagus junction or oesophageal adenocarcinoma cells. In these experiments, oesophageal adenocarcinoma cells replaced the squamous population completely, whereas the Barrett's oesophagus and squamous cells formed stable junctions. Addition of EGF in concentrations similar to physiological levels in the duodenum to Barrett's oesophagus cells appears to block their ability to form stable junctions with squamous cells. In accordance with the effect of EGF on the stability of the Barrett's oesophagus with squamous cells, the adenocarcinoma cell line cultured with EGFR inhibitors forms a stable junction with squamous cells.

Despite being limited to the interaction between two epithelial cell populations, this model could replicate the squamous-columnar junction *in vitro*. It shows that, at least within this experimental setting, EGF promotes the growth of the Barrett's oesophagus segment by replacing the squamous lining. Taken together, the data suggest a gradient of EGF could contribute to the Barrett segment length in the distal oesophagus.

3.3 Introduction

To date, the best-known risk factor for oesophageal cancer is Barrett's oesophagus for which its segment length is used as a prognostic factor for malignancy. Barrett's oesophagus research has predominantly focused on determining the BO cells of origin and the sequential mutations required to acquire malignancy. The mechanisms guiding the replacement of the squamous lining in the lower oesophagus that will determine the segment length however remain poorly understood in BO. As a result, a model to study BO segment growth *in vitro* has not been reported to date.

An *in vitro* model to study BO replacement of healthy squamous cells requires the co-culture of two distinct cell populations. One representing the normal squamous lining and a second the Barrett's oesophagus epithelium. Due to its nature, co-culture models are complex, presenting more variables than single cell systems, including:

- The individual cell behaviour in each population.
- The cell-cell interactions. Both by direct contact or paracrine secretion.
- Collective population behaviour.
- Cell density.
- The effect of the medium contents in each population.
- Evolution of the interactions through time.
- The decay of the nutrients in the media and the culture vessel [193]

The ability to record reproducible and informative results would depend on clear variables and research tools. To achieve this, five elements needed to be defined:

- The BO stages the model wants to replicate.
- The cell lines used to mimic *in vivo* epithelial populations.

- A technique to put the cell populations apart but allowing them to interact in a short period of time.
- A mechanism to label and film the cells for long periods of time using time-lapse microscopy
- A software able to describe and study the different cell interactions.

3.3.1 Choosing the stages of progression to model

To study the expansion of Barrett's oesophagus in the distal oesophagus and the mechanism through which it acquires its final length, the model needs to replicate the junction between early Barrett's oesophagus and the squamous epithelium in the oesophagus. As previously described in the introduction, Barrett's oesophagus expands fast after it originates and remains stable after acquiring its final length. In this thesis we hypothesize that the stable boundary between both populations will occur once the gradient of compounds carried by the reflux becomes too weak to continue promoting BO invasion. Thus, in the absence of any external stimulus, the *in vitro* model replicating this interaction should form a stable junction. If the hypothesis is correct, the presence of EGF or another growth factor in the medium will be able to break this stability and allow the BO cell to expand in detriment of the squamous populations.

Two further cell combinations were used as controls. The first was a negative control for population interaction and junction formation. In it, only a squamous cell line was used. With no columnar cells present, the two populations merge into one without establishing a junction. The second combination was used as positive control for squamous lining replacement and columnar segment growth. For it, an oesophageal adenocarcinoma derived cell line was used to ensure the squamous lining was completely replaced. As once the model is established EGF activation capacity to promote BO segment growth will be tested, this combination would ideally involve an OAC cell line with high EGFR phosphorylation under normal medium conditions. A last combination, using a gastric adenocarcinoma cell line together with squamous

cells was used in comparison with the oesophageal adenocarcinoma cell line in conditions in which E-cadherin mediated cell-cell junctions could not be formed.

3.3.2 Cell line selection

The most used cell lines to study oesophageal adenocarcinoma are tumour derived cell lines. In 1997 Rockett et al. developed three different cell lines from OSCC (OE21), OAC (OE33) and gastric adenocarcinoma from cardia (OE19) [194]. These cell lines are frequently used in *in vitro* experiments involving OAC.

Cancer cell lines are in many cases simple to culture compared to non-tumour derived cell lines and often have a high proliferation rate. Working with cancer cell lines however, can only reliably mimic cancer *in vitro* as they have high metabolic rates, fast proliferation, stem cell-like behaviour and invasive phenotypes. Cancer cells can also acquire new mutations during culture causing cell line divergence [195], [196]. Heterogeneity is also an issue with each patient having a cancer presenting a unique genetic landscape. In our model, the cancer cell line OE33 was used to mimic OAC. OE33 was used as positive control for squamous cell replacement and columnar segment growth. Interestingly, OE33 has both EGFR and HER2 amplifications [197].

In many studies, the cancer cell line OE21 is used to mimic squamous cells *in vitro*. However, it was not derived from a healthy primary cell source. Conversely, HET-1A, a cell line immortalized with the simian virus SV40T, derives from healthy squamous cells. However, studies with this cell line have concluded that it is not a good substitute for squamous cells [198]. The squamous epithelium derived cell line EPC2-hTERT (EPC2) was another alternative. hTERT is the catalytic domain of the telomerase protein. By transfecting the squamous cells using a retroviral vector, the cells are immortalized. This process keeps the cells closer to *in vivo* phenotypes [199]. EPC2 is not invasive and differentiates like the oesophageal epithelium in organotypic culture [200]. Interestingly, EGFR overexpression increases EPC2 migration. Taken together, this makes EPC2 a good candidate for EGF related experimentation [201].

Equally important was finding a cell line to mimic Barrett's oesophagus *in vitro*. The cell line biobank ATCC has available Barrett's oesophagus derived cell lines. These cell lines are also immortalized using hTERT. The four cell lines derived from different stages in BO to OAC progression are: CP-A (non-dysplastic BO), CP-B (high grade dysplasia BO), CP-C (OAC 1) and CP-D (OAC 2) [202]. The stage studied in this chapter is early BO colonization of the distal oesophagus. Thus CP-A derived from early BO was used.

3.3.3 Plating adjacent cell populations

The co-culturing of different cell types in distinct populations prior to study their interaction is a long-standing challenge in tissue engineering. To form clear boundaries between cell populations, most published techniques require fluidics machinery [203] or non-commercial mechanical devices [204]. Other publications directly study the interactions by directly mixing of different cell types while proliferation happens [205] or in response to external stimuli such as the addition of ascorbic acid [206] or all trans-retinoic acid [207]. Experiments in which other cell subtypes like fibroblasts [208], immune cells [209] and adipocytes are used have also been conducted [210]. In none of the reported studies however, separation of the cells into homogeneous populations before interaction was attempted.

Previous work in this group has focused on a droplet method to achieve two uniform cell populations in close proximity to each other. In this method two droplets, each containing the distinct cell populations are placed in close proximity. After attachment of the cells, the medium is replaced and the cells are let to cover the distance between the two cell populations. A major drawback of this approach is the low technical feasibility. Droplets tend to mix when transferred into the incubator and the droplets have a high chance to evaporate before the cells attach and new medium is added. Finally, the distance between the droplets is difficult to control and is thereby prone to large variations. Sometimes so large it even prevents contact between populations.

Another technique consists of tilting the culture plate. This lets the monolayer form in the half well submerged in medium. Then, repeat the process on the other side to let the cells attach adjacent to the first population[211]. This approach however also proved to be technically challenging and very low throughput, thus unsuited for larger studies.

To overcome limitations with the tilted cell plate approach, a third approach was applied based on an aqueous two-phase system using liquids with different densities. The different cell types were resuspended in aqueous solution of different densities using a PEG/Dextran liquid interface, which allowed for the formation of a two-phased aqueous system in which each of the cell types is allowed to attach in close proximity to each other. Once attached to the plate, the medium is replaced and the cells can migrate together [212]. Attempts to use this system for studying the formation of stable cell junctions were unfortunately not successful as cell debris from the droplet method resulted in imaging artefacts challenging the analysis (data not shown).

Better results are achieved by applying a modified divider for wound-healing assays to heterotypic junction formation as was previously described for eardrum cell populations interacting [213]. This method allowed well-defined cell populations separated by a 400 um distance.

3.3.4 Labelling cells for co-culture experiments

The ability to determine the cell identity after the cell populations start interacting is crucial for data collection and analysis. Several strategies can be applied to identify cell identity *in vitro*

The use of columnar and squamous markers allow for label free cell characterisation. This however requires the fixation of the cells and staining the markers using immunofluorescence [214]. This approach is problematic as it requires fixing after each time-point, preventing the study of cellular dynamics of a specific sample over time. Using stable transfection of different fluorescent proteins in each cell line [215], the cellular fluorescence can be kept constant. However, preparation of

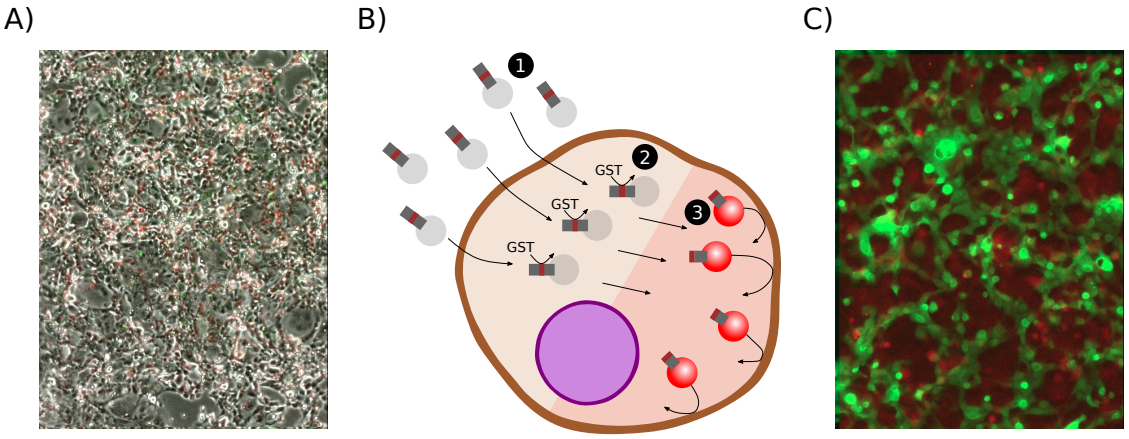

Figure 3.1: Celltracker dyes A) The dyes DiA and DiO label the cancer cell lines OE21 and OE33 weakly, photobleaching after a few hours. B) Celltracker dyes diffuse freely into the cell where they are modified by the glutathione-S-transferase (GST) enzyme into a fluorescent hydrophilic particle unable exit the cell. C) OE21 and Oe33 using Celltracker dyes.

stable transfected cell lines is laborious and time-consuming, reducing throughput and causing delays in testing new cell lines or primary cells. Therefore, another cell labelling approach was pursued.

Commercially available fluorescent dyes allow for quick labelling of cell populations. These dyes label cells for long periods of time allowing microscopy imaging. Previous work in this group focused on the lipophilic dyes DiO and DiA. These dyes intercalate with the phospholipids in the cell membrane and emit fluorescence [216]. Usually used to counterstain neuronal membranes, the dyes did not work in cancer cell lines. High proliferating cells and continuous time-lapse microscopy imaging caused bleaching of the dyes. Therefore, DiO and DiA were considered to be unsuitable for experiments lasting more than 24 hours. Figure 3.1 A, shows the 24 hours frame of an OE21 and OE33 mix experiments with DiA and DiO dyes respectively.

Celltracker dyes (thermofisher) are better suited to label cells for long periods of time in microscope experiments. These dyes are able to enter the cells by free membrane diffusion. Once inside, the dyes are modified by glutathione-S-transferase. The modification prevents the molecule to leave the cell and turns it fluorescent.

(Figure 3.1 B). The fluorescence allows differentiating mixed cell cultures for longer than 24 hours. (Figure 3.1 C) [217]

Imaging was performed using fluorescent time-lapse microscopy. Fluorescent time-lapse microscopy was preferred over confocal imaging as the sample was less likely to be overheated and z-stacks needed to be taken at the confocal microscope to prevent the image from going out of focus. Additional images translate in longer acquisition times and more data collection both increasing the photobleaching of the sample and data storage challenges.

3.3.5 Computational extraction of metrics from cell interaction videos

To analyse the resulting videos, an unsupervised and precise data analysis software is needed. This was achieved by analysing the videos using computer vision in collaboration with Dr. Felix Y. Zhou. To better know how to analyse the videos, the expected cell interactions need to be defined first.

Possible interactions between cell populations

Several different scenarios are possible for the interaction of two different cell populations. Two populations of the same cell type should join into a single population. No interaction will be observed in heterotypic nonproliferative populations lacking a migratory phenotype (Figure 3.2 A). *In vivo*, two different cell populations meeting usually form a stable boundary. Once this boundary is formed, few or no intermixing will happen between both populations [218]. When at least one migrates, the boundary forms closer to the population migrating slower or not migrating. (Figure 3.2 B). The boundary could then remain stable (Figure 3.2 C) or one of the populations continue advancing. The advancing population could either replace (Figure 3.2 D) or grow over the other (Figure 3.2 E). Finally, individual cells in one or both populations could infiltrate the other over time (Figure 3.2 F).

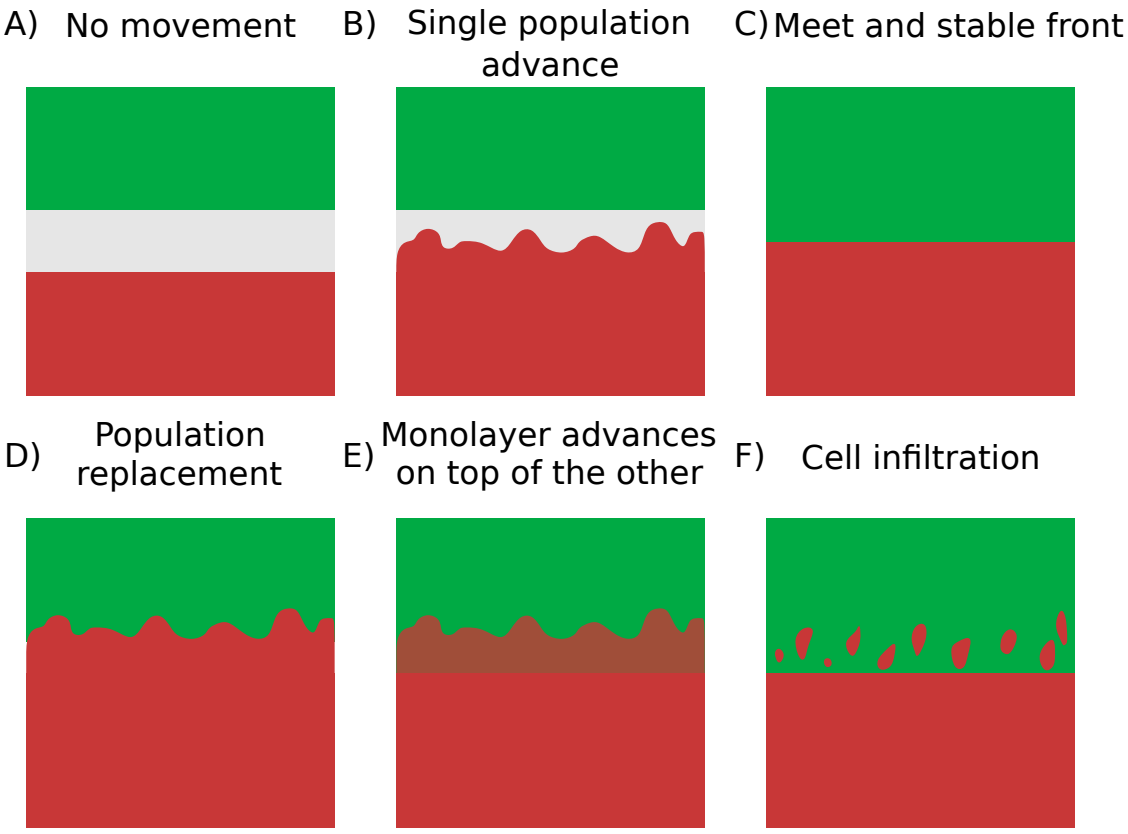

Figure 3.2: Possible population interactions types Summary of the different possible interactions between two different cell populations

Previously existing methods to analyse cell motion

The interest in using live imaging to do high-throughput screenings has increased during the last years [219] , [220], [221]. However, most of the efforts have been put in analysing individual cell behaviour [222] , [223], [224], [225]. In contrast, less efforts have been spent of studying collective motion in confluent monolayers. Most published methods to study individual cellular motion require of cell segmentation. This is not possible with cells in confluent monolayers. As a result, new methods had to be developed to study collective motion.

When the motion is symmetrical a summary of all the frames in the video can be made using a kymograph. A kymograph consists of a single row of pixels from each time point. This row has to be able to represent the symmetrical movement so is taken from the centre of the frame across the symmetry axis. Rows from each time point are then stacked to form a single image. This image captures

the movement across time. This method reduces the time needed to analyse the video but does not output any metrics which makes the comparison of different conditions and replicates difficult [226].

Another method called Particle Image Velocimetry (PIV) was originally developed for hydrodynamics. This technique calculates the correlation between subwindows of the image across different times. Then, it outputs the local displacement and from it the velocity and its direction [227]. PIV was recently adapted to cells in CIV (Cell Image Velocimetry). CIV works in wound healing assays with meeting monolayers [228]. Additionally, CIV can study distinct cell behaviours from subpopulations in the same monolayer [229]. Unfortunately, both methods need a high-quality imaging and prior knowledge of the motion behaviour. They are also not capable to study the behaviour of heterotypic monolayer interactions, highlighting the need for new algorithms to analyse the behaviour of heterotypic monolayer interactions.

3.3.6 MOSES analysis

In order to analyse the behaviour of heterotypic monolayer interactions, Dr Felix Y. Zhou (University of Oxford) developed an algorithm named MOSES. MOSES, an acronym for Motion Sensing superpixels, is a computer vision algorithm. MOSES analyses each fluorescent channel, corresponding to a cell population separately, overcoming limitations of biased analysis and image quality requirements of previously reported methods. In brief, MOSES uses as reference point the fluorescence patterns on each monolayer that vary stochastically (Figure 3.3 A). First, MOSES divides the frame at time 0 into 1000 regular areas known as superpixels (Figure 3.3 B) Each superpixel is linked with its four adjacent superpixels forming a mesh (Figure 3.3 C). MOSES is able to track superpixels through time by analysing the evolution of the stochastic intensity variation patterns in each monolayer (Figure 3.3 D). Then, the Optical flow average of the area in each superpixel is obtained (Figure 3.3 E). Optical Flow is a technique similar to PIV allowing MOSES to track superpixel changes [230] and [231]. This updates the superpixel new location and displacement. By repeating

the process over all the time points a superpixel track can be determined (Figure 3.3 F). The initial mesh linking of the superpixels gets deformed overtime as the motion parameters for each superpixel differ (Figure 3.3 G). This mesh deformation changes captures the local dynamics. Once finished, MOSES generates four distinct metrics for each fluorescent channel analysed. Both fluorescent channels, each corresponding to a cell population, are then correlated. From this analysis four metrics are extracted that explain the population interactions as described below:

Boundary formation index

The boundary formation index allows to quantify the motion in a given region and thereby allows to determine if motions get concentrated in a specific region. MOSES tracks will extend from the initial point to the end of the superpixel motion. If a boundary is formed, the end point of most motions will concentrate at that junction. The boundary formation index counts the quantity of track ends in a region. The higher the concentration of track endings the higher the chances of a boundary at that point.

Mesh stability index

Mesh stability measures the motion between neighbouring superpixels at a given timepoint. How far apart two superpixels that were adjacent at time t0 are at timepoint tn. If none of the cells moved or all moved at the same speed towards the same direction mesh stability would be 1. Values closer to 0 measure more stochastic behaviour.

Mesh order or strain

Strain measures the displacement vectors between a superpixel centroid (the centre of the superpixel area) and the four initially adjacent superpixel centroids. If the neighbouring centroids and the central one move equally, the strain score will stop increasing and plateau. Static superpixels will not separate their centroids from each other. The calculation is made across all superpixels and their cummulative

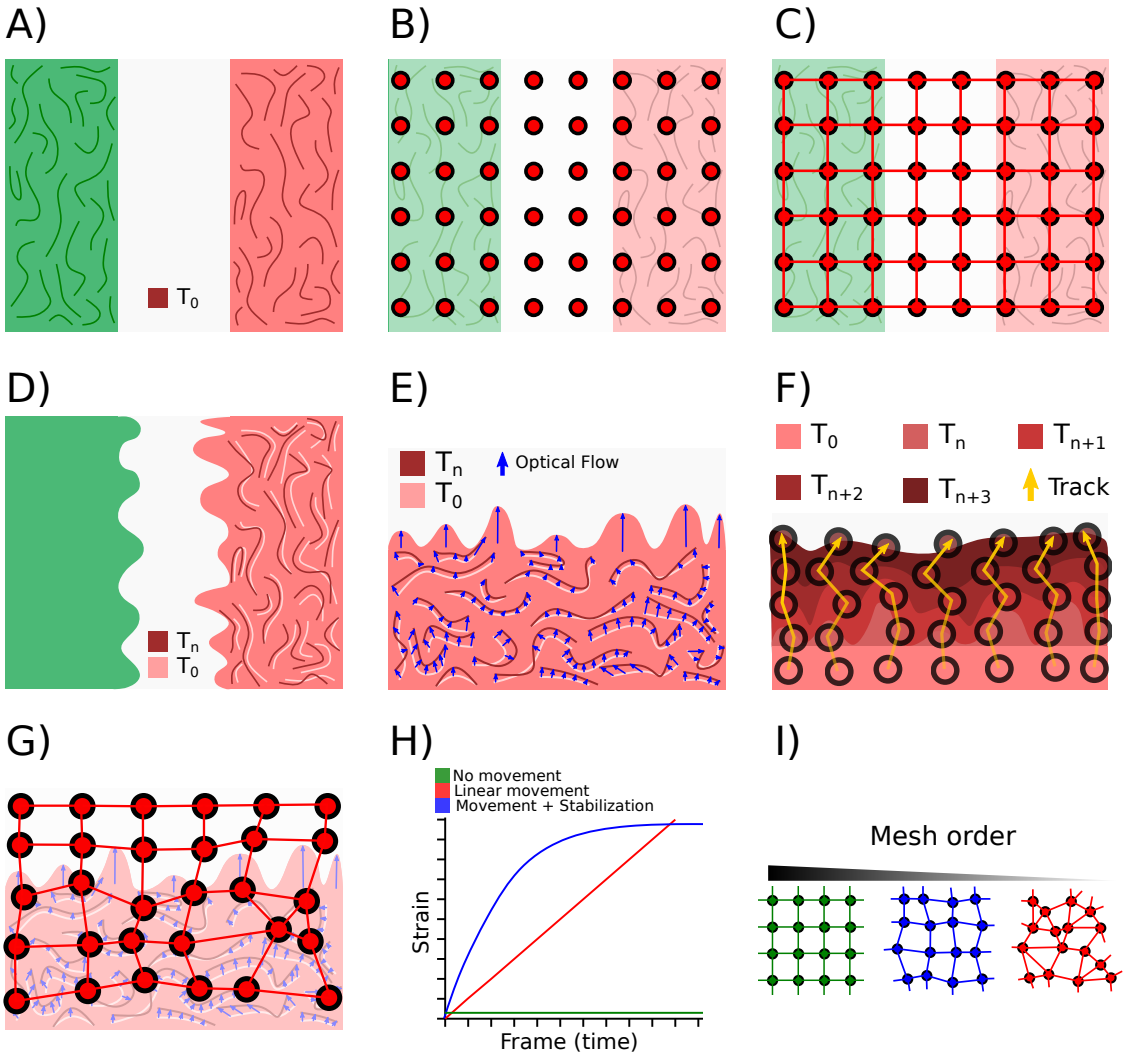

Figure 3.3: Summary of MOSES analysis A) Dyed cell monolayers have features and patterns derived from stochastic intensity changes. This patterns can be detected using computer vision techniques. B) At time 0 (first frame), the field of view is divided into 1000 superpixels. A superpixel a grouping of pixels into a bigger entity with a square area, in the image the centroid of the superpixel is represented. C) The centroids of each superpixel are connected to its four neighbouring centroids forming a regular mesh. D) At time "n" the cells move and the features in the monolayer follow this movement. E) MOSES compares the position in the field of view of the slightly translated features then calculates the optical flow change by extracting a local direction and velocity for the motion in that area. F) The superpixel centroid is moved by the average of the motion vectors in the area it is covering. By doing it every time point, MOSES is able to move the superpixel from frame one to the end frame. It keeps a record and calculates a track with the movement of that superpixel. Metrics like the local motion or the velocity cross-correlation use this track. G) superpixels moving apart over time disrupt the mesh. H) The more the mesh differs from the initial grid, the higher the strain metric outputted by MOSES. If the cells from a monolayer do not move during the experiment the strain will remain 0. The same will happen if all superpixels move in the same direction at the same speed. superpixels separating at constant speed would register as a linear increase in strain. In the absence of movement the strain of the mesh will remain constant forming a plateau in the strain graph. I) Three different mesh order states, this metric is inversely proportional to the strain metric.

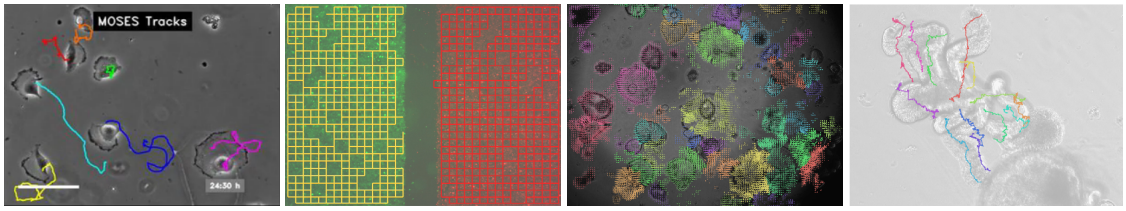

Figure 3.4: Uses of MOSES analysis in *In vitro* models
Besides its use to analyse population interactions, MOSES can also be utilized to study single cell behaviour, organoid growth, organoid branching and embryo development.

value is reported. Thus, strain works as a measure of stability across the field of view (Figure 3.3 H and I). Low mesh stability scores correlate with a high strain index.

Velocity cross-correlation

The Velocity cross-correlation measures how synchronized the motion between the two cell monolayers is. First, MOSES calculates the frame in which the two monolayers meet, or gap closure frame. The correlation before the monolayers meet is used as a baseline. The populations in each side of the boundary will have higher velocity cross-correlation if they are static. This correlation will be lower if a stochastic cell movement is present. Finally, this metric will score the lowest if one cell type is replacing the other as in this behaviour, both population velocities will be opposed.

Infiltration

MOSES can count the cells that infiltrate the other cell population by defining the boundary between the two populations. Then, it counts the fluorescence intensity from a population channel into the other population area.

MOSES can also be used to analyse motion in other experimental models. Besides heterotypic junction analysis this includes: individual cells, organoid growth and branching (Figure 3.4). Further detail for all the metrics can be found in Zhou & Ruiz-Puig et al [232].

	EPC2 - EPC2	EPC2 - CP-A	EPC2 - OE33	EPC2 - AGS	CP-A - CP-A	CP-A - OE33	OE33 - OE33	Total
5% FBS	17	30	20	2	2	6	3	80
0% FBS	16	16	16	0	0	0	0	48
								128

	0 ng/ml EGF	2.5 ng/ml EGF	5 ng/ml EGF	10 ng/ml EGF	20 ng/ml EGF	Total
5% FBS	8	4	10	9	9	40
0% FBS	6	4	6	5	4	25
						65

Figure 3.5: Summary of video number per condition Number of videos per condition used by MOSES to analyse population interactions.

3.4 Results

3.4.1 Experimental design

EPC2 cells were used to mimic the healthy squamous epithelium *in vitro*. By combining them with other cell types three stages of BO progression were mimicked. The EPC2 cells were combined with themselves to have a negative control of junction formation. Then, with CP-A to mimic the interaction between squamous and BO cells. Later, with OE33, an OAC derived cell line with EGFR amplifications. Finally, with AGS cells, a gastric adenocarcinoma derived cell line with wt EGFR [233] and a truncating mutation in E-cadherin [234] (Figure 3.6 A).

A summary of the videos analysed with MOSES to study cell interactions and EGF effect on BO segment growth can be found in Figure 3.5.

The cell types from each combination were labelled using Celltracker dyes and seeded using a divider (Figure 3.6 B). After O/N incubation the divider was removed, and the interaction filmed for either 4 or 6 days.

3.4.2 Oesophageal squamous and Barrett's oesophagus cells form a stable junction *In vitro* in the absence of EGF

Each of the cell combinations displayed distinct behaviour. EPC2-EPC2 cells joined in a single monolayer. In the EPC2-CP-A combination, the BO cells advanced pushing back the squamous cells during the first days. After approximately 72 hours the motion stops, and the junction remained stable. Finally, the combination of EPC2 and OE33 had the tumour cells with the EGFR amplifications advance

during all the time points. In this combination the squamous cells are replaced at a constant rate.

These interactions were interpreted first by using a kymograph (Figure 3.6 C). MOSES was then used to obtain the metrics. In the EPC2-EPC2 combination chaotic movement can be observed as the meshes overlap because the two populations oscillate up and down coordinately. The columnar cells in the EPC2-CP-A combination advance gradually during the first 72 hours. After this, the junction stabilizes and no movement can be observed. Finally, the EPC2-OE33 combination shows the tumour cells replacing the squamous cells completely (Figure 3.7 A). After extracting the strain curves for each of the videos, a principal component analysis on them can summarise the results. This dimensionality reduction technique groups the different repetitions of the experiment together. The clustering indicates different behaviour in each cell combination and low variability and reproducibility between repeats (Figure 3.7 B).

3.4.3 Serum free medium prevents collective cell behaviour in our model

During the experiments the medium used was a 1:1 dilution of the keratinocyte serum free medium, used to culture the immortalized cells, and RPMI with 10% FBS. As a result, 5% of the volume in the medium was fetal bovine serum. When cultured in the absence of serum the interactions of the cell populations changed. The different combinations interacted similarly losing their signature behaviour.

To explain this phenomenon, immunofluorescent staining of the cells in FBS presence and absence was performed. The lack of FBS prevented the formation of cell-cell adherent junctions as shown by E-cadherin staining [235]. This resulted in a change of the actin distribution across the cell, being less concentrated at the cell membrane as a result (Figure 3.8 A). This lack of cell-cell interactions derived in a disruption of the collective behaviour. This can be measured by a reduction of the motion correlation between neighbouring superpixels (Figure 3.8 B and C). This difference in behaviour affects also the strain curves derived from the MOSES

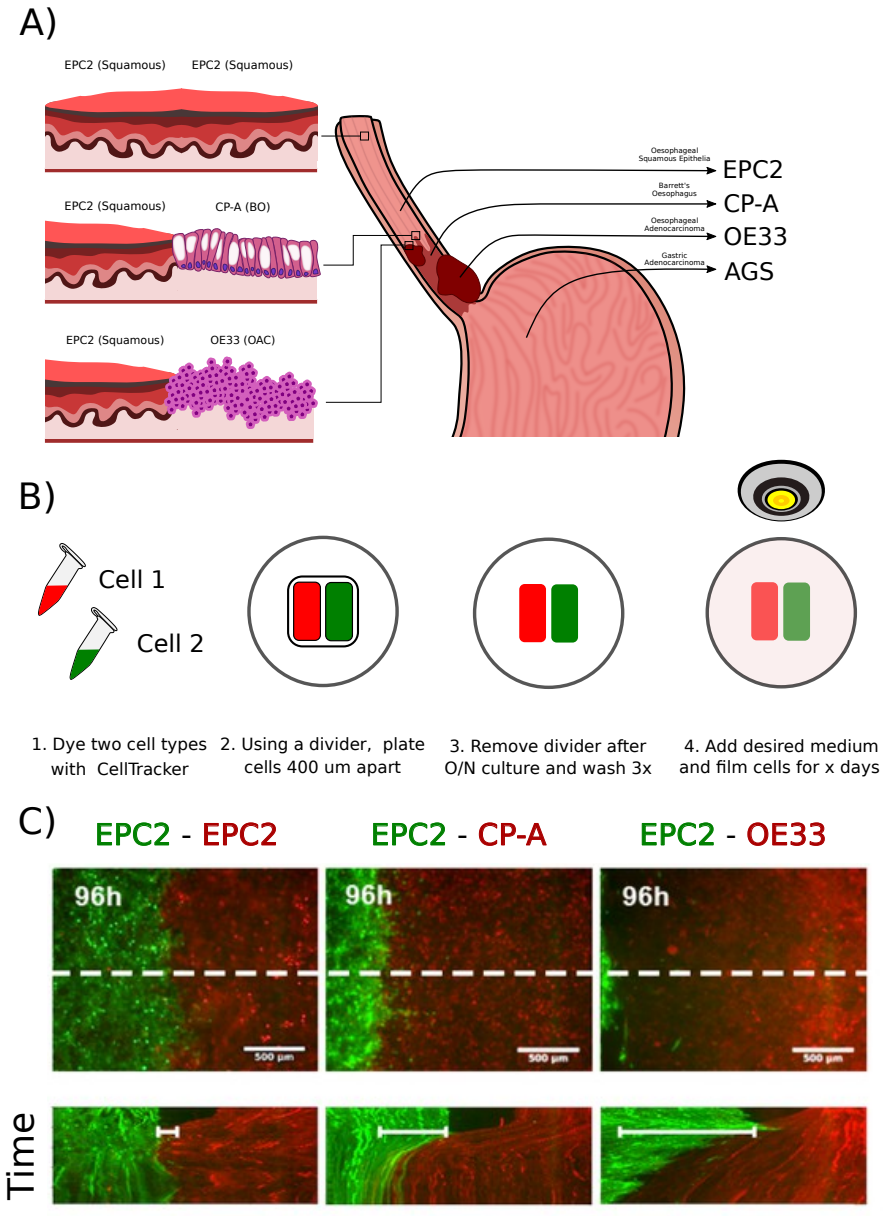

Figure 3.6: EPC2 and CP-A form a stable junction *In vitro* A) We used our model to study three epithelial population interfaces: normal oesophagus (EPC2-EPC2), the squamous-BO junction (EPC2-CP-A), and OAC invasion of the healthy squamous epithelia (EPC2-OAC). The right panel shows the anatomical original for each cell line used in this chapter. B) Experimental design for the heterotypic junction experiments. Two cell types were labelled with fluorescent dyes. Then, using a divider plated at 400 um distance from each other the plate interaction is filmed for 4 to 6 days. C) 96-hour frame for the three cell combinations. By taking a 1 pixel wide section of the centre of each frame and stacking together, we can summarize the video into a kymograph. The kymographs show a small displacement in the EPC2-EPC2 mix. A moderate advance from the BO cells followed by stabilization when combining EPC2-CP-A and a continuous linear advance of the OAC cells in the EPC2-OE33 combination.

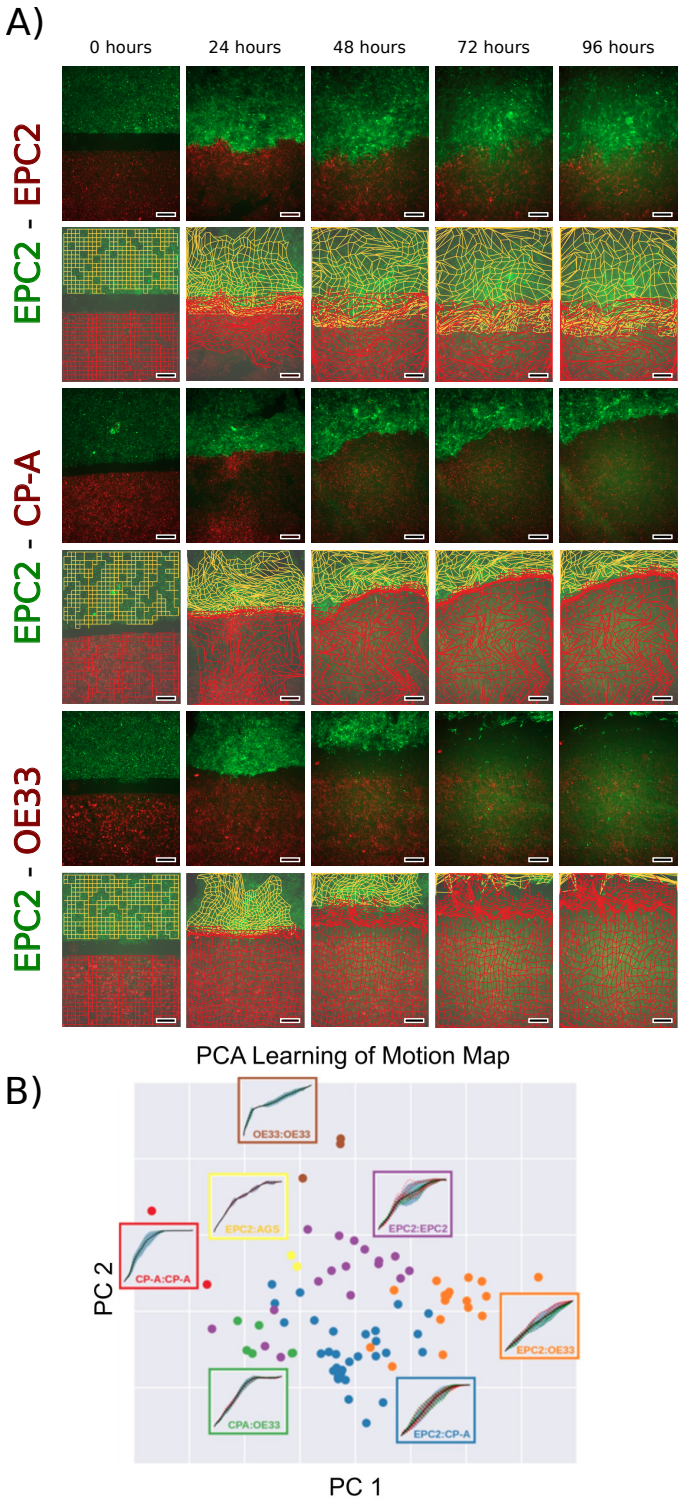

Figure 3.7: MOSES analysis of the three combination in our model A) Frames for 0, 24, 48, 72 and 96 h of EPC2-EPC2, EPC2-CP-A and EPC2-OE33 combinations and MOSES generated mesh. EPC2-CP-A is the only combination that generates an stable junction and the EPC2-OE33 cancer cells continue progressing during all the video length as can be seen by the red mesh. B) Principal component analysis (PCA) of the strain curves for each combination. The PCA is able to cluster the different cell combinations. Scale bar: 500 um

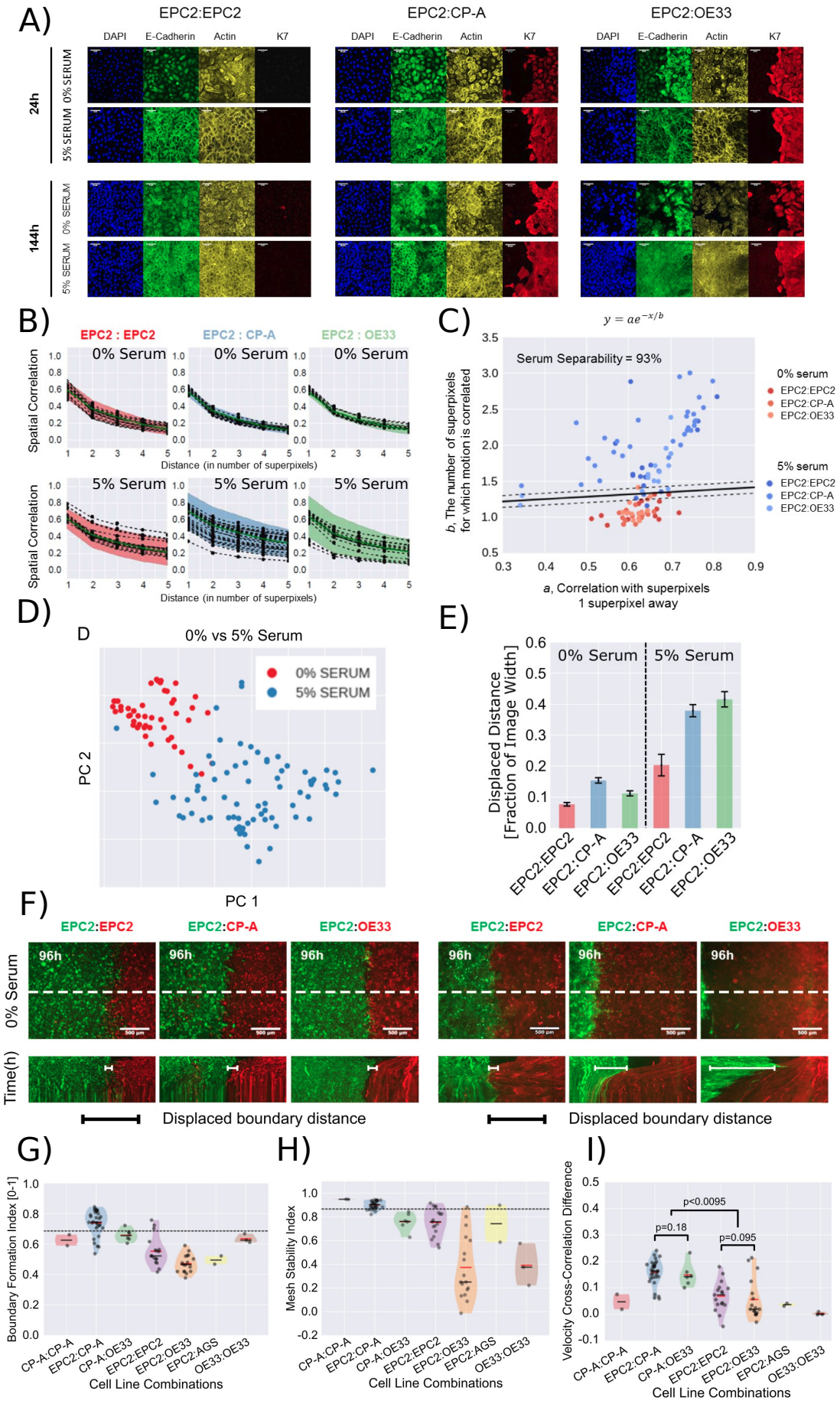
A)
EPC2:EPC2
EPC2:CP-A
EPC2:OE33
DAPI
E-Cadherin
Actin
K7
24h
144h
0% SERUM
5% SERUM
B)
EPC2 : EPC2
EPC2 : CP-A
EPC2 : OE33
0% Serum
5% Serum
Spatial Correlation
Distance (in number of superpixels)
C)
$y = ae^{-x/b}$
Serum Separability = 93%
b, The number of superpixels for which motion is correlated
a, Correlation with superpixels 1 superpixel away
0% serum
5% serum
EPC2:EPC2
EPC2:CP-A
EPC2:OE33
D)
D
0% vs 5% Serum
0% SERUM
5% SERUM
PC 2
PC 1
E)
Displaced Distance [Fraction of Image Width]
0% Serum
5% Serum
F)
96h
0% Serum
Time(h)
Displaced boundary distance
G)
Boundary Formation Index [0-1]
H)
Mesh Stability Index
I)
Velocity Cross-Correlation Difference
p<0.0095
p=0.18
p=0.095
CP-A:CP-A
EPC2:CP-A
CP-A:OE33
EPC2:EPC2
EPC2:OE33
EPC2:AGS
OE33:OE33
Cell Line Combinations

Figure 3.8:

..

Figure 3.8: Serum free medium prevents collective behaviour A) Confocal microscopy immunofluorescence staining for E-cadherin and actin. Serum-free media prevents the formation of adherent junctions. B) Graphic showing the decay in the correlation (y-axis) between superpixels as the distance increases (x-axis). The curves decay faster and reach lower levels in serum-free conditions. each dotted line represents an experiment. Graphic C) summarizes this information. First, plotting how correlated adjacent superpixels are (x-axis). Second, what is the maximum amount of superpixels in which correlation is still higher than a threshold. This plot separates serum and serum-free conditions well. D) Clustering between both conditions can also be achieved by doing a PCA analysis on the strain curves of each experiment. E) Graph plotting the mean displaced distance in each condition. As seen also in the kymographs (F), the displaced distance is reduced in serum-free conditions. The reduced displacement could be linked to the lack of collective motion. G) Violin plot of MOSES boundary formation, mesh stability (H) and velocity cross-correlation (I) indexes. The black dotted line is the mean of that index for the experiments under serum-free medium. The EPC2-CP-A combination is the only one showing higher boundary, stability and velocity cross-correlation indexes than conditions lacking collective motion.

meshes. This can be seen when representing the strain curves as a PCA (Figure 3.8 D). The dimensionality reduction technique separating both conditions.

A kymograph comparison shows that serum-free conditions affect cell migration, making the displacement after gap closure marginal. (Figure 3.8 E). This can also be seen when plotting the distance displaced in each condition as an histogram (Figure 3.8 F). As the serum free condition prevented any collective motion behaviour, we used them as a reference baseline for the interactions occurring when a 5% serum is present. Notably, EPC2-CP-A combination was the only having boundary formation index above the threshold when using serum free conditions as baseline (Figure 3.8 G). This was also true for mesh stability (Figure 3.8 H). Taken together both metrics confirm that EPC2-CP-A is the only combination forming a stable junction. This stability translates in this combination having the higher velocity cross-correlation (Figure 3.8 I).

3.4.4 Gastric adenocarcinoma cell line behaviour differs from OAC cell lines

To further test the effect of the lack of cell-cell junctions in collective motion, the squamous cell line EPC2 was combined with the gastric adenocarcinoma cell line

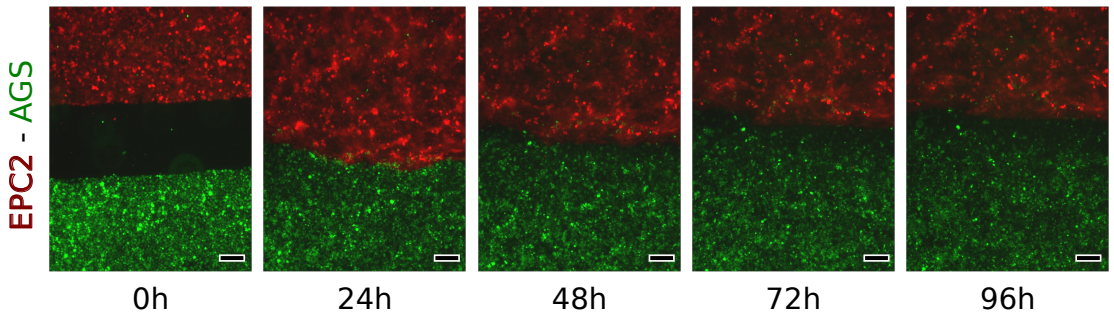

Figure 3.9: Gastric adenocarcinoma cell line and EPC2 co-culture Frames at 0, 24, 48, 72 and 96 hours of the co-culture combining the gastric adenocarcinoma cell line AGS and the squamous epithelium cell line EPC2. After 72h the junction between the AGS and EPC2 cells remains stable as when combining it with the BO cell line CP-A. Scale bar 500 um.

AGS. Besides coming from a different adenocarcinoma type, AGS present two differences with the OAC cell line OE33: First, its EGFR is neither mutated or has copy number variations [236]. Second, AGS cells have a mutation in E-cadherin preventing the formation of cell-cell junctions [234]. Because AGS is unable to form cell-cell junctions the same lack of collective behaviour seen in serum free medium was expected even when cultured in 5% serum. As predicted, after 72h the cells stayed in place and did not continue replacing the squamous epithelium. This result is opposite to the one seen with the other cancer cell line (Figure 3.9).

3.4.5 The use of fluorescent dyes changes cell behaviour under serum conditions but is not colour specific.

The dye used to label our cells could have toxicity affecting the phenotype shown during the interactions. Testing dye toxicity was needed to ensure the dye did not have a notable impact on the results. The experiments were repeated with unlabelled cells or switching the dye colors between cell line. In serum-free conditions there was no difference in the mean squared displacement. In 5% serum conditions we found that both EPC2 and OE33 cells migrated significantly slower when dye was added. Yet, in EPC2 that difference was significant but not important. Change of dyes caused no behaviour differences (Figure 3.10).

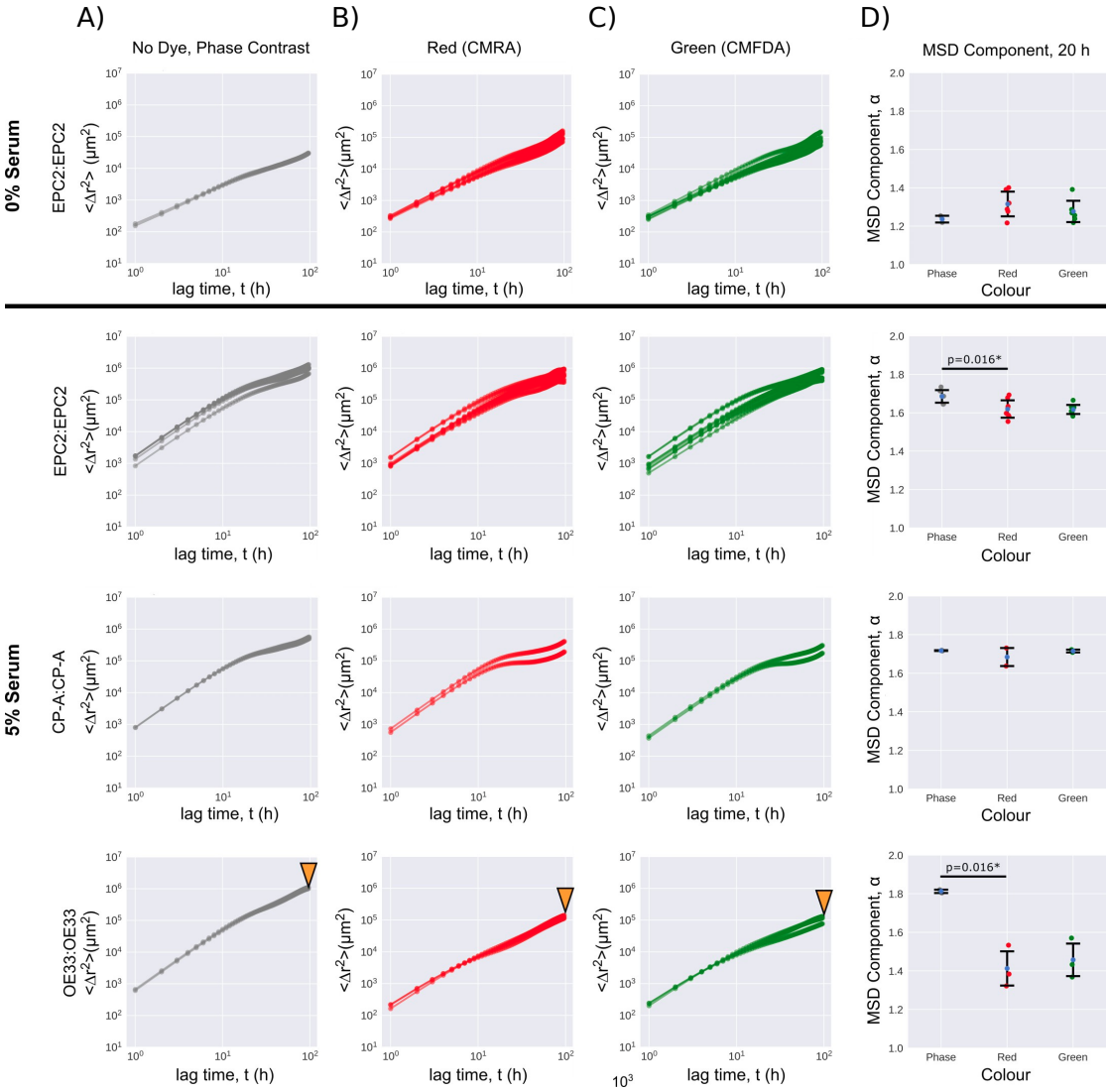

Figure 3.10: Studying dye toxicity across the cell combinations Mean squared displacement (MSD) curves computed from optical flow. Plotted on a log10-log10 axis as a function of the time interval for same cell line combinations in 0% and 5% serum. A–C) MSD curves coloured grey for phase-contrast non-dyed A), red for red-dyed B) and green for green-dyed cells C). D) Error bar plots showing mean extracted exponent alpha from MSD plus/minus one standard deviation. The plots take into consideration the 20 first hours. Each point is an experiment repeat. Two sided t-test was applied assuming identical variances. * denotes $p = < 0.05$. Red and green lipophilic dye reduced the mobility of non-dyed EPC2 and OE33 cells with statistical significance. The size effect was particularly large in OE33, (bottom row marked with orange triangles) with a large drop in the MSD exponent.

3.4.6 High EGF concentrations can disrupt the squamous-columnar junction stability and increase the columnar segment length *In vitro*

The combination of squamous and BO cells *in vitro* formed a stable junction. This junction stability was not changed by dye toxicity. As discussed in the introduction, the formation of a stable junction is also observed *in vivo*, with BO length rarely changing over the course of years. In this section, the hypothesis formulated in the introduction is tested. Can the high EGF concentration that might be contained in the reflux disrupt this junction and enlarge the BO segment? The hypothesis was tested by doing an EGF titration on the junctional model.

The EPC2-CP-A combination was cultured with either low or high EGF concentrations. This concentration levels were based in the *in vivo* EGF concentrations described in the introduction. Low concentrations, 0 and 5 ng/mL, are close to the concentration found in saliva and healthy epithelium. High concentrations, 10 and 20 ng/mL, are similar to pancreatic and duodenal levels respectively.

In vitro, only high EGF concentrations could disrupt junction stability. Under the high EGF conditions, the BO cell line CP-A was able to replace all the squamous EPC2 cells. This was captured by MOSES mesh analysis with the CP-A cells behaving like OE33 and replacing the squamous epithelium after the initial 72 hours. Conversely, under low EGF concentration the columnar cells form stable junctions as in the basal experiments (Figure 3.11).

A deeper analysis of the MOSES meshes can better describe the changes seen using different metrics. First, a significant gradual increase in final displaced distance can be observed. Achieving values similar to the OE33 control combination (Figure 3.12 A). The average movement speed increases as shown by two metrics, average speed and average velocity order (Figure 3.12 B and C). Without junctional stability, both the boundary formation index and the velocity cross-correlation reduce gradually, achieving levels close to EPC2-OE33 (Figure 3.12 D and E). Interestingly, although the mesh stability index reduces, it does not become as chaotic as when the cancer cell line OE33 was involved. This higher mesh stability

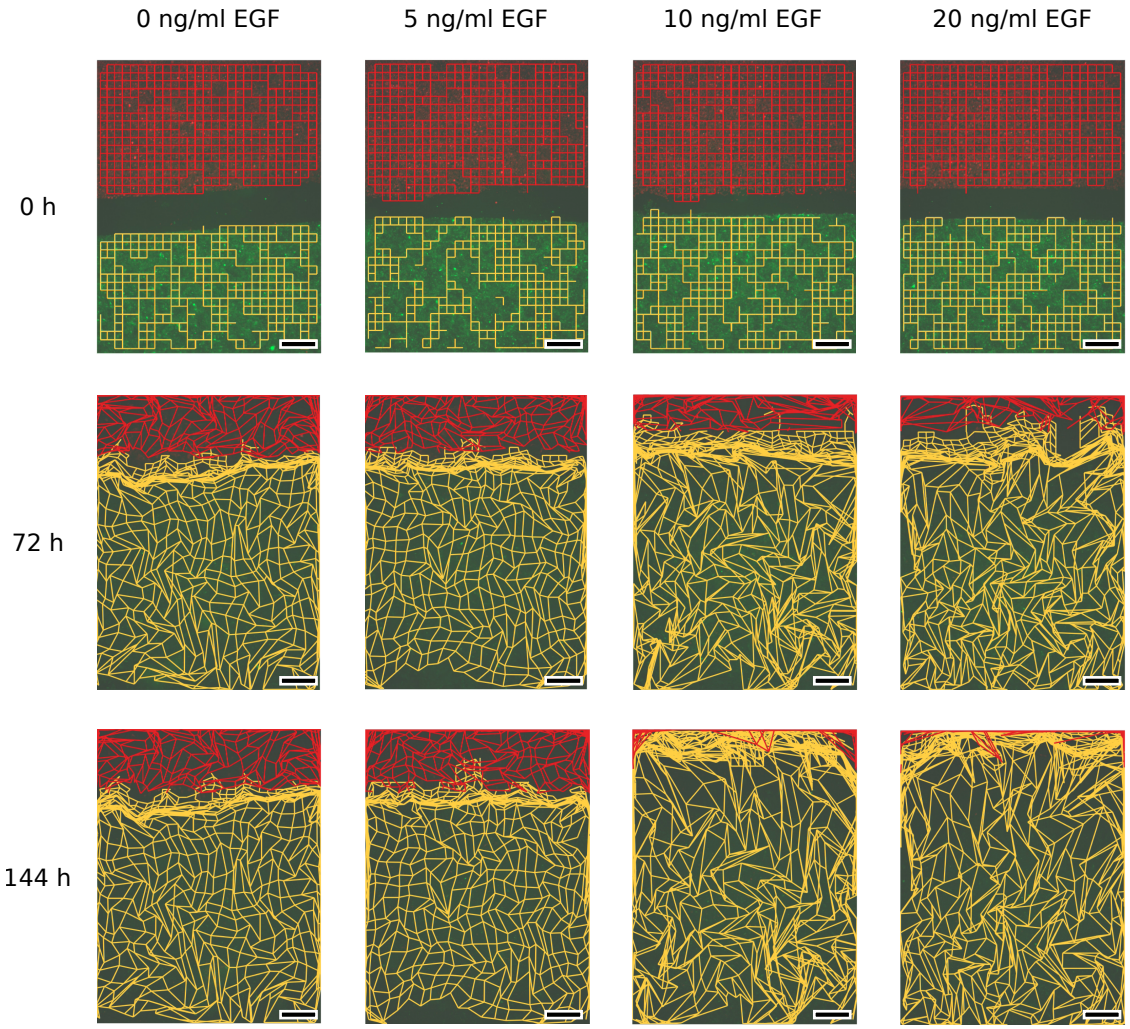

Figure 3.11: MOSES mesh analysis of EGF titration MOSES meshes for frames at 0, 72 and 144 hours during the EGF titration at 0, 5, 10 and 20 nG/mL. Concentrations up to 5 nG/mL do not change basal behaviour, after 72h a stable junction forms. Concentrations of EGF of 10 nG or higher prevent junction stabilization between EPC2 and CP-A cells. This allows the columnar cells to replace the squamous monolayer. Scale bar 500 um.

indicates a more cohesive collective motion (Figure 3.12 F and G). This behaviour suggests that EGF levels in reflux do not necessarily give a cancer-like phenotype to BO cells. The gradual approach of the EPC2-CP-A combination to EPC2-OE33 is captured in their strain curves. As EGF levels increase, a gradual decrease in the plateau happens, indicating a decreasing degree of stability (Figure 3.12 H). Then the strain curves titration experiments were added to the PCA made with basal conditions. The location of these experiments moves from the EPC2-CP-A zone to the EPC2-OE33 area as EGF increases (Figure 3.12 I).

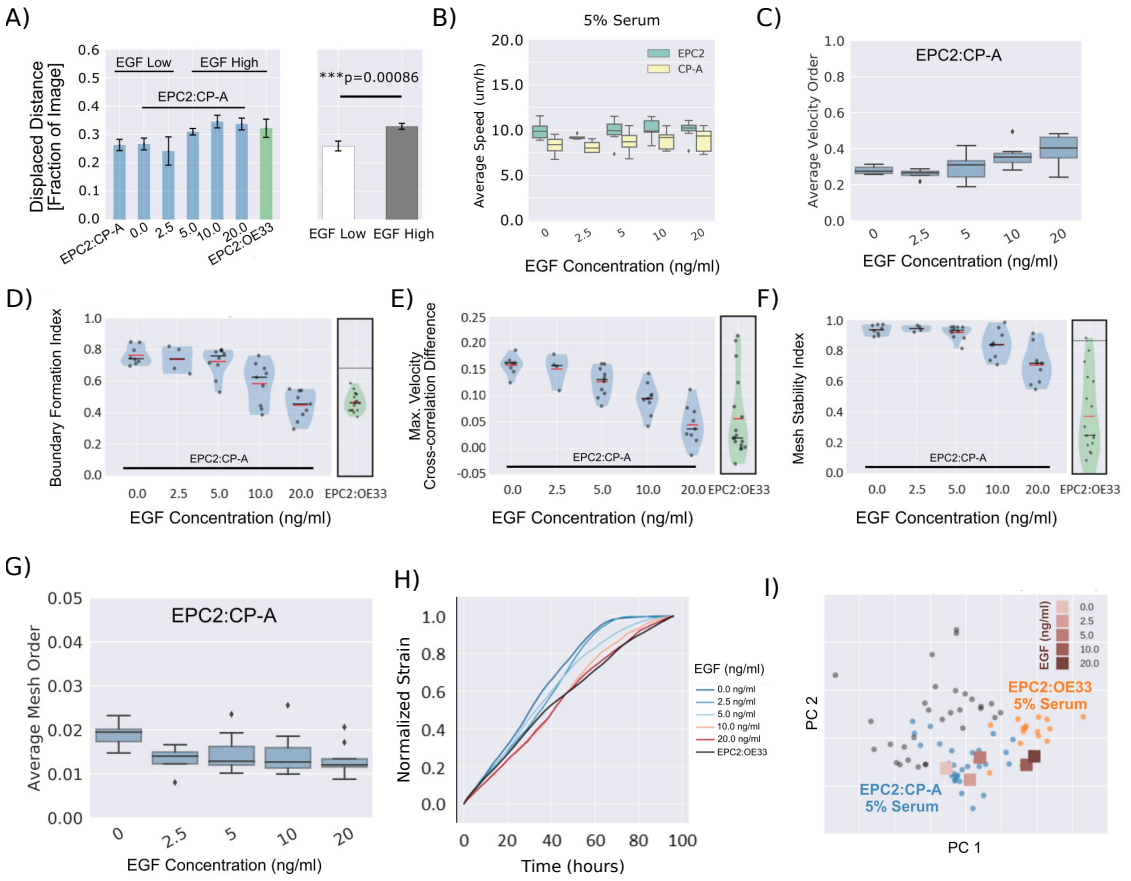

Figure 3.12: MOSES metrics analysis of EGF titration A) Graph showing the increase of mean displaced distance as EGF levels increase (left). The difference between the mean displaced distance in low and high levels is significant (right). B) Boxplot graph showing increase in the average as EGF concentration augments (C) Graph with the average velocity order. Summary of the graph in B taking both cell lines into one metric. D) Violin plot with boundary formation index values. With higher EGF levels the index decreases gradually. It arrives finally reaches values close to the EPC2-CP-A combination. E) A violin plot showing the same trend with velocity cross-correlation. F) Violin plot showing mesh stability trends. As EGF levels increase the mesh stability index decrease but never reaching the EPC2-OE33 combination level. I) Superposed strain curves for each condition. As EGF concentration rises, the strain curves stop plateauing. The strain curve for 20 nG/mL EGF and the EPC2-OE33 combination showing similar trends. H) PCA analysis of the EGF titration experiments on top of the basal condition cell combinations. As shown in the strain curves, the experiments become less similar to EPC2-CP-A as EGF increases. The higher EGF concentration experiments clustering closer to the EPC2-OE33 combination. Scale bar: 500 um

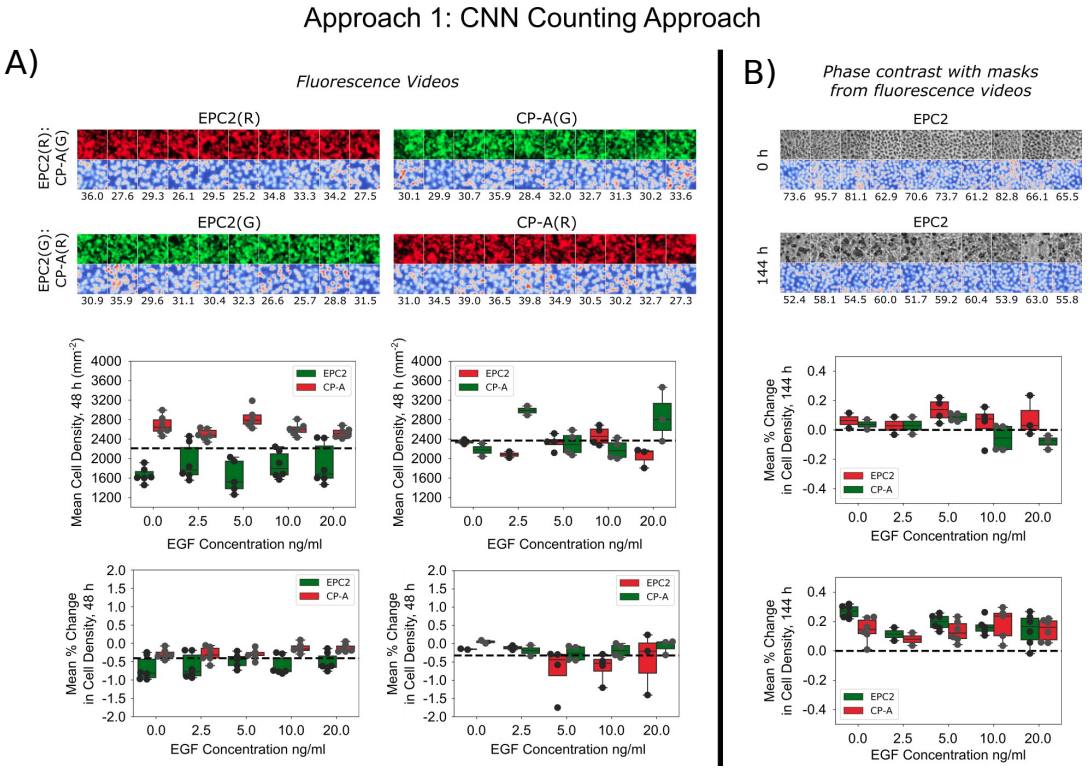

Figure 3.13: Calculating cell proliferation using a CNN Cell counting using the fluorescent channels (A) and the phase contrast channel. Both approaches show a stable cell density (middle panel) and cell density increase as a percentage of total cell population (lower panel).

3.4.7 Columnar invasion of the squamous lining *In vitro* is not determined by cell proliferation

As mentioned in the introduction, EGF increases both migration and cell proliferation. To see which of the two behaviours promoted the junction, the proliferation in each monolayer was studied. Dr Felix Y. Zhou (University of Oxford) used two methods to predict cell proliferation using the videos produced.

In the first approach, cell proliferation was analysed by counting cells in each frame. This was achieved using a convolutional neural networks (CNN), a machine learning approach. In CNN the algorithm learns how to count the cells in the monolayer by looking at annotated data. This approach was used in the fluorescent and phase-contrast channels (Figure 3.13 A and B). In both channels, cell density and mean cell density change remains unchanged in all conditions.

The second approach consisted in studying fluorescence decay over the frames. Cells with higher proliferation rates would have a higher fluorescence decay over time. This happens because the initial dye distributes over the two new cells during cell division. Figure 3.14 A, B and C show the fluorescence intensity decay for both EPC2 and CP-A cell populations over time. This is summarised in the figure 3.14 D and E, with the colour gradient from dark to light indicating time. After doing linear regression, the algorithm computes the proliferation coefficient. Figure 3.14 F and G show the proliferation coefficient with changed dyes. No significant proliferation coefficient changes happen with an increased EGF concentration. Both approaches showed a lack of correlation between EGF concentration and cell proliferation. This suggests that the behaviour change with EGF concentration depends on migration.

3.4.8 Inhibition of EGFR using lapatinib prevents the invasion of BO and OAC derived cell lines *In vitro*

.

The results suggested that EGF was able to enlarge the segment length *In vitro*. To see if EGFR inhibition could cause the opposite effect, the EGFR inhibitor lapatinib was used. In EPC2-CP-A combination, lapatinib stabilized the junction sooner. Instead of having an initial columnar invasion, stabilization occurred where the cells met. Interestingly, the same result happened in the EPC2-OE33 combination when lapatinib was present with higher inhibitor concentrations preventing OE33 advance, forming a stable junction. However, cell death could be seen at 5 um concentration suggesting toxicity at lower concentrations could be responsible for the reduced migration observed in the experiment (Figure 3.15 A).

3.4.9 Deoxycholic acid does not produce the same effects as EGF presence in the medium

The effect of the most commonly studied bile acid, DCA, was tested as well. As it was previously described to activate EGFR, a similar effect to EGF was expected. To study the effect of DCA, three different conditions, 5 uM, 50 uM and 500 uM concentrations were used. None of the concentrations increased columnar

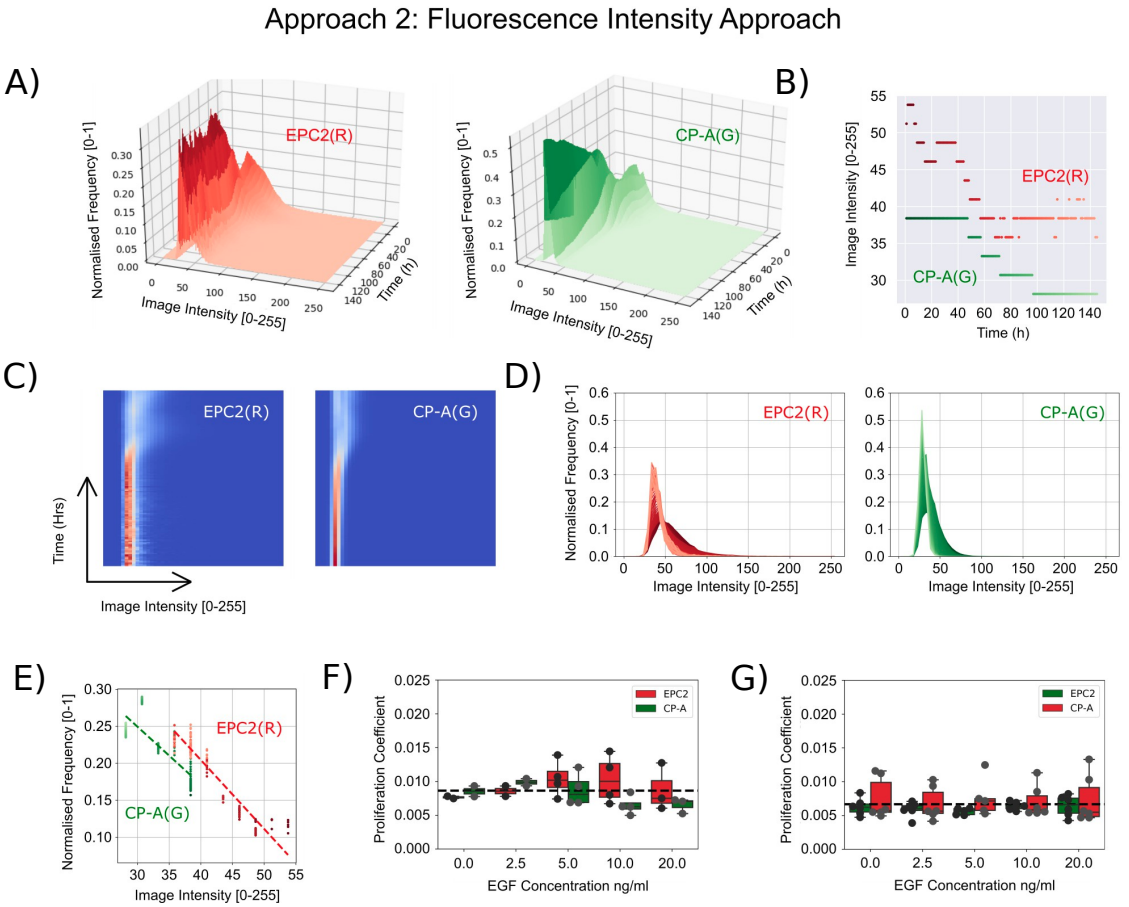

Figure 3.14: Cell proliferation prediction through dye decay A) 3D graph showing the abundance of each fluorescent intensity value as time progresses for EPC2 (red) and CP-A(green). B)Graph summarizing this information in 2D. The most frequent intensity (y axis) for each time point (x axis). The graph shows a intensity decay that can be summarized as a heatmap (C) and a histogram (D). From this information a linear regression of the intensity decay can be obtained (E). From it, the proliferation coefficient is calculated. This proliferation coefficient does not change during the EGF titration. This lack of effect is shown in both dye combination, EPC2(red)-CP-A(green)(F) and EPC2(green)-CP-A(red)(G).

replacement of the squamous cells. The highest concentration, 500 um killed the cells after a few hours (Figure 3.15 B).

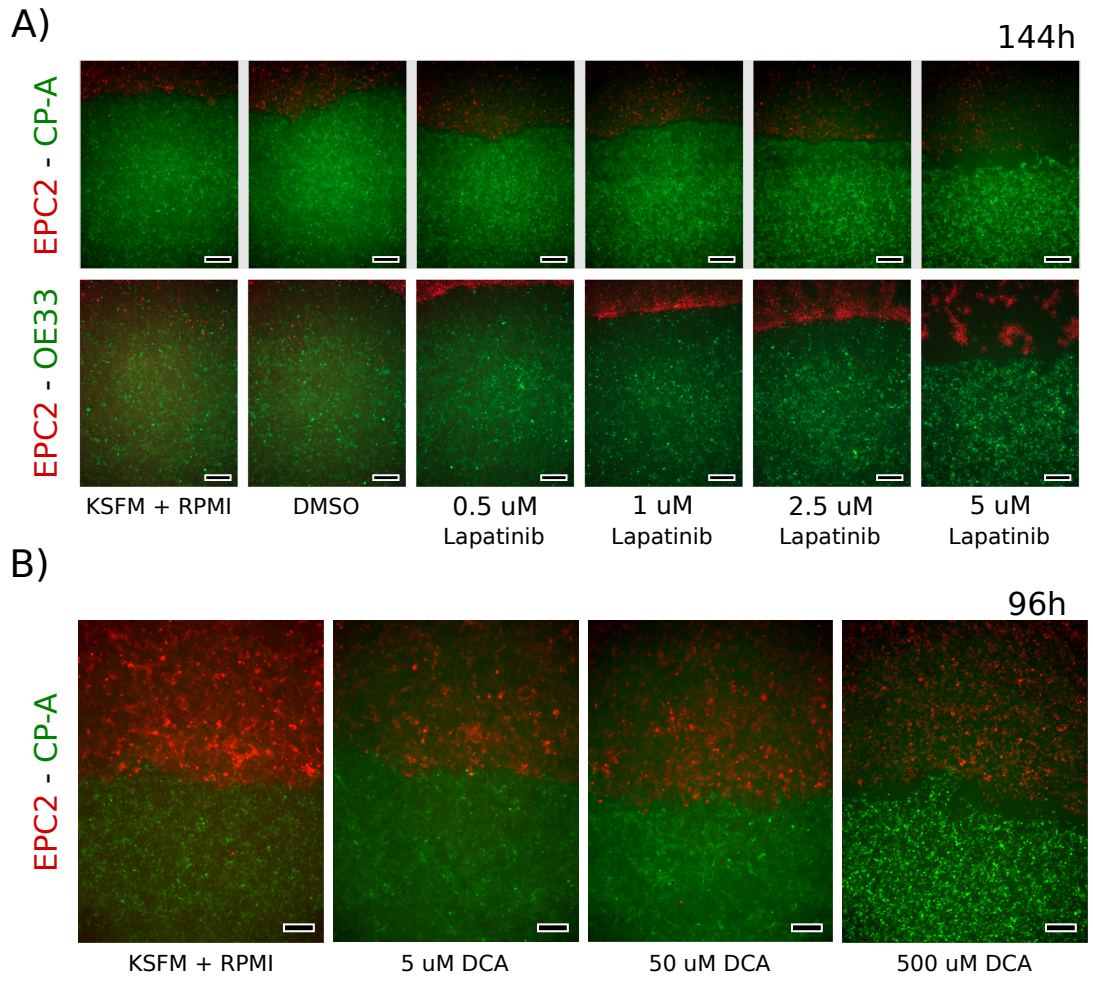

Figure 3.15: Lapatinib and Deoxycholic acid effect on junction stability A) Last frame at the 144 h time point of EPC2-CP-A (higher panel) and EPC2-OE33 (lower panel). In both the stable junction between the columnar and squamous cells forms closer to the meeting point as lapatinib concentration increases. Concentrations of 5 uM or higher induce cell death. B) DCA titration does not increase CP-A replacement of the EPC2 cells. The 500 uM concentration induced cell death after a few hours. Scale bar 500 um.

3.5 Discussion

3.5.1 The combinations selected produce three different interaction phenotypes

In this chapter, a model to study the interaction between the oesophageal squamous cells and premalignant BO is introduced. The aim was testing whether EGF levels in the reflux could affect BO segment length. High EGF concentrations can be brought to the oesophagus from the duodenum. There, the low acidity of the

stomach contents would activate the Brunner's glands EGF secretion. Alternative sources of EGF like the OSG or existing BO segments could be activated through similar mechanisms. BO cells would benefit from EGFR activation mediated by EGF and continue expanding, this expansion lasting until the EGF gradient reduces to healthy oesophagus levels. By understanding the EGF role, new strategies to reduce BO segment length in patients could be developed. This could lower OAC incidence as shorter segments are less prone to malignancy [91].

The first step was to replicate three physiologically relevant conditions *in vitro*. The absence of a junction, a stable squamous-columnar junction and replacement of squamous cells. In this *in vitro* model, these conditions corresponded to three cell combinations. First, the EPC2-EPC2 combination were the two populations formed a junctionless monolayer. Second, EPC2-CP-A, were squamous and premalignant BO cells form a stable junction. Finally, EPC2-OE33, where the tumour cells replace the squamous lining at a constant rate. Interestingly, OE33 has been reported to have already EGFR and HER2 amplifications. We also used AGS cells, derived from a gastric tumour. AGS cells are not reported to have mutated EGFR and invasive phenotypes, as observed from the OE33 cells were not observed. However, cell lines vary between each other in several pathways. Therefore, the differences in phenotypic behaviour between OE33 and AGS cannot be attributed to their different status in the EGFR pathways alone. Further, AGS cells are also known to have mutations in E-cadherin, preventing them from forming cell-cell junctions. This could be an alternative explanation for the differences in behaviour as cells cultured using serum free medium also lacked E-cadherin junctions and behaved similarly.

In this model, the combination between the immortalized squamous cells (EPC2) and the premalignant BO (CP-A) was our baseline. *In vivo*, Barrett's oesophagus length remains stable. The junction formed in our model was also stationary. Interestingly, a short period of columnar cells displacing the squamous happens before junctional stability is reached. A possible explanation is the presence of 2.5 ng/mL EGF in the KSFM medium. Yet, during the EGF titrations, the 0 ng/mL experiment had the same phenotype as when EGF levels were not considered. This

suggests that the signalling between populations needs time to stabilize the junction. This signalling is likely to work through mechano-transcription pathways [237]. It is also possible that squamous cells need more time to strongly attach to the culture plate. The area lost by the squamous cells would then be the initially gained when moving unopposed. Another possibility is that thickening of the squamous epithelia is needed. The epithelial thickness might be closer to the centre of the original area of the divider were the squamous cells were plated. As observed *in vivo*, once the junction between squamous and BO populations is established in the model, it remains stable indefinitely.

After setting-up a system to study the effect of the interaction of two homogenous cell monolayers, behaviour of the celltracker dyes used to mark cells of different origins was tested. The dye had negligible toxicity in the squamous cells and a moderate one in OE33. This toxicity has been reported in previous experiments [238]. The dye had no observable effects in the BO cells. However, the observed toxicity was not considered a major issue for two reasons. First, the interaction behaviour was comparable to the experiments without dye. Second, OE33 was needed as a control for squamous cell replacement. The OE33 cells were able to replace the squamous lining even when dyes were used. Thus, this combination still fulfilled its function as a control. However, this toxicity could become a bigger issue in the future experiments when using primary cells or other cell lines. Alternatives like viral transfection of flurescent markers could be utilized if this problem persists.

3.5.2 *In vitro* results with *In vivo* EGF concentrations suggests EGF in reflux can influence BO length

Next, the effect of EGF on the formation of stable cell junction was tested. EGF is likely to be present in the reflux, as high levels of this growth factor are reported in the duodenum. Like the bile acids, gastroduodenal reflux could carry EGF to the squamous mucosa. No recent reports on the concentration of EGF in reflux have been published which indicate local EGF levels in the oesophagus prior to reflux. In the oesophagus, EGF concentrations are 2 ng/uL of juice, with a slightly

higher concentration of 3 ng/uL in the saliva. Due to interpersonal variability, oesophageal concentration might be higher in some patients. To account for this both 0 and 5 ng/uL concentrations were used. Both concentrations were labelled as low as no changes were predicted at these levels. If those concentrations did promote BO segment growth, BO would replace the squamous lining across all the oesophagus. As predicted, low concentrations were not able to affect junction stability in the *In vitro* model.

The concentrations predicted in the reflux were tested next. The high concentrations were established as 10 to 20 ng/mL EGF. These values are comparable to the concentrations in the pancreatic juice (8.5 ng/mL) and the duodenal lumen (21 ng/mL). Arguably, these concentrations should be lower as the volume in the stomach is larger and duodenal contents might get diluted there. Additionally, low pH might cleave EGF, reducing its activity [239]. Conversely, GORD patients might have higher EGF concentrations in the duodenum. This could be triggered by lower pH in the duodenal lumen, activating a compensation mechanism. The mechanism will increase EGF to inhibit acid secretion [240]. This compensation mechanism might be working as well on the OSG and pre-existing BO epithelium. Taken all together, the prediction of EGF levels in the reflux becomes difficult in the absence of systematic studies measuring EGF levels in reflux in humans. Interestingly, even the lower end of the high concentration range was able to destabilize the junction. This suggest that EGF levels in the reflux might be high enough to promote BO segment expansion.

EGFR and ERBB2 copy number amplifications are common in BO. This protein levels are even further increased during BO dysplastic to OAC progression [241]. In OAC more than 83% patients have receptor tyrosine kinase amplifications [197]. Clones with mutations or copy number alterations increasing EGFR signalling might outcompete neighbouring clones. Successful clones will be more likely to acquire further mutations which potentially trigger malignancy. Taking this into consideration, BO clones under high EGF levels could be using the same advantages to outcompete the squamous cells.

In vivo, EGF levels are likely to vary with reflux episodes. Yet, in the experiments, EGF was kept constant. It would be interesting to check if EGF can also disrupt the junction once it is already formed *in vitro*. To do this, the EPC2-CP-A combination should be cultured during 72h and then medium with EGF added. The BO cells should then start replacing the squamous epithelium. Equally crucial would be to confirm that the junction can be established again when EGF is removed. The new stability when EGF disappears would suggest that lower levels of EGF in the more proximal oesophagus might have similar results.

3.5.3 Migration and not proliferation may drive segment expansion *In vitro*

In order to determine whether migration or proliferation were the elements driving segment expansion *in vitro*, the proliferation of EPC2 and CP-A cells during EGF titration experiments was tested by both CNN cell counting and fluorescence decay. In our model, proliferation from either of the two cell lines in the EPC2-CP-A combination does not increase as EGF increases. This was not expected as EGF has mitogenic properties [163]. The low proliferation rates are likely caused by cell-cell inhibition in confluent monolayers. Another possibility is the activation of a migratory phenotype incompatible with cell division [242]. This suggests that migration is the main factor driving CP-A invasion of the EPC2 monolayer. The specific effect of the EGF concentrations on migration speeds was not tested. The migration induction with EGF could be tested by doing wound healing with a single cell type.

EGFR signalling has been reported to be crucial for mammary gland duct growth [243]. The cuboidal cells from the mammary glands are believed to be similar to the ductal epithelium of the OSG and Brunner's glands in terms of histology. Unfortunately, no published data exists on EGF levels in developing human mammary glands. In mice, the levels of EGF in developing mammary glands were reported to be as high as 8 nG/mG [244]. Notably close to the EGF level threshold of 10 ng/mL considered high EGF concentrations during

our experiments. Therefore it is possible that EGF has a similar effect on the growth of OSG as mammary gland ducts *in vivo*. These cells would migrate and proliferate until a certain length of the oesophagus is colonized. In transitional epithelium, another possible source of BO epithelium, EGFR overexpression has been shown to generate hyperplasia. Examples of these are the urethra epithelium both *in vivo* [245] and *in vitro* [246].

Several experiments could further clarify the EGF role in segment length. These could include testing EGF phosphorylation in the different cell combinations to understand if post-translational modification of EGF correlates with observed phenotypes. These experiments might elucidate if the EPC2-CP-A change in behaviour under EGF is caused by higher sensitivity to EGF levels in the columnar population. If EPC2 is more affected than CP-A, EGF might be promoting a stem cell phenotype in the EPC2 population. This could weaken the cell-cell interactions and allow the more cohesive CP-A to invade the monolayer. This is a possibility as EGFR activation has already been shown to induce EPC2 migration [247]. To test EGF phosphorylation, both mass-spectrometry and western blot assays could be used. Both approaches require fluorescent cell sorting of both populations prior to analysis.

3.5.4 EGFR inhibition might be producing cell toxicity

The EGFR inhibitor lapatinib was used to test if the inhibition of EGFR produces the opposite effect that EGF addition had in the experimental setting [248]. Use of Lapatinib in the growth medium led to a stable junction between BO or OAC cells and squamous cells. In the combination involving the BO derived cell line CP-A this difference consisted in preventing the initial push seen in basal conditions. However, this results might happen due to inhibitor-induced toxicity increasing cell death. To test EGFR inhibitor-related toxicity flow cytometry with a cleaved caspase marker could be used.

Although lapatinib and other EGFR inhibitors have been tested and approved by the FDA [249] to treat OAC, they are unlikely to be used for BO patients.

Side effects of EGFR inhibitors derived from cell toxicity are regarded too severe to recommend its use in patients with a presumable harmless precursor lesion like BO [250]. Alternative use of the EGFR inhibitors could include the limited use after EMR or radio ablation of the BO segment to ensure repopulation by squamous cells. The new squamous lining will be then maintained by using proton pump inhibitors or NSAID. This treatment without EGFR inhibitors has already shown BO segment recession previously [251] , [252]. Although this treatment might reduce EGFR inhibitor induced toxicity, unknown risks caused by reducing mucosal healing after EMR remain. Further, EGFRi treatment after EMR is unlikely more cost-effective than BO surveillance. Further study of the invasion mechanism downstream of EGFR signalling are thus needed.

3.5.5 Deoxycholic acid is not able to disrupt the junction at neutral pH

The deoxycholic acid present in the reflux has both mucosal damaging and mutagenic properties. These properties have made it one of the most studied components of the gastrointestinal reflux. Notably, DCA has been reported to activate EGFR *in vitro* [253]. It can also activate NF-B in OE33 cells, a downstream signalling pathway activated also by IL-1B [254]. IL-1B has been shown to generate Barrett's Oesophagus like hyperplasia in mice [63]. It was thus a good candidate to control junction stability and BO segment length.

In the experimental set up, DCA concentrations up to 500 uM were tested, none of the concentrations however were able to affect junction stability *in vitro*. High DCA concentrations ended killing the cells in a few hours. These results suggest that deoxycholic acid at neutral pH does not promote BO expansion across the distal oesophagus. Because the reflux is a low pH solution, it is possible DCA would have a different effect at lower concentrations in an acid medium, as for example DCA is likely protonated at low pH which would facilitate cell membrane crossing. Indeed, DCA is known to affect cells differently at low pH conditions. However, this combination generates even more cytotoxicity [255]. Mimicking reflux conditions

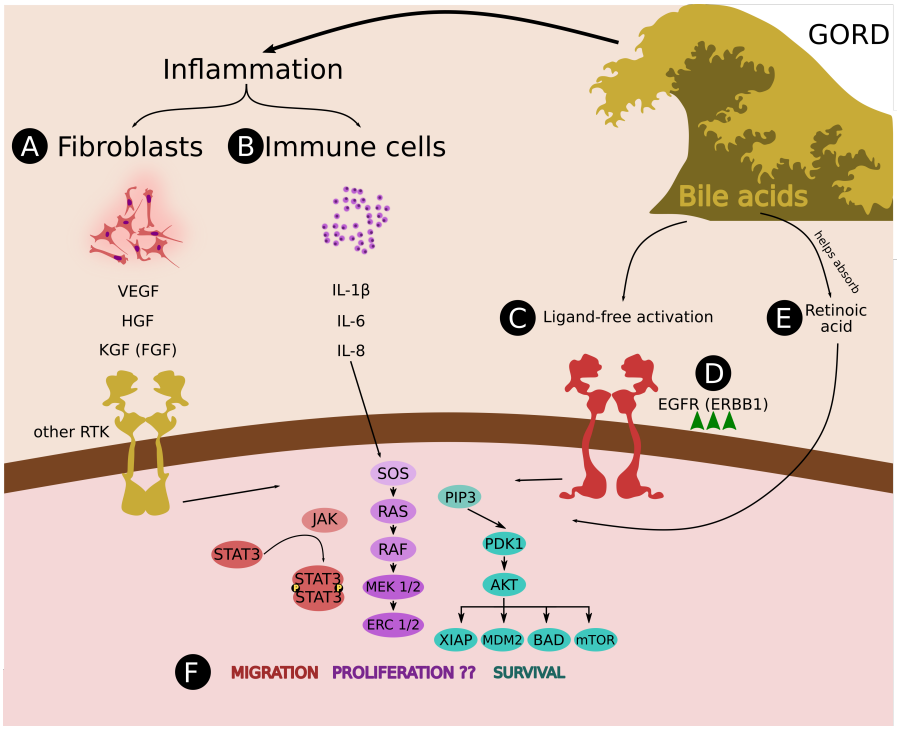

Figure 3.16: Alternatives to EGF activating convergent pathways The signalling pathways activated by EGF through EGFR could be ctived by several other elements present in the SCJ environment. Examples of this elements are: A) Fiboblasts present in the submucosa releasing other RTK ligands like HGF, FGF [257] and VEGF [258] in response to inflammation. B) Immune cells promoting inflammation and releasing cytokines like IL-1, IL-6 and IL-8 [254] into the environment. C) The ligand free activation of EGFR by DCA [253]. D) By increasing the EGFR levels in response to reflux oesophaguitis [161] [259]. E) By bile acid mediated retinoic acid absorption [256] [256]. F) All this different stimuli share some of the signalling pathways leading to migration, proliferation and survival

in the described 2D model however is technically challenging. No devices for the exchange of the media or to mimic temporary pH changes as observed in reflux are available. Efforts for pH control were therefore not pursued in this study.

Other interesting hypotheses related with DCA would have implications for EGF activation as well. One being to study whether low amounts of DCA in our model can lower the EGF threshold needed to break junction stability. Another, testing if retinoic acid, a vitamin absorbed better by epithelial cells when bile acids are present [256] and studied as a promoter of BO metaplasia, could be activating signalling pathways like the MAPK pathway. Of note, this pathway is triggered as well by EGF [256] to promote BO segment growth.

3.5.6 A simple 2D model consisting of only epithelial cells may be insufficient to test the reflux effect on BO segment growth

The model discussed in this chapter could successfully test many of the proposed hypotheses *in vitro*. However, there are several factors involved in BO progression that it is unable to replicate. The following three are examples of these shortcomings.

First, this model lacks other cell types that might be important for the progression of BO, like fibroblasts or immune cells. This lack of key cell populations could explain, for instance, why DCA does not affect BO segment length. DCA induces inflammation in the oesophagus [260]. Inflammation is also generated if DCA is administered somewhere else in the patient [261], [262]. *In vivo*, the fibroblast and immune cells might react to DCA by secreting cytokines and infiltrating into the tissue. Several publications attribute a key role in BO progression to cytokines [63] [263] [264] [265]. Some of them like IL-6 and IL-8 are able to activate the MAPK pathway like EGF [266]. This suggests the EGF experiments executed in this chapter could be only a proxy for the real signalling happening *in vivo*. Additionally, fibroblasts can change the mechanical properties of the model, by editing and secreting extracellular matrix. Fibroblast also secrete growth factors in response to damage or inflammation [267]. *In vitro*, cancer-associated fibroblasts affect OE33 invasiveness [208]. A similar mechanism could promote growth of BO in the lower oesophagus. Other cell types like endothelial cells might also be producing growth factors. For instance, VEGF that have similar signalling mechanisms to EGF, its levels are increased in BO in comparison to squamous epithelium [268][269] and can be produced by either fibroblasts [258] or endothelial cells [270]. A summary of some of the alternative elements that might activate convergent signalling pathways can be found in Figure 3.16.

Secondly, the epithelial cells used could not be faithfully mimicking the *in vivo* populations. Immortalized cell lines might differ from primary tissue. Interaction between them and the DCA or EGF might be cell line dependent. All the cell lines used were isolated from a patient more than a decade ago. In this time they have

probably evolved both genetically and phenotypically [271]. Due to the lack of an air-liquid interphase the cells are also not fully differentiated. This affects both the cell types in the population and its 3D structure. The most noticeable example is the lack of a layered structure in the squamous epithelium. This differences could be mitigated by using primary cells to model the squamous-columnar junction. To expand the primary cells, the organoid culture method would be used. This culture method has been shown to be able to expand cells for an indefinite number of cycles. At the same time it minimizes the number of mutations acquired during passaging, even in already cancerous cells [272].

Finally, reflux episodes happen in short pulses as registered by pH meters. During this short periods of time, the cells could cope with higher concentrations of EGF or DCA and lower pHs *in vitro*. As discussed this can be achieved by regularly changing the medium manually. Yet, after each medium change the same field of view would need to be found for imaging. This adds lots of steps and potential human error. Replicating short reflux pulses would be easier using microfluidics. A programmable pump could then control the pH , compound concentration, volume and duration of the reflux pulses.

All together, several alternative stimuli that could be activating the same signalling pathways as EGF *in vivo*, summarised in Figure 3.17, can not be studied with this model. A model able to replicate the squamous-columnar junction *in vitro* with all these variables does not exist. In the next chapter, the design and execution of a 3D model for the GIT diseases including all the elements discussed is described.

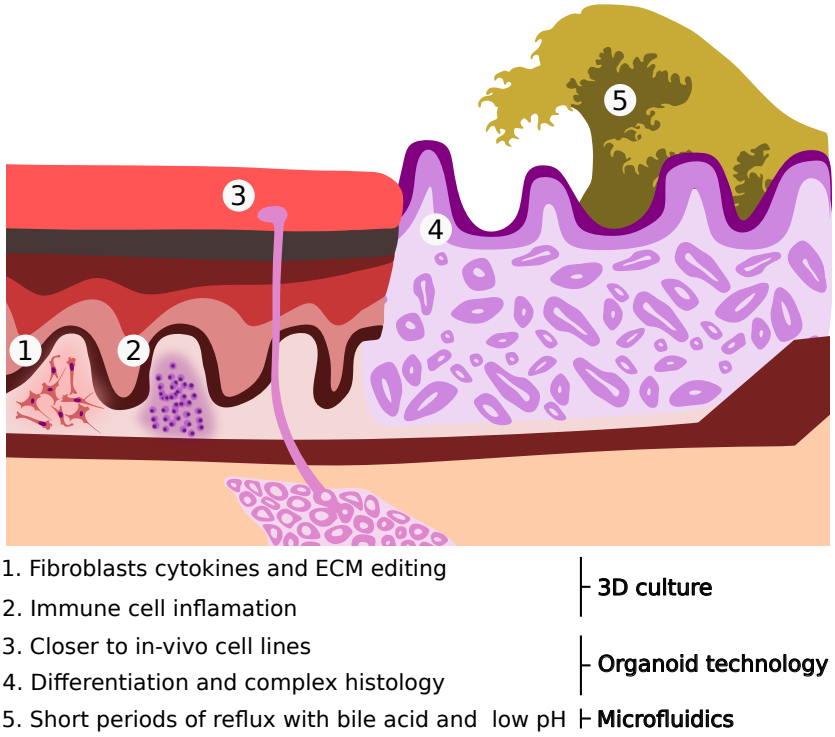

Figure 3.17: Model limitations and proposed solutions The model of the SCJ could better reproduce the *In vivo* conditions of BO if it could incorporate the following factors. 1) Fibroblast cells changing ECM physical properties and releasing growth factors. 2) Immune cells generating inflammation and releasing cytokines as a result. 3) Primary cell lines that would more closely resemble *In vivo* cells. 4) Better control over differentiation and 3D histology. 5) Tight control of when cells are submitted to low pHs and high bile acid concentration. This control would better recapitulate reflux episodes. Points 1-2 could be addressed by changing to a 3D model. 3-4, by using primary organoid cells instead of immortalized cell lines. Finally, 5 by adding a microfluidic device to our model.

4

Using 3D printing techniques to generate a 3D models of heterotypic junctions in the gastrointestinal tract

Contents

4.1 Research aim 100
4.2 Chapter summary 101
4.3 Introduction 102
4.3.1 Animal models 102
4.3.2 Organotypic culture 105
4.3.3 Organoids 106
4.3.4 Organoids use in co-culture methods 108
4.3.5 Organ-on-a-chip and microfabrication 109
4.4 Heterotypic junctions using organoids 110
4.4.1 Printing organic structures with organoid cells 111
4.4.2 Nanoprinting of droplets in an oil-lipid bath 113
4.5 Model required characteristics 114
4.6 Contributions 115
4.7 Results 115
4.7.1 Adapting available organotypic culture systems to generate a differentiated SCJ *In vitro* 115
4.7.2 Organoid nanoprinting using an oil bath 116
4.7.3 Using a 3D printed mould and bigger droplets to enhance organoid fusion 116
4.7.4 Adding fibroblasts changes the extracellular matrix and controls the ring shape 120
4.7.5 Fibroblast mediated contraction of the ring is concentration-dependent 121

4.7.6 Fibroblast concentration define collagen fibre density and fibroblast location . . . 121
4.7.7 Forming heterotypic junctions in the ring using a divider. 122
4.7.8 Using larger moulds to form large tubular collagen scaffolds 125
4.7.9 The collagen tube shape can be altered by using different fibroblasts concentrations in each tube segment . . . 125
4.7.10 Using fibroblast contraction at the tube's edges to attach plastic adapters . . . 126
4.7.11 Populating the tube's lumen with epithelial cells using adapters . . . 127
4.7.12 Infecting tubes with gastric epithelial lining in the lumen 128
4.7.13 The tube's collagen walls stop the diffusion of both medium and air . . . 130
4.8 Discussion . . . 131
4.8.1 Drawbacks of using organotypic culture for heterotypic junctions . . . 131
4.8.2 An improved ring collagen method replicates histological accurate epithelium . . . 131
4.8.3 Fibroblasts contraction as a tool for tissue engineering . 133
4.8.4 Controlling droplet fusion and heterotypic junctions . . 134
4.8.5 Printing self-shaping tubular structures . . . 135
4.8.6 Controlling flow allows for both populating and infection of the tube lumen . . . 136
4.8.7 Properties of collagen walls . . . 137
4.8.8 Future directions . . . 137
4.9 Conclusion . . . 145

4.1 Research aim

In the previous chapter, EGF was shown to disrupt the junctional stability between the squamous and the BO derived cell lines *In vitro*. *In vivo*, several other sources in the complex environment of the squamous-columnar junction could replace EGF and trigger converging signalling pathways. These include: low pH, bile acids, other reflux components and cytokines or growth factors. The latter would be released by fibroblasts, immune cells or other cell populations in response to damage and inflammation occurring during reflux episodes. The simplified 2D model used in the previous chapter can not replicate this complexity *In vitro*. Another limitation of the model was the use of cell lines instead of primary cells. The cell line behaviour

could have diverged from primary cells in such a degree that experimental results might not be transferable. To solve this issue, primary cells could be expanded as organoids to obtain closer to *In vivo* epithelial populations. The objective of this chapter is to design and implement a 3D model able to form heterotypic junctions between epithelial organoid populations. Such a model needs to be able to replicate reflux episodes using microfluidics and to incorporate fibroblasts and immune cell populations into it.

4.2 Chapter summary

The epithelial cells in squamous-columnar junction during Barrett's Oesophagus are part of a complex environment. The epithelial populations coexist with immune cells, endothelial cells, fibroblasts etc. Each of these populations influences the others through a plethora of signalling pathways. These pathways can be activated by direct cell-cell contact, paracrine factors or extracellular matrix remodelling. These interactions occur in a context of intermittent reflux episodes. The reflux lowers the environment pH and carries its own biological compounds. The epithelial cell populations proliferate, stratify, migrate, differentiate and die differently in response to the sum of these stimuli.

The model introduced in the previous chapter is unable to mimic this complex environment. The absence of these other cell populations might explain the lack of effect of the deoxycholic acid. In this chapter, a model able to incorporate additional cell populations present in the SCJ and mimic the reflux episodes is described.

First, adapting the 2D squamous-columnar junction model to the traditional organotypic culture systems was attempted. Then the cell lines were replaced with primary culture organoid cells to increase the similarity with *In vivo* populations. This was made possible by combining 3D printed moulds and collagen printing in oil baths. This method fabricates collagen rings that profit from the collagen contractility to fuse organoids. Combining the ring technology with a removable divider, a heterotypic junction between gastric and duodenal epithelial populations was achieved. By using fibroblasts the possibility of adding additional populations

into the 3D structure was tested. Interestingly, the use of fibroblasts was able to modify the ring structure by promoting the collagen contraction. This contraction was correlated with the fibroblasts concentration and was thus easily controlled.

Finally, the technique was used to generate a new 3D culture model by using longer tubular scaffolds. The tube shape would allow incorporating the tubular structures into a microfluidics system. Fibroblast contraction was then used to shape these tubular structures in a controlled way. Later, these structures were populated with epithelial cells. Unlike previous models this 3D tubular structures with internal epithelial lining were then easily infected with the pathogen *H. Pylori*. The chapter ends discussing the possibilities of this new technology both in primary research and the clinic.

4.3 Introduction

The previous chapter introduced a simplified model of the interaction between the squamous and the BO cells. As discussed at the end of the chapter, this system lacks the complexity present *In vivo*. Different approaches exist to try to replicate this complexity. These models vary in *In vivo* similarity and complexity of use.

4.3.1 Animal models

The *In vivo* complexity in humans can only be reproduced experimentally using animal models. Unfortunately, none of the common animal models is comparable anatomically and histologically with the human squamous-columnar junction. For instance, rodents comprising rats and mice, two of the most used animal models, present significant differences. In rodents, the anatomical location of their SCJ is in the middle of the stomach instead of the gastroesophageal junction (Figure 4.1 A and B). Rodents also lack OSG and do not present reflux episodes [273]. Additionally, their squamous epithelium is fully keratinized, being closer to human skin than oesophagus. Finally, mice and human inflammatory pathways do not behave identically [274].

Although the lack of submucosal glands has not been addressed, a technique does exist to mimic reflux episodes in rodents using surgery. This surgery, known as oesophagojejunostomy, artificially joins the oesophagus with the jejunum. With this technique half of the mice develop inflammation in the oesophagus, intestinal metaplasia and early onset of OAC [275]. Oesophagojejunostomy has three variants (Figure 4.2). Interestingly, the only variant involving the removal of the stomach prevented the mice from developing any metaplastic or dysplastic epithelia. This suggests that the gastric juice might be necessary for the development of BO [276]. Oesophagojejunostomy has also been used in conjunction with genetic engineering. As mentioned previously IL-1B overexpression induces BO and OAC in mice models. This effect is further enhanced when oesophagojejunostomy recycles the intestinal content into the oesophagus [63]. Other models have shown the same synergistic effects when doing a KO of the p53 or p27 genes in mice [277]. Interestingly, some of these models failing to reproduce BO involved again the removal of the stomach [278]. The importance of this organ for metaplasia and OAC can have several explanations. For instance, the absence of gastric fluids with low pH might fail to stimulate the secretion of compounds in the proximal duodenum like EGF. Alternatively, no erosion of the mucosa might occur due to the absence of stomach fluids. Without mucosal damage the colonization of the distal oesophagus becomes more difficult.

Pigs, dogs and primates have been used in BO research as they have submucosal glands. Primates, like the baboons being closer to humans can also suffer from reflux episodes [279]. However, the use of these models is not as extended and working with them is more complex and expensive [280]. A summary of the different animal models used in BO research and the differences they present with the human histology and anatomy can be found in Figure 4.1.

Due to the differences that exist with humans, animal models do not reliably predict outcome or toxicity. This has been shown in other research fields like cancer [281] and Alzheimer's disease [282], [283] research [284]. Animal models are also costly, time-consuming and require specialized personnel and installations. This is especially true if complex surgery like oesophagojejunostomy is needed. These

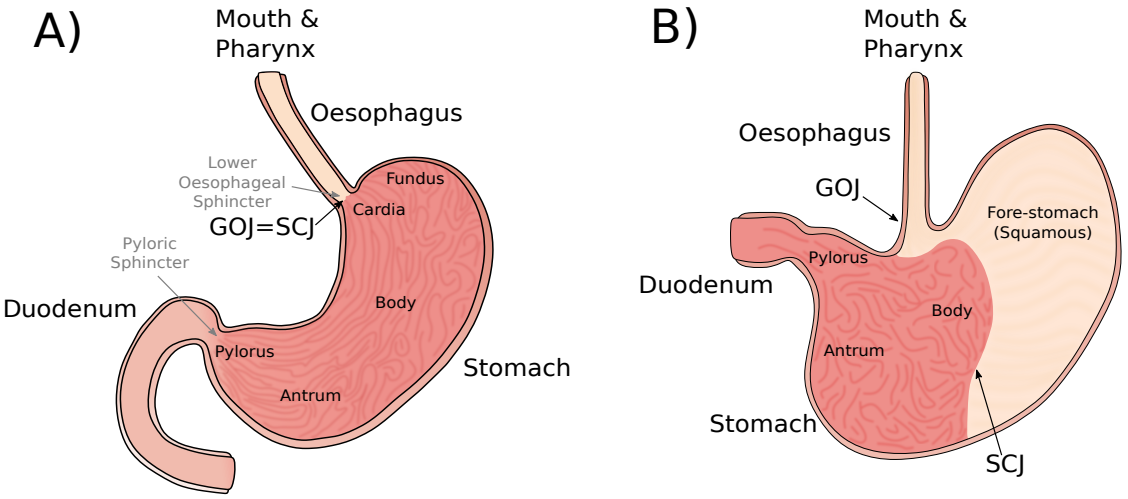

C)

Animal model	Rodents	Dog	Pig	Primates	Human
Oesophageal epithelium non-keratinized					
Oesophageal submucosal glands					
SCJ at GOJ					
Natural reflux					
BO to OAC transition					

Figure 4.1: Animal models for Barrett's oesophagus Comparison of the upper gastrointestinal tract anatomy between A) human and B) mouse. In mice, there is no overlap between the SCJ and the GOJ. C) Table summarizing the differences between humans and animals in the context of Barrett's oesophagus.

factors together with the desire of a part of the population to reduce animal suffering when possible [285], has made governments around the world change policies in favour of alternatives to animal testing. In the UK this commitment became the 3R plan aiming for the reduction, replacement and refinement of animal use in research [286]. One of the leading examples of this plan's implementation is the Open Targets Initiative, a project involving entities like Wellcome Sanger Institute, GSK and Biogen [287]. These institutions aim to replace animal models by combining

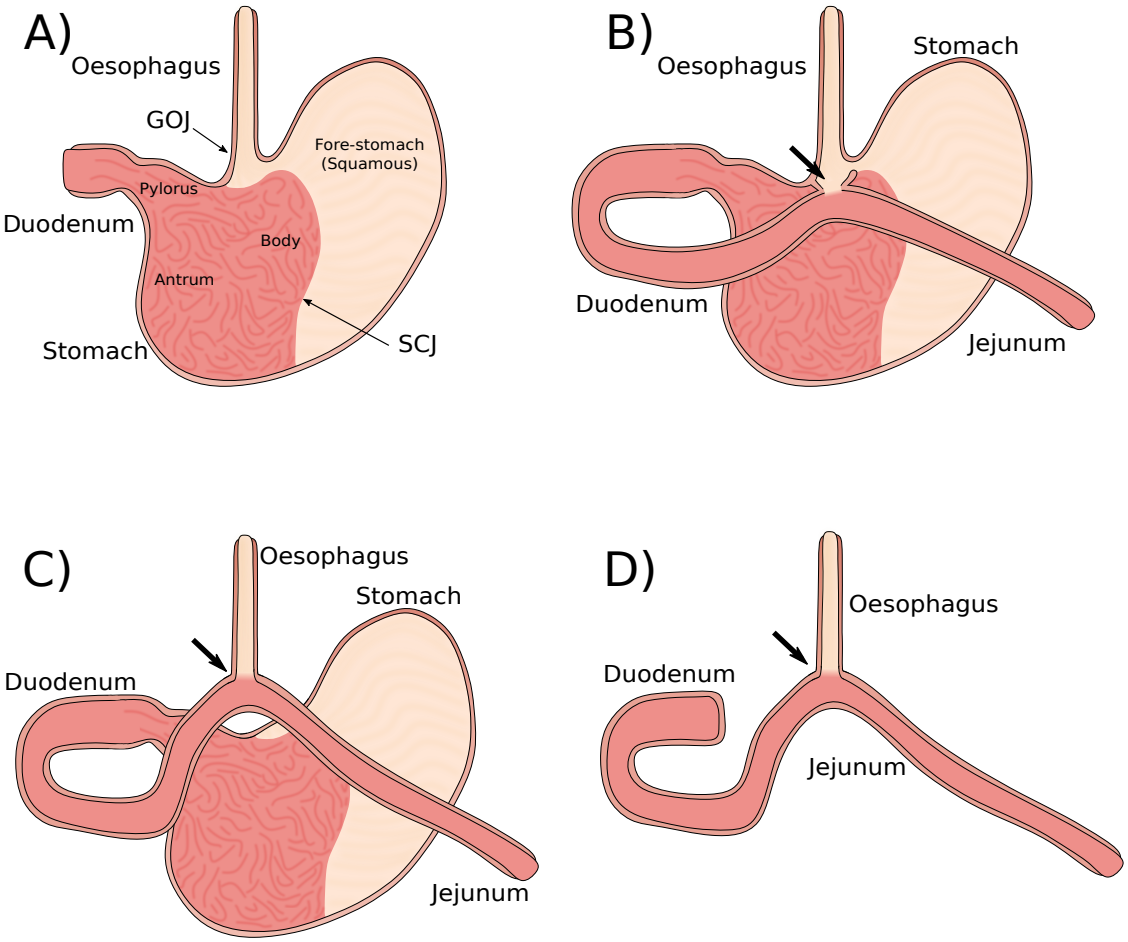

Figure 4.2: Oesophagojejunostomy in rodents Comparison of the different oesophajejunostomy techniques A) Normal rodent upper GIT anatomy B) Oesophajejunomosty by joining the jejunum and the stomach of the mice slightly below the GOJ. C) Oesophajejunostomy by directly joining the oesophagus and the jejunum, leaving the stomach still connected to the duodenum. D) Oesophajejunostomy joining the oesophagus with the jejunum directly and removing the stomach.

organoid culture and big data computer technologies.

4.3.2 Organotypic culture

An alternative to the use of animal models to achieve complexity *In vitro* is organotypic culture [288]. Organotypic culture combines a gel composed of ECM proteins with a transwell insert. The ECM gel usually contains fibroblasts forming what is known as a feeder layer. After the fibroblasts have grown, they contract the feeder layer. Then, epithelial cells either from primary origin or cell lines are seeded on top. When the cells have grown into a monolayer, the medium on top of

them is removed forming an air-liquid interface which helps them to differentiate. These 3D models are supposed to be closer to *In vivo* conditions [289], [290].

All of the cell lines used in the 2D model have been previously studied in the context of organotypic culture. EPC2 generate a multilayered and differentiated oesophageal epithelium in organotypic culture [200]. CP-A, the immortalized BO cell line deriving into a multilayered epithelium containing goblet cells [207],[291]. Finally, OE33 forms a multilayered, poorly differentiated epithelium in organotypic cultures [292]. In this chapter OE21 is used, this cell line derives from OSCC and forms a poorly differentiated multilayered epithelium [198]. Organotypic culture has also been used with primary stem cells isolated from primary squamous and BO tissue [293].

More complex organotypic models including immune cell populations have been reported. For instance, the addition of human peripheral blood mononuclear cells (PBMC) into the feeder layer was used to test oesophagitis in response to interleukin stimulation in squamous and BO cell lines [291], [294]. Organotypic cultures have been used to also test bile acid stimulation. In this model, bile acid stimulation induced the Epithelial Mesenchymal Transition (EMT) phenotype. As a result, invasiveness increased in BO cell lines but not in squamous cells. Interestingly, this phenotype could be prevented by using VEGF inhibitors [295]. VEGF and EGF share signalling pathways and both are inhibited by the compound used in that paper, SU1498 [296]. The bile acid content in the reflux might thus be able to activate either EGF or VEGF to help BO colonize the distal oesophagus through an EMT phenotype. A recent publication showing that EGFR activates as response to bile acids in both 2D and organotypic culture supports a role for either EGF or VEGF *In vivo* [297].

4.3.3 Organoids

As mentioned before, cancer-derived and immortalized cell lines differ from primary cells. The use cell lines sacrifices resemblance with *In vivo* conditions in exchange for a simpler culture protocol. A comaratively new method to expand primary cells

in vitro is organoid culture. In it the primary cells form self contained spherical structures mimicking the organ epithelial lining with an internal lumen. The organoid culture technique enables culture and expansion of primary cells indefinitely. As a result, organoid culture has promoted the use of primary cells *in vitro*.

To grow organoids from a biopsy, the tissue is first dissociated to isolate the stem cells. These stem cells are then plated into a drop of Matrigel and cultured using a cocktail of growth factors. Under these conditions, the primary cells can be expanded indefinitely. In culture, organoid cell populations have similar differentiation patterns to *In vivo* cell epithelium. Through proliferation and differentiation, the *In vivo* tissue architecture is replicated. Additionally, cells expanded as organoids remain genetically stable. The original protocol could be used in columnar tissue with LGR5 positive stem cells [298]. This includes intestinal, Barrett's oesophagus [299] and cancerous cell populations [272]. Recently this technique has been applied squamous oesophageal cells [300], [301]. Interestingly, niche populations in the oesophageal squamous-columnar junction can also be expanded. This niche stem cell populations are potential precursors of BO [72]. The organoid culture method have however several challenges:

First, the medium for organoid culture contains a cocktail of growth factors. These growth factors are at higher concentrations than *In vivo*. For instance, EGF in the organoid medium is present at a concentration of 50 ng/mL. In the previous chapter, the effect of EGF on junction stability was seen in concentrations as low as 10 ng/mL. Thus, EGF titration experiments done in the 2D model can not be replicated using organoid culture medium. Likewise, other growth factors in the cocktail might alter experimental results.

Second, organoids tend become polarized, with their basal side towards the Matrigel and their apical side facing the lumen [302]. This makes dead cells that shed from the monolayer accumulate inside. Polarization also makes infection with pathogens difficult without disrupting the organoid structure [303], [304]. Although mechanisms directing organoid polarity have been published [305], access to the organoids is still prevented by the ECM encapsulation.

Third, organoids grow encapsulated in Matrigel a dense extracellular matrix. Matrigel works as a barrier to secreted components creating pockets with different concentrations of growth factors [306]. The encapsulation makes co-culture difficult as well, preventing immune cells from freely interacting with the epithelial cells. The ECM also results in organoid number attrition when transferring samples, with some of them attaching to plastic surfaces.

Finally, organoid proliferation rates are low compared to cell lines. Organoid culture is also more complex as organoids are cultured in smaller batches. In addition, the plethora of growth factors used to make the culture medium are expensive. Taken together organoid culture is slower and more expensive. This complicates obtaining enough numbers for tissue engineering or screening.

4.3.4 Organoids use in co-culture methods

Organoid co-culture experiments have been reported in several publications. The first approach consists in using cellular subtypes already present in organotypic culture. For instance, immune cell co-culture with epithelial organoids. In them both lymphocytes [307], [308], [309] and macrophages [310] are used (Figure 4.3 A). Fibroblasts have also been added into the matrigel promoting both survival and differentiation (Figure 4.3 B) [311]. Other co-culture models exist that add neurons [312] or endothelial cells [313], [314] to epithelial cell organoids, changing the behaviour and differentiation patterns of the epithelial cells. This again suggests the 2D model used previously might be too simplistic to properly recapitulate *In vivo* conditions. As in organotypic models, transwell inserts have been used to grow the organoid/cell co-culture in an air-liquid interphase to further enhance differentiation [315], [316].

Unfortunately, none of these models is able to control the starting position of the co-cultured cells. Due to the random seeding, chaotic organoid proliferation and their 3D structure, these models have issues with reproducibility. In addition, the ECM still restricts access to the lumen to external compounds and pathogens. To try to standardize the initial experimental layout, several alternatives have appeared.

One of these solutions consists in relegating the organoids to a source of primary cells. In this approach, cells are expanded as organoids and then dissociated to be used in organotypic culture. This method can also be combined with other elements of the organotypic culture. For instance, adding macrophages to increase the height and differentiation of the epithelium [317]. This approach can also simplify the infection of gastric monolayers with pathogens like *Helicobacter Pylori*. Interestingly, when using this method *H. Pylori* was trapped by the mucus layer generated by the epithelial cells. Thus, this approach also enables the study of mucus secretion and composition *In vitro* (Figure 4.3 C) [318].

4.3.5 Organ-on-a-chip and microfabrication

A direct upgrade of combining organotypic culture and organoids is the organ-on-a-chip approach (Figure 4.3 D) [319], [320]. In an organ-on-a-chip, a membrane divides two adjacent chambers. Through each one of the chambers, medium can flown separately using microfluidics [321]. The main addition of this system compared to organotypic culture is flow. The system has two advantages. First, it allows for tight control of the environmental conditions. Second, it has been shown to help intestinal organoid derived cells form villi like structures aided by flow [322].

The production of the organ-on-a-chip is made using microfabrication, normally soft lithography [323]. In soft lithography, a mould is carved using photolithography engraving at a micro or nanometric scale. The mould is then covered with polymeric resins that harden forming an inverted replica of the original [324]. These techniques are used to not only engrave the channels but also recreate histological features. The best well known example are villi-like structures resembling the intestine [325], [326]. However, the organ-on-a-chip approach has limitations:

The first arise from its scaffold, where the rigid resin used during microfabrication hiders downstream processing of the sample. It also prevents the further use of this model in xenografting or human transplants. Xenografting is surgically transplanting donor tissue into an animal. This technique includes using organoids to humanize mice organs and study cancer treatments [327] , [328]. However, the use of orgnanoids

lack the tumour-stroma interaction as they only utilize epithelial cells [329]. An organ-on-a-chip approach without rigid parts able to be xenografted could serve as a platform to xenograft artificial tissue with a more complex design.

Additionally, organ-on-a-chip has not been used yet to generate junctions between different organoid epithelial populations. The closest approach consists on connecting several organ-on-a-chip modules to generate a circuit, a human-on-a-chip [330] , [331]. This system distributes the compounds released into the medium by the different modules. Unfortunately, similar to the membrane dividing the two channels in an organ-on-a-chip, this approach prevents direct interaction between cell populations.

Lastly, chip use is limited by its cost and availability. Although the cost of the material is low, the price of the machinery and the expertise required to use them is high. Until recently, organ-on-a-chip modules were not available for laboratories without expertise in microfabrication or a dedicated facility. Now, some of the simple models can be bought from companies like emulateBio [332]. An interesting alternative to lithography to make the moulds might be plastic 3D printing. Commercially available plastic 3D printers can get resolution as low as few tens of nanometers. Both materials and hardware costs are low, with hardware prices being less than £5000 at the top tier. This moderate investment could make this technique available to most laboratories. However, the cost for the microfluidics machinery still needs to be added. Additionally, unlike resins, using a 3D printed plastic sacrifices the ability to image through the printed material. A solution to this issue would be attaching slides of optical quality and thickness to the 3D printed structure.

4.4 Heterotypic junctions using organoids

Co-culture experiments between different epithelial organoid subtypes exist. In them co-culture is achieved by mixing or seeding the organoids in close proximity and letting them grow until they fuse. These chimeric organoids are known as assembloids. Mechanically joined organoids have been used with both brain [333],

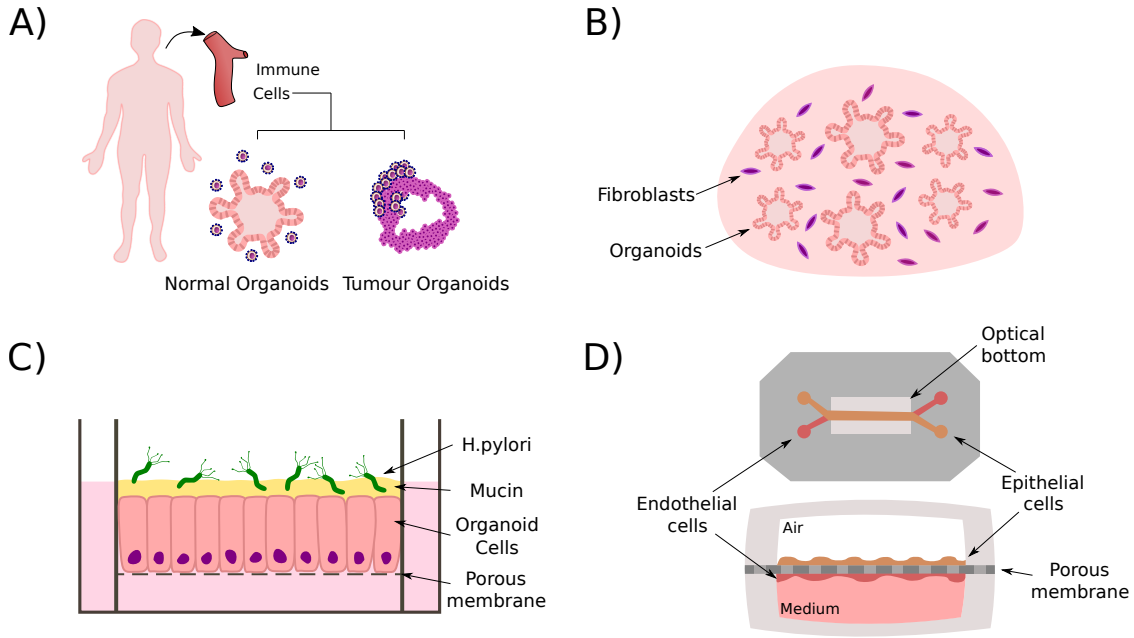

Figure 4.3: Organoids use in co-culture methods Some of the state of the art aproaches to organoid co-culture . A) Co-culture of immune cells of the patient with healthy and tumour organoids. B)Fibroblasts and organoid co-culture in ECM drops to increase differentiation. C) Gastric mucusoid organotypic culture to study infection and mucus production. D)Organ-on-a-chip design. Epithelial and endothelial co-culture in separate rigid channels.

[334] and low gastrointestinal tract [335] organoids to generate complex structures. However, the chaotic seeding does not produce sharp boundaries between cell populations, resulting in disorganized structures. This results in a suboptimal model and complicates functional cell polarization, cell polarization being vital for the epithelium function [336].

4.4.1 Printing organic structures with organoid cells

3D printing has been used in the field of tissue engineering to generate complex structures mimicking native organs. These methods try to generate complex well organized structures by preventing random seeding and chaotic heterogeneity. A plethora of techniques and gel bioinks to 3D print biological structures exists [337]. These techniques have been used to form of heterotypic boundaries [338] and complex structures [339] resembling *In vivo*-like tissue organization [340].

The fabrication of 3D printed tissue requires of dedicated facilities. Besides

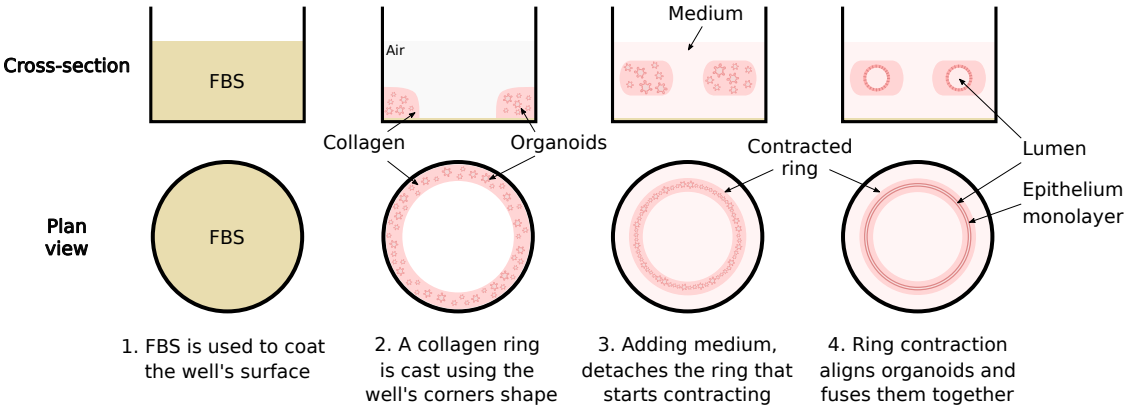

Figure 4.4: Hans Clevers' method to fuse organoids in collagen rings The published methods exploits collagen gelation to form rings loaded with organoids. The fibre reorganization in the rings pushes the organoids together. This movement fuses them in an epithelial mucosa with a lumen.

the need of specialized hardware, bioprinting has additional limitations. One issue when bioprinting organic structures using hydrogels is deformation due to gravity [341]. Gravity causes big hydrogel structures to deform, collapse or even break due to its own weight [339]. Additionally, most hydrogels can be easily damaged during manipulation.

These techniques are often used with cell lines and spheroids [342], [343]. Bioprinting with organoids is much less extended and limited, consisting in populating scaffolds or seeding them in a certain area of a plastic chip [344]. Other advance printing methods use spheroids as construction block, this generates stable and fast printing but the resulting tissue is very densely packed with cells producing aberrant histology [345].

In 2017 Sachs et al. from the Hans Clevers laboratory in Utrecht developed a technique to fuse organoids using collagen rings (Figure 4.4). Instead of printing, this method used the edge of the culture well as a mould where to manually pipette the collagen. Once the collagen gelated, the medium is added making the ring float. The ring's collagen fibres then align contracting slightly. This contraction brings the organoids together and makes them fuse. This generates a continuous epithelial monolayer with an internal lumen [346].

A similar approach was successful in using printing and cell lines derived from healthy mammary tissue. The cells were printed in close proximity inside a ECM matrix and cultured using organoid medium. The technique used 3D printing to distribute the cell colonies in the wells at a chosen distance. The budding cells then fused forming the desired structures. The same technique can generate heterotypic structures between cells labelled with different fluorescent proteins [347] , [348]. A drawback of both techniques is that the cells continue being encapsulated inside the ECM used as bioink.

4.4.2 Nanoprinting of droplets in an oil-lipid bath

A recent method consisting on printing into and oil-lipid bath could improve bioprinting methods. In this technique, aqueous droplets are printed inside an oil bath containing phospholipids. The phospholipids form a bilayer around the printed droplets generating an interphase between them [349]. By controlling the coordinates where droplets are released, layered structures can be formed. Once the desired structure is made the phospholipids in the oil are diluted. The drop in phospholipid concentration removes the phospholipid coating of the droplets and fuses them together [350] (Figure 4.5).

This has similarities with the reported in [339] where a gelatine bath is used to print alginate. This is followed by melting of the gelatine to release the alginate construct. However, the oil-lipid bath technique is cleaner and does not depend on a temperature variations.

This 3D printing approach has several other advantages. First, it can reach a nanoscale resolution. Second, the oil bath prevents the evaporation of the water in the droplets. This allows for longer printing times without risking desiccation. Longer printing times permit changing the bioink and cells during the printing process and thus increase the printing complexity. Third, it can use any aqueous bioink making it more flexible than alginate/gelatin printing. Finally, the oil bath density reduces the effect of gravity on the structure. This allows printing more stable and larger structures. Together with Dr Linna Zhou from Prof. Hagan

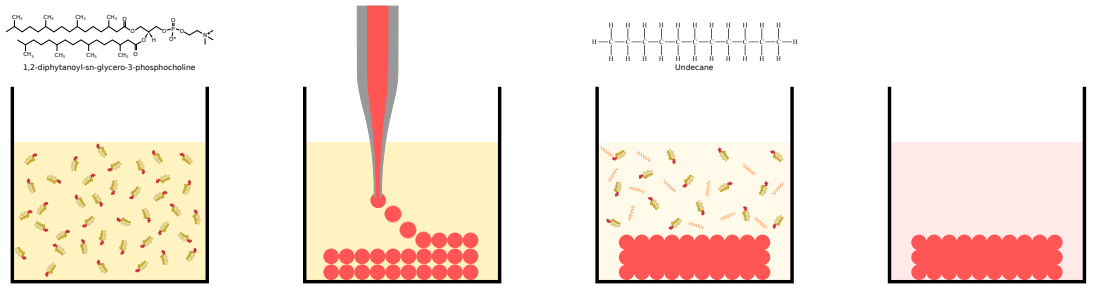

Figure 4.5: Nanoprinting using an oil-lipid bath An oil-phospholipid mixture bath fills the printing container. The phopholipids form bilayers around each aqueous droplet printed preventing fusion.This allows layer by layer printing. Once the lipid is diluted, the droplets fuse into a continuous structure.

Bayley's laboratory, we modified this technique to generate GIT models. These models solve some of the current issues in bioprinting and incorporate organoids.

4.5 Model required characteristics

To design an *In vitro* model able to incorporate all the advantages seen in the available models without their drawbacks. This must include:

- Complex cell populations including epithelial and stromal cells.
- Control of the location of each population.
- Compatibility with microfluidics devices.
- Production of large self assembling structures.
- Lack of rigid parts to allow direct interaction of the cell populations with the ECM. This also enabling xenographting or even organ replacement.
- Printing should not require expensive machinery.

4.6 Contributions

Carlos Ruiz-Puig and Dr. Linna Zhou designed the and printed the models. Carlos Ruiz-Puig and Richard Lisle designed and printed the 3D plastic moulds. Carlos Ruiz-Puig cultured the cells, processed the samples and did the staining of the sections.

4.7 Results

4.7.1 Adapting available organotypic culture systems to generate a differentiated SCJ *In vitro*

To try to obtain a 3D heterotypic junction model the standard organotypic culture method was adapted. This approach involved using the same divider as in the previous chapter on a transwell insert. Unfortunately, the membrane of the inserts used were too stiff and the liquid contents leaked out of the divider. Coating the membrane with a Matrigel layer prevented leakage by cushioning the union between it and the divider. However, the divider weight caused damage on the Matrigel layer. This prevented the cells to migrate towards each other and form a junction. This issue was solved by using a porous sponge instead of the usual stiff membrane (Figure 4.6 A) as transwell bottom. The Matrigel coating was then able to bend in response to the divider weight, minimizing the damage. The alvetex sponge was also populated with fibroblasts before seeding the epithelial cells.

This approach was successful in forming 3D squamous-columnar junctions *In vitro*. The junction was reproduced with cancer and immortalized cell lines. For the cancer cell line junction, OE21 derived from OSCC and OE33 from OAC were used (Figure 4.6 B). After optimization with the cancer cell lines, the immortalized cells from the 2D BO junction model, EPC2 and CP-A, were successfully used (Figure 4.6 C).

Unfortunately, this method still damaged the Matrigel often. Additionally, this approach requires a large number of cells. As organoids proliferate at a lower rate the amount of cells needed would slow down experimental output. The

organotypic culture was also time consuming, requiring a month to do a full experiment. The length of the experiment made it impossible to study population dynamics using fluorescent dyes and would significantly increase the expenses in reagents if organoid medium was used.

4.7.2 Organoid nanoprinting using an oil bath

To avoid the drawbacks with organotypic culture, the oil-lipid bath printing system was used. Organoids were mixed into the collagen and the mix used as bioink for printing. The organoids used were from duodenal origin as they have higher proliferation rates. The high proliferation allowed to perform experiments more often and speeded up the formation of a monolayer after organoid fusion. The bioink containing the organoids was printed in droplets forming a ring. As in Hans Clevers' publication, the ring contracted and the organoids fused together.

The first problem with this approach was the printer nozzle. Being of higher density than the medium, the organoids settled and clogged the tip (Figure 4.7 A). This is known to happen when printing with droplets instead of extruding [351]. To solve the clogging problem, organoid dissociation before printing was tried. Unfortunately, this released dead cells into the collagen. These dead cells tend to accumulate in the organoid lumen after shedding. When the organoids are dissociated, the dead and healthy cells get mixed (Figure 4.7 B). This resulted in the epithelial monolayer presenting apoptotic events and necrosis instead of resembling a healthy epithelium (Figure 4.7 C).

4.7.3 Using a 3D printed mould and bigger droplets to enhance organoid fusion

To prevent dead cells from mixing with the collagen full organoids had to be used. As full organoids would clog the nozzle, the printing method had to be changed. As a result, the technique was simplified to allow pipetting the droplets manually. Because manual pipetting makes droplet printing less precise a 3D printed plastic mould was required. The use of mould allowed the droplets to consistently form ring

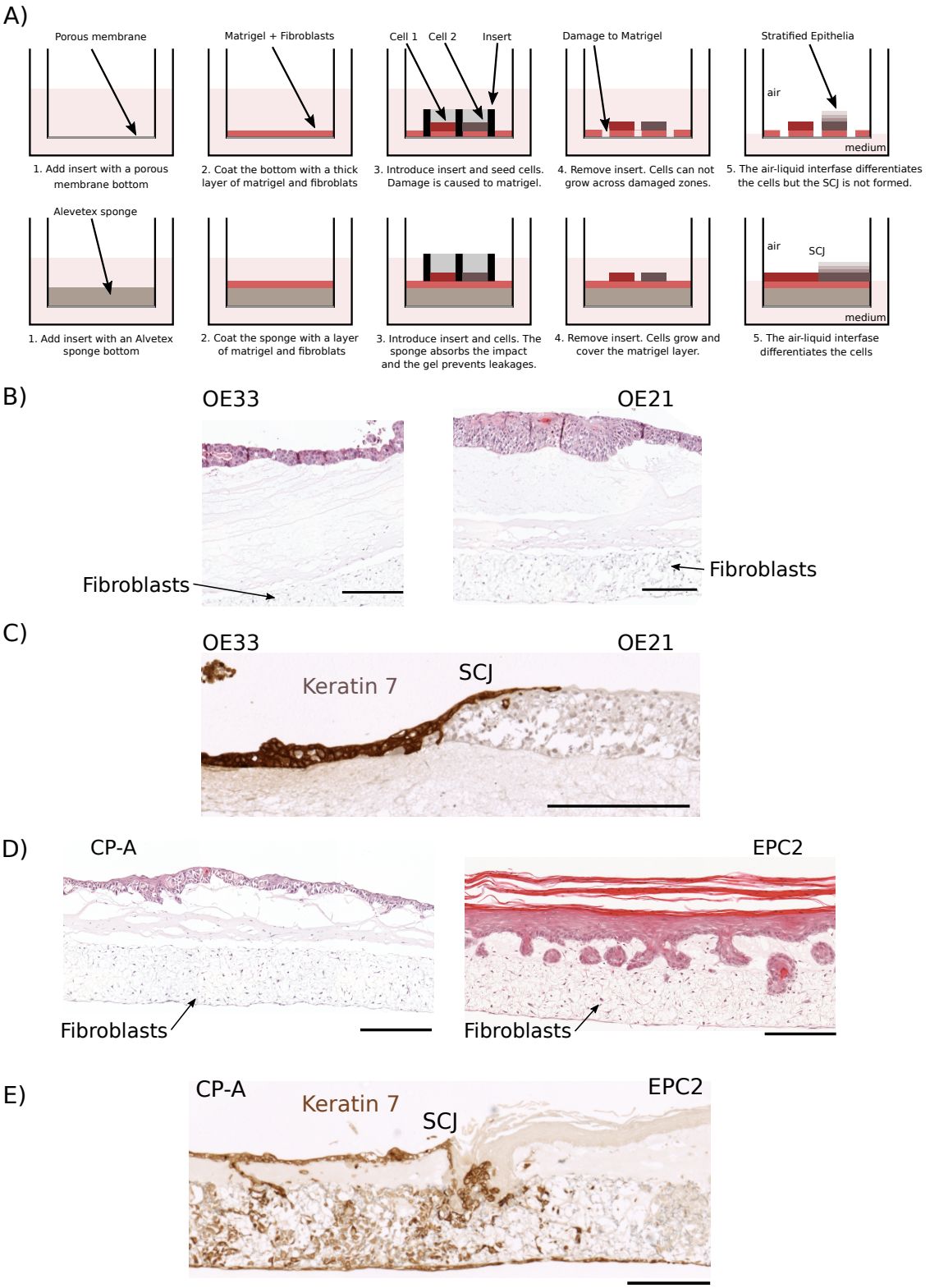

Figure 4.6: Organotypic models of the heterotypic junction A) Cartoon summary of the problematic with using a divider and the solution using an alvetex sponge. B) H&E of the OE21 and OE33 cancer cell lines in organotypic culture. C) Keratin 7 immunohistochemistry of the squamous columnar junction between OE21 and OE33. D) H&E of the EPC2 and CP-A immortalized cell lines in organotypic culture. E) Keratin 7 immunohistochemistry of the squamous columnar junction between EPC2 and CP-A. Scale bar: 100 um

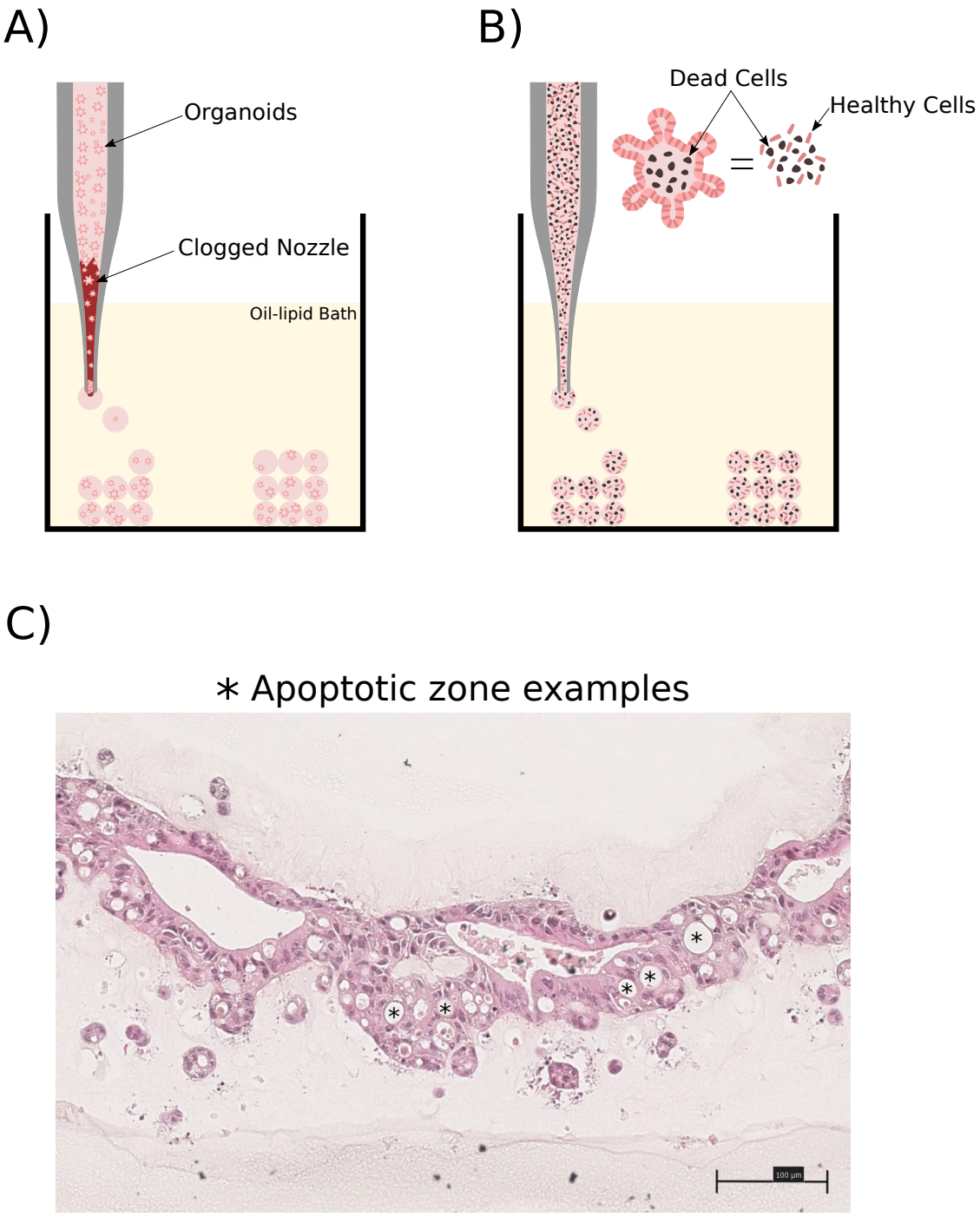

Figure 4.7: Dissociating organoid into cells for nanoprinting A) The narrow nozzle used for bioprinting clogged when using full organoids. B) To solve this issue dissociating the organoids before printing was tried. C) H&E staining of the tissue printed with dissociated organoids. Apoptotic areas , some marked with (*), can be seen across the epithelium. Scale bar: 100 um

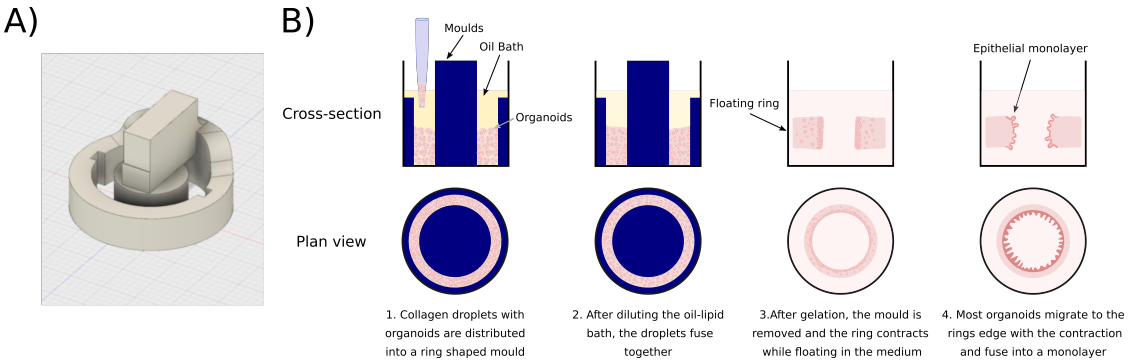

Figure 4.8: Combining plastic 3D printing and oil-lipid baths A) Computer rendering of the mould blueprint used to make the collagen rings. B) Steps to form collagen rings with organoid combining oil-lipid bath and 3D printed moulds.

structures (Figure 4.8) and also increased printing speed. Thanks to the oil-lipid bath surface tension, the aqueous droplets stayed in the mould. This prevented the leakage issues found in the organotypic model.

As in Hans Clevers' publication, the organoids in the ring fused into a single monolayer. However, using the oil-lipid bath and mould combination had two advantages. First, unlike in the previously published method, the ring was unlikely to dry during gelation. Second, the ring was kept from flattening due to gravity giving the rings a more regular shape (Figure 4.9 A).

This resulted in a change in organoid migration inside the structure and the in the epithelial monolayer final organization. In Clevers' method organoids migrated towards the centre of the ring wall section. There, the cells formed into a hollow tube with an internal lumen. In the new method organoids migrated towards the edge of the ring's inner circumference. Then, organoids fused into a single monolayer having the inner ring as the lumen. This change in epithelial organization was confirmed using immunofluorescence. E-cadherin staining was used to counterstain epithelial cells. Villin, a polarity marker for duodenal cells, confirming the lumen location (Figure 4.9 B). Finally, collagen 1 staining showed where the limits of the collagen ring were (Figure 4.9 C). Interestingly, H&E staining showed segments of the monolayer forming villi-like structures (Figure 4.9 D). This histological structure resembled a real cross-section of the duodenum more closely.

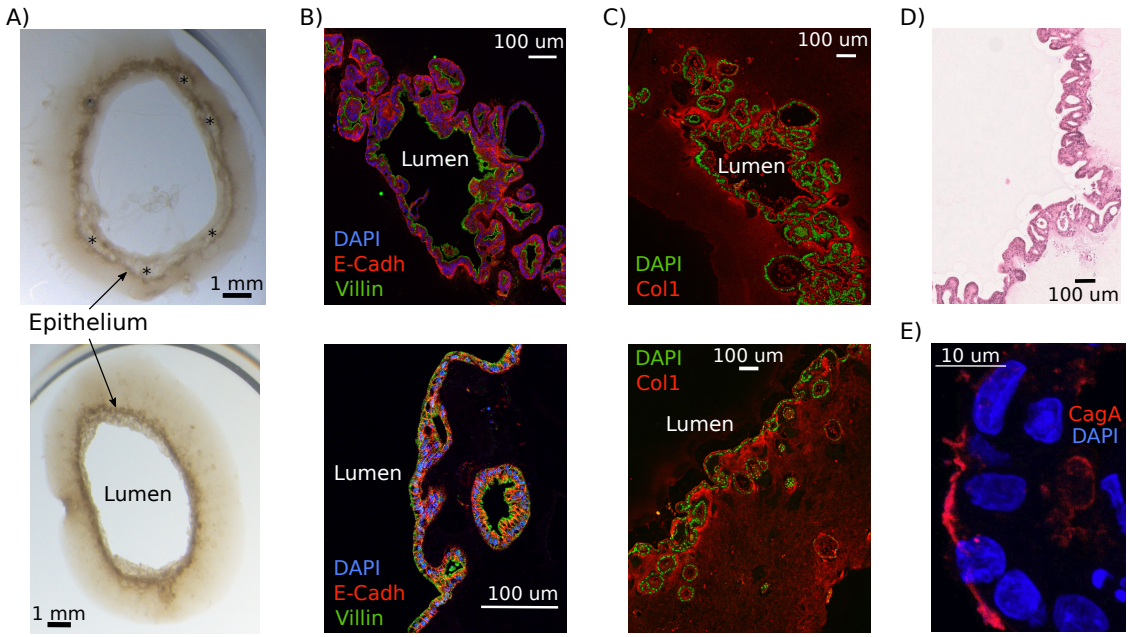

Figure 4.9: Collagen ring method comparison A) Transmitted light image of rings done with the Hans Clevers' approach and the presented in this thesis. The former forms internal lumens inside the ring. The new methods forms epithelium in the inner edge, transforming it into the lumen. B) Detail of the same rings with immunofluorescense staining for villin and E-cadherin. Villin indicates apical polarization towards the lumen. C) Collagen 1 immunofluorescent staining of the same rings. The nucleous of the cells can be seen next to the collagen edge in the new method while they remain inside the collagen in the previosuly existing approach. D) H&E staining of the new method epithelium. Some areas presenting villiform structures. E) CagA staining of the ring epithelium infected with *H. Pylori*.

This change is not only aesthetic. As shown by collagen staining the epithelial layer on the inner edge is not covered by collagen. The lack of encapsulation facilitates interaction with the medium. This was shown by adding *H. Pylori* in a ring with an epithelial monolayer of gastric organoid cells. By simply adding *H. Pylori* into the medium, the gastric cells were infected (Figure 4.9 E).

4.7.4 Adding fibroblasts changes the extracellular matrix and controls the ring shape

Organotypic cultures use fibroblasts to differentiate epithelial populations and change ECM characteristics. To obtain the same benefits, fibroblasts were mixed with the organoids and the collagen (Figure 4.10 A). After ring gelation, the fibroblasts remained in the collagen and the organoids migrated to the edge of the

ring. Surprisingly, the fibroblasts contracted the collagen fibres of the ring. This contraction reduced the ring circumference (Figure 4.10 B). As expected, the H&E staining of the ring epithelium showed a taller, more differentiated epithelium. This polarized epithelium had the nuclei migating closer to the ECM containing the fibroblasts (Figure 4.10 C). Unexpectedly, fibroblasts changed the side towards which the organoids migrated. The epithelial monolayer now forming at the outer edge of the ring.

4.7.5 Fibroblast mediated contraction of the ring is concentration-dependent

Ring contraction had some potential advantages. By bringing the organoids together fusion was enhanced. Additionally, with a smaller circumference to cover fewer organoids were needed. Finally, the reduction of the circumference could potentially be exploited in screenings making large rings fit into screening plates.

To understand contraction in our model, its relationship with fibroblasts numbers was tested. This was studied by making rings with titrated fibroblasts concentrations. As expected, higher fibroblast concentrations increased the contraction speed and its extent. Ring contraction was faster at the initial timepoints and started to stabilize after 48 hours (Figure 4.10 E).

Another cell population present in the BO environment are immune cells. To be able to define the ring final size and the organoids needed, knowing the effect these cells will have in ring contraction is crucial. To study this, a small population of 10 thousand Jurkat cells was added. Jurkat is a T-lymphocyte cancer-derived cell line [352]. As expected, the Jurkat cells by themselves were unable to contract the ring. When both immune cells and fibroblasts were in the matrix, the contraction was reduced (Figure 4.10 F).

4.7.6 Fibroblast concentration define collagen fibre density and fibroblast location

The collagen fibres in the ring's extracellular matrix could also work as a barrier for immune cell migration. To study collagen fibre density, the rings used in

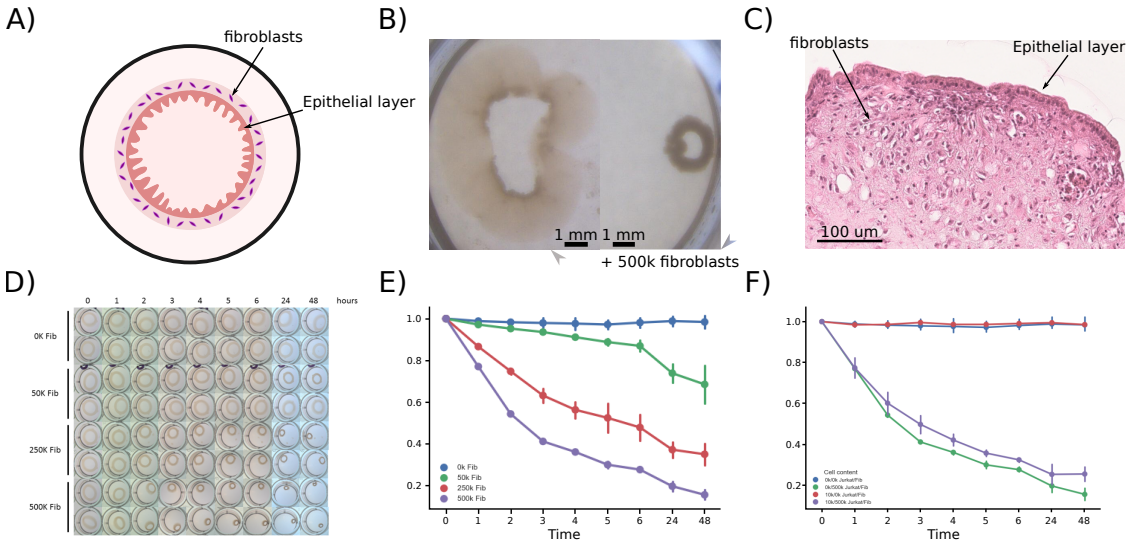

Figure 4.10: Fibroblasts ring contraction is concentration dependant A) Schematic fibroblats-organoid co-culture ring. B) Transmitted light images of ring contraction comparison when 500K fibroblasts are added to the collagen. C) H&E staining of co-culture cross-section. An epithelial cell monolayer is form on the outer ring while fibroblasts remain in the collagen. D)Transmitted light image of ring contraction over time as fibroblast concentration changes. E) Graph showing ring contraction over-time with different fibroblast concentrations. Standard deviation is used to represent variability of three replicates. F) Graph showing the effect of adding an additional cell population in the matrix to contraction. 10K Jurkat cells reduce ring contraction. Cell numbers are given per millilitre of collagen.

the fibroblast titration were stained for collagen I. As expected, fibroblast driven contraction increased fibre density. This could be seen by the reducing amounts of black areas between the fibres. Interestingly, this also resulted in a different fibroblast distribution. Nuclear staining shows that at the highest fibroblast concentration used, fibroblasts stop being regularly distributed. Instead, the fibroblasts concentrate near the inner edge of the ring. This migration pattern could explain why organoids migrate to the outer edge when co-cultured with fibroblasts (Figure 4.11).

4.7.7 Forming heterotypic junctions in the ring using a divider.

The next step was to replicate the heterotypic epithelial junctions of our 2D model. This could be achieved by using a removable 3D printed plastic divider. The divider was first inserted in the mould and both introduced into the oil-lipid

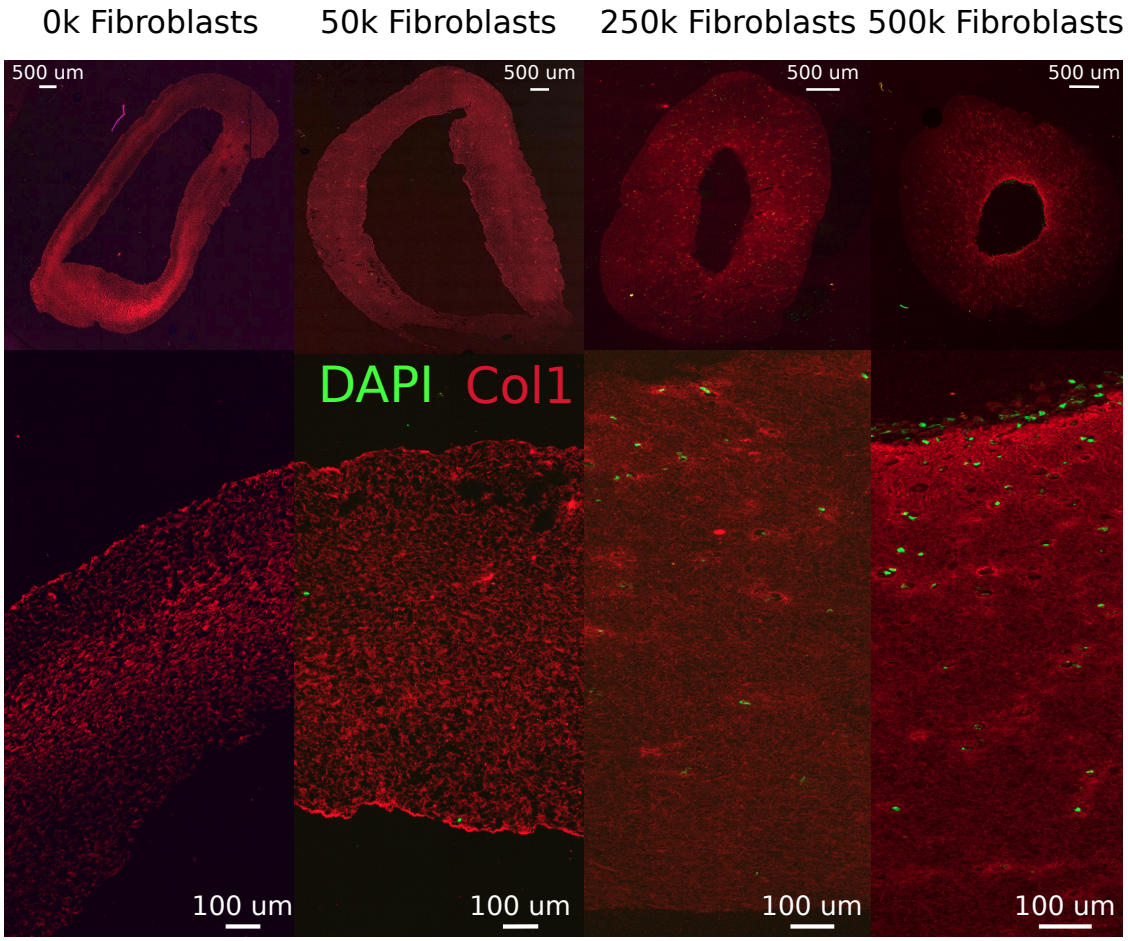

Figure 4.11: Fibroblasts contraction changes collagen fibre packing Immunofluorescense staining of the ring wall of collagen 1 and nuclear DNA. The space between the fibres is reduce gradually. Fibroblasts migrate to the centre of the ring at the highest concentration. Fibroblasts numbers are given per millilitre of collagen.

bath. Then, each of the two chambers were filled with collagen droplets with different organoid populations. When the divider was removed, the droplets moved towards each other but did not fuse because of the phospholipid coating. Once this lipid was removed, fusion joined both halves into a single ring with a sharp boundary. The organoids then migrated to the edge and a single heterotypic monolayer was formed (Figure 4.12).

This approach was used to make mixed rings with organoids from gastric and duodenal origin. The junction between both organoid populations could be seen using immunofluorescence against tissue specific markers. Mucin 5A and villin were used as gastric and duodenal markers respectively. The staining showed the rings

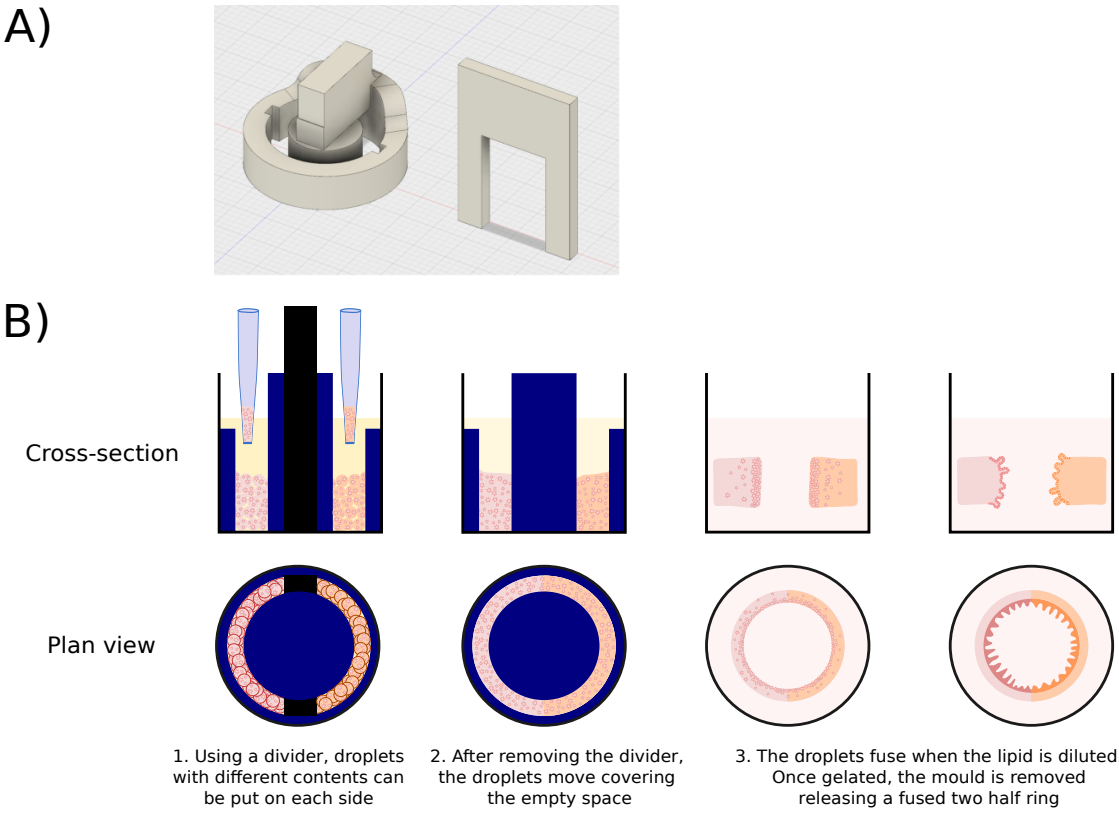

Figure 4.12: Heterotypic junction formation using a divider A) Computer rendering of mould and divider designs. B) Steps to fabricate heterotypic junctions in collagen rings.

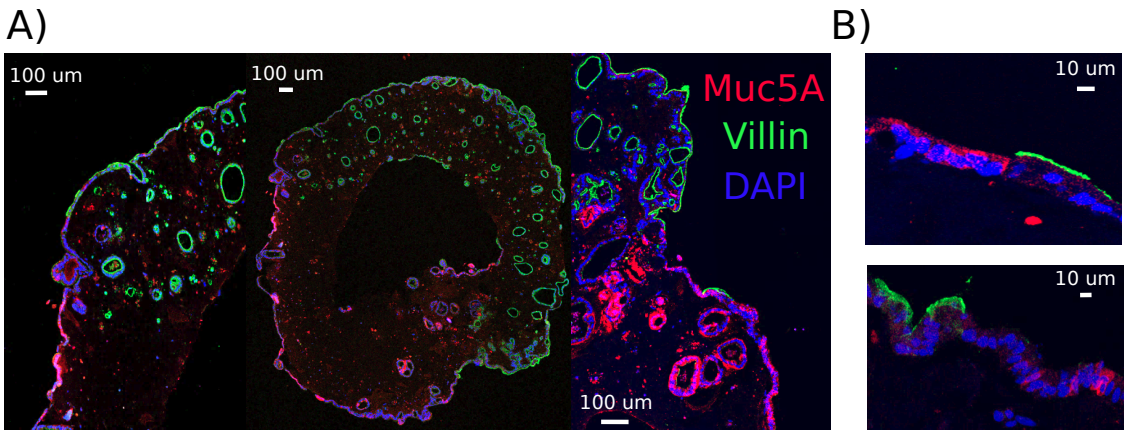

Figure 4.13: Heterotypic junction immunofluorescense staining Fluorescense staining of the gastric and duodenal marquers muc5A and villin. A) Complete ring image with detail of junction between both epithelial lining. B) 63x detail of both junctional populations. Muc5A is only expressed in the secretory gastric cells. Thus, staining is not present in all the gastric epithelium.

divided into two halves with a distinct epithelial population (Figure 4.13).

4.7.8 Using larger moulds to form large tubular collagen scaffolds

The gastrointestinal tract is a tubular structure. By using different epithelial lining, the material ingested is digested and absorbed. This epithelium transitions along the tube forming heterotypic junctions. By using the same principles applied in the ring formation, long tubular segments could be formed. There were several advantages of forming tubes instead of rings as a model. First, two different mediums could potentially be used, one inside and another outside the tube. Second, the tubular structure could be adapted to use in microfluidics like an organ-on-a-chip. Third, heterotypic junctions could potentially be formed without a divider. This would be achieved by stacking droplets with different organoid populations and letting them migrate towards the inner lumen. Finally, being made of organic elements, the complex structure could be xenografted.

To form tubular structures the next steps were followed (Figure 4.14 A). First, a 15 mL falcon tube conical bottom was cut. This tube was used as a container for the longer mould required. Then, new moulds were 3D printed with length of either 4 or 10 cm (Figure 4.14 B). The new mould was introduced into the tube and the tube filled with an oil-lipid bath. Droplets of collagen were then introduced until they reached the top. Once the fused droplets gelated, PBS was flowed through one end to release the tube into the medium (Figure 4.14 C). Interestingly, the collagen structures fabricated in this way could be manipulated with forceps. This makes them more resilient than structures printed using alginate.

4.7.9 The collagen tube shape can be altered by using different fibroblasts concentrations in each tube segment

The width of the tubular section of the gastrointestinal tract varies across its length. It is narrower in organs like the oesophagus or duodenum getting wider in the stomach and colon segments. Shaping the mould with different widths in each section would complicate the release the collagen structure. To compartmentalise the tube, the contractile properties seen in rings with fibroblasts were used.

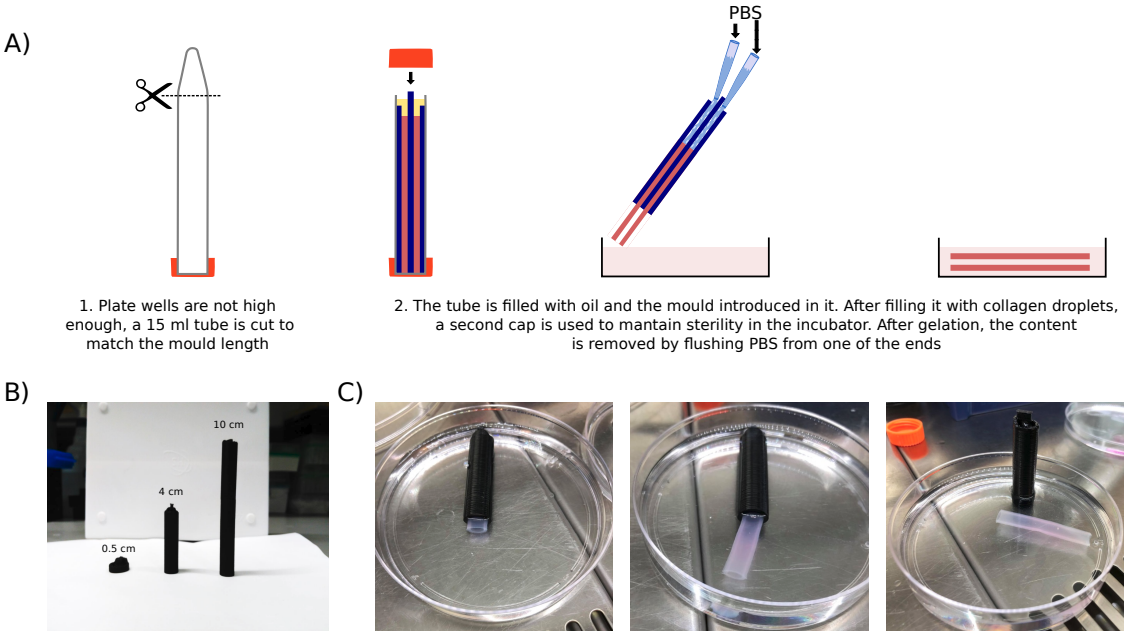

Figure 4.14: Experimental design to form tubular collagen structures A) Squematic of the steps needed to form collagen tubular structures. B) Size of the new mould compared to the mould used for the rings. C) Release of 4 cm long tube structure steps.

The tube was treated as a stack of consecutive rings. In each ring, the fibroblast number could be changed using bioink with different concentrations. This principle was tested to try to form a stomach-like structure. This structure would be narrow at the ends and more dilated in its centre. To achieve this, a higher concentration of fibroblast was used in the edge droplets. Then the fibroblats gradient reduced gradually towards the centre (Figure 4.15 A). The tubes were filmed for 5 days. The collagen tubes changed shape gradually until stabilizing with the desired shape after 96 hours (Figure 4.15 B). More complex structures using the 10 cm mould. A combination of different fibroblast concentrations forming a simplified version of the GIT (Figure 4.15 C).

4.7.10 Using fibroblast contraction at the tube's edges to attach plastic adapters

The aforementioned advantages for constructing tubular structures were only possible if there is control over the contents of the lumen. To control the flow into the lumen, adapters were needed at the tube's ends.

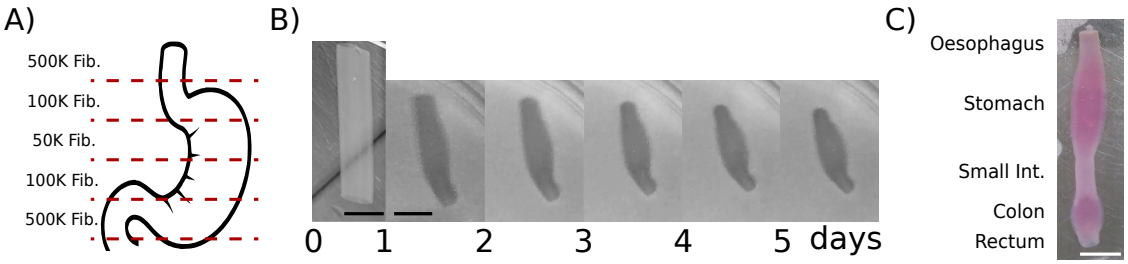

Figure 4.15: Self-shaping tubular structures A) Fibroblast/mL concentration in each segment to form a stomach-like collagen structure. B) Time-lapse frames every 24 hour showing self-shaping of the tube into the designed structure. C) Tube shaped into GIT-like contraction pattern after 5 days. Scale bars: 1 cm

Four different options were tested. Two of them, wire and cotton strings were used to tie the ends of the tube. This approach was useful to stop flow in the tube. However, reopening the tube was complicated and usually damaged the tube. The other two, steel and plastic adapters, depended on the contraction from the fibroblasts attached to the tube's ends. Steel adapters were too heavy and smooth. These adapters detached easily from the tube when moving the sample or pipetting volumes inside. The last option were plastic adapters. The surface of pre-existing plastic tubes, from pen ink cartridges, proved to be also too smooth. Finally, the best option was a 3D printed plastic adapter (Figure 4.16 A). The layered structure was irregular allowing better attachment of the contracting collagen. Flow into the adapters could be stopped using caps. These caps were made by introducing 0.2 um filter meshes into a pipette tip and cutting around it. The tip segment with the mesh sealed the lumen from outside cells but allowed the medium to flow in. Caps not allowing the medium to pass through could also be 3D printed (Figure 4.16 B).

4.7.11 Populating the tube's lumen with epithelial cells using adapters

The adapters were used to populate the lumen of the tube with epithelial populations. First, the adapters were introduced into the collagen tube. The fibroblast populations contracted the ends of the tube fixing the adapters. Then, epithelial cells were added into the lumen through the hollow adapter and a cap was used to

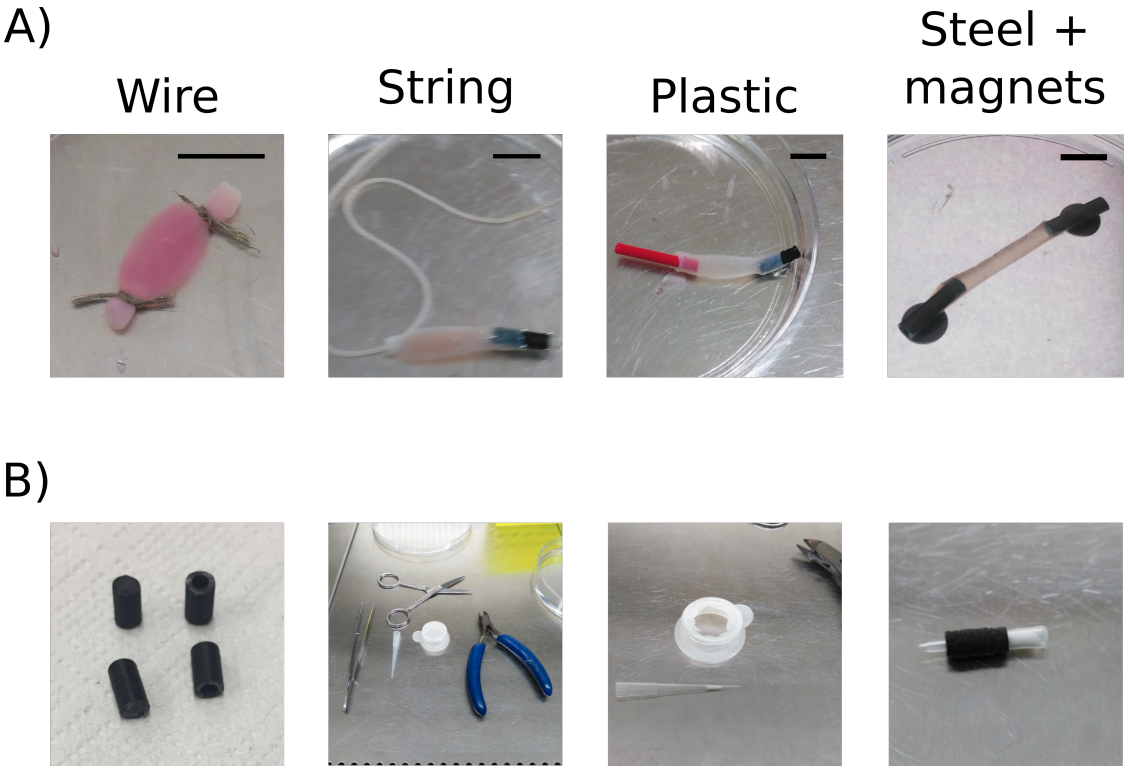

Figure 4.16: Adapter and cap variations A) Different adapters tried to control flow into the tubes. B) From left to right: 3D printed adapters and steps to form caps for the adapter using a pipette tip and a filter mesh. Scale bars: 1 cm

seal the cells inside. After incubation O/N and the caps removal, the lumen was flushed to remove all the non-attached epithelial cells (Figure 4.17 A).

Both gastric (AGS) and colon (Caco-2) cancer epithelial cell lines were used. For AGS a stomach structure shaped using fibroblast gradients was used. The Caco-2 cells were introduced into a contracted tube with 500k fibroblasts per mL. In both cases the cells covered the interior of the tube with an epithelial layer. The epithelial layer thickness varied with the cell type and was thicker in one half of the tube's circumference. This phenomenon was probably caused by gravity, grouping the cells in that lower part more densely.

4.7.12 Infecting tubes with gastric epithelial lining in the lumen

Tubes with AGS epithelial lining were further manipulated, infecting them with *Helicobacter Pylori*. The infection was executed by removing the cap and introducing

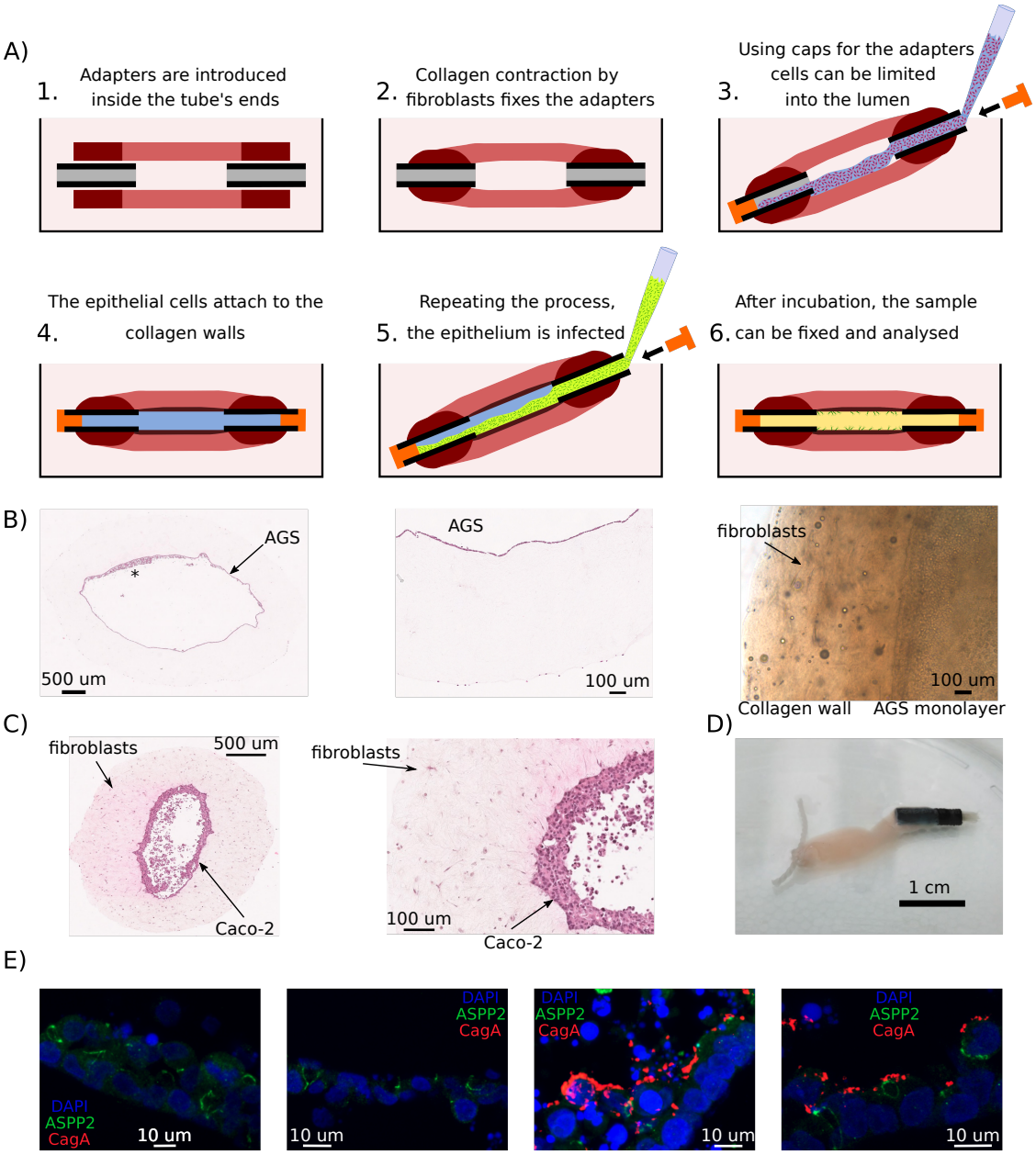

Figure 4.17: Populating and infecting the tubes lumen A)Steps to populate the lumen with epithelium using the adapters and infect the cells. B) H&E staining of tube with AGS lining and 50K fibroblasts/mL. C) Light microscopy detail of the collagen wall and AGS lining. D) H&E staining of tube with Caco-2 cell lining 500K fibroblasts/mL. E) Collagen tube with AGS lining and *H. Pylori* infection before fixing. F)Immunofluorescense staining of ASPP2 and CagA. *H. Pylori* marker CagA staining next to epithelial cells together with ASPP2 rearrangement confirms epithelial infection.

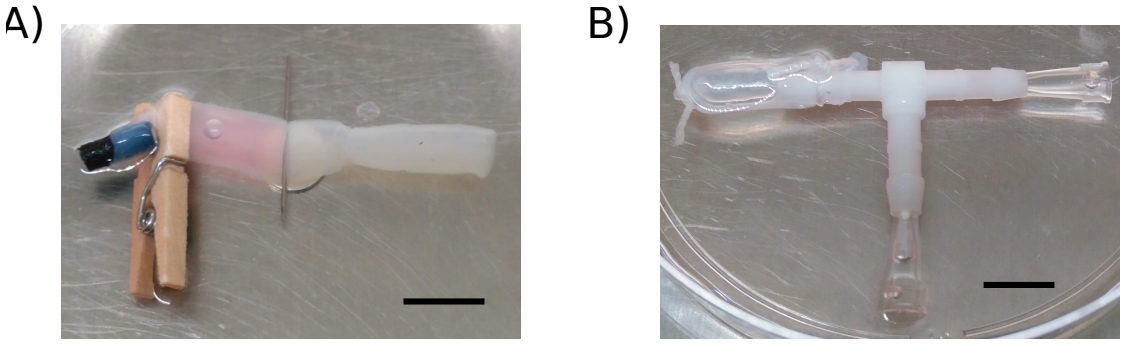

Figure 4.18: Collagen wall impermeability A) Phenol red dyed medium does not diffuse after an hour submerged in phenol red free medium. Air bubble remains inside as well B) Air in the tube lumen fills the structure and stays in the tube after an hour.

the bacteria into the lumen. After a 6 hour infection, the cap was opened and the bacteria washed out. Samples were then processed and cut. Finally, immunofluorescence staining was used to assess the efficacy of the infection. The *Helicobacter Pylori* marker CagA was used to identify cells infected with *H. Pylori*. The samples were also stained for ASPP2 a junctional protein recruited in successful infections. The tube samples infected presented CagA-ASPP2 staining indicating successful infection.

4.7.13 The tube's collagen walls stop the diffusion of both medium and air

microfluidics devices. To use the tube structures for microfluidics, the diffusion through the collagen wall needs to be slow. To test this, a magnet and a needle were used to pinch the tube in two.

Half the tube was filled with phenol red-dyed medium. The other half with PBS. The phenol red-dyed medium was unable to diffuse out of the tube. This suggests the collagen wall might be impermeable to liquids at least in periods of time under one 1h (Figure 4.18 A). The air was also unable to cross the collagen wall. Injecting it inside the tube dilated the structure but did not go out of the walls (Figure 4.18 B).

4.8 Discussion

In this chapter, two preexisting technologies were combined to generate an alternative 3D model of the GIT. This technique has features of the preexisting models without their drawbacks.

The necessary properties of this model were the following: First, being able to include stromal cell populations. Second, reproducing *In vivo* heterotypic junctions using primary cells expanded using organoid technology. Third, enhancing differentiation and histological resemblance to *In vivo* organs. Finally, being able to incorporate microfluidics to control medium conditions and pathogens.

4.8.1 Drawbacks of using organotypic culture for heterotypic junctions

First, the 2D model in chapter one was adapted to organotypic culture requirements. The same divider may be used to separate the epithelial populations and stroma cells could added to the alvetex sponge at the bottom of the well insert. Although this model worked, it had several drawbacks. The model was easily damaged during manipulation. Additionally, large amounts of epithelial cells were needed to construct a single model. This made the use of organoids difficult and too resource demanding for screening. Lastly, both wound closure and differentiation processes took weeks. This increased the chance of errors and the volume of reagents needed. This method could be used together with fluidics, using 6 well plates with channels. Yet, this fluidics setting requires large volumes of medium and incubator space [353]. Taken together, the organotypic culture approach had too many drawbacks.

4.8.2 An improved ring collagen method replicates histological accurate epithelium

To solve these issues the organotypic culture was replaced with a 3D printing technique using and a lipid-oil bath. As the nozzle for nanoprinting is too thin, the organoids blocked the nozzle. Dissociating the cells to solve this issue generated another: dead cells from the organoid lumen were released into the collagen lowering

the tissue quality. To solve this issue, a 3D printed plastic scaffold was added, enabling the use of bigger droplets. This droplets could then be added pipetting by hand. This reduced the precision of the droplets but allowed for a faster and simpler methodology.

We based our ring structure in a previous publication from the Clevers' laboratory [346] aiming to improve their methodology. Heterogeneity in the ring shape was a drawback of Clevers' method. The use of an oil-lipid bath and a mould solved this issue and presented other advantages. The time point when the droplets fuse could be controlled and the oil bath protected the droplets from drying. In addition, the oil mitigated the effect of gravity preventing flattening of the structures. The resulting structures were identical to the mould used, standardizing the resulting circumference and thickness.

Interestingly, this resulted in a different migration pattern for organoids in the collagen. The Clevers' method formed a hollow tube around the centre of the ring cross-section, both the epithelium and the lumen being embedded in the collagen. Instead, our model had the organoids migrate towards the inner edge of the ring and then fuse. This migration pattern made the centre of the ring in the lumen of the epithelium lining. The final structure resembled a cross-section of the GIT circumference. As in the *In vivo* mucosa, the cell shed in our model's epithelium were released into the lumen (data not shown).

This conformation had advantages over the previously published technique. For instance, the epithelium was no longer covered by the collagen simplifying the interaction with the epithelial lining. An example of this was infection with *H. Pylori*, which became easier than in previously reported organoid models. Organoids needed to either be microinjected or broken and then infected. An alternative was growing the cells on a membrane, [318] but in this case, the mucus needed to be washed and the 3D structure was lost. In addition, these epithelium monolayers needed to be cultured for a longer time than in the ring model. Arguably, our model cultured for shorter periods of time and would be equally simple to infect. Interestingly, this suggest the ring model could be better differentiated and produce

a thick mucous layer if cultured for longer times. Short culture times in the ring model were used to have a higher output. Having established the culture system , studying differentiation in shorter and longer culture times would be interesting.

4.8.3 Fibroblasts contraction as a tool for tissue engineering

3D organotypic cultures use fibroblasts to improve differentiation and polarization of epithelial cells. These cells are added into the ECM beforehand and then the epithelial cell lines are seeded on top once the ECM is already contracted. This was not an option in the ring model, where both the ECM and the cells were added when printing the ring. Fortunately, the organoids still migrated to the edge of the ring when co-cultured with fibroblasts. As in previous publications, fibroblasts seemed to help the epithelial cells polarize. Unfortunately, the extent of the polarization has not been tested by immunofluorescence in rings with and without fibroblasts. Nevertheless, rings with duodenal cells both with and without fibroblasts presented polarization shown with villin staining.

Interestingly, the fibroblast were able to contract the ring structure. The reproducibility of the result and its dependency on concentration can make it a tool for tissue engineering. Unfortunately, time limitations prevented further research in the contraction potential. For instance, patterning the ring with different fibroblast concentrations across the circumference could form villiform structures.

It is worth mentioning that the fibroblasts used in our model were human foetal fibroblasts (HFF). The use of oesophageal derived fibroblast could bring the model closer to *In vivo* conditions. Further, the use of cancer-associated fibroblasts could also be an interesting addition to this model. Fibroblasts engineered to secrete a growth factor, for instance, EGF could also be used. For instance they could be seeded in only half a section of the ring to assess if the BO cells outcompete squamous cells in that segment.

Even when the contraction of the collagen structures could have interesting uses, it might generate problems as well. The original idea for this model was to populate

the ECM with both fibroblasts and immune cells. The Jurkat cell experiments showed that adding another cell type changes fibroblast contraction. In addition, fibroblast contraction increased fibber density, making the structure more resilient to manipulation but potentially preventing immune cell migration. Further research needs to be done to achieve cell migration in the ECM. A solution to this issue could be starting with a lower collagen density or mixing additional ECM proteins. Laminin, for instance, has been shown to help organoid growth in culture [354].

4.8.4 Controlling droplet fusion and heterotypic junctions

One of the advantages over the previously published collagen ring methods was controlling droplet fusion. Using this property combined with a removable divider, two half rings could be printed and then fused after the divider is removed. The use of this divider permitted the formation of heterotypic epithelial junction in our model. Unfortunately, the squamous-columnar junction could not be reproduced using this method, as the squamous biopsies obtained did not grow into organoids. Instead, a gastroduodenal junction was replicated. This approach successfully generated a heterotypic junction between both gastric and duodenal populations. Once this technique is perfected, the next step would be going back to growing squamous organoids. The ability to use a divider to separate cell populations could have additional uses. As commented before, segments of the rings could be made with different fibroblasts, for example CAFs. The same approach could be done with immune cell populations, for example analysing cancer organoid growth in a half ring with Tregs compared with the other half without them. More complex dividers could be made to increase the number of different segments or make them asymmetric. A possible use for asymmetric segment ring structures could be cancer invasion assays, where a small segment of the ring contains cancer cells and the rest of the lining is healthy epithelium. Having this standardized experimental setting would allow for comparative studies of cell invasiveness under different stimuli or genetic modifications.

4.8.5 Printing self-shaping tubular structures

The ring model presented here could form heterotypic junctions and had a similar histologyto a GIT cross-section. However, it could not be used in combination with microfluidics. This is one of the advantages of the organ-on-a-chip approach. The objective was to generate long tubular structures that could be connected to a fluidics system in both ends. To achieve this the technique was modified using longer moulds.

The tubular structures printed could be as long as 10 cm. This length is larger than the used in most 3D bioprinting techniques thanks to the oil bath, as the oil reduced the effect of gravity during the process, preventing breakage. To our knowledge, the combination of mould plastic 3D printing with oil-bath technologies has not been used before. Most of the materials used during the experiments were intended to do other functions. The design of dedicated materials could increase size, speed and the complexity in which structures are made even further,.

The presence of fibroblast-controlled collagen contraction was utilised in the tube structures. By controlling fibroblast concentrations, the tube sections could be designed to have different contraction levels. This could make the tube self-shape during culture. By designing the model beforehand, structures with an anatomical resemblance to the stomach or the GIT were made. This would not have been possible without postponed contraction as the release of the collagen structure from the mould requires it to be regular across its length. To our knowledge, this is the only 3D printed model benefiting of the inherent contraction of fibroblasts to change its architecture.

In this thesis, the capacity of these structures to self-shape was used to add adapters to the edges. These adapters were strongly fixed to the ends by collagen contraction. Once attached they were used to control flow in and out of the tube lumen. In the future, the same approach could be used to incorporate the tubes to microfluidics circuits.

Self-shaping structures could be used for several other applications. For instance, to design xenografts for mice with the desired anatomical conformation. They could later be used to produce replacements for human like intestine, oesophageal or

vascular segments. This contraction could be driven further by combining fibroblasts with muscle cells to form artificial sphincters. Finally, they could facilitate the study of mechanotranscription or developmental pathways *in vitro*.

4.8.6 Controlling flow allows for both populating and infection of the tube lumen

The adapters used were plastic 3D printed hollow tubes. To control flow we needed two different elements to block the holes: the first a plastic piece capable of blocking medium inflow and the second a piece able to keep cells and bacteria inside while allowing medium exchange. For the latter, a cap could easily be made by using a pipette tip with a compressed filter mesh inside and cutting it to size. One of the inconveniences of this approach was the cap and adapter floatability. In the future, the use of metal microfluidic adaptors or denser plastic would be preferred. To improve collagen attachment to the adapter in metal the outer surface could be engraved.

Control of the flow into the lumen was used to populate it with epithelial cells. The coating worked with both cell types used but varied in thickness depending on the cell line. These experiments were performed with high concentrations of cells. Cell number titration experiments will be needed in the future to improve resource efficiency. This is especially important if organoids instead of cell lines are to be used. Organoids grow slower and the growth factors used in their medium are costly. Unfortunately, organoid migration when added to the collagen was not tested in the tube model. In the rings, the organoids migrated to the inner or outer ring edge in the presence of fibroblasts. For microfluidics experiments, it is important that the epithelium is found in the lumen, even when fibroblasts are used. Thus, the simplest approach might be to dissociate the cells and use them as cell lines to populate the lumen. This approach could also be more resource-efficient, requiring a lesser number of cells.

Further, the epithelial lining of the tube's lumen could be infected using *H. Pylori*. Unfortunately, AGS cells don't form tight junctions due to a mutation in E-cadherin. Thus, ASPP2 recruitment was not as clear as when stomach organoids were infected.

4.8.7 Properties of collagen walls

Finally, the permeability of the collagen wall was tested. This property is needed to efficiently flow medium through the tube's lumen. Both liquid and air were unable to cross the collagen wall of the tube. This is in conditions were pressure was not applied. It is possible that in conditions when a flow is applied the diffusion happens. Further experiments are needed to test for how long the diffusion is prevented. In addition, the use of fluorescent markers might be more precise than using phenol red. However, near impermeability of thick collagen walls has already been reported. With collagen containing cells having a permeability of 10-11 cm2 [355], this value considered in the transition between semipermeable and impermeable [356].

The impermeability of collagen is interesting for two future applications: first, creating air-liquid interfaces to promote cell differentiation and stratification in squamous cells. Full impermeability however, could become a problem as cells might be isolated from the external medium and thus dry out. This is however unlikely as collagen is a humidity reservoir. Second, it could prevent the mixing of the flowing medium in the lumen and the outer medium, thus enabling the more precise control of the concentrations of molecules in the medium during flow. With the impermeability of the wall confirmed, the difference between using solid caps or caps with filters becomes more important. Cells left isolated in the lumen for too long will lack the necessary nutrients unless the medium is replaced. Additional measures, like shortening the collagen fibers used in the bioprinting process, could regulate permeability if needed [355].

4.8.8 Future directions

The model presented here is potentially able to cover all the applications we defined as objectives. These are heterotypic junctions, immune cell co-culture, air-

liquid interphase and usable together with microfluidics. However, time limitations prevented us from doing experiments with all these elements together. The following section describes and discusses some of the innovative uses the model could have. It also comments additional improvements to the model.

Time and growth factors in differentiation

In vivo, the epithelium lining the different organs consists of cells in different differentiation subtypes. Unfortunately, no experimental setting to test differentiation in the models presented in this chapter was done. Immunofluorescence staining for differentiation markers is a priority in future experiments. Two factors could be easy changed to improve differentiation: culture times and medium composition.

The models in this thesis were cultured for four to seven days. Most of the other organotypic models presented in the discussion are cultured for periods of no less than two weeks. Longer culture times could potentially translate in a more differentiated mucosa. For instance, higher epithelium, more villi branching formation and more mucus production.

The medium is another factor determining differentiation. Organoids can be both cultured in proliferation or differentiation medium [299]. To ensure fusion and continuous epithelial lining in the models, proliferation of the cells was a priority. Thus all models containing organoids were cultured in proliferation medium. In longer culture experiments, however, differentiation medium could be used to promote a more diverse differentiation pattern and a more complex gland architecture. An alternative would be to use already differentiated organoids from the start. This will shorten the differentiation time but could potentially make monolayer formation more difficult.

Cancer metastases model

In this chapter the tubular model was presented as a tool to mimic GIT segments and illnesses. However, other organs in the body present tubular structures as well. A interesting application of tubular collagen structures would be studying vascular structures. One of the most direct applications would be studying metastases

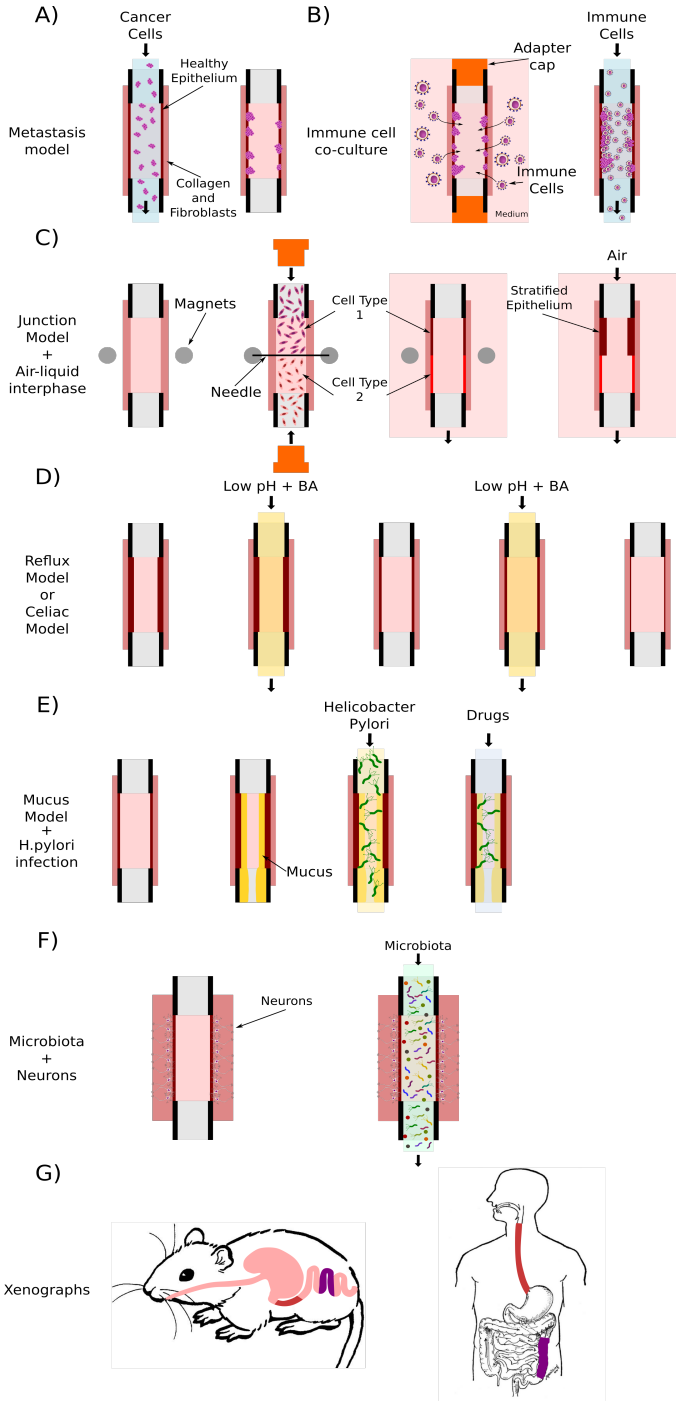

Figure 4.19: Summary of future directions A) Use of tube structures as a metastasis model and B) immune cell co-culture methods (right). C) Forming heterotypic junctions in the tubular structure using magnets. Followed by air-liquid interphase culture. D)Model to study reflux episodes *In vitro*. E) Model to study mucus production, cell infection and drug treatments. F) *In vitro* model to study microbiota and gut-brain axis cross-talk using tube structures. G) Tube segments used for xenografting and as organ replacement.

into other tissues. By populating the lumen with endothelial cells, a metastases model with cancer cells flowing through the lumen could be made. In it, drugs or genetic modifications promoting or preventing metastases could be studied. For instance, both cancer and endothelial cells could carry mutations that might facility extravasation of the tumour outside the vasculature. Flowing tumour cells into the lumen would also be a mechanism to seed them for co-culture with immune cells experiments (Figure 4.19 A).

Immune cell interaction model

In the previous chapter alternatives to EGF promoting BO invasion of the epithelium were proposed. One of them was using cytokines like IL-1B or IL-6 which activate similar pathways. These cytokines would be released during inflammation by immune cells in response to reflux. To test this hypothesis, immune cells need to be present in the model. This can be achieved in three ways. First, the immune cells can be present in the collagen when printing, however the migration could be prevented by the collagen fibers being too dense. Second, immune cells could be added in the medium outside the tube. In this approach, fiber density might also prevent migration of the immune cells into the lumen. Finally, cells could be flown inside the lumen using microfluidics. This has the advantage of direct contact with the epithelium. However, polarized epithelium cells would be interacting with the wrong side of the cell (Figure 4.19 B).

Heterotypic junction and air-liquid interfaces

In the previous chapter, a 2D model of the squamous-columnar junction was reproduced. In this chapter, the 3D heterotypic junction between gastric and duodenal was replicated. However, the BO SCJ was not shown. As mentioned before, squamous organoids could not be grown from biopsies. However, once this is solved there are two possible approaches to achieve heterotypic junction formation. First, stack two segments of the tube with organoids from each type. The organoids should migrate to the edge of the ring and fuse into a monolayer. This approach is likely to need a lot of cells and, if fibroblasts are present, might migrate to

the external edge of the tube instead of the inner lumen. The second approach is introducing the cells into the lumen. This approach requires a mechanism to separate both populations until they attach. This can be achieved by using a magnet attached to the bottom of the plate and a needle as observed in the medium difussion experiment. However this approach is likely to damage the collagen wall slightly. To prevent this damage, coated needles or knots using string could be used.

Previous experiments suggest that the collagen wall is impermeable to liquid and air. As a result, air could be flown into the lumen using microfluidics or a pipette. With the adapters blocked, the air would enhance differentiation and stratification of the mucosa (Figure 4.19 C) [357]. Caution will need to be taken not to dry the surface epithelium. As in microscopy, humidity of the air inflow can be controlled to prevent desiccation of the epithelium.

Gastroesophageal reflux disease model

During GORD reflux episodes are short and punctual [358]. During these episode the pH, bile acid and other compounds concentrations change rapidly . By using our model in a microfluidics device, we can imitate these changing conditions. Controlled reflux events will prevent cells from dying from continues exposure to the pH and bile acids (Figure 4.19 D).

Mucusoids and *Helicobacter Pylori*

Infections are another source of cancer in the GIT [359]. *Helicobacter Pylori* is a pathogenic bacterium that causes gastric adenocarcinoma a similar tumour to OAC. Like other bacteria, *H. Pylori* has been known to acquire resistance to the drugs commonly used to treat infected patients. Organoids have been shown to be a promising model to study the interaction between these bacteria and the epithelial cells. For instance, to find drugs to treat them [360]. Some issues remain when infecting organoids with cumbersome methods like microinjection or breaking them before infecting what can result in the polarized epithelial cells infected from any direction. To simplify infection, methods like the mucusoids have been developed. This study also emphasizes the importance of mucus having antibacterial properties

[318]. As in our model, this system simplifies infection and makes sure it happens only on the apical side. The tube model could be used to study the mucus by letting the cells secrete into the lumen and then milk it using slow microfluidics. This presents several advantages over the mucusoid method: First, the bacteria will only be in the interior of the lumen. Additionally, other cell populations like immune cells could be added to see how inflammation changes the outcome. Lastly, segments of human *H. Pylori*-infected tube could be xenografted into mice. Otherwise, mice would need to be humanized to effectively be infected with *H. Pylori*. Adding an artificial segment after the stomach with humanized epithelium would enable profiting of the mouse immune system (Figure 4.19 E).

Xenografting and organ replacement

One of the differences between the collagen tube model and organ-on-a-chip approaches is the lack of hard scaffolding. The absence of rigid scaffolding could make them a good candidate for xenografting. This tissue implants could be use in animal models or as a replacement parts in human patients.

In animals, one use would be to add controlled sections of GIT with the desired mutations and humanised epithelium. Sections with tumours with controlled progression stages, size and location could also be added. This might make a valuable model for new drugs and increasing reproducibility. For instance, using this approach we could test our EGF hypothesis. A segment of tube with half squamous and half BO lining of human origin could be introduced between the duodenum and the jejunum of mice. After a couple of weeks it would be removed for analysis.

For human replacement parts, the system would need to be scaled up. Further research and tests are required to study the complications derived from scaling up. Replacement parts are needed in cancer patients that have oesophageal or intestinal resections. These patients suffer loss in quality of life due to lack of ideal replacements [361] and complications like oesophageal structures [362], [363]. Currently, replacement is done with decellularized ECM matrix coming from pig intestine [364] or urinary bladder [365]. With studies showing that adding epithelial

layers to the decellularized surfaces help reduce strictures and improve quality of life [366]. The use of collagen tubes populated with fibroblasts and epithelial layers could potentially improve the quality of life of patients. This will be challenging and require several elements. First, obtaining cells from the patients beforehand. Then, expanding them as organoids or culturing them fast enough and in sufficient numbers to print a biocompatible structure. Second, to shape the implant with the native architecture. Finally, to vascularize the segments implanted to ensure their survival in the host (Figure 4.19 F).

Using nanoprinting in the future

An advantage of the tube method over bioprinting is the ability to construct structures using a laboratory pipette and a commercial plastic 3D printer. This will allow other laboratories to use this technique with few investments. It also leaves room for improvement if more complex structures are needed.

However, *In vivo* organs have complex structures and function, and a complex 3D architecture. An intestinal model, for example, should have a neuromuscular structure generating contractions to induce peristaltic movements. A differentiated and organized villi epithelium to be able to absorb nutrients and generate mucus. And finally, a vascular and lymphatic network to bring immune cells and oxygen to the system is crucial for the structure to be successful [367], [368]. Vascularization could be achieved by printing channels using sacrificial bioink as previously published in [345] or using aqueous droplets containing only PBS layer by layer forming channels. This level of complexity is not achievable with our actual model and would need to rely on nanoprinting.

During this chapter, nanoprinting resulted in a damaged and apoptotic epithelium. Probably due to dead cells in the lumen. There are two options to bypass the issue generated by dead cells and nanoprint with good results. The first is using commercially available products that clean up dead cells [369]. The other is using a printer with a bigger nozzle or changing to an extrusion printer. Being able to use a 3D printer to build our tubes would allow for more complex structures. For instance,

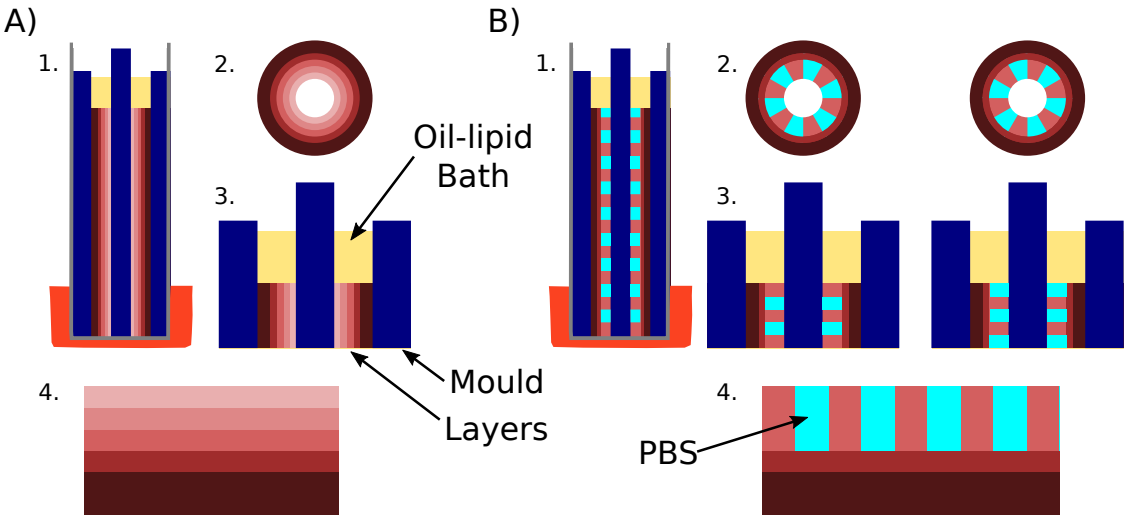

Figure 4.20: Using nanoprinting to increase complexity A) Use of nanoprinting to for layers from inside out at the same height. B) Using nanoprinting to form villi-like structures in the tube wall. 1) side view of printed tissue. 2 and 3) Top and lateral view of ring structure layer rotation. In villi formation the pattern rotates to form empty pockets. 4) Closer detail of side view and wall cross-section

using nanoprinting, lateral layerization can be achieved at the same tube segment. Each height could have different levels with epithelium, muscularis and serosa parts. This would make the model more similar to *In vivo* structures. Cell populations in distinct areas, for instance glands or tumours with different invasiveness could also be printed. A similar approach has been successfuly executed using spheroids with poor histological resemblance to *In vivo* structures [342] , [370] (Figure 4.20 A).

Nanoprinting could be used also to form villi structures. During this chapter only collagen droplets have been used. However, by using droplets of PBS empty spaces could be formed. The aqueous droplets would serve as a scaffold in oil and collagen could be layered on top. Then the droplets would dilute when the oil bath is replaced with medium leaving an empty space. The areas next to the lumen where aqueous droplets are would rotate every certain layers. When the medium is added they would dilute generating invaginations in the collagen. This invaginations can then be populated with cell lines or organoids (Figure 4.20 B).

Microbiota models for the gut

The study of human gut microbiota has experienced a marked increase during the past years. Microbiota has been linked to areas as diverse child development [371], [372], illnesses like cancer [373], [374] and infections [375], obesity, diabetes [376] and the human the psyche through what is known as the gut-brain axis [377], [378], [379].

The renewed interest in this field increases the need for new models to study the microbiome *In vitro*. In animal models, study of the microbiota has been attempted *In vivo* by transplanting human microbiota from ill patients to germ-free mice. However due to diet and the disparities between two species, the model presents many challenges [380]. Recently, organ-in-a-chip models have been developed that are able to co-culture epithelial, endothelial and microbiota populations. These models use the flow to keep the bacteria populations in check preventing overgrowth from happening [381], [382]. Today an *In vitro* model able to study the gut-brain axis does not exist, although ERC grants to projects like MINERVA ' (MIcrobiota-Gut-BraiN EngineeRed platform to eVAluate intestinal microflora impact on brain functionality) are trying to promote it [383]. Using our method, we could include neurons and immune cells into the models in a complex 3D architecture to better mimic the gut-brain axis. Neurons are difficult to culture *In vitro*, having complex medium requirements. Thus, this would require solving the issue with medium conditions first (Figure 4.19 G).

4.9 Conclusion

The tube model introduced in this chapter presents several novelties: one being the use of an oil-lipid bath together with a plastic 3D printer, the other profiting from fibroblast contraction to shape and connect the printed structures to the desired non-organic element. Overall, this method is close to the organ-in-a-chip system. It can be used to co-culture organoid cells with stromal cells, be used in microfluidics and be infected easily. Yet, the tube model presents three additional advantages.

First, the lack of any rigid or inorganic parts. This increases the possibilities for processing and manipulating the model, a potential use being xenografting them into animal models to humanize them or doing replacement parts.

A second, is generating heterotypic junctions by organoid migration from the ECM or by limiting the access of cells to only a segment of the tube.

Finally, all the process is done with limited investment in machinery. Instead of having a dedicated hardware, the use of a relatively cheap 3D printer allows the model to be adapted to the requirements needed.

Further research is needed to fully develop its potential as most of the proposed uses have not been tested. This model would also benefit from better understanding the three steps of BO progression to OAC. This steps are BO cell of origin, colonization of the distal oesophagus and transformation to OAC. In the next chapter we propose a process to study this steps focusing in the activated pathways and the compounds that might secrete them. Hypotheses arising from such a study could be later used in models like the collagen tubes.

5

Combining microdissection and proteomics to study Barrett's oesophagus progression

Contents

5.1 Research aim 148
5.2 Introduction 149
5.2.1 Barrett's Oesophagus to OAC progression occurs in a complex environment 149
5.2.2 Techniques to study complex microenvironments driving Barrett's oesophagus at a cellular subtype level 150
5.2.3 Advantages of working with proteins 153
5.2.4 Using microdissection and proteomics to study Barrett's oesophagus 154
5.3 Experimental design 155
5.4 Contributions 156
5.5 Results 157
5.5.1 Patient case selection pipeline 157
5.5.2 Sectioning FFPE blocks pattern 158
5.5.3 Sample annotation 158
5.5.4 Sample selection and microdissection 161
5.6 Discussion 162
5.6.1 Mounting thinner sections on microdissection slides . . 163
5.6.2 Use of biopsies in place of paraffin blocks 168
5.6.3 Using results to study pathologists lack of consensus . . 168

5.1 Research aim

The origin, colonization and progression of Barrett's Oesophagus to OAC happens in a complex environment. In the previous chapter a model trying to replicate this complexity *in vitro* was described. However, the knowledge of the *in vivo* regulatory pathways, cell populations, differentiation, growth factor gradients and mutations shaping these events is still limited.

In the last decade, several studies have been conducted trying to better describe this complex environment. The main approach of these studies has been the bulk sequencing of either DNA and RNA. These techniques lack the spatial information required to know the cell origin and location in the tissue. This translates into a loss of signal, as information coming from the different tissue types when the sample is processed in a single batch is mixed together. Techniques like single-cell sequencing and tissue microdissection are being used to try to prevent this loss of spatial information.

In the clinic, most samples are stored embedded in paraffin after being fixed to preserve them. This process reduces the quality of both DNA and RNA. Proteins are by nature more resilient to these processes than nucleic acids. By studying proteins using proteomics techniques, details on both protein abundance and post-translational modification can be obtained. In this chapter, the aim is to combine microdissection and proteomics to study BO.

This combination would achieve both spatial information and good quality data from paraffin-embedded samples. Unfortunately, due to technical and time constraints this chapter does not contain proteomics data results.

5.2 Introduction

5.2.1 Barrett's Oesophagus to OAC progression occurs in a complex environment

The previous chapter aimed to improve the study of BO colonization of the lower oesophagus by adding complexity to the model. *In vivo* this complexity arises from the different cell populations present, their differentiation status and their interactions. This populations include epithelial, immune, endothelial and, other cell types. These complex interactions have an effect during all the stages of Barrett's oesophagus progression.

The origin of BO has been attributed to several of these cell populations through the following means. First, through the transdifferentiation of either gastric or squamous epithelial cells. Second, the migration from endothelial, oesophageal submucosal glands or immune cells progenitors into the damaged mucosa. Third, the ability of stem cell niche populations to colonize the lower oesophagus [71], [384], [72].

The reflux reaching the distal oesophagus influences its environmental conditions. The low pH damages the squamous mucosa activating apoptotic and inflammation signalling. This inflammation recruits immune cells [385] to the mucosa increasing the signal. Cytokines released by these cells, bile acids, retinoic acid [386] or the effect of EGF discussed previously could help BO achieve its final length.

The transition from BO to dysplasia and OAC happens in a context of inflammation. The tissue is infiltrated by immune cells, showing higher levels of cytokines like IL-1B and IL-8 and nf-KB activation [265].

In the early stage of OAC, the presence of cancer-associated fibroblasts could help the tumour cells invade the stroma. This increases its staging and reduces the chance of survival of those patients [208]. The treatment of OAC is also affected by neighbouring immune cell populations. For instance, the presence of tumour infiltrating lymphocyte improves prognosis in patients [387], [388]. Although no studies have been published for OAC yet, tumour associated macrophages (TAMs) [389] and regulatory T cells (Tregs) [390] are inversely correlated with prognosis in most cancers.

Bulk DNA and RNA next-generation sequencing technologies have been the most successful methods to study this progression [391]. However, these interactions are also influenced by the spatial location of each element. By processing all the samples in a batch there is a risks of losing the signal attributable to each cell type and its spatial information. To solve this issue, different techniques have been developed that are starting to be used in the context of BO and OAC.

5.2.2 Techniques to study complex microenvironments driving Barrett's oesophagus at a cellular subtype level

Flow cytometry and Fluorescence activated cell sorting

Antibodies against extracellular proteins that are cell-type specific can be used to label a specific cell population. By using a fluorescense activated cell sorter (FACS) the proportion of cells of each subtype can be analysed and the cells sorted for posterior analysis [392]. This technique has several drawbacks. First, the markers for the cells need to be known beforehand. Second, the number of populations it can label concurrently is limited. Finally, it needs a substantial amount of tissue to study the least frequent cell populations.

Magnetic-activated cell sorting and Mass cytometry

An alternative to FACS is the use of magnetic nanoparticles coated with antibodies against the cell-specific protein. With the use of magnets, the population can be removed or extracted for further processing. This technique is known as Magnetic Activated Cell Sorting (MACS) [393]. MACS has the same drawbacks and less purity but can be used with smaller volumes.

By labelling the antibodies with metal isotopes, the single-cell resolution of flow cytometry can be combined with mass-spectrometry. This technology is known as mass cytometry or cytometry by time of flight (CyTOF). With CyTOF up to 40 different isotopically labelled antibodies can be used. The drawbacks however remain similar to FACS. CyTOF is only useful for a panel of already known genes and needs to process big tissue samples to obtain certain populations. To this factors

we have to add the cost of the technique, the slow cell analysis throughput and the destruction of the sample during the process preventing further analysis [394].

Single cell sequencing

Single-cell RNA sequencing (scRNA-seq) uses a microfluidic device to separate the sample into a flow of single cells. These cells are then isolated by cutting the solvent flow into droplets using a secondary oil current. To each one of the droplets digestion enzymes and a barcoded handle to the RNA are added giving each sample a unique code. The RNA is then pooled and sequenced. Finally, computer analysis methods allow to assign each read to a cell. Then, the cells are grouped and analysed through dimensionality reduction techniques [395].

The advantage of this technique is the lack of a requirement for markers. This enables the description of cell populations previously unknown in the samples. It also gives RNA level information for each population although the overall quality is usually not as good as in bulk sequencing [396]. This technique still has the drawback of needing a substantial amount of starting material and lacks spatial resolution [397]. The cell markers found using this technique can however be used to label these cell types in tissue slides in downstream experiments.

Bulk sequencing deconvolution

Attempts to infer the information for a specific cell population using bulk sequencing data have been done. This can be done by using the RNA-seq data from a purified cell type and extracting the signatures from these populations. Once the signature is established, batch deconvolution computer analysis tools like CYBERSORT can infer the abundance of each cell type in batch tumour sample [398], [399]. Recently, techniques have appeared that rely on single-cell sequencing data instead of purified populations to extract the cell signatures [400]. The scRNA-seq data can benefit from bulk RNA-seq as well by inferring cell abundance from bulk RNA-seq. This prevents the bias from occurring in scRNA-seq [401]. This however does not produce any further detail of signal pathway activation besides cell specialization, for instance M1 or M2 macrophages, and their abundance.

Immunohistochemistry and Slide-seq

A handicap of all the previous techniques is the absence of spatial resolution. Some information for the different cell types can be extracted, normally abundance, but the position and relative abundance of those cells in the context of the histology cannot be obtained. Traditionally, this can be addressed by staining tissue slides from a part of the biopsy that will be sequenced using the markers for those cell populations. This staining can consist of either histochemistry or immunofluorescence. These techniques are usually limited to a few cell populations due to the difficulty of multiplexing.

Techniques like Slide-seq try to join both sequencing data quality with spatial resolution. First the tissue slide is covered with DNA coded beads with known coordinates. The tissue is then digested, and the RNA attaches to the DNA. After amplification and sequencing the results can be mapped to the slide coordinates [402]. Although this techniques might revolutionize how Barrett's oesophagus is studied, they are still at a prototyping stage and are not easily available to many laboratories.

MALDI imaging

A similar approach analysing proteins both quantitatively and spatially information from a tissue sample slide is MALDI-TOF. This technique consists of two steps happening continuously, Matrix-assisted laser desorption/ionization (MALDI) and Time of Flight (TOF) mass-spectrometry. In MALDI the tissue slide is covered with droplets of matrix at regular distances. These matrix spots are then ionised using a ultraviolet laser. Proteins carried with the matrix can be studied using a time of flight mass-spectrometry [403] [404].

Tissue microdissection

One of the drawbacks of MALDI imaging is the need to use frozen tissue. Most clinical institutions store patient tissue extracted after pathologist annotation in formalin fixed paraffin embedded (FFPE) blocks.

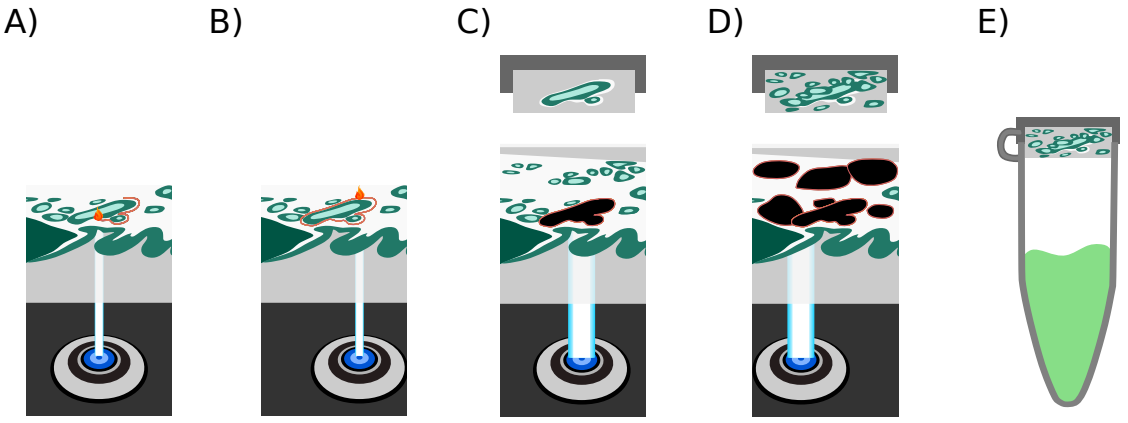

Figure 5.1: Steps during tissue microdissection A) Using focused laser the membrane and the tissue were cut. B) The laser completely separates the area of interest from the rest of the tissue section. C) Using a broader laser, the tissue is pushed up into the sticky cap of a special tube for tissue microdissection. D) By repeating the process in other areas with the desired feature, the cap is filled with the desired tissue type. E) The tube is closed after including the desired reactive to start processing the sample for protein, RNA or DNA extraction.

An alternative to MALDI for FFPE samples is the use of a tissue microdissection. In this technique sample sections are put on special microdissection slides coated with a light responsive element. The samples are then deparaffinised and counterstained. With the help of an automated plate controlled by software, a laser cuts the sample which is then catapulted into a collector tube. By repeating this process over the desired area of the slide a sample consisting of only a histology subtype can be obtained (Figure 5.1). This technique has been used to study the squamous-columnar junction in the cervix [405].

With this technique DNA, RNA and protein can be extracted. However, RNA quality is low after fixing and storage [406] and DNA-seq can only be used to study mutations and copy number variations in the cell. This gives proteins several advantages that make them interesting to study BO using FFPE samples obtained from the clinic.

5.2.3 Advantages of working with proteins

- Proteins are the functional unit of the cell. Their abundance in a certain tissue should give a closer representation of the phenotype than RNA levels.

- Proteins extracted from FFPE tissue are less damaged than DNA and RNA molecules.

- Mass-spectrometry also detects post-translational modifications present in the proteins. This would allow studying which pathways are activated. For example, the phosphorylation of RTK like EGFR during BO colonization of the lower oesophagus [407].

- Proteins can also be used to study the ECM of the tissue slide. ECM has been reported to have an environmental effect of BO to OAC evolution [408].

5.2.4 Using microdissection and proteomics to study Barrett's oesophagus

Proteomics markers for Barrett's oesophagus progression

Barrett's oesophagus progression to cancer through dysplasia has been studied with DNA and RNA sequencing. However, the proteomic landscape at the different progression stages has not been studied using microdissection. The characterization of the protein levels through the different stages could have clinical applications. For instance, comparing the results in microdissected tissue from low-grade and high-grade dysplasia with early BO could be used to find new markers for progression. The new markers could then be used for early detection in biopsy histology analysis or even cytosponge studies. Recently, the use of cell free DNA [409] and protein [410] in the bloodstream as diagnosis markers have been tested with success. The knowledge of new DNA and protein markers could be used to replace endoscopy or make its need less frequent. This could result in a decrease in costs for public healthcare and better quality of life for the patients.

Barrett's oesophagus origin

The OSG hypothesis for BO origin was proposed by Leedham et al. [74] using microdissected samples of these epithelial types. Recent work by our lab [14], suggests that submucosal glands and BO share cell populations. Using microdissection of the glands plus DNA-seq and proteomics analysis a purified population could produce further evidence on this hypothesis. With this approach both DNA and protein mutations and how they relate could be studied but also copy number variations and clonality.

EGFR and other tyrosine kinases phosphorylation

In this thesis a gradient of EGF promoting BO invasion of the distal oesophagus was proposed. In this hypothesis, the cells closer to the gastroesophageal junction will be exposed to higher levels of EGF. In the 2D *in vitro* model presented in this thesis, the results with EGF titration suggest that this gradient could be able to promote BO segment growth. The EGF gradient could also explain why these populations have also been reported to have more goblet cells [188], [189], [190]. Using microdissection, we can try to confirm whether BO populations without goblet cells have less phosphorylation of the EGFR receptor. Concurrently OSG gland populations under the squamous epithelium should also present less EGFR phosphorylation but have a similar protein signature to BO. A last interesting point to address for EGF in BO is how abundant EGF secretion from the BO epithelium and OSG is. Of note, the intrinsic amount of EGF present in the BO can make that of the reflux irrelevant in comparison.

5.3 Experimental design

This chapter aims to combine tissue microdissection with simultaneous DNA and Protein extraction. A better understanding of the microenvironment of BO and its evolution to OAC can be obtained by following this steps:

- Obtain access to EMR patient samples containing OSG, BO, LGD, HGD and OAC histological features.
- Process and store slides for H&E staining, microdissection and future research.
- Annotate the samples by at least 3 pathologists.
- Microdissect and extract RNA and Protein from the tissue subtypes.
- Define protein signatures for each progression stage in BO and study its evolution as devolves into OAC.
- Study the relationship between mutations, copy number and protein levels in BO.
- Define the proteomics profile for the BO, LGD and HGD transition axis and the changes between them.
- Find new markers for LGD and HGD that could be used in the clinic.
- Study if EGFR phosphorylation across the different histological features. Compare proximal and distal BO sections, different progression stages and EGFR phosphorilation of EGFR.

5.4 Contributions

Partial funding was obtained from CancerUK to support this projects thanks to the help of Dr Richard Peter Owen, who also thought of the experimental design. The samples were obtained from the Imperial College through the help of Professor Robert Goldin. Professor Robert Goldin, Professor Viktor Koezler and Dr. Lai-Mun Wang annotated the histology.

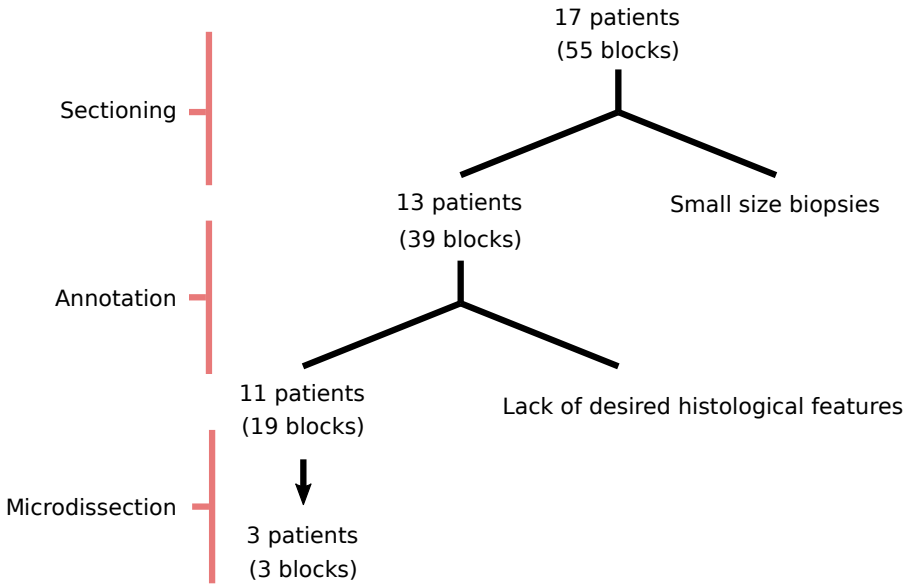

Figure 5.2: Pipeline of sample selection for microdissection Pipeline with the number of patients and blocks processed and attrition in each step of the process (Sectioning, annotation, microdissection.)

5.5 Results

5.5.1 Patient case selection pipeline

Due to the time requirement of the microdissection technique, only a few patients could be processed at the same time. After processing this small batch, the objective was to confirm that good quality data could be obtained with old FFPE samples. Then the study of a larger patient batch could be considered. As the time was limited, the samples were subjected to several filter steps to shortlist the most interesting cases. Priority was put in samples with different stages of BO progression in the same FFPE block. The following process was used to select the final candidates for microdissection (Figure 5.2):

First, samples in which the biopsy was too small were discarded. Second, blocks were sectioned into the slides and H&E stained. Third, after annotation by three pathologists the samples with only few BO progression histological features were discarded. Finally, the top three samples from different patients with the most diverse BO features were selected for microdissection.

5.5.2 Sectioning FFPE blocks pattern

Each block needed to be sectioned in sufficient slides to ensure sample availability during the downstream processing. First, H&E staining and annotation by pathologists. Second, microdissection slides with 10 um thick sections to counterstain and microdissect. These sections were cut thicker to obtain more tissue from the same slide. Finally, additional sections were taken in glass slides to keep for future experimental work. To ensure enough slides were available for each step, 14 slides were sectioned from each FFPE block. The two first being 4 um thick samples on glass slides. These slides were followed by two 10 um thick samples on microdissection slides. This pattern was then repeated twice more. Lastly, two additional 4 um sections on glass slides are sectioned. The slide number 6 of each sequence was H&E stained and then annotated. 10 um slides were stained with methyl green and then microdissected. Finally, unused 4 um slides were stored for later use.

5.5.3 Sample annotation

The H&E stained slides were annotated by three different pathologists. Each slide was annotated for the different steps in BO progression. The different annotation classes were the following: Squamous epithelium, oesophageal submucosal glands, reactive epithelium (BO without globlet cells), Barrett's oesophagus with goblet cells (BWG), Low-grade dysplasia (LGD), High-grade dysplasia (HGD) and oesophageal adenocarcinoma. An example for each tissue type can be found in Figure 5.4.

The areas where all three pathologists agreed were outlined in black. Where the annotations did not match, a red or blue color highlighted the area of controversy with the first pathologist. A second overlay was made color coding the areas with the annotations. Areas where there was disagreement were labelled with the class two of the three pathologist had agreed upon. The result for each block was kept in a table (Figure 5.5). The samples with at least three different histological features were shortlisted for microdissection.

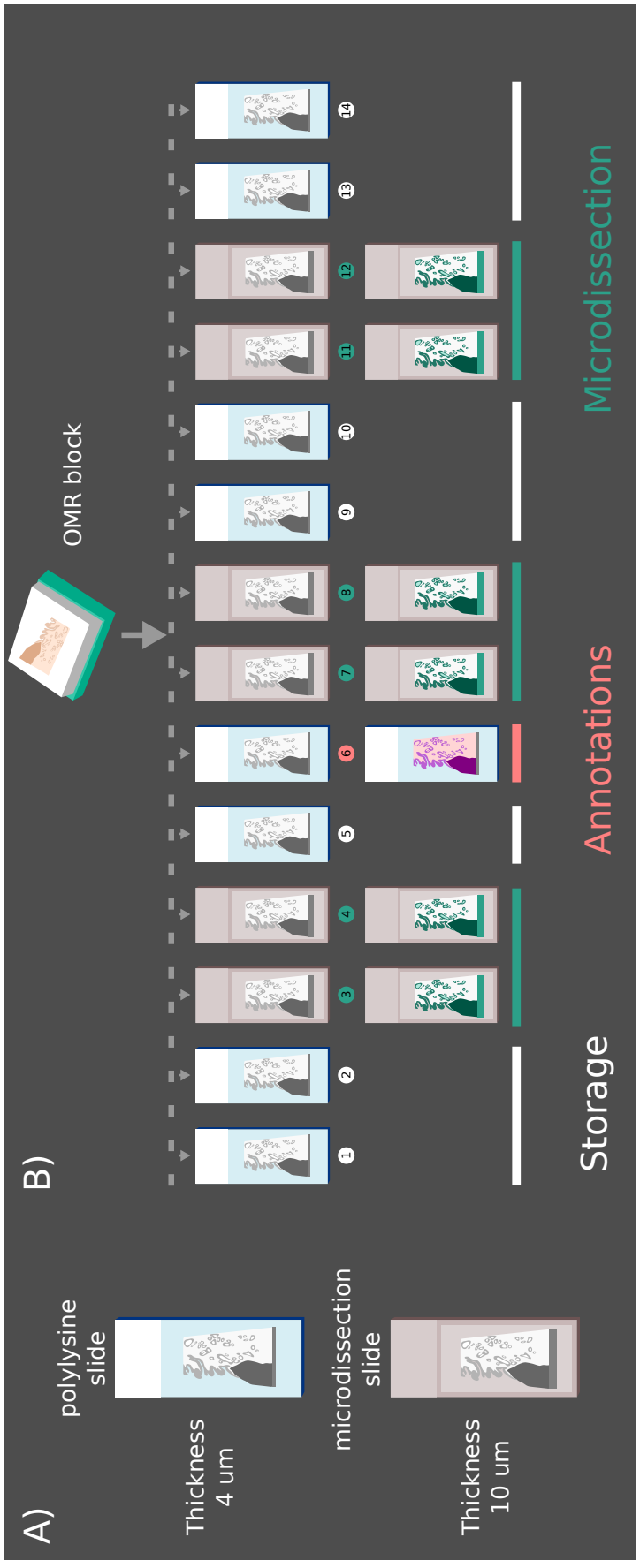

Figure 5.3: Block processing protocol A) Block sections were cut at 4 and 10 um on glass and microdissection slides respectively. B) Detail of sectioning steps and its final use. Slide 6 is H&E stained and annotated. 10 um slides are stained with methyl green and microdissected.

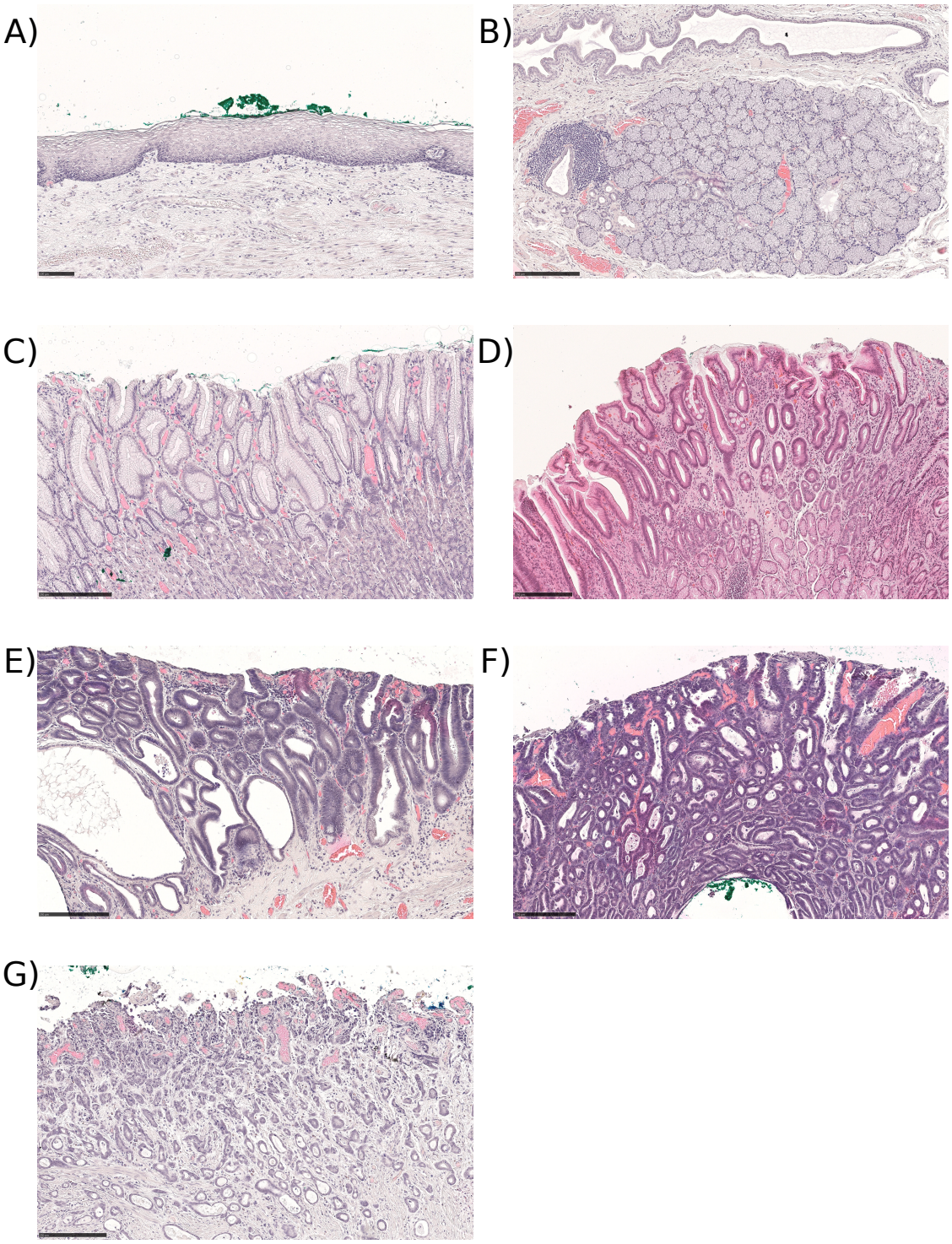

Figure 5.4: Example of histology annotations for microdissection Each sample was annotated for the following tissue types: A) Squamous epithelium, B) Oesophageal submucosal glands (OSG), C) Reactive columnar epithelium (Reactive), D) Barrett's with goblet cells (BWG), E) Low grade dysplasia (LGD), F) High grade dysplasia (HGD) and G) Oesophageal adenocarcinoma.(OAC). Scale bar: 100 um for A) image and then 250 um

Main code	Id	Block	Squamous	Glands	Reactive	BWG	LGD	HGD	OAC	Total
MS17	821	A1	1	1	0	0	0	0	1	3
		A2	1	1	0	0	0	0	1	3
		A3	1	1	0	0	0	0	1	3
MS17	1145	A1	0	0	0	0	0	0	0	0
		B1	0	0	1	0	1	0	0	2
		B2	0	0	1	0	1	0	0	2
		C1	0	0	1	0	1	0	0	2
		C2	0	0	1	1	0	0	0	2
		D1	0	0	1	0	1	0	0	2
		D2	0	0	1	0	0	0	0	1
		E1	0	0	1	1	1	0	0	3
		E2	0	0	1	0	1	0	0	2
MS17	2392	B2	1	0	1	1	1	0	0	4
MS17	2698	A2	1	1	1	1	1	1	0	6
		B2	1	0	1	0	0	0	0	2
		C2	1	1	1	0	1	0	0	4
MS17	5060	A2	1	1	1	0	1	1	0	5
		B2	1	1	1	1	0	0	0	4
		C2	1	0	1	1	1	0	0	4
MS17	8938	B1	0	0	1	1	0	0	0	2
MS17	18751	A1	0	0	1	1	1	0	0	3
		A2			1	1	1			
MS17	20276	A1	0	0	0	1	0	0	0	1
		A2	0	0	1	1	1	0	0	3
		A3	0	0	1	1	0	0	0	2
		A4	0	1	1	0	0	0	0	2
		A5	0	0	1	1	1	0	0	3
MS17	1216	A2	1	0	0	0	0	0	0	1
MS17	14510	A2	0	0	1	1	1	0	0	3
		B2	0	1	1	1	1	0	0	4
MS17	9431	A1	0	0	1	0	1	0	0	2
		A2	0	0	1	1	1	0	0	3
MS17	8938	A1	0	0	1	0	1	0	0	2
		A2	0	0	1	1	0	0	0	2
		B2	0	0	1	0	1	0	0	
		C1	0	0	1	1	0	1	0	
		D2	0	1	1	1	0	1	0	4
MS17	23857	A1	0	1	1	1	0	0	0	3
		A2	0	0	1	0	0	1	0	2
		A3	0	1	1	1	1	1	0	5

Figure 5.5: Annotation table for selected Color-coded table of block annotations, each patient has its own color heading. The presence of each histological feature is represented a 1 (green). They absence of a tissue type with a 0 (red). The total column adds the number of different tissue types.

5.5.4 Sample selection and microdissection

For the first microdissection batch three blocks were selected. The details of the annotations and the microdissection of the samples selected can be found in the following figures:

- 1) Figure 5.6 and Figure 5.7 corresponding to the ID MS17-821-A2.
- 2) Figure 5.8 and Figure 5.9 corresponding to the ID MS17-2698-A2.
- 3) Figure 5.10 and Figure 5.11 corresponding to the ID MS17-14510-B2.

The samples were then stored ready for DNA and protein to be extracted for sequencing and Mass-spectrometry (MS) analysis. Unfortunately, due to time limitations the samples were not processed further.

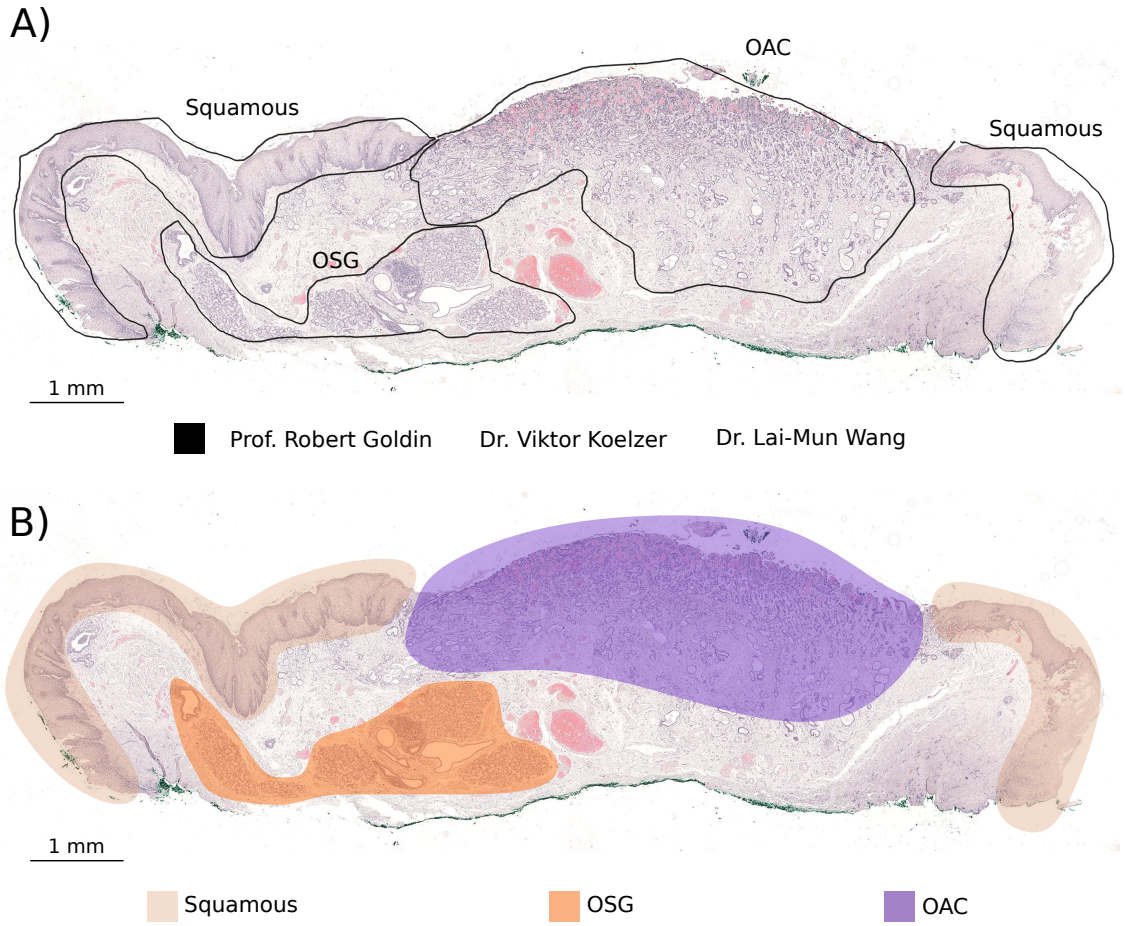

Figure 5.6: Block MS17-821-A2 annotations A) Annotation by three pathologist. B) Color-coded areas of interest for microdissection.

5.6 Discussion

During this chapter the different approaches to study complex tissues with several cell populations were described. Due to the availability of EMR blocks in the clinics where endoscopy resection of advanced BO segment is made, the use of proteomics combined with microdissection was suggested. To make a pilot experiment, a small study of 17 patient and 55 blocks was started. Then the samples were processed to ensure there was enough tissue for pathology annotation, microdissection followed by proteomics and spare slides for future experiments. Later, the samples were annotated by the pathologists. Finally, the slides from the three patients with the most diverse histological features were microdissected.

Unfortunately, the time span that the experiments would take was underesti-

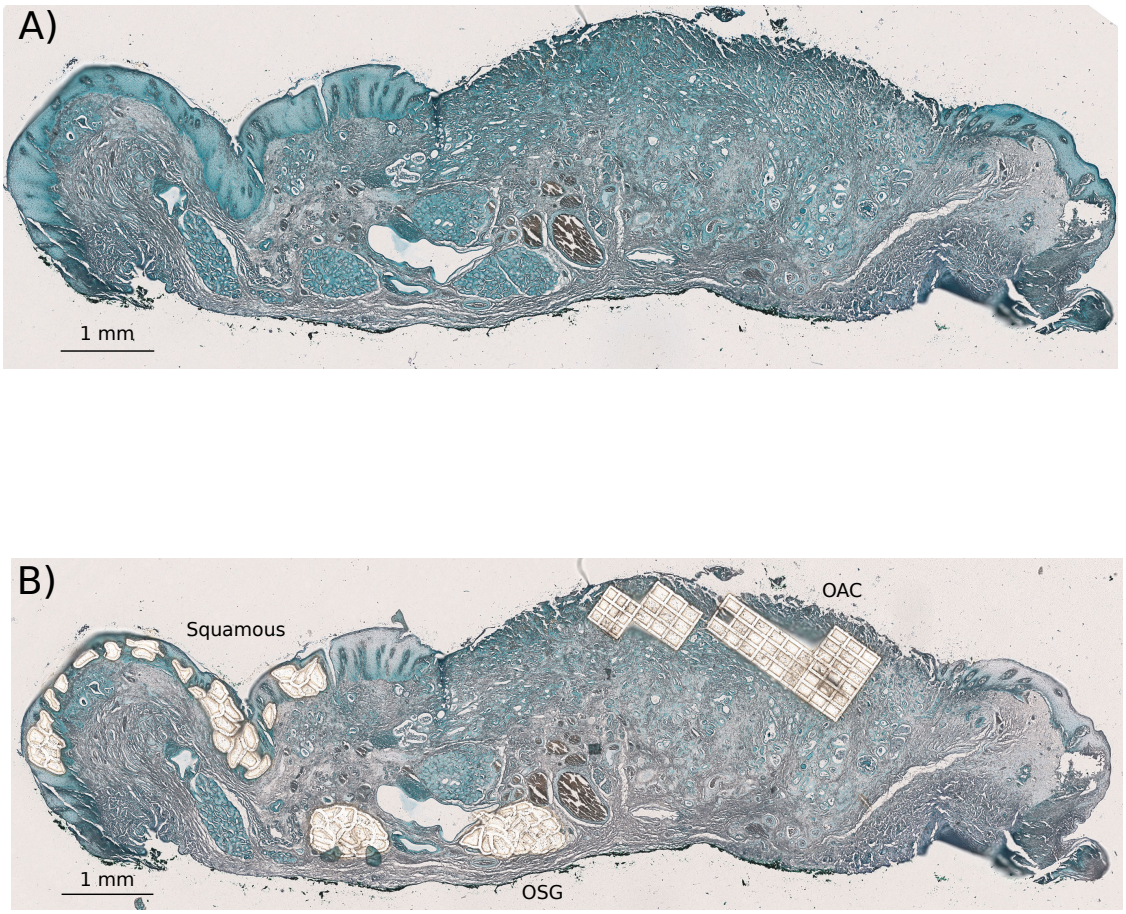

Figure 5.7: Block MS17-821-A2 microdissection A) Scan of one of the six slides stained with methyl green previous to microdissection B) Areas extracted from the same slide after the microdissection process.

mated. At the initial point, the goal was to process samples from a minimum of ten patients. This number was suggested to reduce the batch effects in sequencing and proteomics runs. Due to inexperience in processing the samples the processing times were underestimated. Next, several factors that could improve the project pipeline are discussed.

5.6.1 Mounting thinner sections on microdissection slides

To increase the amount of sample cut from the same slide, the FFPE blocks sections were sliced to a 10 um thickness. Once the tissue was being microdissected, this generated several issues. The tissue was more difficult to cut, often requiring several rounds of laser to detach it from the wax. Additionally, the increased

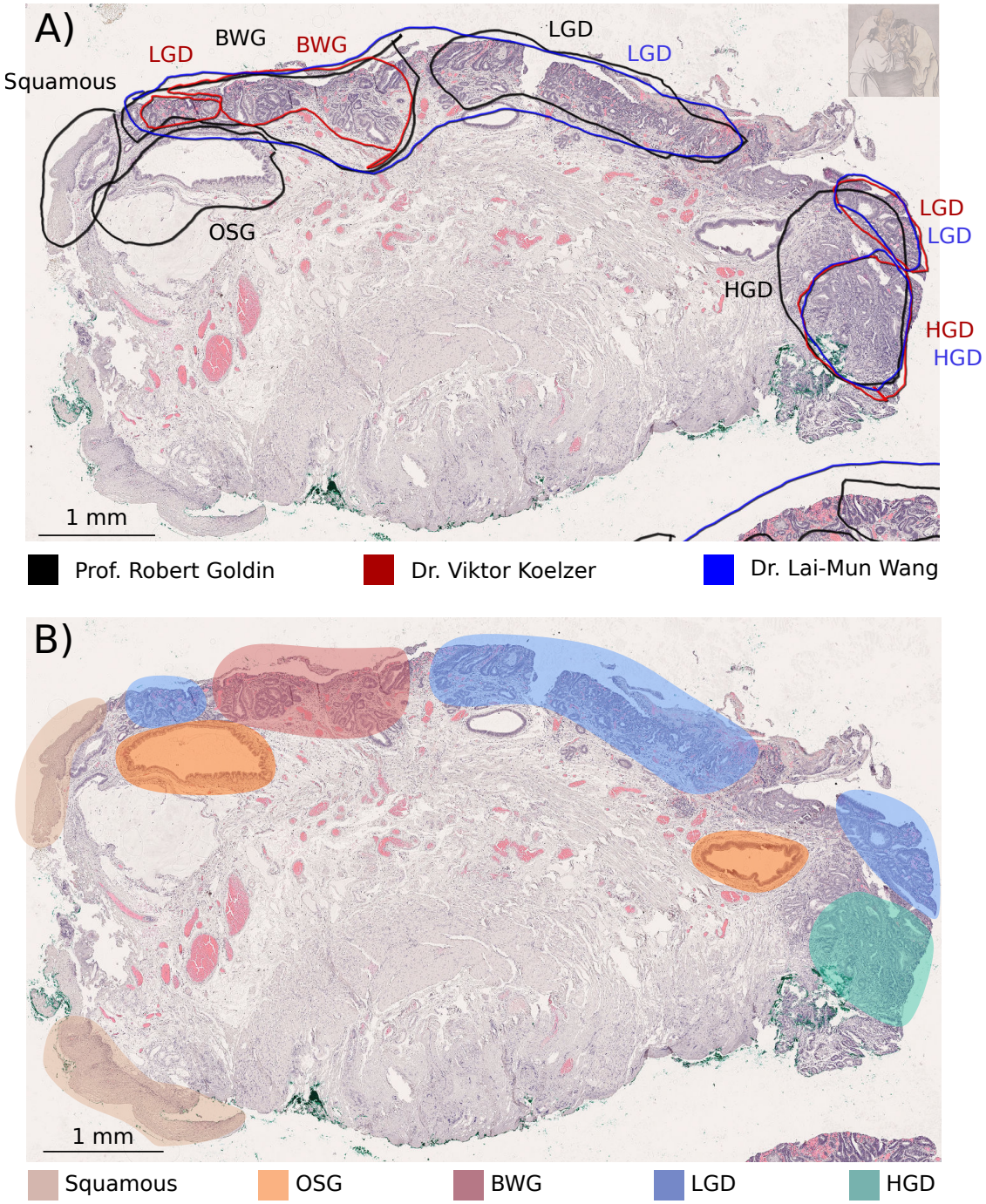

Figure 5.8: Block MS17-2698-A2 annotations A) Annotation by three pathologist. B) Color-coded areas of interest for microdissection.

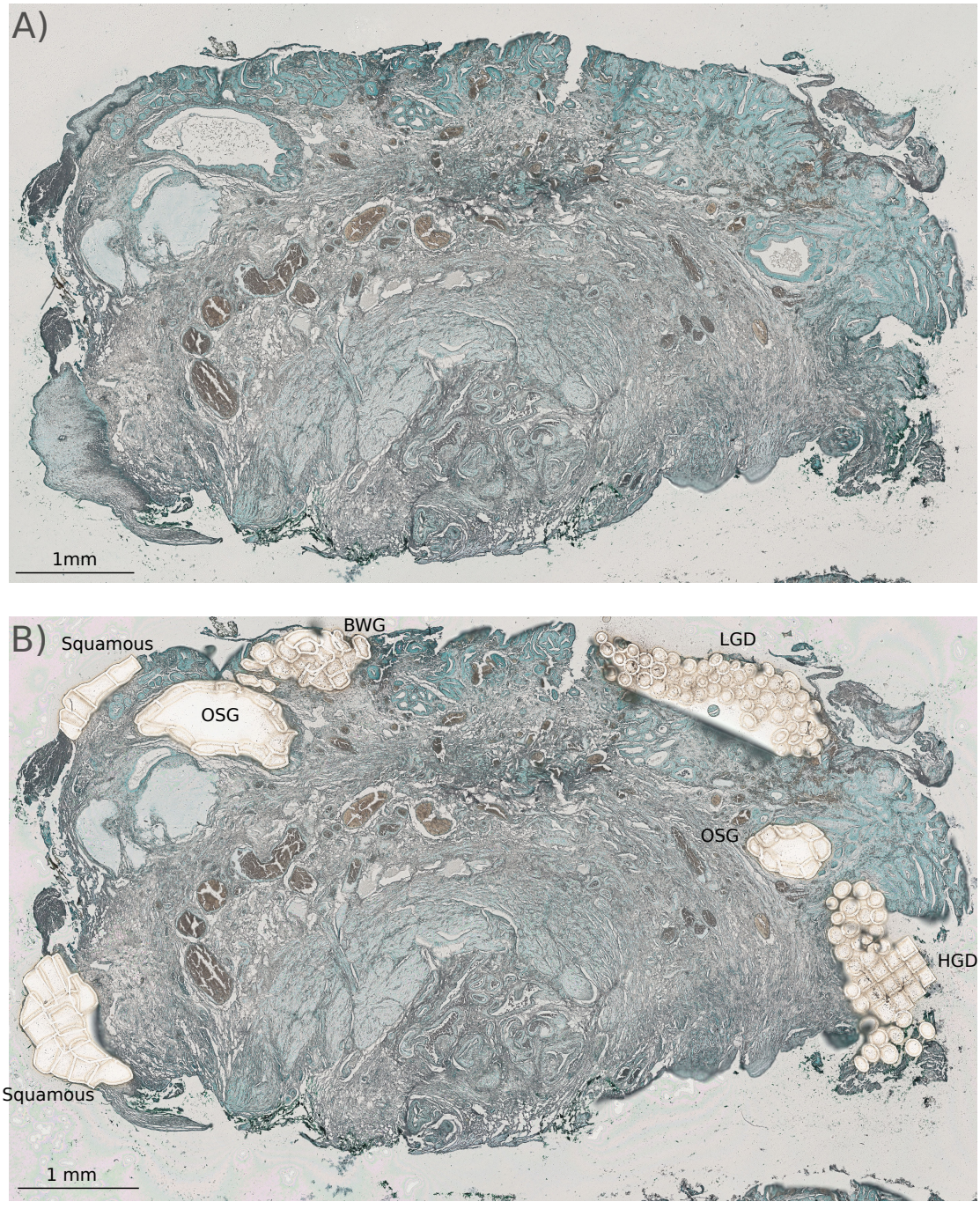

Figure 5.9: Block MS17-2698-A2 microdissection A) Scan of one of the six slides stained with methyl green previous to microdissection B) Areas extracted from the same slide after the microdissection process.

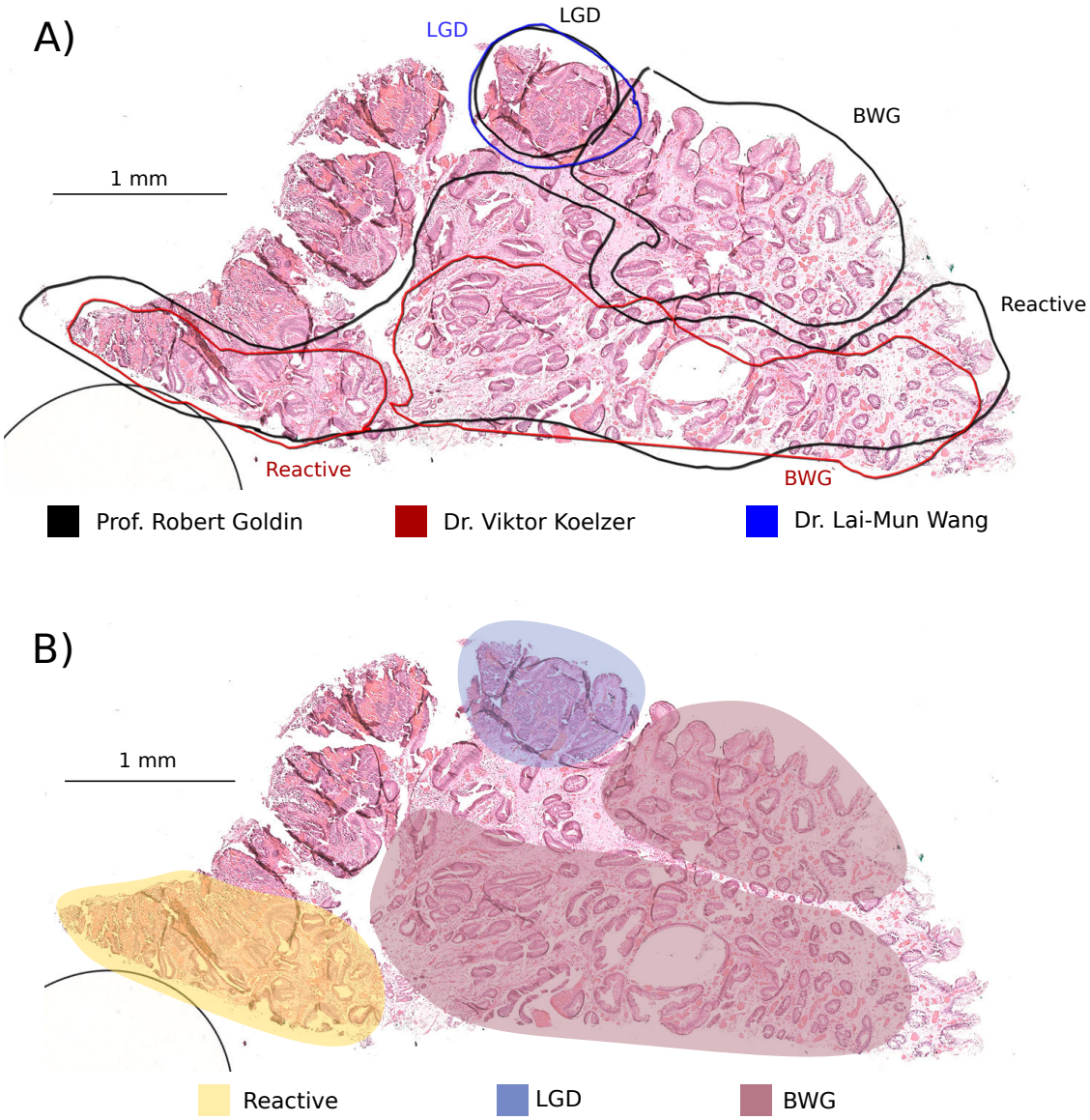

Figure 5.10: Block MS17-15410-B2 annotations A) Annotation by three pathologist. B) Color-coded areas of interest for microdissection.

thickness increased the weight. This affected the process of catapulting the tissue into the collection tube. Thus, the area cut from the slide needed to be reduced. This increased microdissection processing time investment contributing to the overall delay project of the.

Another problem with microdissection increasing time expenditure were the number of slides to microdissect. Instead of fours slides like in previously described studies, six were used in this project, each slide having two sample sections.

These design decisions were taken to ensure that there was enough tissue to

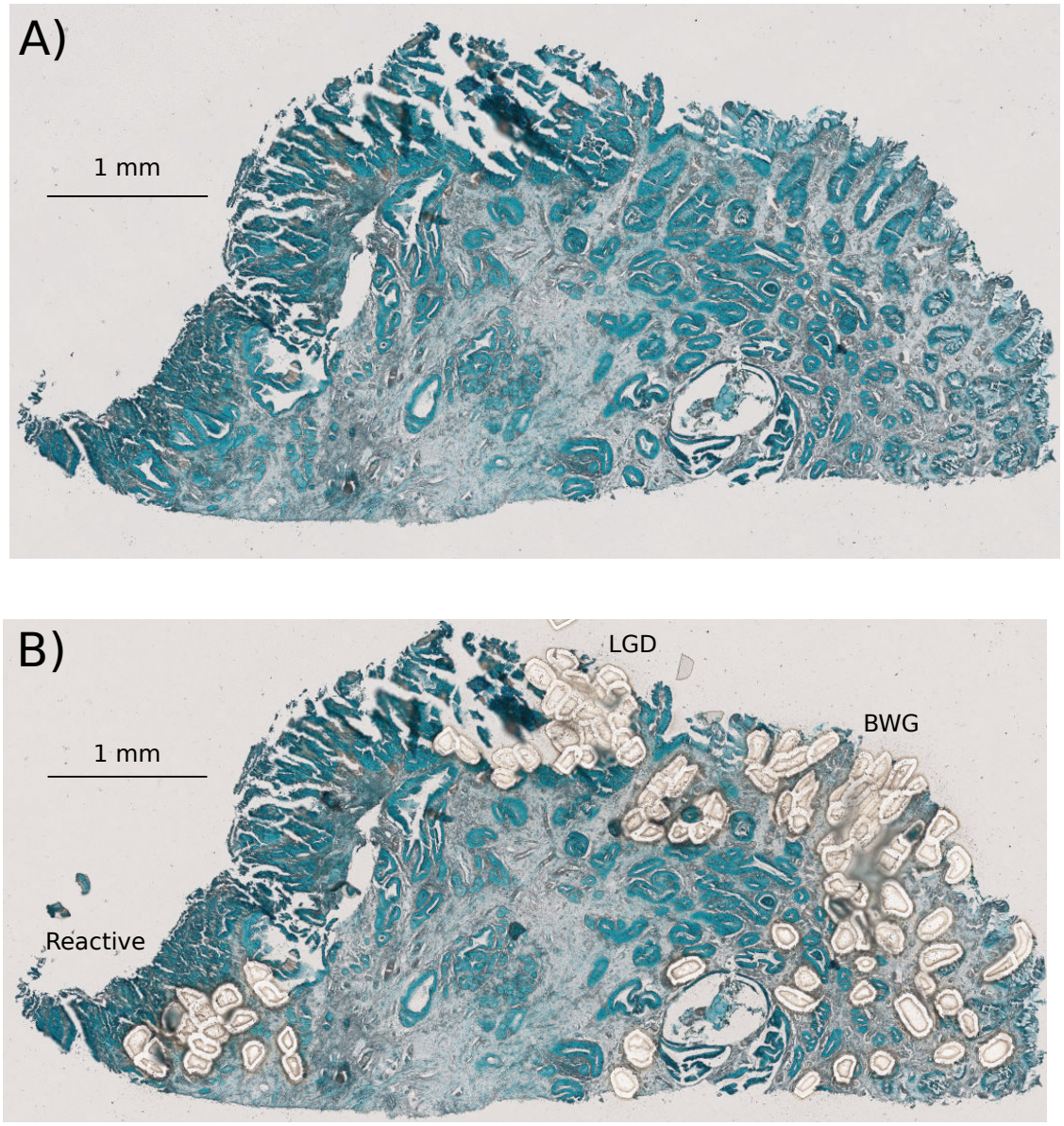

Figure 5.11: Block MS17-15410-B2 microdissection A) Scan of one of the six slides stained with methyl green previous to microdissection B) Areas extracted from the same slide after the microdissection process.

obtain good proteomics results. Extra precaution was taken because the FFPE samples were already two years old. However, this approach ended enlarging microdissection times and preventing the completion of the project. After the first batch of samples results are analysed, if good quality results are obtained, the number of slides processed could be reduced speeding up the process.

5.6.2 Use of biopsies in place of paraffin blocks

EMR samples were selected because of their large volume and the increased chances of obtaining BO segments with advanced progression, as this technique is used to remove LGD, HGD and early OAC sections. However, in future experiments focusing in testing different hypotheses, fresh biopsies from endoscopy samples could be used. The samples obtained in endoscopy could then be either frozen or FFPE depending on the results obtained with the paraffin samples.

A future project that would benefit from switching the tissue origin from FFPE EMR samples to fresh endoscopy biopsies would be studying EGFR activation gradients. In this project, the biopsies could be taken in a sequential pattern. A biopsy could be taken close to the gastroesophageal junction and then every certain number of centimetres advancing proximally. Using this approach, the existence of an EGFR phosphorylation gradient could be studied. EGF production by OSG and BO would be expected to be higher in the biopsies taken more distally. Besides the EGF role, these experiments could lead to interesting observations of how long-segment and short-segment BO differ and through which signalling pathways this difference arises.

A last advantage of this approach is that reflux samples could be taken from the patients and analysed through mass-spectrometry to study their composition. Then this information could be analysed in conjunction with the biopsy results. This will be specially informative in the study of reflux generated EGF gradients.

5.6.3 Using results to study pathologists lack of consensus

When annotating histology samples from BO, pathologists agree easily in which histological features are early BO or oesophageal adenocarcinoma. More difficult is the distinction across the dysplasia axis, with BO, LGD and HGD being the histological features where less consensus is reached. As a result of the efforts in biobank generation and annotation, a reasonable sized amount of annotated image data was acquired. After proteomics, access to clinical data could also be obtained. Once the dataset is generated, machine learning methods could be

used to classify histology using the annotations, proteomics data and image scans accumulated. This would enable the comparison of the annotations of the different pathologists to the sequencing and proteomics data and better understand when the transition between the different subtypes occur.

6
Conclusions

Contents

6.1 Conclusion 171
6.1.1 Designing a model of the interaction between squamous and BO cell populations 171
6.1.2 EGF can disrupt the stability between squamous and oesophageal cell types and promote columnar segment growth *in vitro* 172
6.1.3 EGF activates BO segment growth is not proliferation dependant *in vitro* 175
6.1.4 The use of a divider can generate 3D models of the squamous-columnar junction in organotypic models . . . 177
6.1.5 Combining oil-lipid bath with 3D printed moulds improves existing technique to fuse epithelial organoids 177
6.1.6 Control over the cell populations of each ring segment to form heterotypic junctions 178
6.1.7 Fibroblasts populations contract the collagen scaffold in a concentration dependant manner 178
6.1.8 Production of longer tubular structures and shaping them using fibroblast concentrations 179
6.1.9 Adapters allow the control over the contents in the tube's lumen enabling lining of the internal wall with epithelial cells 180
6.1.10 The collagen wall is impermeable enabling future use into microfluidic circuits 180
6.1.11 Design of future xenografting experiments in mice models 182
6.1.12 Microdissection and proteomics analysis approach . . . 184

6.1 Conclusion

6.1.1 Designing a model of the interaction between squamous and BO cell populations

Using immortalized cell lines coming from the healthy squamous lining of the oesophagus and early Barrett's oesophagus epithelium plated adjacently, a 2D model to study the interactions between these populations was generated *in vitro*. The cell types used were labelled beforehand using fluorescent dyes and their interaction studied by applying a software named MOSES to footage obtained by time-lapse microscopy. In this model, without stimulation the squamous and columnar populations reached junctional stability. This result contrasted greatly with the continuous advance that oesophageal adenocarcinoma cell lines showed when co-cultured with squamous cells or the fusion into a unique monolayer when co-culturing the same cell type.

As a control, the same combinations were cultured under no-serum conditions. This prevented the formation of cell-cell junctions and thus collective behaviour. These combinations were used as negative controls to set the threshold for the computational analysis. This was further confirmed by using AGS, a cancer cell line with a deleterious mutation in E-cadherin that, unlike the oesophageal adenocarcinoma cell line OE33, was unable to push the squamous epithelium. Future work may test the effect of the lack of cell-cell junction by performing a KO of E-cadherin directly in OE33. Concurrently, doing a KO of E-cadherin in the immortalized squamous EPC2 cells and then combining them with the BO derived CP-A cell line under normal conditions would mimic a different phenomenon during reflux episodes. During reflux episodes, low pH has been described to disturb cell-cell junction stability and increase the space between the cells [119]. This works by acidic cleavage of the junctional protein E-cadherin [411]. It would be interesting

to test if this effect by itself is sufficient to promote BO segment growth or if it still requires stimulation by reflux components.

6.1.2 EGF can disrupt the stability between squamous and oesophageal cell types and promote columnar segment growth *in vitro*

Once the model was established, EGF concentrations were shown to be able to disrupt the formation of junctional stability and promote the growth of the segment length at the detriment of the squamous lining. Interestingly, the concentrations found to cause this change in behaviour are within the expected physiological ranges in the duodenum [178], [149]. Thus, it is possible that gastroduodenal reflux episodes carrying EGF to the distal oesophagus generate the same effect *in vivo*.

One question that arose after this experiment is the real origin of EGF signalling *in vivo*. As discussed before, several compounds and growth factors present in the reflux environment have converging signalling pathways with EGF Figure 3.16. For instance, low pH has been shown to increase BO cell proliferation and differentiation as EGF does [115]. At the same time, EGF can be produced in response to low pH as a compensation mechanism or be carried to the distal oesophagus by reflux [178]. To test whether low pH is enough to make the BO produce EGF and trigger EGFR activation, human biopsies could be used and cultured in neutral pH and pH 3.5, previously described to promote proliferation [115]. If EGF is produced by BO epithelium under these conditions, production of EGF in the medium could be tested by ELISA. The biopsy can then be used to assess EGFR and other proteins of the downstream signalling pathway activation. The same experiments could be done with BO organoids grown from BO biopsies. In this experiment, the stromal component will disappear, and the ELISA would only detect EGF production by the columnar epithelial cells. Even more important would be to test EGF levels during reflux episodes to confirm observations carried out during the 80s and 90s [178], [149] (Figure 6.1).

In addition to this experiment, high levels of EGF had been previously reported to promote hyperplasia in glandular structures like Brunner glands [184] or migration

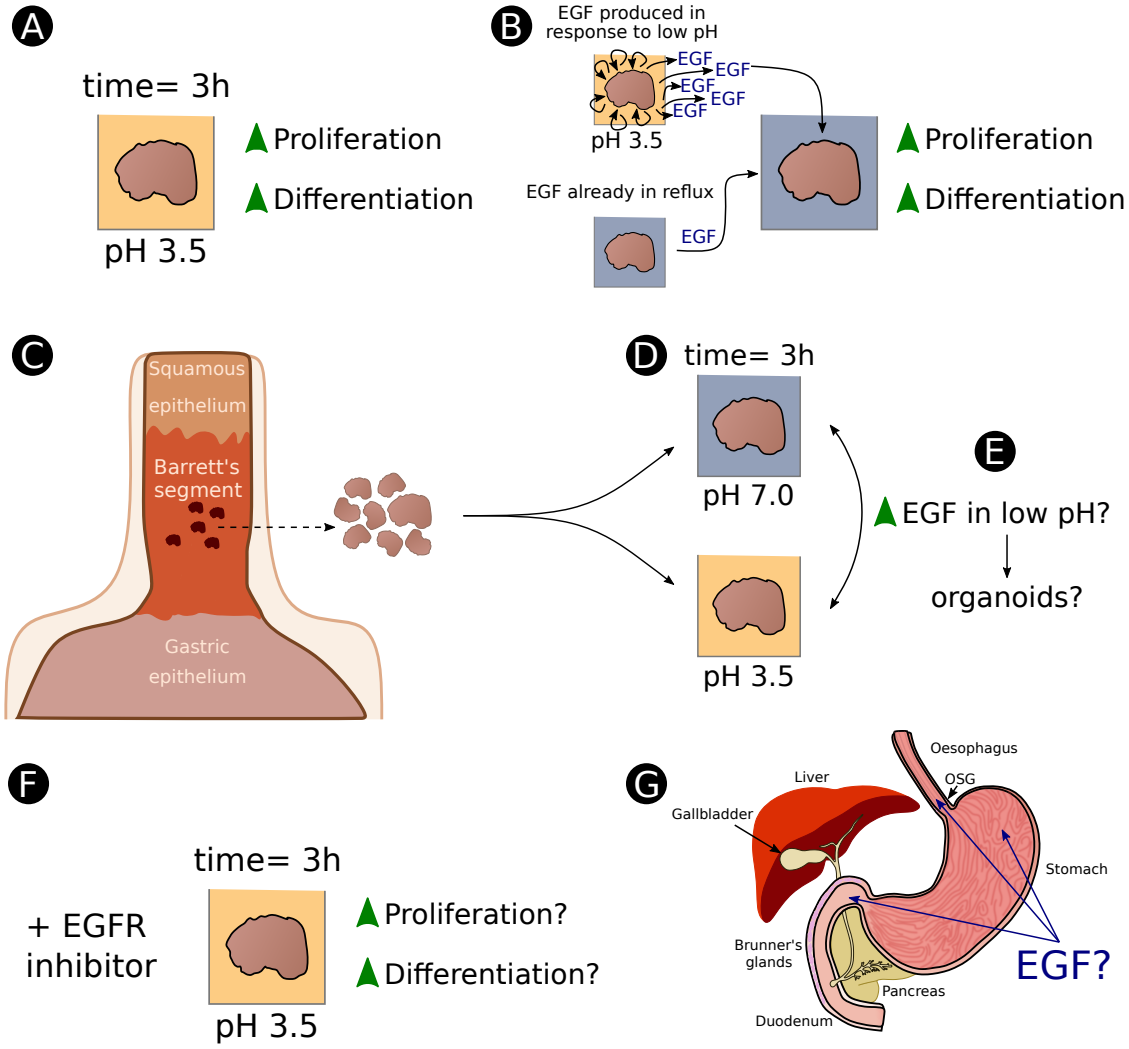

Figure 6.1: Low pH effect on EGF production in the BO segment A) Previous work reported increase in proliferation and differentiation when BO biopsies are cultured during three hours in pH 3.5 medium. B) This effect could link with the EGF hypothesis by having low pH increase EGF production (top panel). Another possibility is that EGF levels coming from reflux are sufficient to promote proliferation and differentiation C) This could be tested *in vitro* using endoscopic biopsies of the same region of the BO segment. D) Some biopsies would be incubated at a neutral pH and the other in low pH medium. E) After incubation, the EGF and EGFR activation in both conditions can be compared. If the hypothesis is right EGF levels should be higher in the sample incubated in low pH medium. Organoids can be grown to do the same experiment to remove the stromal compartment and ensure a similar amount of epithelial tissue. F) An alternative method to evaluate if low pH induced proliferation and differentiation is linked with EGF is using an EGFR inhibitor. G) To evaluate the real effect of the EGF that might be produced by the BO epithelium the EGF levels present in the reflux need to be studied. Depending on the reflux concentrations the effect might be negligible.

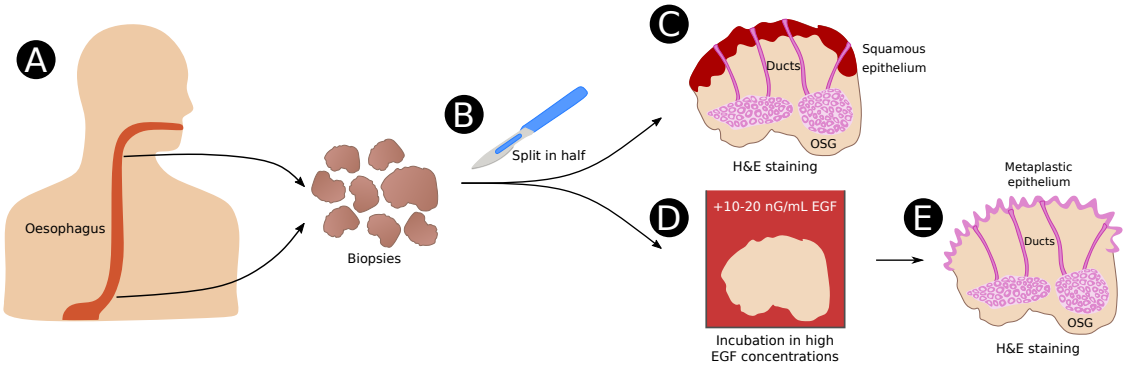

Figure 6.2: Human biopsies to study EGF in BO expansion This experiment replicates [142] replacing retinoic acid for EGF to observe if the effects in the 2D model are transferable. A) Biopsies from the upper and lower oesophagus are taken. B) The samples are first cut in half. C) One half is sectioned into slides to confirm there is no BO epithelium and the presence or absence of OSG. D) The other half is cultured in EGF during 72 hours. E) The sample is then processed and stained to study if EGF promoted columnar epithelium replacement of the squamous lining.

in mammary gland cells [157]. Thus, a similar effect in OSG or BO could also be expected. A simple experiment to test high levels of EGF in the laboratory would be to adapt previous experimental work done with human oesophageal biopsies using retinoic acid. In this study by Chang et al. in the Fitzgerald laboratory, retinoic acid applied to squamous biopsies was described as being able to generate BO epithelium in squamous biopsies. This process occurred in only a 20% of the samples. In the paper it is suggested that retinoic acid might be promoting either submucosal gland colonization of the surface or transdifferentiating [142]. A similar experiment consisting of splitting squamous biopsies in half, staining one half to test for OSG presence and submerging the other half in high EGF concentrations, would be able to test our hypothesis in a setting closer to *in vivo* conditions (Figure 6.2). Retinoic acid and EGF signalling pathways have redundancies. If the hypothesis presented in this thesis is correct, high EGF concentrations should promote replacement of the squamous lining by OSG cells in the biopsies. This effect should be observed at rates higher than the 20% conversion rate, obtained when random sampling was done instead of using only the OSG positive biopsies [142].

One of the design decisions of this experiment was to add EGF to the medium at time 0, before the junction stability was reached after 72h. This leaves two

questions that need to be studied in the future. First, can high EGF concentrations disrupt junctional stability once it has already been established, or is another stimulus found *in vivo*, e.g. low pH, required to trigger the replacement? Next, once EGF is removed from the medium, what time expend is required to obtain junction stability again? Both experiments could be easily performed in the 2D experimental model. The first would consist of culturing the cells for 72h and once junction stability has been reached, exchange the medium for medium containing EGF. The second would require for the medium with EGF to be replaced after 72h for medium without the growth factor.

6.1.3 EGF activates BO segment growth is not proliferation dependant *in vitro*

In vivo, EGFR activation signalling branches into different subpathways promoting proliferation, survival, cell migration, differentiation, cellular mobility and exoskeleton rearrangement [156]. During the publication of the MOSES paper, the reviewers queried whether BO segment elongation promoted by EGF activation was proliferation dependant. The two methods used, (counting the cells with machine learning methods and studying fluorescence decay in the sample) showed no significant change in proliferation in higher EGF levels. However, the question of which of the different sub-pathways was activated during BO segment growth still remains unanswered.

A possible solution to discern which of the different routes influences BO behaviour would be testing the key proteins in each pathway using an inhibitor screening. This would require for the 2D model shown in this thesis to be adapted to a screening format. First, the commercial divider needs to be down-scaled to fit a square well screening plate (Figure 6.3 A and B). The mould can then be produced by using a laser cutter or a 3D printer (Figure 6.3 C). This was done in the laboratory as a prototype but because the moulds were made of hard plastic instead of silicone, the cells leaked underneath. Interestingly, a solution for this issue arose during the 3D model project development. By covering each of the down-scaled

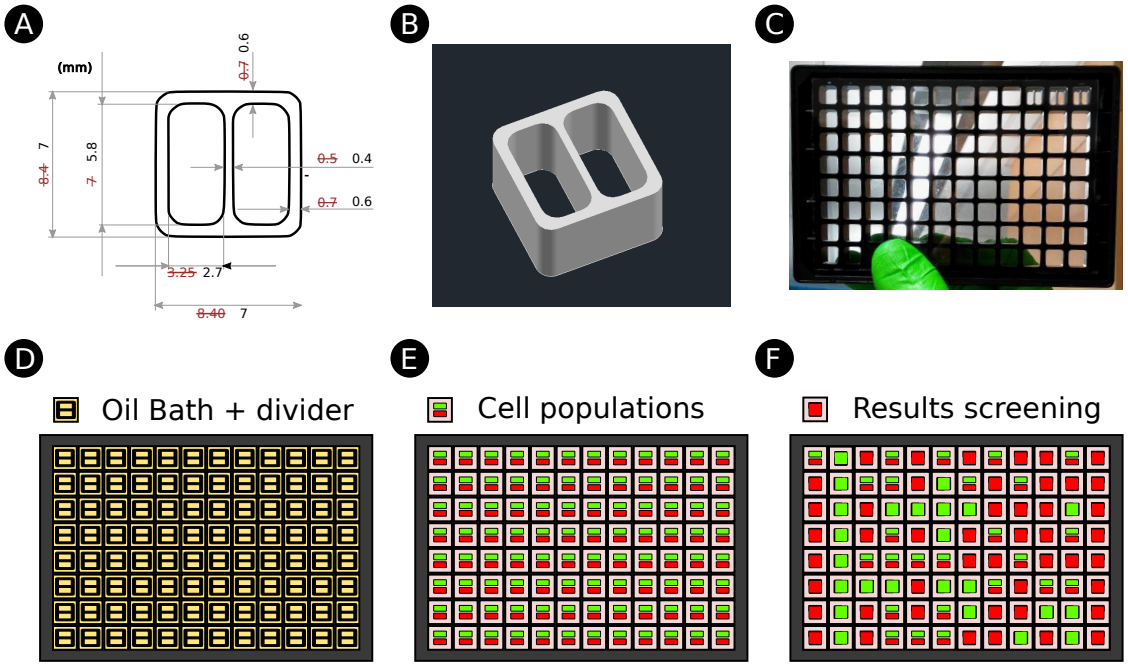

Figure 6.3: Adapting the 2D model to a screening platform A) Blueprint of the commercial divider design after being down-scaled to fit 96 well plates. B) 3D rendering of the new divider. C) Image of the dividers in an optical bottom 96 well plate. D) By covering the wells with an oil-lipid bath, the leakage of the cells under the divider can be prevented. E) The cells are then plated. After the cells attach to the bottom of the well, the oil exchanged for medium with the screening drug. F) Screenings results can be analysed using MOSES or by comparing the end point with the control.

moulds in the wells with an oil-lipid bath, the aqueous droplets containing medium with cells could not leak under the mould (Figure 6.3 D). Cells could then be plated using this method and the compounds for the screening added after washing the oil (Figure 6.3 E). The results could be analysed using MOSES for major detail or by comparing frames 0 and 140 h of the experiment (Figure 6.3 F). With this screening method it would possible to screen for activation downstream EGF in its different signalling pathways to narrow down the pathway responsible for BO segment growth *in vitro*. This could potentially help to develop targets for drugs that could be used after BO segment ablation experiments to prevent regrowth of the squamous epithelium without high toxicity.

6.1.4 The use of a divider can generate 3D models of the squamous-columnar junction in organotypic models

Although the 2D model could be used to test the desired hypothesis, the simplified design consisting uniquely of immortalized epithelial cell lines and without being able to replicate the reflux pulses could not be representative of the mechanisms occurring *in vivo*. To add this complexity *in vivo*, the model was adapted to organotypic culture. However, the method required of long culture times and the divider often damaged the Matrigel layer. As with the screening model adaptation, the solution to this lack of reproducibility might be using an oil-lipid bath, this would prevent leakage occurring when using normal transwell inserts, which will make the Matrigel coating unnecessary. The fibroblasts and immune cell populations could still be cultured in the alvetex sponge. Unfortunately, adapting this model to replicate reflux episodes would still be challenging and growth plus differentiations times still long.

6.1.5 Combining oil-lipid bath with 3D printed moulds improves existing technique to fuse epithelial organoids

To simplify the formation of heterotypic junctions, 3D printing was used. However, this generated technical difficulties due to the organoid size and dead cell content. To be able to use bigger droplets a ring mould was added. The objective was to generate collagen rings with organoid contents that would fuse together. This was inspired by a similar technique using the edge of the ring as a mould for the collagen without any liquid environment [346]. Adding the oil-lipid bath and mould elements into the model prevented desiccation and increased the control and reproducibility of the fabricated rings. Interestingly, this also changed the migration and fusion pattern of the organoids. This change migrated the lumen from being located in the interior of the ring to the inner edge. This effectively converted the centre of the ring into the lumen of the newly formed epithelium. Besides having a closer resemblance to a cross-section of the GIT tube, this prevented encapsulation by collagen of the epithelium allowing better interaction with it during experiments. An example of this is direct *H. Pylori* infection instead of

using on microinjection or breaking the organoids. Future experiments testing this model should be focused on obtaining metrics of size reproducibility compared to the previously published method by Hans Clevers' team.

6.1.6 Control over the cell populations of each ring segment to form heterotypic junctions

The use of an oil-lipid bath also allowed for controlled fusion of the droplets containing organoids. By adding a divider to the mould, the droplets could be separated into two different sections and fused after divider removal by diluting the lipid. This allowed the formation of rings with a unique epithelial monolayer formed by populations from two different organoid subtypes. Unfortunately, even when published protocols are available [300], [301], the production of squamous organoids was not successful, and the focus had to be transferred to a junction of another anatomical origin. In the end, the gastroduodenal junction was replicated by using organoids from gastric and duodenal origin. In the future, efforts should be centred in generating squamous organoids or obtaining them from a collaborator with more expertise. This approach could also be useful to generate models with different cell populations that are not necessarily epithelial in origin. For instance, to test mutations in fibroblasts or immune cells to see how the affect epithelial behaviour.

6.1.7 Fibroblasts populations contract the collagen scaffold in a concentration dependant manner

One of the objectives of the 3D model was to add non-epithelial cell populations. As a major source of growth factors to help repair the epithelium and trigger inflammation [267] fibroblasts were a convenient option. Interestingly, the fibroblast populations included in the collagen bioink influenced collagen contraction to the point of being able to dictate its final size. The extent of the contraction and the speed in which it happened was proportional to fibroblasts concentration. Adding another cell population of immune origin like Jurkat cells reduced the ring contractility. This contraction also caused the fibres to pack tighter. It would be crucial to design experiments to test whether this contraction prevents immune

cell migration to know if this could still be used as a model for epithelial-immune cell interaction. This would be done by profiting from the ability to divide the ring in two sections. Immune cells, preferentially a cell line that can be polarized towards macrophages like THP-1 cells, would only be plated in half the ring. If the fibres are too packed for cells to migrate, posterior immunofluorescence staining of the ring would only show immune cell population in one of the two halves. The use of drugs promoting migration might be necessary to have a clear read-out in case migration distances are short in normal conditions.

6.1.8 Production of longer tubular structures and shaping them using fibroblast concentrations

The use of ring structures to form heterotypic junctions was able to incorporate non-epithelial cell types in the ECM but failed to achieve one of the objectives, replicate reflux episodes *in vitro*. This could be achieved by having the ring floating in a chamber connected to a microfluidics system. This approach, however, would have affected equally all the cell populations and prevented the epithelial cells from mimicking the normal defence mechanisms against reflux like cell polarization and mucus production. To solve this issue an elongated version of the ring model was fabricated. This required the design and production of new moulds, containers and a mechanism to remove the casted gel from the mould. The fabrication process was faster and the results more resilient to manipulation than in other printing methods used to generate tubular structures [412].

Interestingly, the collagen contraction phenomenon observed in the rings when fibroblasts are added into the ECM can be used to shape the tubes by adding different fibroblast concentrations in each segment. This enables the formation of structures resembling a simplified anatomy the GIT organs. The delayed contraction simplifies the gel casting process. Otherwise, a mould with the desired shape would prevent removal of the collagen structure after gelation. To solve the issue with complex gel shapes at the initial casting timepoint the mould should have consisted of two different sections joined to form the mould and separated after gelation,

a more complex process than that which is presented in this thesis. The use of additional cell types, such as smooth muscle myofibroblasts or endothelial cells, to populate the collagen matrix and test their effect on the final tube conformation would be useful to investigate new applications for this fabrication technique. For instance, smooth muscle cells could potentially be used to generate sphincter-like structures in the tube structures to add resistance to flow e.g. during cell plating. Endothelial cells could solve an issue this model may encounter to be used in animal xenografting experiments in the future, vascularization. Without vascularization the epithelial cells in the tube would not survive *in vivo* and the immune cells would not be able to reach the epithelium [367], [368].

6.1.9 Adapters allow the control over the contents in the tube's lumen enabling lining of the internal wall with epithelial cells

In addition to being able to form shapes resembling organ anatomy, fibroblast contraction was shown to allow the incorporation of 3D printed extensions to the tube. Adapters may be firmly attached and can be manipulated without the risk of removal. Using the adapters, the contents inside the lumen of the tube were controlled. This permitted the introduction of high cell concentrations inside the small volume of the lumen that could line the tube overnight. One drawback observed from this technique was the thickening of the epithelium of one side of the tube in comparison to the other. This phenomenon is likely caused by gravity. By using rotating culture containers, for instance falcon tubes with a cap allowing gas exchange or turning the sample manually after a few hours, this effect could be prevented in the future. Using the same adapters, the cells lining the lumen was infected with *Helicobacter pylori*.

6.1.10 The collagen wall is impermeable enabling future use into microfluidic circuits

After testing the tube permeability to medium and air, it was found that there was no diffusion of either through the wall, at least when the tube was submerged

in another liquid. This phenomenon was already observed in structures formed of a mix of fibroblasts and dense collagen fibres e.g. blood vessels [355]. This property is vital to use this model in conjunction with microfluidics. However, two potential drawbacks require further investigation: first, study whether the populations added to the collagen wall can still migrate through the collagen; second, ensure that cell populations in the lumen can still obtain enough moisture to grow in an air-liquid interphase. If this is the case, air blown into the lumen could be used to stratify squamous cell populations present in the lumen as well as help differentiate columnar cells.

Once the properties have been established, the next step would be to obtain a microfluidics pump and test the model under medium flow. Once the previously commented issues with the squamous organoids have been solved, heterotypic junctions between squamous and BO cells should be replicated in this new model. The separation between the cell populations could be achieved by two different approaches: one possibility is stacking segments with different organoid populations and letting them migrate into the lumen and form a continuous monolayer; the other involves using magnets or string to physically divide the tube into two segments and populate the inner lumen through the end adaptors using dissociated organoids. (Figure 6.4 A). To study the interaction between these populations, it would be necessary to mark the spot in which the two epithelial monolayers meet. This could be achieved by labelling the segment between the cells using a dye for collagen [413] or mixing the collagen with a protein like laminin in that segment so it can be detected using immunofluorescence (Figure 6.4 B).

Once this heterotypic junction can be established, medium with the desired compound, e.g. EGF, DCA, or low pH, can be injected into the lumen at controlled pulses. The effect of the compound would be evaluated by comparing the distance travelled by the BO organoid cells away from the labelled collagen segment in the control and the desired compound (Figure 6.4 C). A more complex version of this model could be designed by adding a third hollow adapter in the middle of the tube. Two different mediums could then be flown from each of the tube's ends forming a

gradient. The mixed medium would then flow out through the side adapter where the cells would stop advancing (Figure 6.4 D).This technique might allow producing tube segments with the desired qualities for xenografting into *in vivo* models.

6.1.11 Design of future xenografting experiments in mice models

Due to time limitations, the lack of squamous organoids, and the surgical training required, the tubular model was never xenografted into mice. In addition, the lack of a vascularization might prevent the survival of the xenografted tissue [367], [368]. Cross-section resolution allowing vascularization could be obtained by using 3D printing with a bigger nozzle.

Prior to using the artificially generated segments, two experiments could be performed by xenografting segments of the mice's own digestive system to another section. The first experiment would be to transfer a part of the mouse small intestine into the middle of the oesophagus. This segment could serve as a proxy for intestinal metaplasia in the oesophagus. This surgery is known as jejunal interposition and is used in human patients when the stomach cannot be used to replace an oesophageal resection [414].If the experimental results from the 2D model are correct, the intestinal segment should form stable junctions with the squamous cells in the oesophagus under normal conditions. If this occurs, the mouse's water supply could be supplemented with DCA, as in previous experiments [63] , or EGF. This should promote intestinal cell replacement of the squamous epithelium in the mouse's oesophagus. By doing the opposite experiment and xenografting a segment of the squamous epithelium distally to the duodenum, replacement of the squamous epithelium by intestinal cells should be seen naturally happening due to the compounds transiting down the duodenum. This model has the advantage that there is no immune response against the xenografted tissue as the donor is the same mouse and only wt specimens are required (Figure 6.5 A).

If these experiments are successful and can be used to form segments of tube with human squamous-columnar junctions between squamous and BO cells *in vitro*,

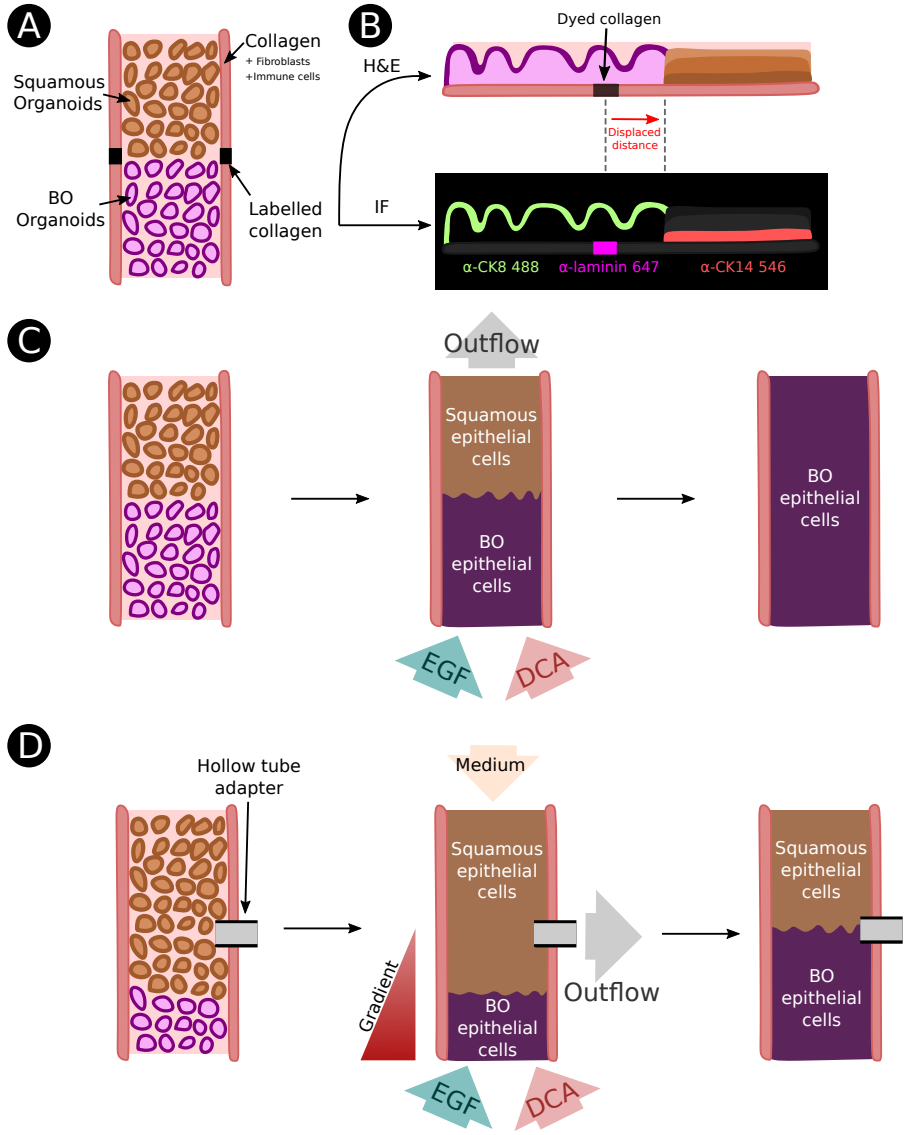

Figure 6.4: Organoid use in combination with the tube model A) By stacking segments with two different organoid populations or lining the lumen using adapters, heterotypic junctions in the tube model could be generated. B) To study the migration patterns of the interaction between the different cell populations the segment of the ring between the two populations needs to be labelled. This can be done with a collagen dye visible in H&E staining or by adding a protein, for example laminin, only in that section. This protein could then be used as reference point in IF imaging. The displaced distance will be calculated from the labelled segment to the cell population front. C)Once the organoids migrate to the inner edge and fuse into a monolayer. EGF, DCA or other compounds are flown into the lumen using microfluidics, either continuously or in pulses. The resulting epithelium composition is evaluated after the experiment. D) By adding a side adapter into the tubes side, the gradient of the compound tested can be controlled. By changing the flow from each end, the gradient can be controlled and the cell migration stopped at the desired point.

these segments can be then used *in vivo* by using rodent models. A humanized version of the xenograft can be performed using the tube technology. As with the mouse xenograft, the segment will firstly be added to the middle of the oesophagus to confirm that it remains stable when no external chemical insult is present (Figure 6.5 B I). Once this is confirmed, compounds like EGF will be added to the mouse's water supply promoting the growth of the BO segment (Figure 6.5 B II). The same result should be observed in a mouse model having the human tube segment interposed between the duodenum and the jejunum (Figure 6.5 B III). Finally, a last experiment could be performed interposing the segment between the duodenum and the jejunum and removing the stomach. This will determine whether the stomach is required for the intestinal metaplasia growth to occur *in vivo*, as was previously reported in oesophajejunostomy experiments (Figure 6.5 B IV). In addition to the need of immunosuppressed mice to perform this experiment, there is an additional challenge to this approach. Vascularization might be required to pump blood through the implant, which would only be possible by incorporating 3D printing techniques at a micrometric resolution. An alternative to this would be decellularizing the epithelium of the removed mouse section and populating it with squamous and intestinal cells using the Sato technique [327] for *in vivo* humanization of the epithelium but with the descellularized segment *in vitro*.

6.1.12 Microdissection and proteomics analysis approach

The final project presented in this thesis consisted of combining two different techniques, tissue microdissection with protein mass-spectrometry analysis to study BO progression to OAC. With the microdissection, the aim was to obtain a single cell type resolution presently absent in the most commonly used high-throughput technologies while capturing the spatial information that would be lost in a single-cell approach. Proteomics analysis using mass-spectrometry presented three other advantages: first, protein in FFPE samples, the most common processing method for human samples in the clinic, preserves better than DNA or RNA; second, proteins should give more valuable information of the phenotypes as they are the functional

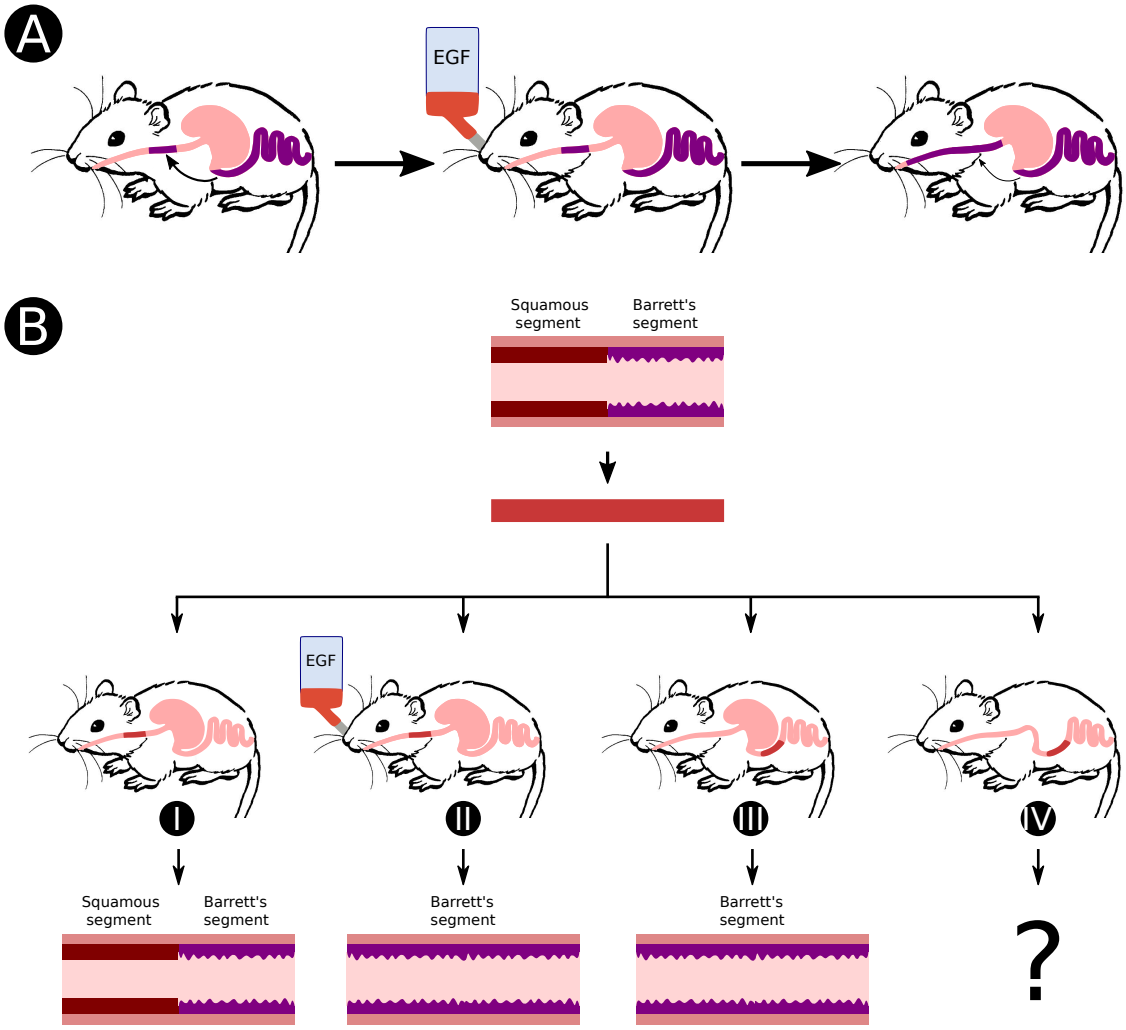

Figure 6.5: ***in vivo*** **experiments with mice** A) A section of the duodenum is surgically attached to the middle of the oesophagus. High EGF concentrations are then added to the mice drinking water. If the hypothesis is correct EGF should trigger columnar intestinal cell invasion of the squamous epithelium in the oesophagus. B) By xenografting the tube model into the mouse, we can obtain a humanised heterotyic junction segment interacting with the *in vivo* microenvironment. I) Adding the segment to the middle of the oesophagus should not result in junction instability as the EGF concentrations in the oesophagus are low. II) This could changed by adding EGF into the drinking water of the mouse. III) If the segment is located just after the duodenum the high levels of EGF, low acidity and bile acids should be able to disrupt the junction promoting growth of the columnar cells. IV) As seen in oesophagojejunostomy experiments, the removal of the stomach might prevent columnar metaplasia from extending. If removal of the stomach prevents this phenotype adding EGF into the drinking water will give more information on the mechanism. If the BO segment growth phenotype is rescued, EGF levels and not mucosal damage generated by low pH might be triggering the growth

unit of the cell; finally, a proteomics analysis can also provide information of posttranslational modifications such as phosphorylation, expanding the knowledge of the signalling pathways activation status.

For this project, FFPE samples were processed, annotated and microdisected. Unfortunately, due to time limitations, no results were obtained from the pilot cohort used to study the feasibility of the project. Following the analysis of the results, the experimental design can be adapted to study the signalling pathways that activate during reflux episodes that influence BO length.

To study this, fresh biopsies instead of FFPE endoscopic mucosal resection specimens would be used. This will be performed to ensure the biopsies fulfil the required characteristics by working together with an endoscopist. These biopsies will be taken from long BO segments at regular intervals, for instance every centimetre, starting at the proximal end and finishing at the gastroesophageal junction (Figure 6.6 A and B). The samples will then be annotated and the epithelial cells microdissected (Figure 6.6 C, D and E). Once the epithelial tissue is obtained, it will be processed using mass-spectrometry (Figure 6.6 F). For the proteins phosphorylated by gradients generated during reflux episodes, the levels of phosphorylation should be highest close to the GOJ and diminish as the samples are closer to the squamous epithelium in the proximal end of the BO segment. If the initial hypothesis suggesting EGF activates EGFR during reflux episodes, and this increases BO segment and also induces goblet cell formation, is true, we should see this trend with EGFR (Figure 6.6 G). This analysis should also indicate which downstream processes are activated during reflux. In addition to these experiments, confirming that EGF is present in the reflux at the estimated concentrations would be an added evidence of EGF role in determining the final length of the BO segment.

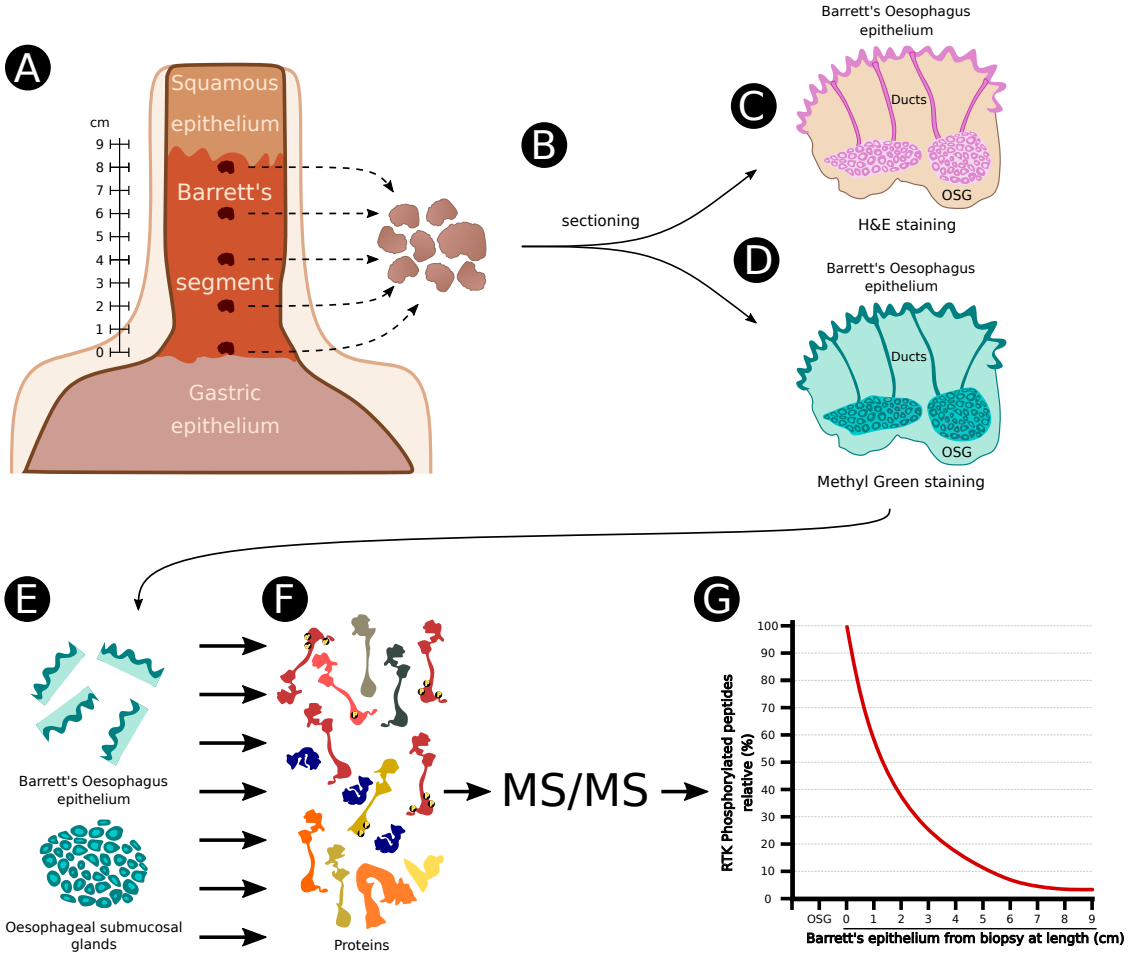

Figure 6.6: Sequential biopsy microdisection and MS analysis A) Biopsies are taken from patients with long BO segments at fix distance intervals. B) The biopsy is cut into slides C) One slide is used for pathologists annotation. D) The others are stained with methyl green and microdissected into E) The BO epithelium and OSG. F) The proteins for each samples are extracted and analysed using MS/MS. G) Plot with result hypothesis. If the EGF hypothesis is correct a phosphorylation gradient for EGFR or other RTK should be highest next to the GOJ and decrease as the biopsy origin is more proximal.

References

[1] Steven a. Frank. *Dynamics of Cancer. Incidence, Inheritance, and Evolution.* 2007.

[2] F G DeNardi and R H Riddell. "The normal esophagus." In: *The American journal of surgical pathology* 15.3 (Mar. 1991), pp. 296–309. URL: http://www.ncbi.nlm.nih.gov/pubmed/1996732.

[3] Cédric Blanpain and Elaine Fuchs. "Epidermal homeostasis: a balancing act of stem cells in the skin." In: *Nature reviews. Molecular cell biology* 10.3 (Mar. 2009), pp. 207–17. URL: http://www.ncbi.nlm.nih.gov/pubmed/19209183%20http://www.pubmedcentral.nih.gov/articlerender.fcgi?artid=PMC2760218.

[4] Mariagnese Barbera et al. "The human squamous oesophagus has widespread capacity for clonal expansion from cells at diverse stages of differentiation." In: *Gut* 64.1 (Jan. 2015), pp. 11–9. URL: http://www.ncbi.nlm.nih.gov/pubmed/24572143%20http://www.pubmedcentral.nih.gov/articlerender.fcgi?artid=PMC4283695.

[5] Rebecca A Coad et al. "On the histogenesis of Barrett's oesophagus and its associated squamous islands: a three-dimensional study of their morphological relationship with native oesophageal gland ducts." In: *The Journal of pathology* 206.4 (Aug. 2005), pp. 388–94. URL: http://www.ncbi.nlm.nih.gov/pubmed/15926200.

[6] J D Long and R C Orlando. "Esophageal submucosal glands: structure and function." In: *The American journal of gastroenterology* 94.10 (Oct. 1999), pp. 2818–24. URL: http://www.ncbi.nlm.nih.gov/pubmed/10520827.

[7] Mark Rishniw et al. "Molecular aspects of esophageal development." In: *Annals of the New York Academy of Sciences* 1232 (Sept. 2011), pp. 309–15. URL: http://www.ncbi.nlm.nih.gov/pubmed/21950820%20http://www.pubmedcentral.nih.gov/articlerender.fcgi?artid=PMC3568516.

[8] Y van Nieuwenhove, H Destordeur, and G Willems. "Spatial distribution and cell kinetics of the glands in the human esophageal mucosa." In: *European journal of morphology* 39.3 (July 2001), pp. 163–8. URL: http://www.ncbi.nlm.nih.gov/pubmed/11910535.

[9] Roy C Orlando. "The integrity of the esophageal mucosa. Balance between offensive and defensive mechanisms." In: *Best practice & research. Clinical gastroenterology* 24.6 (Dec. 2010), pp. 873–82. URL: http://www.ncbi.nlm.nih.gov/pubmed/21126700%20http://www.pubmedcentral.nih.gov/articlerender.fcgi?artid=PMC2995989.

[10] Nick Barker et al. "Lgr5(+ve) stem cells drive self-renewal in the stomach and build long-lived gastric units in vitro." In: *Cell stem cell* 6.1 (Jan. 2010), pp. 25–36. URL: http://www.ncbi.nlm.nih.gov/pubmed/20085740.

[11] Nick Barker et al. "Identification of stem cells in small intestine and colon by marker gene Lgr5." In: *Nature* 449.7165 (Oct. 2007), pp. 1003–7. URL: http://www.ncbi.nlm.nih.gov/pubmed/17934449.

[12] Pottayan Ayyappakutty Nandagopalan, Kanapilly Francis Magdalene, and Areekal Binu. "Effect of Aging on the Quantitative Number of Brunner's Glands." In: *Journal of clinical and diagnostic research : JCDR* 8.3 (Mar. 2014), pp. 4–6. URL: http://www.ncbi.nlm.nih.gov/pubmed/24783064%20http://www.pubmedcentral.nih.gov/articlerender.fcgi?artid=PMC4003680.

[13] K G Botros, S L El-Hady, and E A El-Mohandes. "Prenatal development of the human Brunner's glands." In: *Anatomischer Anzeiger* 171.1 (1990), pp. 23–30. URL: http://www.ncbi.nlm.nih.gov/pubmed/2403210.

[14] Richard Peter Owen et al. "Single cell RNA-seq reveals profound transcriptional similarity between Barrett's oesophagus and oesophageal submucosal glands." In: *Nature communications* 9.1 (2018), p. 4261. URL: http://www.ncbi.nlm.nih.gov/pubmed/30323168%20http://www.pubmedcentral.nih.gov/articlerender.fcgi?artid=PMC6189174.

[15] W J Krause. "Brunner's glands: a structural, histochemical and pathological profile." In: *Progress in histochemistry and cytochemistry* 35.4 (2000), pp. 259–367. URL: http://www.ncbi.nlm.nih.gov/pubmed/11148980.

[16] Eric J Yang et al. "Microanatomy of the cervical and anorectal squamocolumnar junctions: a proposed model for anatomical differences in HPV-related cancer risk." In: *Modern pathology : an official journal of the United States and Canadian Academy of Pathology, Inc* 28.7 (July 2015), pp. 994–1000. URL: http://www.ncbi.nlm.nih.gov/pubmed/25975286%20http://www.pubmedcentral.nih.gov/articlerender.fcgi?artid=PMC4490106.

[17] Jelena Mirkovic et al. "Carcinogenic HPV infection in the cervical squamo-columnar junction." In: *The Journal of pathology* 236.3 (July 2015), pp. 265–71. URL: http://www.ncbi.nlm.nih.gov/pubmed/25782708%20http://www.pubmedcentral.nih.gov/articlerender.fcgi?artid=PMC4457596.

[18] Stuart J Spechler and Rhonda F Souza. "Barrett's esophagus." In: *The New England journal of medicine* 371.9 (Aug. 2014), pp. 836–45. URL: http://www.ncbi.nlm.nih.gov/pubmed/25162890.

[19] Global Burden of Disease Cancer Collaboration et al. "The Global Burden of Cancer 2013." In: *JAMA oncology* 1.4 (July 2015), pp. 505–27. URL: http://www.ncbi.nlm.nih.gov/pubmed/26181261%20http://www.pubmedcentral.nih.gov/articlerender.fcgi?artid=PMC4500822.

[20] Katrina F Trivers, Susan A Sabatino, and Sherri L Stewart. "Trends in esophageal cancer incidence by histology, United States, 1998-2003." In: *International journal of cancer* 123.6 (Sept. 2008), pp. 1422–8. URL: http://www.ncbi.nlm.nih.gov/pubmed/18546259.

[21] S Barona, J Tebar, and A Avila. "[Restoration of incisors with ceramic veneers]." In: *Soproden* 2.3 (Sept. 1986), pp. 131–3. URL: http://www.ncbi.nlm.nih.gov/pubmed/3078819.

[22] Jun Zhao et al. "Analysis of esophageal cancer time trends in China, 1989- 2008." In: *Asian Pacific journal of cancer prevention : APJCP* 13.9 (2012), pp. 4613–7. URL: http://www.ncbi.nlm.nih.gov/pubmed/23167389.

[23] Gustaf Edgren et al. "A global assessment of the oesophageal adenocarcinoma epidemic." In: *Gut* 62.10 (Oct. 2013), pp. 1406–14. URL: http://www.ncbi.nlm.nih.gov/pubmed/22917659.

[24] Judith Offman, Francesca Pesola, and Peter Sasieni. "Trends and projections in adenocarcinoma and squamous cell carcinoma of the oesophagus in England from 1971 to 2037." In: *British journal of cancer* 118.10 (2018), pp. 1391–1398. URL: http://www.ncbi.nlm.nih.gov/pubmed/29563637%20http://www.pubmedcentral.nih.gov/articlerender.fcgi?artid=PMC5959941.

[25] Shao-Hua Xie and Jesper Lagergren. "A global assessment of the male predominance in esophageal adenocarcinoma." In: *Oncotarget* 7.25 (June 2016), pp. 38876–38883. URL: http://www.ncbi.nlm.nih.gov/pubmed/27145283%20http://www.pubmedcentral.nih.gov/articlerender.fcgi?artid=PMC5122437.

[26] T D L Crosby et al. "Definitive chemoradiation in patients with inoperable oesophageal carcinoma." In: *British journal of cancer* 90.1 (Jan. 2004), pp. 70–5. URL: http://www.ncbi.nlm.nih.gov/pubmed/14710209%20http://www.pubmedcentral.nih.gov/articlerender.fcgi?artid=PMC2395332.

[27] T Crosby et al. "Long-term results and recurrence patterns from SCOPE-1: a phase II/III randomised trial of definitive chemoradiotherapy +/- cetuximab in oesophageal cancer." In: *British journal of cancer* 116.6 (Mar. 2017), pp. 709–716. URL: http://www.ncbi.nlm.nih.gov/pubmed/28196063%20http://www.pubmedcentral.nih.gov/articlerender.fcgi?artid=PMC5355926.

[28] Cancer Research UK. *Oesophageal cancer statistics*. Aug 2019. URL: https://www.cancerresearchuk.org/health-professional/cancer-statistics/statistics-by-cancer-type/oesophageal-cancer.

[29] William H Allum et al. "Long-term results of a randomized trial of surgery with or without preoperative chemotherapy in esophageal cancer." In: *Journal of clinical oncology : official journal of the American Society of Clinical Oncology* 27.30 (Oct. 2009), pp. 5062–7. URL: http://www.ncbi.nlm.nih.gov/pubmed/19770374.

[30] P van Hagen et al. "Preoperative chemoradiotherapy for esophageal or junctional cancer." In: *The New England journal of medicine* 366.22 (May 2012), pp. 2074–84. URL: http://www.ncbi.nlm.nih.gov/pubmed/22646630.

[31] Joel Shapiro et al. "Neoadjuvant chemoradiotherapy plus surgery versus surgery alone for oesophageal or junctional cancer (CROSS): long-term results of a randomised controlled trial." In: *The Lancet. Oncology* 16.9 (Sept. 2015), pp. 1090–1098. URL: http://www.ncbi.nlm.nih.gov/pubmed/26254683.

[32] Francisco Schlottmann and Marco G. Patti. "Esophageal Adenocarcinoma: Pathogenesis and Epidemiology". In: *Esophageal Cancer*. Cham: Springer International Publishing, 2018, pp. 21–28. URL: http://link.springer.com/10.1007/978-3-319-91830-3%7B%5C_%7D3.

[33] Mahul B. Amin et al., eds. *AJCC Cancer Staging Manual*. Cham: Springer International Publishing, 2017. URL: http://link.springer.com/10.1007/978-3-319-40618-3.

[34] J R Siewert and H J Stein. "Classification of adenocarcinoma of the oesophagogastric junction." In: *The British journal of surgery* 85.11 (Nov. 1998), pp. 1457–9. URL: http://www.ncbi.nlm.nih.gov/pubmed/9823902.

[35] Cancer Research UK. *Oesophageal cancer statistics, survival*. Aug 2019. URL: www.cancerresearchuk.org/health-professional/cancer-statistics/statistics-by-cancer-type/oesophageal-cancer/survival#heading-Zero.

[36] Cancer.org. *Esophagus cancer: Detection, diagnosis and staging. Survival rates.* Aug 2019. URL: https://www.cancer.org/cancer/esophagus-cancer/detection-diagnosis-staging/survival-rates.html.

[37] CancerUK. *Tackling hard-to-treat cancers – what, how and why?* 2016. URL: https://scienceblog.cancerresearchuk.org/2016/07/20/tackling-hard-to-treat-cancers-what-how-and-why/.

[38] Jun Wu et al. "Endotherapy versus surgery for early neoplasia in Barrett's esophagus: a meta-analysis." In: *Gastrointestinal endoscopy* 79.2 (Feb. 2014), 233–241.e2. URL: http://www.ncbi.nlm.nih.gov/pubmed/24079410.

[39] Elizabeth C Smyth et al. "Oesophageal cancer." In: *Nature reviews. Disease primers* 3 (July 2017), p. 17048. URL: http://www.ncbi.nlm.nih.gov/pubmed/28748917%20http://www.pubmedcentral.nih.gov/articlerender.fcgi?artid=PMC6168059.

[40] Tom Waddell et al. "Epirubicin, oxaliplatin, and capecitabine with or without panitumumab for patients with previously untreated advanced oesophagogastric cancer (REAL3): a randomised, open-label phase 3 trial." In: *The Lancet. Oncology* 14.6 (May 2013), pp. 481–9. URL: http://www.ncbi.nlm.nih.gov/pubmed/23594787%20http://www.pubmedcentral.nih.gov/articlerender.fcgi?artid=PMC3669518.

[41] Florian Lordick et al. "Capecitabine and cisplatin with or without cetuximab for patients with previously untreated advanced gastric cancer (EXPAND): a randomised, open-label phase 3 trial." In: *The Lancet. Oncology* 14.6 (May 2013), pp. 490–9. URL: http://www.ncbi.nlm.nih.gov/pubmed/23594786.

[42] Susan J Dutton et al. "Gefitinib for oesophageal cancer progressing after chemotherapy (COG): a phase 3, multicentre, double-blind, placebo-controlled randomised trial." In: *The Lancet. Oncology* 15.8 (July 2014), pp. 894–904. URL: http://www.ncbi.nlm.nih.gov/pubmed/24950987.

[43] Manish A Shah et al. "Effect of Fluorouracil, Leucovorin, and Oxaliplatin With or Without Onartuzumab in HER2-Negative, MET-Positive Gastroesophageal Adenocarcinoma: The METGastric Randomized Clinical Trial." In: *JAMA oncology* 3.5 (May 2017), pp. 620–627. URL: http://www.ncbi.nlm.nih.gov/pubmed/27918764%20http://www.pubmedcentral.nih.gov/articlerender.fcgi?artid=PMC5824210.

[44] Daniel V T Catenacci et al. "Rilotumumab plus epirubicin, cisplatin, and capecitabine as first-line therapy in advanced MET-positive gastric or gastro-oesophageal junction cancer (RILOMET-1): a randomised, double-blind, placebo-controlled, phase 3 trial." In: *The Lancet. Oncology* 18.11 (2017), pp. 1467–1482. URL: http://www.ncbi.nlm.nih.gov/pubmed/28958504%20http://www.pubmedcentral.nih.gov/articlerender.fcgi?artid=PMC5898242.

[45] E Van Cutsem et al. "A randomized, open-label study of the efficacy and safety of AZD4547 monotherapy versus paclitaxel for the treatment of advanced gastric adenocarcinoma with FGFR2 polysomy or gene amplification." In: *Annals of oncology : official journal of the European Society for Medical Oncology* 28.6 (June 2017), pp. 1316–1324. URL: http://www.ncbi.nlm.nih.gov/pubmed/29177434.

[46] Charles S Fuchs et al. "Ramucirumab monotherapy for previously treated advanced gastric or gastro-oesophageal junction adenocarcinoma (REGARD): an international, randomised, multicentre, placebo-controlled, phase 3 trial." In: *Lancet (London, England)* 383.9911 (Jan. 2014), pp. 31–39. URL: http://www.ncbi.nlm.nih.gov/pubmed/24094768.

[47] Charles S Fuchs et al. "Ramucirumab with cisplatin and fluoropyrimidine as first-line therapy in patients with metastatic gastric or junctional adenocarcinoma (RAINFALL): a double-blind, randomised, placebo-controlled, phase 3 trial." In: *The Lancet. Oncology* 20.3 (Mar. 2019), pp. 420–435. URL: http://www.ncbi.nlm.nih.gov/pubmed/30718072.

[48] Yung-Jue Bang et al. "Trastuzumab in combination with chemotherapy versus chemotherapy alone for treatment of HER2-positive advanced gastric or gastro-oesophageal junction cancer (ToGA): a phase 3, open-label, randomised controlled trial." In: *Lancet (London, England)* 376.9742 (Aug. 2010), pp. 687–97. URL: http://www.ncbi.nlm.nih.gov/pubmed/20728210.

[49] Yoon-Koo Kang et al. "Nivolumab in patients with advanced gastric or gastro-oesophageal junction cancer refractory to, or intolerant of, at least two previous chemotherapy regimens (ONO-4538-12, ATTRACTION-2): a randomised, double-blind, placebo-controlled, phase 3 trial." In: *Lancet (London, England)* 390.10111 (Dec. 2017), pp. 2461–2471. URL: http://www.ncbi.nlm.nih.gov/pubmed/28993052.

[50] Yelena Y Janjigian et al. "CheckMate-032 Study: Efficacy and Safety of Nivolumab and Nivolumab Plus Ipilimumab in Patients With Metastatic Esophagogastric Cancer." In: *Journal of clinical oncology : official journal of the American Society of Clinical Oncology* 36.28 (2018), pp. 2836–2844. URL: http://www.ncbi.nlm.nih.gov/pubmed/30110194%20http://www.pubmedcentral.nih.gov/articlerender.fcgi?artid=PMC6161834.

[51] Elie Dolgin. "Bringing down the cost of cancer treatment." In: *Nature* 555.7695 (2018), S26–S29. URL: http://www.ncbi.nlm.nih.gov/pubmed/29517030.

[52] Sir Marc Feldmann. "Cancer immunotherapy in routine cost-effective cancer care?" In: *EMBO molecular medicine* 10.11 (2018). URL: http://www.ncbi.nlm.nih.gov/pubmed/30322840%20http://www.pubmedcentral.nih.gov/articlerender.fcgi?artid=PMC6220302.

[53] Rocco Maurizio Zagari et al. "Prevalence of upper gastrointestinal endoscopic findings in the community: A systematic review of studies in unselected samples of subjects." In: *Journal of gastroenterology and hepatology* 31.9 (Sept. 2016), pp. 1527–38. URL: http://www.ncbi.nlm.nih.gov/pubmed/26840528.

[54] Rebecca C Fitzgerald et al. "British Society of Gastroenterology guidelines on the diagnosis and management of Barrett's oesophagus." In: *Gut* 63.1 (Jan. 2014), pp. 7–42. URL: http://www.ncbi.nlm.nih.gov/pubmed/24165758.

[55] P Chaves et al. "Gastric and intestinal differentiation in Barrett's metaplasia and associated adenocarcinoma." In: *Diseases of the esophagus : official journal of the International Society for Diseases of the Esophagus* 18.6 (2005), pp. 383–7. URL: http://www.ncbi.nlm.nih.gov/pubmed/16336609.

[56] M Griffin and E C Sweeney. "The relationship of endocrine cells, dysplasia and carcinoembryonic antigen in Barrett's mucosa to adenocarcinoma of the oesophagus." In: *Histopathology* 11.1 (Jan. 1987), pp. 53–62. URL: http://www.ncbi.nlm.nih.gov/pubmed/2881873.

[57] N R BARRETT. "Chronic peptic ulcer of the oesophagus and 'oesophagitis'." In: *The British journal of surgery* 38.150 (Oct. 1950), pp. 175–82. URL: http://www.ncbi.nlm.nih.gov/pubmed/14791960.

[58] N R BARRETT. "The lower esophagus lined by columnar epithelium." In: *Surgery* 41.6 (June 1957), pp. 881–94. URL: http://www.ncbi.nlm.nih.gov/pubmed/13442856.

[59] J HAYWARD. "The lower end of the oesophagus." In: *Thorax* 16 (Mar. 1961), pp. 36–41. URL: http://www.ncbi.nlm.nih.gov/pubmed/13712529%20http://www.pubmedcentral.nih.gov/articlerender.fcgi?artid=PMC1018600.

[60] Y Nakanishi et al. "Distribution and significance of the oesophageal and gastric cardiac mucosae: a study of 131 operation specimens." In: *Histopathology* 51.4 (Oct. 2007), pp. 515–9. URL: http://www.ncbi.nlm.nih.gov/pubmed/17711448.

[61] P T Chandrasoma et al. "Distribution and significance of epithelial types in columnar-lined esophagus." In: *The American journal of surgical pathology* 25.9 (Sept. 2001), pp. 1188–93. URL: http://www.ncbi.nlm.nih.gov/pubmed/11688579.

[62] Nicole M White et al. "Barrett's esophagus and cardiac intestinal metaplasia: two conditions within the same spectrum." In: *Canadian journal of gastroenterology = Journal canadien de gastroenterologie* 22.4 (Apr. 2008), pp. 369–75. URL: http://www.ncbi.nlm.nih.gov/pubmed/18414711%20http://www.pubmedcentral.nih.gov/articlerender.fcgi?artid=PMC2662894.

[63] Michael Quante et al. "Bile acid and inflammation activate gastric cardia stem cells in a mouse model of Barrett-like metaplasia." In: *Cancer cell* 21.1 (Jan. 2012), pp. 36–51. URL: http://www.ncbi.nlm.nih.gov/pubmed/22264787%20http://www.pubmedcentral.nih.gov/articlerender.fcgi?artid=PMC3266546.

[64] R Farré et al. "Short exposure of oesophageal mucosa to bile acids, both in acidic and weakly acidic conditions, can impair mucosal integrity and provoke dilated intercellular spaces." In: *Gut* 57.10 (Oct. 2008), pp. 1366–74. URL: http://www.ncbi.nlm.nih.gov/pubmed/18593808.

[65] Anna M Nicholson et al. "Barrett's metaplasia glands are clonal, contain multiple stem cells and share a common squamous progenitor." In: *Gut* 61.10 (Oct. 2012), pp. 1380–9. URL: http://www.ncbi.nlm.nih.gov/pubmed/22200839.

[66] H Kazumori et al. "Bile acids directly augment caudal related homeobox gene Cdx2 expression in oesophageal keratinocytes in Barrett's epithelium." In: *Gut* 55.1 (Jan. 2006), pp. 16–25. URL: http://www.ncbi.nlm.nih.gov/pubmed/16118348%20http://www.pubmedcentral.nih.gov/articlerender.fcgi?artid=PMC1856383.

[67] David J Morrow et al. "Pathogenesis of Barrett's esophagus: bile acids inhibit the Notch signaling pathway with induction of CDX2 gene expression in human esophageal cells." In: *Surgery* 146.4 (Oct. 2009), 714–21, discussion 721–2. URL: http://www.ncbi.nlm.nih.gov/pubmed/19789031%20http://www.pubmedcentral.nih.gov/articlerender.fcgi?artid=PMC3371765.

[68] Maria E Vega et al. "Inhibition of Notch signaling enhances transdifferentiation of the esophageal squamous epithelium towards a Barrett's-like metaplasia via KLF4." In: *Cell cycle (Georgetown, Tex.)* 13.24 (2014), pp. 3857–66. URL: http://www.ncbi.nlm.nih.gov/pubmed/25558829%20http://www.pubmedcentral.nih.gov/articlerender.fcgi?artid=PMC4614677.

[69] Marie Reveiller et al. "Bile exposure inhibits expression of squamous differentiation genes in human esophageal epithelial cells." In: *Annals of surgery* 255.6 (June 2012), pp. 1113–20. URL: http://www.ncbi.nlm.nih.gov/pubmed/22498892.

[70] G Sarosi et al. "Bone marrow progenitor cells contribute to esophageal regeneration and metaplasia in a rat model of Barrett's esophagus." In: *Diseases of the esophagus : official journal of the International Society for Diseases of the Esophagus* 21.1 (2008), pp. 43–50. URL: http://www.ncbi.nlm.nih.gov/pubmed/18197938.

[71] Xia Wang et al. "Residual embryonic cells as precursors of a Barrett's-like metaplasia." In: *Cell* 145.7 (June 2011), pp. 1023–35. URL: http://www.ncbi.nlm.nih.gov/pubmed/21703447%20http://www.pubmedcentral.nih.gov/articlerender.fcgi?artid=PMC3125107.

[72] Ming Jiang et al. "Transitional basal cells at the squamous-columnar junction generate Barrett's oesophagus." In: *Nature* 550.7677 (2017), pp. 529–533. URL: http://www.ncbi.nlm.nih.gov/pubmed/29019984%20http://www.pubmedcentral.nih.gov/articlerender.fcgi?artid=PMC5831195.

[73] Ester Lörinc, Lennart Mellblom, and Stefan Öberg. "The immunophenotypic relationship between the submucosal gland unit, columnar metaplasia and squamous islands in the columnar-lined oesophagus." In: *Histopathology* 67.6 (Dec. 2015), pp. 792–8. URL: http://www.ncbi.nlm.nih.gov/pubmed/25898799.

[74] S J Leedham et al. "Individual crypt genetic heterogeneity and the origin of metaplastic glandular epithelium in human Barrett's oesophagus." In: *Gut* 57.8 (Aug. 2008), pp. 1041–8. URL: http://www.ncbi.nlm.nih.gov/pubmed/18305067%20http://www.pubmedcentral.nih.gov/articlerender.fcgi?artid=PMC2564832.

[75] Frederik Hvid-Jensen et al. "Incidence of adenocarcinoma among patients with Barrett's esophagus." In: *The New England journal of medicine* 365.15 (Oct. 2011), pp. 1375–83. URL: http://www.ncbi.nlm.nih.gov/pubmed/21995385.

[76] Marjolein Sikkema et al. "Risk of esophageal adenocarcinoma and mortality in patients with Barrett's esophagus: a systematic review and meta-analysis." In: *Clinical gastroenterology and hepatology : the official clinical practice journal of the American Gastroenterological Association* 8.3 (Mar. 2010), 235–44, quiz e32. URL: http://www.ncbi.nlm.nih.gov/pubmed/19850156.

[77] Danielle L Lavery et al. "Evolution of oesophageal adenocarcinoma from metaplastic columnar epithelium without goblet cells in Barrett's oesophagus." In: *Gut* 65.6 (2016), pp. 907–13. URL: http://www.ncbi.nlm.nih.gov/pubmed/26701877%20http://www.pubmedcentral.nih.gov/articlerender.fcgi?artid=PMC4893117.

[78] Shivaram Bhat et al. "Risk of malignant progression in Barrett's esophagus patients: results from a large population-based study." In: *Journal of the National Cancer Institute* 103.13 (July 2011), pp. 1049–57. URL: http://www.ncbi.nlm.nih.gov/pubmed/21680910%20http://www.pubmedcentral.nih.gov/articlerender.fcgi?artid=PMC3632011.

[79] N S Buttar et al. "Extent of high-grade dysplasia in Barrett's esophagus correlates with risk of adenocarcinoma." In: *Gastroenterology* 120.7 (June 2001), pp. 1630–9. URL: http://www.ncbi.nlm.nih.gov/pubmed/11375945.

[80] Konstantin Pogorelov et al. "KVASIR: A Multi-Class Image Dataset for Computer Aided Gastrointestinal Disease Detection". In: *Proceedings of the 8th ACM on Multimedia Systems Conference*. MMSys'17. Taipei, Taiwan: ACM, 2017, pp. 164–169. URL: http://doi.acm.org/10.1145/3083187.3083212.

[81] Massachusetts General Hospital. 2019. URL: https://www.massgeneral.org.

[82] Hopkins Medicine. 2019. URL: www.hopkinsmedicine.org.

[83] Joel H Rubenstein, Nora Mattek, and Glenn Eisen. "Age- and sex-specific yield of Barrett's esophagus by endoscopy indication." In: *Gastrointestinal endoscopy* 71.1 (Jan. 2010), pp. 21–7. URL: http://www.ncbi.nlm.nih.gov/pubmed/19748616%20http://www.pubmedcentral.nih.gov/articlerender.fcgi?artid=PMC2813379.

[84] D J Stein et al. "The association of body mass index with Barrett's oesophagus." In: *Alimentary pharmacology & therapeutics* 22.10 (Nov. 2005), pp. 1005–10. URL: http://www.ncbi.nlm.nih.gov/pubmed/16268976.

[85] Tomoyuki Akiyama et al. "Visceral obesity and the risk of Barrett's esophagus in Japanese patients with non-alcoholic fatty liver disease." In: *BMC gastroenterology* 9 (July 2009), p. 56. URL: http://www.ncbi.nlm.nih.gov/pubmed/19622165%20http://www.pubmedcentral.nih.gov/articlerender.fcgi?artid=PMC2718904.

[86] Cadman L Leggett et al. "Metabolic syndrome as a risk factor for Barrett esophagus: a population-based case-control study." In: *Mayo Clinic proceedings* 88.2 (Feb. 2013), pp. 157–65. URL: http://www.ncbi.nlm.nih.gov/pubmed/23374619%20http://www.pubmedcentral.nih.gov/articlerender.fcgi?artid=PMC3771537.

[87] Rami Eliakim et al. "A prospective study of the diagnostic accuracy of PillCam ESO esophageal capsule endoscopy versus conventional upper endoscopy in patients with chronic gastroesophageal reflux diseases." In: *Journal of clinical gastroenterology* 39.7 (Aug. 2005), pp. 572–8. URL: http://www.ncbi.nlm.nih.gov/pubmed/16000923.

[88] Caryn S Ross-Innes et al. "Risk stratification of Barrett's oesophagus using a non-endoscopic sampling method coupled with a biomarker panel: a cohort study." In: *The lancet. Gastroenterology & hepatology* 2.1 (2017), pp. 23–31. URL: http://www.ncbi.nlm.nih.gov/pubmed/28404010.

[89] Liam Zakko et al. "Cytosponge use in risk stratification of Barrett's oesophagus." In: *The lancet. Gastroenterology & hepatology* 2.1 (2017), pp. 3–4. URL: http://www.ncbi.nlm.nih.gov/pubmed/28404011.

[90] Heiko Pohl et al. "Length of Barrett's oesophagus and cancer risk: implications from a large sample of patients with early oesophageal adenocarcinoma." In: *Gut* 65.2 (Feb. 2016), pp. 196–201. URL: http://www.ncbi.nlm.nih.gov/pubmed/26113177.

[91] Dipesh Solanky et al. "Barrett Esophagus Length, Nodularity, and Low-grade Dysplasia are Predictive of Progression to Esophageal Adenocarcinoma." In: *Journal of clinical gastroenterology* 53.5 (), pp. 361–365. URL: http://www.ncbi.nlm.nih.gov/pubmed/29608452.

[92] S Y Iftikhar et al. "Length of Barrett's oesophagus: an important factor in the development of dysplasia and adenocarcinoma." In: *Gut* 33.9 (Sept. 1992), pp. 1155–8. URL: http://www.ncbi.nlm.nih.gov/pubmed/1427364%20http://www.pubmedcentral.nih.gov/articlerender.fcgi?artid=PMC1379476.

[93] Nour Hamade et al. "Lower Annual Rate of Progression of Short-Segment vs Long-Segment Barrett's Esophagus to Esophageal Adenocarcinoma." In: *Clinical gastroenterology and hepatology : the official clinical practice journal of the American Gastroenterological Association* 17.5 (Apr. 2019), pp. 864–868. URL: http://www.ncbi.nlm.nih.gov/pubmed/30012433.

[94] R E Rudolph et al. "Effect of segment length on risk for neoplastic progression in patients with Barrett esophagus." In: *Annals of internal medicine* 132.8 (Apr. 2000), pp. 612–20. URL: http://www.ncbi.nlm.nih.gov/pubmed/10766679.

[95] Benjamin Avidan et al. "Hiatal hernia size, Barrett's length, and severity of acid reflux are all risk factors for esophageal adenocarcinoma." In: *The American journal of gastroenterology* 97.8 (Aug. 2002), pp. 1930–6. URL: http://www.ncbi.nlm.nih.gov/pubmed/12190156.

[96] David C Whiteman et al. "Australian clinical practice guidelines for the diagnosis and management of Barrett's esophagus and early esophageal adenocarcinoma." In: *Journal of gastroenterology and hepatology* 30.5 (May 2015), pp. 804–20. URL: http://www.ncbi.nlm.nih.gov/pubmed/25612140.

[97] Caryn S Ross-Innes et al. "Whole-genome sequencing provides new insights into the clonal architecture of Barrett's esophagus and esophageal adenocarcinoma." In: *Nature genetics* 47.9 (Sept. 2015), pp. 1038–1046. URL: http://www.ncbi.nlm.nih.gov/pubmed/26192915%20http://www.pubmedcentral.nih.gov/articlerender.fcgi?artid=PMC4556068.

[98] Pierre Martinez et al. "Evolution of Barrett's esophagus through space and time at single-crypt and whole-biopsy levels." In: *Nature communications* 9.1 (2018), p. 794. URL: http://www.ncbi.nlm.nih.gov/pubmed/29476056%20http://www.pubmedcentral.nih.gov/articlerender.fcgi?artid=PMC5824808.

[99] James A Evans and Stuart A C McDonald. "The Complex, Clonal, and Controversial Nature of Barrett's Esophagus." In: *Advances in experimental medicine and biology* 908 (), pp. 27–40. URL: http://www.ncbi.nlm.nih.gov/pubmed/27573766.

[100] Pierre Martinez et al. "Dynamic clonal equilibrium and predetermined cancer risk in Barrett's oesophagus." In: *Nature communications* 7 (2016), p. 12158. URL: http://www.ncbi.nlm.nih.gov/pubmed/27538785%20http://www.pubmedcentral.nih.gov/articlerender.fcgi?artid=PMC4992167.

[101] Fouad J Moawad et al. "Barrett's oesophagus length is established at the time of initial endoscopy and does not change over time: results from a large multicentre cohort." In: *Gut* 64.12 (Dec. 2015), pp. 1874–80. URL: http://www.ncbi.nlm.nih.gov/pubmed/25652086.

[102] P Sharma, R E Sampliner, and E Camargo. "Normalization of esophageal pH with high-dose proton pump inhibitor therapy does not result in regression of Barrett's esophagus." In: *The American journal of gastroenterology* 92.4 (Apr. 1997), pp. 582–5. URL: http://www.ncbi.nlm.nih.gov/pubmed/9128303.

[103] A Malesci et al. "Partial regression of Barrett's esophagus by long-term therapy with high-dose omeprazole." In: *Gastrointestinal endoscopy* 44.6 (Dec. 1996), pp. 700–5. URL: http://www.ncbi.nlm.nih.gov/pubmed/8979061.

[104] R E Sampliner. "Effect of up to 3 years of high-dose lansoprazole on Barrett's esophagus." In: *The American journal of gastroenterology* 89.10 (Oct. 1994), pp. 1844–8. URL: http://www.ncbi.nlm.nih.gov/pubmed/7942680.

[105] "An evidence-based appraisal of reflux disease management–the Genval Workshop Report." In: *Gut* 44 Suppl 2 (Apr. 1999), S1–16. URL: http://www.ncbi.nlm.nih.gov/pubmed/10741335%20http://www.pubmedcentral.nih.gov/articlerender.fcgi?artid=PMC1766645.

[106] Nimish Vakil et al. "The Montreal definition and classification of gastroesophageal reflux disease: a global evidence-based consensus." In: *The American journal of gastroenterology* 101.8 (Aug. 2006), 1900–20, quiz 1943. URL: http://www.ncbi.nlm.nih.gov/pubmed/16928254.

[107] A Ruigómez et al. "Natural history of gastro-oesophageal reflux disease diagnosed in general practice." In: *Alimentary pharmacology & therapeutics* 20.7 (Oct. 2004), pp. 751–60. URL: http://www.ncbi.nlm.nih.gov/pubmed/15379835.

[108] Stuart J Thomas et al. "Ghrelin and Leptin Have a Complex Relationship with Risk of Barrett's Esophagus." In: *Digestive diseases and sciences* 61.1 (Jan. 2016), pp. 70–9. URL: http://www.ncbi.nlm.nih.gov/pubmed/26396004%20http://www.pubmedcentral.nih.gov/articlerender.fcgi?artid=PMC5549859.

[109] Joel H Rubenstein et al. "Associations of diabetes mellitus, insulin, leptin, and ghrelin with gastroesophageal reflux and Barrett's esophagus." In: *Gastroenterology* 145.6 (Dec. 2013), 1237–44.e1–5. URL: http://www.ncbi.nlm.nih.gov/pubmed/23999171%20http://www.pubmedcentral.nih.gov/articlerender.fcgi?artid=PMC3914630.

[110] T L Peeters. "Ghrelin: a new player in the control of gastrointestinal functions." In: *Gut* 54.11 (Nov. 2005), pp. 1638–49. URL: http://www.ncbi.nlm.nih.gov/pubmed/16227363%20http://www.pubmedcentral.nih.gov/articlerender.fcgi?artid=PMC1774760.

[111] K Clément et al. "A mutation in the human leptin receptor gene causes obesity and pituitary dysfunction." In: *Nature* 392.6674 (Mar. 1998), pp. 398–401. URL: http://www.ncbi.nlm.nih.gov/pubmed/9537324.

[112] R C Fitzgerald. "Barrett's oesophagus and oesophageal adenocarcinoma: how does acid interfere with cell proliferation and differentiation?" In: *Gut* 54 Suppl 1 (Mar. 2005), pp. i21–6. URL: http://www.ncbi.nlm.nih.gov/pubmed/15711004%20http://www.pubmedcentral.nih.gov/articlerender.fcgi?artid=PMC1867792.

[113] M C Sevilla Mantilla et al. "Manometry and 24-hour ambulatory pH monitoring at two levels of the esophagus in patients with and without esophagitis." In: *Revista espanola de enfermedades digestivas : organo oficial de la Sociedad Espanola de Patologia Digestiva* 90.3 (Mar. 1998), pp. 145–54. URL: http://www.ncbi.nlm.nih.gov/pubmed/9595935.

[114] N A Tobey et al. "The role of pepsin in acid injury to esophageal epithelium." In: *The American journal of gastroenterology* 96.11 (Nov. 2001), pp. 3062–70. URL: http://www.ncbi.nlm.nih.gov/pubmed/11721751.

[115] R C Fitzgerald, M B Omary, and G Triadafilopoulos. "Dynamic effects of acid on Barrett's esophagus. An ex vivo proliferation and differentiation model." In: *The Journal of clinical investigation* 98.9 (Nov. 1996), pp. 2120–8. URL: http://www.ncbi.nlm.nih.gov/pubmed/8903332%20http://www.pubmedcentral.nih.gov/articlerender.fcgi?artid=PMC507657.

[116] Rhonda F Souza et al. "Acid exposure activates the mitogen-activated protein kinase pathways in Barrett's esophagus." In: *Gastroenterology* 122.2 (Feb. 2002), pp. 299–307. URL: http://www.ncbi.nlm.nih.gov/pubmed/11832445.

[117] R Fass et al. “Correlation of oesophageal acid exposure with Barrett’s oesophagus length.” In: *Gut* 48.3 (Mar. 2001), pp. 310–3. URL: http://www.ncbi.nlm.nih.gov/pubmed/11171818%20http://www.pubmedcentral.nih.gov/articlerender.fcgi?artid=PMC1760147.

[118] Benjamin Avidan et al. “Hiatal hernia and acid reflux frequency predict presence and length of Barrett’s esophagus.” In: *Digestive diseases and sciences* 47.2 (Feb. 2002), pp. 256–64. URL: http://www.ncbi.nlm.nih.gov/pubmed/11855539.

[119] Arne Kandulski and Peter Malfertheiner. “Gastroesophageal reflux diseaseĝ€"from reflux episodes to mucosal inflammation”. In: *Nature Reviews Gastroenterology and Hepatology* 9.1 (Jan. 2012), pp. 15–22. URL: http://www.nature.com/articles/nrgastro.2011.210.

[120] Christopher P. Wild and Laura J. Hardie. “Reflux, Barrett’s oesophagus and adenocarcinoma: burning questions”. In: *Nature Reviews Cancer* 3.9 (Sept. 2003), pp. 676–684. URL: http://www.nature.com/articles/nrc1166.

[121] D J Bowrey. “Histological changes in the oesophageal squamous mucosa: correlation with ambulatory 24 hour pH monitoring”. In: *Journal of Clinical Pathology* 56.3 (Mar. 2003), pp. 205–208. URL: http://jcp.bmj.com/cgi/doi/10.1136/jcp.56.3.205.

[122] Rhonda Frances Souza. “Reflux esophagitis and its role in the pathogenesis of Barrett’s metaplasia.” In: *Journal of gastroenterology* 52.7 (July 2017), pp. 767–776. URL: http://www.ncbi.nlm.nih.gov/pubmed/28451845%20http://www.pubmedcentral.nih.gov/articlerender.fcgi?artid=PMC5488728.

[123] H B El-Serag et al. “The length of newly diagnosed Barrett’s oesophagus and prior use of acid suppressive therapy.” In: *Alimentary pharmacology & therapeutics* 19.12 (June 2004), pp. 1255–60. URL: http://www.ncbi.nlm.nih.gov/pubmed/15191506.

[124] Ram Dickman et al. “Clinical predictors of Barrett’s esophagus length.” In: *Gastrointestinal endoscopy* 62.5 (Nov. 2005), pp. 675–81. URL: http://www.ncbi.nlm.nih.gov/pubmed/16246678.

[125] Janusz A Z Jankowski et al. “Esomeprazole and aspirin in Barrett’s oesophagus (AspECT): a randomised factorial trial.” In: *Lancet (London, England)* 392.10145 (2018), pp. 400–408. URL: http://www.ncbi.nlm.nih.gov/pubmed/30057104%20http://www.pubmedcentral.nih.gov/articlerender.fcgi?artid=PMC6083438.

[126] Mario Anders et al. “Long-term recurrence of neoplasia and Barrett’s epithelium after complete endoscopic resection.” In: *Gut* 63.10 (Oct. 2014), pp. 1535–43. URL: http://www.ncbi.nlm.nih.gov/pubmed/24389236.

[127] Vasiliy Ivanovich Reshetnyak. “Physiological and molecular biochemical mechanisms of bile formation.” In: *World journal of gastroenterology* 19.42 (Nov. 2013), pp. 7341–60. URL: http://www.ncbi.nlm.nih.gov/pubmed/24259965%20http://www.pubmedcentral.nih.gov/articlerender.fcgi?artid=PMC3831216.

[128] I Björkhem and G Eggertsen. “Genes involved in initial steps of bile acid synthesis.” In: *Current opinion in lipidology* 12.2 (Apr. 2001), pp. 97–103. URL: http://www.ncbi.nlm.nih.gov/pubmed/11264980.

[129] L J Bennion et al. "Effects of oral contraceptives on the gallbladder bile of normal women." In: *The New England journal of medicine* 294.4 (Jan. 1976), pp. 189–92. URL: http://www.ncbi.nlm.nih.gov/pubmed/1244533.

[130] Gerd A Kullak-Ublick, Bruno Stieger, and Peter J Meier. "Enterohepatic bile salt transporters in normal physiology and liver disease." In: *Gastroenterology* 126.1 (Jan. 2004), pp. 322–42. URL: http://www.ncbi.nlm.nih.gov/pubmed/14699511.

[131] David W Russell. "The enzymes, regulation, and genetics of bile acid synthesis." In: *Annual review of biochemistry* 72 (2003), pp. 137–74. URL: http://www.ncbi.nlm.nih.gov/pubmed/12543708.

[132] John Y L Chiang. "Bile acids: regulation of synthesis." In: *Journal of lipid research* 50.10 (Oct. 2009), pp. 1955–66. URL: http://www.ncbi.nlm.nih.gov/pubmed/19346330%20http://www.pubmedcentral.nih.gov/articlerender.fcgi?artid=PMC2739756.

[133] J. W. COOK, E. L. KENNAWAY, and N. M. KENNAWAY. "Production of Tumours in Mice by Deoxycholic Acid". In: *Nature* 145.3677 (Apr. 1940), pp. 627–627. URL: http://www.nature.com/articles/145627a0.

[134] H Bernstein et al. "Bile acids as carcinogens in human gastrointestinal cancers." In: *Mutation research* 589.1 (Jan. 2005), pp. 47–65. URL: http://www.ncbi.nlm.nih.gov/pubmed/15652226.

[135] D Nehra et al. "Toxic bile acids in gastro-oesophageal reflux disease: influence of gastric acidity." In: *Gut* 44.5 (May 1999), pp. 598–602. URL: http://www.ncbi.nlm.nih.gov/pubmed/10205192%20http://www.pubmedcentral.nih.gov/articlerender.fcgi?artid=PMC1727508.

[136] H Bernstein et al. "Activation of the promoters of genes associated with DNA damage, oxidative stress, ER stress and protein malfolding by the bile salt, deoxycholate." In: *Toxicology letters* 108.1 (July 1999), pp. 37–46. URL: http://www.ncbi.nlm.nih.gov/pubmed/10472808.

[137] R J Sokol et al. "Generation of hydroperoxides in isolated rat hepatocytes and hepatic mitochondria exposed to hydrophobic bile acids." In: *Gastroenterology* 109.4 (Oct. 1995), pp. 1249–56. URL: http://www.ncbi.nlm.nih.gov/pubmed/7557092.

[138] Dun-Fa Peng et al. "Glutathione Peroxidase 7 Suppresses Bile Salt-Induced Expression of Pro-Inflammatory Cytokines in Barrett's Carcinogenesis." In: *Journal of Cancer* 5.7 (2014), pp. 510–7. URL: http://www.ncbi.nlm.nih.gov/pubmed/24963355%20http://www.pubmedcentral.nih.gov/articlerender.fcgi?artid=PMC4067510.

[139] Masato Inayama et al. "Involvement of oxidative stress in experimentally induced reflux esophagitis and esophageal cancer." In: *Hepato-gastroenterology* 54.75 (), pp. 761–5. URL: http://www.ncbi.nlm.nih.gov/pubmed/17591057.

[140] G J S Jenkins et al. "The bile acid deoxycholic acid has a non-linear dose response for DNA damage and possibly NF-kappaB activation in oesophageal cells, with a mechanism of action involving ROS." In: *Mutagenesis* 23.5 (Sept. 2008), pp. 399–405. URL: http://www.ncbi.nlm.nih.gov/pubmed/18515815.

[141] David P Doupé et al. "A single progenitor population switches behavior to maintain and repair esophageal epithelium." In: *Science (New York, N.Y.)* 337.6098 (Aug. 2012), pp. 1091–3. URL: http://www.ncbi.nlm.nih.gov/pubmed/22821983%20http://www.pubmedcentral.nih.gov/articlerender.fcgi?artid=PMC3527005.

[142] Chih-Long Chang et al. "Retinoic acid-induced glandular differentiation of the oesophagus." In: *Gut* 56.7 (July 2007), pp. 906–17. URL: http://www.ncbi.nlm.nih.gov/pubmed/17185354%20http://www.pubmedcentral.nih.gov/articlerender.fcgi?artid=PMC1994378.

[143] S Oberg et al. "Determinants of intestinal metaplasia within the columnar-lined esophagus." In: *Archives of surgery (Chicago, Ill. : 1960)* 135.6 (June 2000), 651–5, discussion 655–6. URL: http://www.ncbi.nlm.nih.gov/pubmed/10843360.

[144] Yuji Naito et al. "Role of pancreatic trypsin in chronic esophagitis induced by gastroduodenal reflux in rats." In: *Journal of gastroenterology* 41.3 (Mar. 2006), pp. 198–208. URL: http://www.ncbi.nlm.nih.gov/pubmed/16699853.

[145] Katarina B Greer et al. "Association of insulin and insulin-like growth factors with Barrett's oesophagus." In: *Gut* 61.5 (May 2012), pp. 665–72. URL: http://www.ncbi.nlm.nih.gov/pubmed/21930730%20http://www.pubmedcentral.nih.gov/articlerender.fcgi?artid=PMC3669672.

[146] Prasad G Iyer et al. "Association of Barrett's esophagus with type II Diabetes Mellitus: results from a large population-based case-control study." In: *Clinical gastroenterology and hepatology : the official clinical practice journal of the American Gastroenterological Association* 11.9 (Sept. 2013), 1108–1114.e5. URL: http://www.ncbi.nlm.nih.gov/pubmed/23591277%20http://www.pubmedcentral.nih.gov/articlerender.fcgi?artid=PMC3865768.

[147] J I Isenberg et al. "Human duodenal mucosal bicarbonate secretion. Evidence for basal secretion and stimulation by hydrochloric acid and a synthetic prostaglandin E1 analogue." In: *Gastroenterology* 91.2 (Aug. 1986), pp. 370–8. URL: http://www.ncbi.nlm.nih.gov/pubmed/3087810.

[148] Markus Sjöblom. "The duodenal mucosal bicarbonate secretion." In: *Upsala journal of medical sciences* 110.2 (2005), pp. 115–49. URL: http://www.ncbi.nlm.nih.gov/pubmed/16075893.

[149] J Sarosiek et al. "Evidence on secretion of epidermal growth factor by the esophageal mucosa in humans." In: *The American journal of gastroenterology* 88.7 (July 1993), pp. 1081–7. URL: http://www.ncbi.nlm.nih.gov/pubmed/8317410.

[150] J B Elder et al. "Cellular localisation of human urogastrone/epidermal growth factor." In: *Nature* 271.5644 (Feb. 1978), pp. 466–7. URL: http://www.ncbi.nlm.nih.gov/pubmed/342970.

[151] P U Heitz et al. "Immunohistochemical localisation of urogastrone to human duodenal and submandibular glands." In: *Gut* 19.5 (May 1978), pp. 408–13. URL: http://www.ncbi.nlm.nih.gov/pubmed/350728%20http://www.pubmedcentral.nih.gov/articlerender.fcgi?artid=PMC1412104.

[152] G Carpenter and S Cohen. "Epidermal growth factor." In: *The Journal of biological chemistry* 265.14 (May 1990), pp. 7709–12. URL: http://www.ncbi.nlm.nih.gov/pubmed/2186024.

[153] M D Hollenberg and H Gregory. "Epidermal growth factor-urogastrone: biological activity and receptor binding of derivatives." In: *Molecular pharmacology* 17.3 (May 1980), pp. 314–20. URL: http://www.ncbi.nlm.nih.gov/pubmed/6248761.

[154] H Gregory. "Isolation and structure of urogastrone and its relationship to epidermal growth factor." In: *Nature* 257.5524 (Sept. 1975), pp. 325–7. URL: http://www.ncbi.nlm.nih.gov/pubmed/1161035.

[155] Roy S Herbst. "Review of epidermal growth factor receptor biology." In: *International journal of radiation oncology, biology, physics* 59.2 Suppl (2004), pp. 21–6. URL: http://www.ncbi.nlm.nih.gov/pubmed/15142631.

[156] Yosef Yarden and Ben-Zion Shilo. "SnapShot: EGFR signaling pathway." In: *Cell* 131.5 (Nov. 2007), p. 1018. URL: http://www.ncbi.nlm.nih.gov/pubmed/18045542.

[157] Menachem Katz et al. "A reciprocal tensin-3-cten switch mediates EGF-driven mammary cell migration." In: *Nature cell biology* 9.8 (Aug. 2007), pp. 961–9. URL: http://www.ncbi.nlm.nih.gov/pubmed/17643115.

[158] Ajaz A Bhat et al. "Exposure of Barrett's and esophageal adenocarcinoma cells to bile acids activates EGFR-STAT3 signaling axis via induction of APE1." In: *Oncogene* 37.46 (2018), pp. 6011–6024. URL: http://www.ncbi.nlm.nih.gov/pubmed/29991802%20http://www.pubmedcentral.nih.gov/articlerender.fcgi?artid=PMC6328352.

[159] Jung-Hwan Yoon et al. "Bile acids induce cyclooxygenase-2 expression via the epidermal growth factor receptor in a human cholangiocarcinoma cell line." In: *Gastroenterology* 122.4 (Apr. 2002), pp. 985–93. URL: http://www.ncbi.nlm.nih.gov/pubmed/11910351.

[160] Laure Rittié et al. "Retinoid-induced epidermal hyperplasia is mediated by epidermal growth factor receptor activation via specific induction of its ligands heparin-binding EGF and amphiregulin in human skin in vivo." In: *The Journal of investigative dermatology* 126.4 (Apr. 2006), pp. 732–9. URL: http://www.ncbi.nlm.nih.gov/pubmed/16470170.

[161] Guilherme Pretto et al. "Increase of epidermal growth factor receptor expression in progression of GERD, Barrett, and adenocarcinoma of esophagus." In: *Digestive diseases and sciences* 58.1 (Jan. 2013), pp. 115–22. URL: http://www.ncbi.nlm.nih.gov/pubmed/22875307.

[162] Jesper Lagergren et al. "Oesophageal cancer." In: *Lancet (London, England)* 390.10110 (Nov. 2017), pp. 2383–2396. URL: http://www.ncbi.nlm.nih.gov/pubmed/28648400.

[163] Atsushi Suzuki et al. "EGF signaling activates proliferation and blocks apoptosis of mouse and human intestinal stem/progenitor cells in long-term monolayer cell culture." In: *Laboratory investigation; a journal of technical methods and pathology* 90.10 (Oct. 2010), pp. 1425–36. URL: http://www.ncbi.nlm.nih.gov/pubmed/20714325.

[164] Daisuke Nanba et al. "Recent advances in the epidermal growth factor receptor/ligand system biology on skin homeostasis and keratinocyte stem cell regulation." In: *Journal of dermatological science* 72.2 (Nov. 2013), pp. 81–6. URL: http://www.ncbi.nlm.nih.gov/pubmed/23819985.

[165] Mark R Frey, Anastasia Golovin, and D Brent Polk. "Epidermal growth factor-stimulated intestinal epithelial cell migration requires Src family kinase-dependent p38 MAPK signaling." In: *The Journal of biological chemistry* 279.43 (Oct. 2004), pp. 44513–21. URL: http://www.ncbi.nlm.nih.gov/pubmed/15316018.

[166] P Geimer and E G Bade. "The epidermal growth factor-induced migration of rat liver epithelial cells is associated with a transient inhibition of DNA synthesis." In: *Journal of cell science* 100 (Pt 2 (Oct. 1991), pp. 349–55. URL: http://www.ncbi.nlm.nih.gov/pubmed/1757491.

[167] Z Lu et al. "Epidermal growth factor-induced tumor cell invasion and metastasis initiated by dephosphorylation and downregulation of focal adhesion kinase." In: *Molecular and cellular biology* 21.12 (June 2001), pp. 4016–31. URL: http://www.ncbi.nlm.nih.gov/pubmed/11359909%20http://www.pubmedcentral.nih.gov/articlerender.fcgi?artid=PMC87064.

[168] Hyung-Do Kim et al. "Epidermal growth factor-induced enhancement of glioblastoma cell migration in 3D arises from an intrinsic increase in speed but an extrinsic matrix- and proteolysis-dependent increase in persistence." In: *Molecular biology of the cell* 19.10 (Oct. 2008), pp. 4249–59. URL: http://www.ncbi.nlm.nih.gov/pubmed/18632979%20http://www.pubmedcentral.nih.gov/articlerender.fcgi?artid=PMC2555959.

[169] N T Bennett and G S Schultz. "Growth factors and wound healing: biochemical properties of growth factors and their receptors." In: *American journal of surgery* 165.6 (June 1993), pp. 728–37. URL: http://www.ncbi.nlm.nih.gov/pubmed/8506974.

[170] M Itoh and Y Matsuo. "Gastric ulcer treatment with intravenous human epidermal growth factor: a double-blind controlled clinical study." In: *Journal of gastroenterology and hepatology* 9 Suppl 1 (1994), S78–83. URL: http://www.ncbi.nlm.nih.gov/pubmed/7881024.

[171] W Haedo et al. "Oral human recombinant epidermal growth factor in the treatment of patients with duodenal ulcer." In: *Revista espanola de enfermedades digestivas : organo oficial de la Sociedad Espanola de Patologia Digestiva* 88.6 (June 1996), pp. 409–18. URL: http://www.ncbi.nlm.nih.gov/pubmed/8755321.

[172] G L Brown et al. "Enhancement of wound healing by topical treatment with epidermal growth factor." In: *The New England journal of medicine* 321.2 (July 1989), pp. 76–9. URL: http://www.ncbi.nlm.nih.gov/pubmed/2659995.

[173] V Joshi, G S Ray, and J R Goldenring. "Inhibition of parietal cell acid secretion is mediated by the classical epidermal growth factor receptor." In: *Digestive diseases and sciences* 42.6 (June 1997), pp. 1194–8. URL: http://www.ncbi.nlm.nih.gov/pubmed/9201084.

[174] L Wang et al. "Epidermal growth factor and transforming growth factor-alpha directly inhibit parietal cell function through a similar mechanism." In: *The Journal of pharmacology and experimental therapeutics* 265.1 (Apr. 1993), pp. 308–13. URL: http://www.ncbi.nlm.nih.gov/pubmed/8474014.

[175] U Finke et al. "Effects of epidermal growth factor on acid secretion from guinea pig gastric mucosa: in vitro analysis." In: *Gastroenterology* 88.5 Pt 1 (May 1985), pp. 1175–82. URL: http://www.ncbi.nlm.nih.gov/pubmed/2984079.

[176] J F Hatt and P J Hanson. "Inhibition of gastric acid secretion by epidermal growth factor. Effects on cyclic AMP and on prostaglandin production in rat isolated parietal cells." In: *The Biochemical journal* 255.3 (Nov. 1988), pp. 789–94. URL: http://www.ncbi.nlm.nih.gov/pubmed/2463831%20http://www.pubmedcentral.nih.gov/articlerender.fcgi?artid=PMC1135310.

[177] J J Lewis et al. "Effects of epidermal growth factor on signal transduction in rabbit parietal cells." In: *The American journal of physiology* 258.3 Pt 1 (Mar. 1990), G476–83. URL: http://www.ncbi.nlm.nih.gov/pubmed/2156444.

[178] J W Konturek et al. "Distribution and release of epidermal growth factor in man." In: *Gut* 30.9 (Sept. 1989), pp. 1194–200. URL: http://www.ncbi.nlm.nih.gov/pubmed/2806986%20http://www.pubmedcentral.nih.gov/articlerender.fcgi?artid=PMC1434230.

[179] A M Tunio, J Holton, and M Hobsley. "Gastric juice epidermal growth factor concentration and Helicobacter pylori in patients with duodenal ulcer." In: *The British journal of surgery* 82.9 (Sept. 1995), pp. 1204–6. URL: http://www.ncbi.nlm.nih.gov/pubmed/7551996.

[180] A M Tunio and M Hobsley. "Epidermal growth factor in saliva and gastric juice: response to histamine." In: *Gut* 37.3 (Sept. 1995), pp. 335–9. URL: http://www.ncbi.nlm.nih.gov/pubmed/7590427%20http://www.pubmedcentral.nih.gov/articlerender.fcgi?artid=PMC1382812.

[181] S COHEN. "Isolation of a mouse submaxillary gland protein accelerating incisor eruption and eyelid opening in the new-born animal." In: *The Journal of biological chemistry* 237 (May 1962), pp. 1555–62. URL: http://www.ncbi.nlm.nih.gov/pubmed/13880319.

[182] S Fiorucci et al. "Gastric acidity and gastroesophageal reflux patterns in patients with esophagitis." In: *Gastroenterology* 103.3 (Sept. 1992), pp. 855–61. URL: http://www.ncbi.nlm.nih.gov/pubmed/1499935.

[183] Emily Foltz et al. "An assessment of human gastric fluid composition as a function of PPI usage." In: *Physiological reports* 3.1 (Jan. 2015). URL: http://www.ncbi.nlm.nih.gov/pubmed/25626870%20http://www.pubmedcentral.nih.gov/articlerender.fcgi?artid=PMC4387745.

[184] I E Farkas and G Gerö. "The role of Brunner's glands in the mucosal protection of the proximal part of duodenum." In: *Acta physiologica Hungarica* 73.2-3 (1989), pp. 257–60. URL: http://www.ncbi.nlm.nih.gov/pubmed/2596316.

[185] James R Goldenring. "Pyloric metaplasia, pseudopyloric metaplasia, ulcer-associated cell lineage and spasmolytic polypeptide-expressing metaplasia: reparative lineages in the gastrointestinal mucosa." In: *The Journal of pathology* 245.2 (2018), pp. 132–137. URL: http://www.ncbi.nlm.nih.gov/pubmed/29508389%20http://www.pubmedcentral.nih.gov/articlerender.fcgi?artid=PMC6026529.

[186] N A Wright, C Pike, and G Elia. "Induction of a novel epidermal growth factor-secreting cell lineage by mucosal ulceration in human gastrointestinal stem cells." In: *Nature* 343.6253 (Jan. 1990), pp. 82–5. URL: http://www.ncbi.nlm.nih.gov/pubmed/2296294.

[187] Danielle L Lavery et al. "The stem cell organisation, and the proliferative and gene expression profile of Barrett's epithelium, replicates pyloric-type gastric glands." In: *Gut* 63.12 (Dec. 2014), pp. 1854–63. URL: http://www.ncbi.nlm.nih.gov/pubmed/24550372%20http://www.pubmedcentral.nih.gov/articlerender.fcgi?artid=PMC4251192.

[188] S Marina Casalino-Matsuda, Maria E Monzón, and Rosanna M Forteza. "Epidermal growth factor receptor activation by epidermal growth factor mediates oxidant-induced goblet cell metaplasia in human airway epithelium." In: *American journal of respiratory cell and molecular biology* 34.5 (May 2006), pp. 581–91. URL: http://www.ncbi.nlm.nih.gov/pubmed/16424381%20http://www.pubmedcentral.nih.gov/articlerender.fcgi?artid=PMC2644222.

[189] Min He et al. "Activation of the EGF Receptor by Histamine Receptor Subtypes Stimulates Mucin Secretion in Conjunctival Goblet Cells." In: *Investigative ophthalmology & visual science* 59.8 (2018), pp. 3543–3553. URL: http://www.ncbi.nlm.nih.gov/pubmed/30025103%20http://www.pubmedcentral.nih.gov/articlerender.fcgi?artid=PMC6049985.

[190] L Li et al. "Effect of esophageal intraluminal mechanical and chemical stressors on salivary epidermal growth factor in humans." In: *The American journal of gastroenterology* 88.10 (Oct. 1993), pp. 1749–55. URL: http://www.ncbi.nlm.nih.gov/pubmed/8213719.

[191] T Lembo et al. "Inflammation of the gastro-oesophageal junction (carditis) in patients with symptomatic gastro-oesophageal reflux disease: a prospective study." In: *Gut* 45.4 (Oct. 1999), pp. 484–8. URL: http://www.ncbi.nlm.nih.gov/pubmed/10486352%20http://www.pubmedcentral.nih.gov/articlerender.fcgi?artid=PMC1727693.

[192] Promega. *Dual Luciferase Reporter Assay*. Aug 2019. URL: https://www.promega.com/-/media/files/resources/protcards/dual-luciferase-reporter-assay-and-dual-luciferase-reporter-1000-assay-systems-quick-protocol.pdf?la=en.

[193] Lisa Goers, Paul Freemont, and Karen M Polizzi. "Co-culture systems and technologies: taking synthetic biology to the next level." In: *Journal of the Royal Society, Interface* 11.96 (July 2014). URL: http://www.ncbi.nlm.nih.gov/pubmed/24829281%20http://www.pubmedcentral.nih.gov/articlerender.fcgi?artid=PMC4032528.

[194] J C Rockett et al. "Five newly established oesophageal carcinoma cell lines: phenotypic and immunological characterization." In: *British journal of cancer* 75.2 (1997), pp. 258–63. URL: http://www.ncbi.nlm.nih.gov/pubmed/9010035%20http://www.pubmedcentral.nih.gov/articlerender.fcgi?artid=PMC2063267.

[195] Andre Kleensang et al. "Genetic variability in a frozen batch of MCF-7 cells invisible in routine authentication affecting cell function." In: *Scientific reports* 6 (2016), p. 28994. URL: http://www.ncbi.nlm.nih.gov/pubmed/27456714%20http://www.pubmedcentral.nih.gov/articlerender.fcgi?artid=PMC4960662.

[196] Jurjen J Boonstra et al. "Mistaken identity of widely used esophageal adenocarcinoma cell line TE-7." In: *Cancer research* 67.17 (Sept. 2007), pp. 7996–8001. URL: http://www.ncbi.nlm.nih.gov/pubmed/17804709.

[197] Maria Secrier et al. "Mutational signatures in esophageal adenocarcinoma define etiologically distinct subgroups with therapeutic relevance." In: *Nature genetics* 48.10 (2016), pp. 1131–41. URL: http://www.ncbi.nlm.nih.gov/pubmed/27595477%20http://www.pubmedcentral.nih.gov/articlerender.fcgi?artid=PMC5957269.

[198] Timothy J Underwood et al. "A comparison of primary oesophageal squamous epithelial cells with HET-1A in organotypic culture." In: *Biology of the cell* 102.12 (Dec. 2010), pp. 635–44. URL: http://www.ncbi.nlm.nih.gov/pubmed/20843300.

[199] Hideki Harada et al. "Telomerase induces immortalization of human esophageal keratinocytes without p16INK4a inactivation." In: *Molecular cancer research : MCR* 1.10 (Aug. 2003), pp. 729–38. URL: http://www.ncbi.nlm.nih.gov/pubmed/12939398.

[200] Jiri Kalabis et al. "Isolation and characterization of mouse and human esophageal epithelial cells in 3D organotypic culture." In: *Nature protocols* 7.2 (Jan. 2012), pp. 235–46. URL: http://www.ncbi.nlm.nih.gov/pubmed/22240585%20http://www.pubmedcentral.nih.gov/articlerender.fcgi?artid=PMC3505594.

[201] Takaomi Okawa et al. "The functional interplay between EGFR overexpression, hTERT activation, and p53 mutation in esophageal epithelial cells with activation of stromal fibroblasts induces tumor development, invasion, and differentiation." In: *Genes & development* 21.21 (Nov. 2007), pp. 2788–803. URL: http://www.ncbi.nlm.nih.gov/pubmed/17974918%20http://www.pubmedcentral.nih.gov/articlerender.fcgi?artid=PMC2045132.

[202] M Corinna A Palanca-Wessels et al. "Extended lifespan of Barrett's esophagus epithelium transduced with the human telomerase catalytic subunit: a useful in vitro model." In: *Carcinogenesis* 24.7 (July 2003), pp. 1183–90. URL: http://www.ncbi.nlm.nih.gov/pubmed/12807723%20http://www.pubmedcentral.nih.gov/articlerender.fcgi?artid=PMC1559990.

[203] S Takayama et al. "Patterning cells and their environments using multiple laminar fluid flows in capillary networks." In: *Proceedings of the National Academy of Sciences of the United States of America* 96.10 (May 1999), pp. 5545–8. URL: http://www.ncbi.nlm.nih.gov/pubmed/10318920%20http://www.pubmedcentral.nih.gov/articlerender.fcgi?artid=PMC21896.

[204] Elliot E Hui and Sangeeta N Bhatia. "Micromechanical control of cell-cell interactions." In: *Proceedings of the National Academy of Sciences of the United States of America* 104.14 (Apr. 2007), pp. 5722–6. URL: http://www.ncbi.nlm.nih.gov/pubmed/17389399%20http://www.pubmedcentral.nih.gov/articlerender.fcgi?artid=PMC1851558.

[205] Jia Zeng et al. "Transcriptional regulation by normal epithelium of premalignant to malignant progression in Barrett's esophagus." In: *Scientific reports* 6 (2016), p. 35227. URL: http://www.ncbi.nlm.nih.gov/pubmed/27731371%20http://www.pubmedcentral.nih.gov/articlerender.fcgi?artid=PMC5059688.

[206] Lauren M F Merlo et al. "An in vitro co-culture model of esophageal cells identifies ascorbic acid as a modulator of cell competition." In: *BMC cancer* 11 (Oct. 2011), p. 461. URL: http://www.ncbi.nlm.nih.gov/pubmed/22026449%20http://www.pubmedcentral.nih.gov/articlerender.fcgi?artid=PMC3213018.

[207] Rachelle E Kosoff et al. "Development and characterization of an organotypic model of Barrett's esophagus." In: *Journal of cellular physiology* 227.6 (June 2012), pp. 2654–9. URL: http://www.ncbi.nlm.nih.gov/pubmed/21882191%20http://www.pubmedcentral.nih.gov/articlerender.fcgi?artid=PMC3352665.

[208] Timothy J Underwood et al. "Cancer-associated fibroblasts predict poor outcome and promote periostin-dependent invasion in oesophageal adenocarcinoma." In: *The Journal of pathology* 235.3 (Feb. 2015), pp. 466–77. URL: http://www.ncbi.nlm.nih.gov/pubmed/25345775%20http://www.pubmedcentral.nih.gov/articlerender.fcgi?artid=PMC4312957.

[209] Joan Somja et al. "Dendritic cells in Barrett's esophagus carcinogenesis: an inadequate microenvironment for antitumor immunity?" In: *The American journal of pathology* 182.6 (June 2013), pp. 2168–79. URL: http://www.ncbi.nlm.nih.gov/pubmed/23619476.

[210] Emma H Allott et al. "The SGBS cell strain as a model for the in vitro study of obesity and cancer." In: *Clinical & translational oncology : official publication of the Federation of Spanish Oncology Societies and of the National Cancer Institute of Mexico* 14.10 (Oct. 2012), pp. 774–82. URL: http://www.ncbi.nlm.nih.gov/pubmed/22855155.

[211] Sahar Javaherian, Katherine J Li, and Alison P McGuigan. "A simple and rapid method for generating patterned co-cultures with stable interfaces." In: *BioTechniques* 55.1 (July 2013), pp. 21–6. URL: http://www.ncbi.nlm.nih.gov/pubmed/23834381.

[212] John P Frampton et al. "Cell co-culture patterning using aqueous two-phase systems." In: *Journal of visualized experiments : JoVE* 73 (Mar. 2013). URL: http://www.ncbi.nlm.nih.gov/pubmed/23567187%20http://www.pubmedcentral.nih.gov/articlerender.fcgi?artid=PMC3640839.

[213] Hideru Togashi et al. "Nectins establish a checkerboard-like cellular pattern in the auditory epithelium." In: *Science (New York, N.Y.)* 333.6046 (Aug. 2011), pp. 1144–7. URL: http://www.ncbi.nlm.nih.gov/pubmed/21798896.

[214] Carolyn L Smith. "Basic confocal microscopy." In: *Current protocols in molecular biology* Chapter 14 (Jan. 2008), Unit 14.11. URL: http://www.ncbi.nlm.nih.gov/pubmed/18231980.

[215] O SHIMOMURA, F H JOHNSON, and Y SAIGA. "Extraction, purification and properties of aequorin, a bioluminescent protein from the luminous hydromedusan, Aequorea." In: *Journal of cellular and comparative physiology* 59 (June 1962), pp. 223–39. URL: http://www.ncbi.nlm.nih.gov/pubmed/13911999.

[216] M G Honig and R I Hume. "Fluorescent carbocyanine dyes allow living neurons of identified origin to be studied in long-term cultures." In: *The Journal of cell biology* 103.1 (July 1986), pp. 171–87. URL: http://www.ncbi.nlm.nih.gov/pubmed/2424918%20http://www.pubmedcentral.nih.gov/articlerender.fcgi?artid=PMC2113786.

[217] Zhang. "New fluorescent-probes for long-term tracing of living cells". In: *FASEB* 6.5 (1992), A1835.

[218] Christian Dahmann, Andrew C Oates, and Michael Brand. "Boundary formation and maintenance in tissue development." In: *Nature reviews. Genetics* 12.1 (Jan. 2011), pp. 43–55. URL: http://www.ncbi.nlm.nih.gov/pubmed/21164524.

[219] Michael H A Schmitz et al. "Live-cell imaging RNAi screen identifies PP2A-B55alpha and importin-beta1 as key mitotic exit regulators in human cells." In: *Nature cell biology* 12.9 (Sept. 2010), pp. 886–93. URL: http://www.ncbi.nlm.nih.gov/pubmed/20711181%20http://www.pubmedcentral.nih.gov/articlerender.fcgi?artid=PMC3839080.

[220] Michael Held et al. "CellCognition: time-resolved phenotype annotation in high-throughput live cell imaging." In: *Nature methods* 7.9 (Sept. 2010), pp. 747–54. URL: http://www.ncbi.nlm.nih.gov/pubmed/20693996.

[221] Gregoire Pau et al. "Dynamical modelling of phenotypes in a genome-wide RNAi live-cell imaging assay." In: *BMC bioinformatics* 14 (Oct. 2013), p. 308. URL: http://www.ncbi.nlm.nih.gov/pubmed/24131777%20http://www.pubmedcentral.nih.gov/articlerender.fcgi?artid=PMC3827932.

[222] Dirk Padfield, Jens Rittscher, and Badrinath Roysam. "Coupled minimum-cost flow cell tracking for high-throughput quantitative analysis." In: *Medical image analysis* 15.4 (Aug. 2011), pp. 650–68. URL: http://www.ncbi.nlm.nih.gov/pubmed/20864383.

[223] Martin Maška et al. "A benchmark for comparison of cell tracking algorithms." In: *Bioinformatics (Oxford, England)* 30.11 (June 2014), pp. 1609–17. URL: http://www.ncbi.nlm.nih.gov/pubmed/24526711%20http://www.pubmedcentral.nih.gov/articlerender.fcgi?artid=PMC4029039.

[224] Martin Schiegg et al. "Graphical model for joint segmentation and tracking of multiple dividing cells." In: *Bioinformatics (Oxford, England)* 31.6 (Mar. 2015), pp. 948–56. URL: http://www.ncbi.nlm.nih.gov/pubmed/25406328.

[225] Thomas A Nketia et al. "Analysis of live cell images: Methods, tools and opportunities." In: *Methods (San Diego, Calif.)* 115 (2017), pp. 65–79. URL: http://www.ncbi.nlm.nih.gov/pubmed/28242295.

[226] Jessica S Martinez, Joseph B Schlenoff, and Thomas C S Keller. "Collective epithelial cell sheet adhesion and migration on polyelectrolyte multilayers with uniform and gradients of compliance." In: *Experimental cell research* 346.1 (2016), pp. 17–29. URL: http://www.ncbi.nlm.nih.gov/pubmed/27292313%20http://www.pubmedcentral.nih.gov/articlerender.fcgi?artid=PMC4967014.

[227] L Petitjean et al. "Velocity fields in a collectively migrating epithelium." In: *Biophysical journal* 98.9 (May 2010), pp. 1790–800. URL: http://www.ncbi.nlm.nih.gov/pubmed/20441742%20http://www.pubmedcentral.nih.gov/articlerender.fcgi?artid=PMC2862185.

[228] Florian Milde et al. "Cell Image Velocimetry (CIV): boosting the automated quantification of cell migration in wound healing assays." In: *Integrative biology : quantitative biosciences from nano to macro* 4.11 (Nov. 2012), pp. 1437–47. URL: http://www.ncbi.nlm.nih.gov/pubmed/23047374.

[229] Assaf Zaritsky et al. "Emergence of HGF/SF-induced coordinated cellular motility." In: *PloS one* 7.9 (2012), e44671. URL: http://www.ncbi.nlm.nih.gov/pubmed/22970283%20http://www.pubmedcentral.nih.gov/articlerender.fcgi?artid=PMC3435317.

[230] Thomas Brox et al. "High Accuracy Optical Flow Estimation Based on a Theory for Warping". In: 2004, pp. 25–36. URL: http://link.springer.com/10.1007/978-3-540-24673-2%7B%5C_%7D3.

[231] T. Brox and J. Malik. "Large Displacement Optical Flow: Descriptor Matching in Variational Motion Estimation". In: *IEEE Transactions on Pattern Analysis and Machine Intelligence* 33.3 (Mar. 2011), pp. 500–513.

[232] Felix Y Zhou et al. "Motion sensing superpixels (MOSES) is a systematic computational framework to quantify and discover cellular motion phenotypes." In: *eLife* 8 (2019). URL: http://www.ncbi.nlm.nih.gov/pubmed/30803483%20http://www.pubmedcentral.nih.gov/articlerender.fcgi?artid=PMC6391079.

[233] Simone Keller et al. "Evaluation of epidermal growth factor receptor signaling effects in gastric cancer cell lines by detailed motility-focused phenotypic characterization linked with molecular analysis." In: *BMC cancer* 17.1 (2017), p. 845. URL: http://www.ncbi.nlm.nih.gov/pubmed/29237412%20http://www.pubmedcentral.nih.gov/articlerender.fcgi?artid=PMC5729506.

[234] Masato Suzuki et al. "Helicobacter pylori CagA Phosphorylation-Independent Function in Epithelial Proliferation and Inflammation". In: *Cell Host & Microbe* 5.1 (Jan. 2009), pp. 23–34. URL: https://linkinghub.elsevier.com/retrieve/pii/S1931312808004022.

[235] F van Roy and G Berx. "The cell-cell adhesion molecule E-cadherin." In: *Cellular and molecular life sciences : CMLS* 65.23 (Nov. 2008), pp. 3756–88. URL: http://www.ncbi.nlm.nih.gov/pubmed/18726070.

[236] Zhi Jiang Zang et al. "Genetic and structural variation in the gastric cancer kinome revealed through targeted deep sequencing." In: *Cancer research* 71.1 (Jan. 2011), pp. 29–39. URL: http://www.ncbi.nlm.nih.gov/pubmed/21097718%20http://www.pubmedcentral.nih.gov/articlerender.fcgi?artid=PMC3719377.

[237] Akiko Mammoto, Tadanori Mammoto, and Donald E Ingber. "Mechanosensitive mechanisms in transcriptional regulation." In: *Journal of cell science* 125.Pt 13 (July 2012), pp. 3061–73. URL: http://www.ncbi.nlm.nih.gov/pubmed/22797927%20http://www.pubmedcentral.nih.gov/articlerender.fcgi?artid=PMC3434847.

[238] Joseph D Tario et al. "Monitoring Cell Proliferation by Dye Dilution: Considerations for Probe Selection." In: *Methods in molecular biology (Clifton, N.J.)* 1678 (2018), pp. 249–299. URL: http://www.ncbi.nlm.nih.gov/pubmed/29071683%20http://www.pubmedcentral.nih.gov/articlerender.fcgi?artid=PMC5831513.

[239] R J Playford et al. "Epidermal growth factor is digested to smaller, less active forms in acidic gastric juice." In: *Gastroenterology* 108.1 (Jan. 1995), pp. 92–101. URL: http://www.ncbi.nlm.nih.gov/pubmed/7806067.

[240] P S Olsen et al. "Effect of secretin and somatostatin on secretion of epidermal growth factor from Brunner's glands in the rat." In: *Digestive diseases and sciences* 39.10 (Oct. 1994), pp. 2186–90. URL: http://www.ncbi.nlm.nih.gov/pubmed/7924740.

[241] Yaping Xu, Liming Sheng, and Weimin Mao. "Role of epidermal growth factor receptor tyrosine kinase inhibitors in the treatment of esophageal carcinoma and the suggested mechanisms of action." In: *Oncology letters* 5.1 (Jan. 2013), pp. 19–24. URL: http://www.ncbi.nlm.nih.gov/pubmed/23255886%20http://www.pubmedcentral.nih.gov/articlerender.fcgi?artid=PMC3525339.

[242] Jin-Hong Kim et al. "Tunable interplay between epidermal growth factor and cell-cell contact governs the spatial dynamics of epithelial growth." In: *Proceedings of the National Academy of Sciences of the United States of America* 106.27 (July 2009), pp. 11149–53. URL: http://www.ncbi.nlm.nih.gov/pubmed/19549816%20http://www.pubmedcentral.nih.gov/articlerender.fcgi?artid=PMC2708686.

[243] Mark D Sternlicht et al. "Mammary ductal morphogenesis requires paracrine activation of stromal EGFR via ADAM17-dependent shedding of epithelial amphiregulin." In: *Development (Cambridge, England)* 132.17 (Sept. 2005), pp. 3923–33. URL: http://www.ncbi.nlm.nih.gov/pubmed/16079154%20http://www.pubmedcentral.nih.gov/articlerender.fcgi?artid=PMC2771180.

[244] R W Engelman et al. "Mammary and submandibular gland epidermal growth factor expression is reduced by calorie restriction." In: *Cancer research* 55.6 (Mar. 1995), pp. 1289–95. URL: http://www.ncbi.nlm.nih.gov/pubmed/7882324.

[245] Jin Cheng et al. "Overexpression of epidermal growth factor receptor in urothelium elicits urothelial hyperplasia and promotes bladder tumor growth." In: *Cancer research* 62.14 (July 2002), pp. 4157–63. URL: http://www.ncbi.nlm.nih.gov/pubmed/12124355.

[246] W I de Boer et al. "Characterization of distinct functions for growth factors in murine transitional epithelial cells in primary organotypic culture." In: *Experimental cell research* 214.2 (Oct. 1994), pp. 510–8. URL: http://www.ncbi.nlm.nih.gov/pubmed/7925644.

[247] Claudia D Andl et al. "Epidermal growth factor receptor mediates increased cell proliferation, migration, and aggregation in esophageal keratinocytes in vitro and in vivo." In: *The Journal of biological chemistry* 278.3 (Jan. 2003), pp. 1824–30. URL: http://www.ncbi.nlm.nih.gov/pubmed/12435727.

[248] Patrick J Medina and Susan Goodin. "Lapatinib: a dual inhibitor of human epidermal growth factor receptor tyrosine kinases." In: *Clinical therapeutics* 30.8 (Aug. 2008), pp. 1426–47. URL: http://www.ncbi.nlm.nih.gov/pubmed/18803986.

[249] Food and Drugs Administration. *TYKERB (lapatinib) tablets*. 2007. URL: https://www.accessdata.fda.gov/drugsatfda_docs/label/2010/022059s007lbl.pdf.

[250] Bernd Tischer et al. "Dermatologic events from EGFR inhibitors: the issue of the missing patient voice." In: *Supportive care in cancer : official journal of the Multinational Association of Supportive Care in Cancer* 25.2 (2017), pp. 651–660. URL: http://www.ncbi.nlm.nih.gov/pubmed/27718067%20http://www.pubmedcentral.nih.gov/articlerender.fcgi?artid=PMC5196015.

[251] G Triadafilopoulos. "Proton pump inhibitors for Barrett's oesophagus." In: *Gut* 46.2 (Feb. 2000), pp. 144–6. URL: http://www.ncbi.nlm.nih.gov/pubmed/10644301%20http://www.pubmedcentral.nih.gov/articlerender.fcgi?artid=PMC1727807.

[252] R E Sampliner et al. "Squamous mucosa overlying columnar epithelium in Barrett's esophagus in the absence of anti-reflux surgery." In: *The American journal of gastroenterology* 83.5 (May 1988), pp. 510–2. URL: http://www.ncbi.nlm.nih.gov/pubmed/3364411.

[253] Nelly E Avissar et al. "Bile acid alone, or in combination with acid, induces CDX2 expression through activation of the epidermal growth factor receptor (EGFR)." In: *Journal of gastrointestinal surgery : official journal of the Society for Surgery of the Alimentary Tract* 13.2 (Feb. 2009), pp. 212–22. URL: http://www.ncbi.nlm.nih.gov/pubmed/18854960.

[254] G J S Jenkins et al. "The bile acid deoxycholic acid (DCA) at neutral pH activates NF-kappaB and induces IL-8 expression in oesophageal cells in vitro." In: *Carcinogenesis* 25.3 (Mar. 2004), pp. 317–23. URL: http://www.ncbi.nlm.nih.gov/pubmed/14656946.

[255] Gareth J S Jenkins et al. "Deoxycholic acid at neutral and acid pH, is genotoxic to oesophageal cells through the induction of ROS: The potential role of anti-oxidants in Barrett's oesophagus." In: *Carcinogenesis* 28.1 (Jan. 2007), pp. 136–42. URL: http://www.ncbi.nlm.nih.gov/pubmed/16905748.

[256] A Piskunov and C Rochette-Egly. "A retinoic acid receptor RARα pool present in membrane lipid rafts forms complexes with G protein αQ to activate p38MAPK." In: *Oncogene* 31.28 (July 2012), pp. 3333–45. URL: http://www.ncbi.nlm.nih.gov/pubmed/22056876.

[257] Lorraine B. Ware and Michael A. Matthay. "Keratinocyte and hepatocyte growth factors in the lung: roles in lung development, inflammation, and repair". In: *American Journal of Physiology-Lung Cellular and Molecular Physiology* 282.5 (May 2002), pp. L924–L940. URL: https://www.physiology.org/doi/10.1152/ajplung.00439.2001.

[258] Sabrina Kellouche et al. "Platelets, thrombospondin-1 and human dermal fibroblasts cooperate for stimulation of endothelial cell tubulogenesis through VEGF and PAI-1 regulation." In: *Experimental cell research* 313.3 (Feb. 2007), pp. 486–99. URL: http://www.ncbi.nlm.nih.gov/pubmed/17126831.

[259] Yasuhiro Fujiwara et al. "Increased expression of transforming growth factor-alpha and epidermal growth factor receptors in rat chronic reflux esophagitis." In: *Journal of gastroenterology and hepatology* 19.5 (May 2004), pp. 521–7. URL: http://www.ncbi.nlm.nih.gov/pubmed/15086595.

[260] R C Fitzgerald et al. "Inflammatory gradient in Barrett's oesophagus: implications for disease complications." In: *Gut* 51.3 (Sept. 2002), pp. 316–22. URL: http://www.ncbi.nlm.nih.gov/pubmed/12171950%20http://www.pubmedcentral.nih.gov/articlerender.fcgi?artid=PMC1773354.

[261] Su Jin Chung et al. "The role of phosphatidylcholine and deoxycholic acid in inflammation." In: *Life sciences* 108.2 (July 2014), pp. 88–93. URL: http://www.ncbi.nlm.nih.gov/pubmed/24880073.

[262] Shengnan Zhao et al. "Deoxycholic Acid Triggers NLRP3 Inflammasome Activation and Aggravates DSS-Induced Colitis in Mice." In: *Frontiers in immunology* 7 (2016), p. 536. URL: http://www.ncbi.nlm.nih.gov/pubmed/27965665%20http://www.pubmedcentral.nih.gov/articlerender.fcgi?artid=PMC5124666.

[263] Katerina Dvorak and Bohuslav Dvorak. "Role of interleukin-6 in Barrett's esophagus pathogenesis." In: *World journal of gastroenterology* 19.15 (Apr. 2013), pp. 2307–12. URL: http://www.ncbi.nlm.nih.gov/pubmed/23613623%20http://www.pubmedcentral.nih.gov/articlerender.fcgi?artid=PMC3631981.

[264] R C Fitzgerald et al. "Diversity in the oesophageal phenotypic response to gastro-oesophageal reflux: immunological determinants." In: *Gut* 50.4 (Apr. 2002), pp. 451–9. URL: http://www.ncbi.nlm.nih.gov/pubmed/11889061%20http://www.pubmedcentral.nih.gov/articlerender.fcgi?artid=PMC1773186.

[265] J M O'Riordan et al. "Proinflammatory cytokine and nuclear factor kappa-B expression along the inflammation-metaplasia-dysplasia-adenocarcinoma sequence in the esophagus." In: *The American journal of gastroenterology* 100.6 (June 2005), pp. 1257–64. URL: http://www.ncbi.nlm.nih.gov/pubmed/15929754.

[266] Christoph Garbers et al. "Interleukin-6: designing specific therapeutics for a complex cytokine." In: *Nature reviews. Drug discovery* 17.6 (2018), pp. 395–412. URL: http://www.ncbi.nlm.nih.gov/pubmed/29725131.

[267] R S Smith et al. "Fibroblasts as sentinel cells. Synthesis of chemokines and regulation of inflammation." In: *The American journal of pathology* 151.2 (Aug. 1997), pp. 317–22. URL: http://www.ncbi.nlm.nih.gov/pubmed/9250144%20http://www.pubmedcentral.nih.gov/articlerender.fcgi?artid=PMC1858004.

[268] Antonio Taddei et al. "Cyclooxygenase-2 and Inflammation Mediators Have a Crucial Role in Reflux-Related Esophageal Histological Changes and Barrett's Esophagus". In: *Digestive Diseases and Sciences* 59.5 (May 2014), pp. 949–957. URL: http://link.springer.com/10.1007/s10620-013-2975-4.

[269] Merja I Auvinen et al. "Incipient angiogenesis in Barrett's epithelium and lymphangiogenesis in Barrett's adenocarcinoma." In: *Journal of clinical oncology : official journal of the American Society of Clinical Oncology* 20.13 (July 2002), pp. 2971–9. URL: http://www.ncbi.nlm.nih.gov/pubmed/12089227.

[270] Anne Eichmann and Michael Simons. "VEGF signaling inside vascular endothelial cells and beyond." In: *Current opinion in cell biology* 24.2 (Apr. 2012), pp. 188–93. URL: http://www.ncbi.nlm.nih.gov/pubmed/22366328%20http://www.pubmedcentral.nih.gov/articlerender.fcgi?artid=PMC4030755.

[271] Uri Ben-David et al. "Genetic and transcriptional evolution alters cancer cell line drug response." In: *Nature* 560.7718 (2018), pp. 325–330. URL: http://www.ncbi.nlm.nih.gov/pubmed/30089904%20http://www.pubmedcentral.nih.gov/articlerender.fcgi?artid=PMC6522222.

[272] Marc van de Wetering et al. "Prospective derivation of a living organoid biobank of colorectal cancer patients." In: *Cell* 161.4 (May 2015), pp. 933–45. URL: http://www.ncbi.nlm.nih.gov/pubmed/25957691%20http://www.pubmedcentral.nih.gov/articlerender.fcgi?artid=PMC6428276.

[273] Charles C Horn et al. "Why can't rodents vomit? A comparative behavioral, anatomical, and physiological study." In: *PloS one* 8.4 (2013), e60537. URL: http://www.ncbi.nlm.nih.gov/pubmed/23593236%20http://www.pubmedcentral.nih.gov/articlerender.fcgi?artid=PMC3622671.

[274] Junhee Seok et al. "Genomic responses in mouse models poorly mimic human inflammatory diseases." In: *Proceedings of the National Academy of Sciences of the United States of America* 110.9 (Feb. 2013), pp. 3507–12. URL: http://www.ncbi.nlm.nih.gov/pubmed/23401516%20http://www.pubmedcentral.nih.gov/articlerender.fcgi?artid=PMC3587220.

[275] Matthias Raggi et al. "Successful evaluation of a new animal model using mice for esophageal adenocarcinoma." In: *Langenbeck's archives of surgery* 395.4 (Apr. 2010), pp. 347–50. URL: http://www.ncbi.nlm.nih.gov/pubmed/20300770.

[276] Fabio Terabe et al. "Columnar Metaplasia in Three Types of Surgical Mouse Models of Esophageal Reflux." In: *Cellular and molecular gastroenterology and hepatology* 4.1 (July 2017), pp. 115–123. URL: http://www.ncbi.nlm.nih.gov/pubmed/28593183%20http://www.pubmedcentral.nih.gov/articlerender.fcgi?artid=PMC5453905.

[277] M Fein et al. "Loss of function of Trp53, but not Apc, leads to the development of esophageal adenocarcinoma in mice with jejunoesophageal reflux." In: *The Journal of surgical research* 83.1 (May 1999), pp. 48–55. URL: http://www.ncbi.nlm.nih.gov/pubmed/10210642.

[278] Jing Hao et al. "Gastroesophageal reflux leads to esophageal cancer in a surgical model with mice." In: *BMC gastroenterology* 9 (July 2009), p. 59. URL: http://www.ncbi.nlm.nih.gov/pubmed/19627616%20http://www.pubmedcentral.nih.gov/articlerender.fcgi?artid=PMC2723127.

[279] E J Glover et al. "Gastroesophageal reflux disease in baboons (Papio sp.): a new animal model." In: *Journal of medical primatology* 37.1 (Feb. 2008), pp. 18–25. URL: http://www.ncbi.nlm.nih.gov/pubmed/18199068.

[280] Harit Kapoor et al. "Animal Models of Barrett's Esophagus and Esophageal Adenocarcinoma-Past, Present, and Future." In: *Clinical and translational science* 8.6 (Dec. 2015), pp. 841–7. URL: http://www.ncbi.nlm.nih.gov/pubmed/26211420%20http://www.pubmedcentral.nih.gov/articlerender.fcgi?artid=PMC4703452.

[281] Steve Perrin. "Preclinical research: Make mouse studies work." In: *Nature* 507.7493 (Mar. 2014), pp. 423–5. URL: http://www.ncbi.nlm.nih.gov/pubmed/24678540.

[282] Anthony King. "The search for better animal models of Alzheimer's disease." In: *Nature* 559.7715 (2018), S13–S15. URL: http://www.ncbi.nlm.nih.gov/pubmed/30046083.

[283] Sara Reardon. "Frustrated Alzheimer's researchers seek better lab mice." In: *Nature* 563.7733 (2018), pp. 611–612. URL: http://www.ncbi.nlm.nih.gov/pubmed/30482928.

[284] Paul McGonigle and Bruce Ruggeri. "Animal models of human disease: challenges in enabling translation." In: *Biochemical pharmacology* 87.1 (Jan. 2014), pp. 162–71. URL: http://www.ncbi.nlm.nih.gov/pubmed/23954708.

[285] www.gov.uk. *Public attitudes to animal testing*. 2014. URL: https://www.gov.uk/government/news/public-attitudes-to-animal-testing.

[286] www.gov.uk. *Animal testing and research: Replacement, Reduction and Refinement*. 2019. URL: https://www.gov.uk/guidance/research-and-testing-using-animals.

[287] Open Targets. *Animal testing and research: Replacement, Reduction and Refinement*. 2019. URL: https://www.opentargets.org/.

[288] Eliah R Shamir and Andrew J Ewald. "Three-dimensional organotypic culture: experimental models of mammalian biology and disease." In: *Nature reviews. Molecular cell biology* 15.10 (Oct. 2014), pp. 647–64. URL: http://www.ncbi.nlm.nih.gov/pubmed/25237826%20http://www.pubmedcentral.nih.gov/articlerender.fcgi?artid=PMC4352326.

[289] Francesco Pampaloni, Emmanuel G Reynaud, and Ernst H K Stelzer. "The third dimension bridges the gap between cell culture and live tissue." In: *Nature reviews. Molecular cell biology* 8.10 (Oct. 2007), pp. 839–45. URL: http://www.ncbi.nlm.nih.gov/pubmed/17684528.

[290] Maddaly Ravi et al. "3D cell culture systems: advantages and applications." In: *Journal of cellular physiology* 230.1 (Jan. 2015), pp. 16–26. URL: http://www.ncbi.nlm.nih.gov/pubmed/24912145.

[291] Dorottya Laczkó et al. "Modeling Esophagitis Using Human Three-Dimensional Organotypic Culture System." In: *The American journal of pathology* 187.8 (Aug. 2017), pp. 1787–1799. URL: http://www.ncbi.nlm.nih.gov/pubmed/28627413%20http://www.pubmedcentral.nih.gov/articlerender.fcgi?artid=PMC5974532.

[292] Chase Taylor et al. "Activin a signaling regulates cell invasion and proliferation in esophageal adenocarcinoma." In: *Oncotarget* 6.33 (Oct. 2015), pp. 34228–44. URL: http://www.ncbi.nlm.nih.gov/pubmed/26447543%20http://www.pubmedcentral.nih.gov/articlerender.fcgi?artid=PMC4741448.

[293] Yusuke Yamamoto et al. "Mutational spectrum of Barrett's stem cells suggests paths to initiation of a precancerous lesion." In: *Nature communications* 7 (Jan. 2016), p. 10380. URL: http://www.ncbi.nlm.nih.gov/pubmed/26783136%20http://www.pubmedcentral.nih.gov/articlerender.fcgi?artid=PMC4735693.

[294] Khvaramze Shaverdashvili et al. "KLF4 activates NFκB signaling and esophageal epithelial inflammation via the Rho-related GTP-binding protein RHOF." In: *PloS one* 14.4 (2019), e0215746. URL: http://www.ncbi.nlm.nih.gov/pubmed/30998758%20http://www.pubmedcentral.nih.gov/articlerender.fcgi?artid=PMC6472825.

[295] Qiuyang Zhang et al. "Acidic Bile Salts Induce Epithelial to Mesenchymal Transition via VEGF Signaling in Non-Neoplastic Barrett's Cells." In: *Gastroenterology* 156.1 (2019), 130–144.e10. URL: http://www.ncbi.nlm.nih.gov/pubmed/30268789%20http://www.pubmedcentral.nih.gov/articlerender.fcgi?artid=PMC6309503.

[296] George Boguslawski et al. "SU1498, an inhibitor of vascular endothelial growth factor receptor 2, causes accumulation of phosphorylated ERK kinases and inhibits their activity in vivo and in vitro." In: *The Journal of biological chemistry* 279.7 (Feb. 2004), pp. 5716–24. URL: http://www.ncbi.nlm.nih.gov/pubmed/14625306.

[297] Zhangjian Zhou et al. "Activation of EGFR-DNA-PKcs pathway by IGFBP2 protects esophageal adenocarcinoma cells from acidic bile salts-induced DNA damage." In: *Journal of experimental & clinical cancer research : CR* 38.1 (Jan. 2019), p. 13. URL: http://www.ncbi.nlm.nih.gov/pubmed/30626422%20http://www.pubmedcentral.nih.gov/articlerender.fcgi?artid=PMC6327430.

[298] Toshiro Sato et al. "Single Lgr5 stem cells build crypt-villus structures in vitro without a mesenchymal niche." In: *Nature* 459.7244 (May 2009), pp. 262–5. URL: http://www.ncbi.nlm.nih.gov/pubmed/19329995.

[299] Toshiro Sato et al. "Long-term expansion of epithelial organoids from human colon, adenoma, adenocarcinoma, and Barrett's epithelium." In: *Gastroenterology* 141.5 (Nov. 2011), pp. 1762–72. URL: http://www.ncbi.nlm.nih.gov/pubmed/21889923.

[300] Youngtae Jeong et al. "Identification and genetic manipulation of human and mouse oesophageal stem cells." In: *Gut* 65.7 (2016), pp. 1077–86. URL: http://www.ncbi.nlm.nih.gov/pubmed/25897018.

[301] Stephen L Trisno et al. "Esophageal Organoids from Human Pluripotent Stem Cells Delineate Sox2 Functions during Esophageal Specification." In: *Cell stem cell* 23.4 (2018), 501–515.e7. URL: http://www.ncbi.nlm.nih.gov/pubmed/30244869%20http://www.pubmedcentral.nih.gov/articlerender.fcgi?artid=PMC6225525.

[302] Sarah P Short, Patricia W Costacurta, and Christopher S Williams. "Using 3D Organoid Cultures to Model Intestinal Physiology and Colorectal Cancer." In: *Current colorectal cancer reports* 13.3 (June 2017), pp. 183–191. URL: http://www.ncbi.nlm.nih.gov/pubmed/29276469%20http://www.pubmedcentral.nih.gov/articlerender.fcgi?artid=PMC5736147.

[303] Sina Bartfeld et al. "In vitro expansion of human gastric epithelial stem cells and their responses to bacterial infection." In: *Gastroenterology* 148.1 (Jan. 2015), 126–136.e6. URL: http://www.ncbi.nlm.nih.gov/pubmed/25307862%20http://www.pubmedcentral.nih.gov/articlerender.fcgi?artid=PMC4274199.

[304] S S Wilson et al. "A small intestinal organoid model of non-invasive enteric pathogen-epithelial cell interactions." In: *Mucosal immunology* 8.2 (Mar. 2015), pp. 352–61. URL: http://www.ncbi.nlm.nih.gov/pubmed/25118165%20http://www.pubmedcentral.nih.gov/articlerender.fcgi?artid=PMC4326599.

[305] Julia Y Co et al. "Controlling Epithelial Polarity: A Human Enteroid Model for Host-Pathogen Interactions." In: *Cell reports* 26.9 (2019), 2509–2520.e4. URL: http://www.ncbi.nlm.nih.gov/pubmed/30811997%20http://www.pubmedcentral.nih.gov/articlerender.fcgi?artid=PMC6391775.

[306] Katherine W Rogers and Alexander F Schier. "Morphogen gradients: from generation to interpretation." In: *Annual review of cell and developmental biology* 27 (2011), pp. 377–407. URL: http://www.ncbi.nlm.nih.gov/pubmed/21801015.

[307] Caroline A Lindemans et al. "Interleukin-22 promotes intestinal-stem-cell-mediated epithelial regeneration." In: *Nature* 528.7583 (Dec. 2015), pp. 560–564. URL: http://www.ncbi.nlm.nih.gov/pubmed/26649819%20http://www.pubmedcentral.nih.gov/articlerender.fcgi?artid=PMC4720437.

[308] Krijn K Dijkstra et al. "Generation of Tumor-Reactive T Cells by Co-culture of Peripheral Blood Lymphocytes and Tumor Organoids." In: *Cell* 174.6 (2018), 1586–1598.e12. URL: http://www.ncbi.nlm.nih.gov/pubmed/30100188%20http://www.pubmedcentral.nih.gov/articlerender.fcgi?artid=PMC6558289.

[309] Jayati Chakrabarti et al. "Mouse-Derived Gastric Organoid and Immune Cell Co-culture for the Study of the Tumor Microenvironment." In: *Methods in molecular biology (Clifton, N.J.)* 1817 (2018), pp. 157–168. URL: http://www.ncbi.nlm.nih.gov/pubmed/29959712.

[310] Vicki Plaks et al. "Adaptive Immune Regulation of Mammary Postnatal Organogenesis." In: *Developmental cell* 34.5 (Sept. 2015), pp. 493–504. URL: http://www.ncbi.nlm.nih.gov/pubmed/26321127%20http://www.pubmedcentral.nih.gov/articlerender.fcgi?artid=PMC4573906.

[311] Agnieszka Pastuła et al. "Three-Dimensional Gastrointestinal Organoid Culture in Combination with Nerves or Fibroblasts: A Method to Characterize the Gastrointestinal Stem Cell Niche." In: *Stem cells international* 2016 (2016), p. 3710836. URL: http://www.ncbi.nlm.nih.gov/pubmed/26697073%20http://www.pubmedcentral.nih.gov/articlerender.fcgi?artid=PMC4677245.

[312] Michael J Workman et al. "Engineered human pluripotent-stem-cell-derived intestinal tissues with a functional enteric nervous system." In: *Nature medicine* 23.1 (2017), pp. 49–59. URL: http://www.ncbi.nlm.nih.gov/pubmed/27869805%20http://www.pubmedcentral.nih.gov/articlerender.fcgi?artid=PMC5562951.

[313] Giuseppe Pettinato et al. "Generation of fully functional hepatocyte-like organoids from human induced pluripotent stem cells mixed with Endothelial Cells." In: *Scientific reports* 9.1 (June 2019), p. 8920. URL: http://www.ncbi.nlm.nih.gov/pubmed/31222080%20http://www.pubmedcentral.nih.gov/articlerender.fcgi?artid=PMC6586904.

[314] Kimberly A Homan et al. "Flow-enhanced vascularization and maturation of kidney organoids in vitro." In: *Nature methods* 16.3 (2019), pp. 255–262. URL: http://www.ncbi.nlm.nih.gov/pubmed/30742039%20http://www.pubmedcentral.nih.gov/articlerender.fcgi?artid=PMC6488032.

[315] Takahito Katano et al. "Establishment of a long-term three-dimensional primary culture of mouse glandular stomach epithelial cells within the stem cell niche." In: *Biochemical and biophysical research communications* 432.4 (Mar. 2013), pp. 558–63. URL: http://www.ncbi.nlm.nih.gov/pubmed/23485463.

[316] Xingnan Li et al. "Oncogenic transformation of diverse gastrointestinal tissues in primary organoid culture." In: *Nature medicine* 20.7 (July 2014), pp. 769–77. URL: http://www.ncbi.nlm.nih.gov/pubmed/24859528%20http://www.pubmedcentral.nih.gov/articlerender.fcgi?artid=PMC4087144.

[317] Gaelle Noel et al. "A primary human macrophage-enteroid co-culture model to investigate mucosal gut physiology and host-pathogen interactions." In: *Scientific reports* 7 (2017), p. 45270. URL: http://www.ncbi.nlm.nih.gov/pubmed/28345602%20http://www.pubmedcentral.nih.gov/articlerender.fcgi?artid=PMC5366908.

[318] Francesco Boccellato et al. "Polarised epithelial monolayers of the gastric mucosa reveal insights into mucosal homeostasis and defence against infection." In: *Gut* (Feb. 2018). URL: http://www.ncbi.nlm.nih.gov/pubmed/29467166%20http://www.pubmedcentral.nih.gov/articlerender.fcgi?artid=PMC6580761.

[319] Takanori Takebe, Boyang Zhang, and Milica Radisic. "Synergistic Engineering: Organoids Meet Organs-on-a-Chip." In: *Cell stem cell* 21.3 (2017), pp. 297–300. URL: http://www.ncbi.nlm.nih.gov/pubmed/28886364.

[320] Sunghee Estelle Park, Andrei Georgescu, and Dongeun Huh. "Organoids-on-a-chip." In: *Science (New York, N.Y.)* 364.6444 (2019), pp. 960–965. URL: http://www.ncbi.nlm.nih.gov/pubmed/31171693.

[321] Dongeun Huh et al. "Reconstituting organ-level lung functions on a chip." In: *Science (New York, N.Y.)* 328.5986 (June 2010), pp. 1662–8. URL: http://www.ncbi.nlm.nih.gov/pubmed/20576885.

[322] Magdalena Kasendra et al. "Development of a primary human Small Intestine-on-a-Chip using biopsy-derived organoids." In: *Scientific reports* 8.1 (2018), p. 2871. URL: http://www.ncbi.nlm.nih.gov/pubmed/29440725%20http://www.pubmedcentral.nih.gov/articlerender.fcgi?artid=PMC5811607.

[323] G M Whitesides et al. "Soft lithography in biology and biochemistry." In: *Annual review of biomedical engineering* 3 (2001), pp. 335–73. URL: http://www.ncbi.nlm.nih.gov/pubmed/11447067.

[324] Younan Xia and George M Whitesides. "Soft Lithography." In: *Angewandte Chemie (International ed. in English)* 37.5 (Mar. 1998), pp. 550–575. URL: http://www.ncbi.nlm.nih.gov/pubmed/29711088.

[325] Yuli Wang et al. "A microengineered collagen scaffold for generating a polarized crypt-villus architecture of human small intestinal epithelium." In: *Biomaterials* 128 (2017), pp. 44–55. URL: http://www.ncbi.nlm.nih.gov/pubmed/28288348%20http://www.pubmedcentral.nih.gov/articlerender.fcgi?artid=PMC5392043.

[326] Yuli Wang et al. "Formation of Human Colonic Crypt Array by Application of Chemical Gradients Across a Shaped Epithelial Monolayer." In: *Cellular and molecular gastroenterology and hepatology* 5.2 (2018), pp. 113–130. URL: http://www.ncbi.nlm.nih.gov/pubmed/29693040%20http://www.pubmedcentral.nih.gov/articlerender.fcgi?artid=PMC5904049.

[327] Shinya Sugimoto et al. "Reconstruction of the Human Colon Epithelium In Vivo." In: *Cell stem cell* 22.2 (2018), 171–176.e5. URL: http://www.ncbi.nlm.nih.gov/pubmed/29290616.

[328] Alyssa J Miller et al. "In Vitro Induction and In Vivo Engraftment of Lung Bud Tip Progenitor Cells Derived from Human Pluripotent Stem Cells." In: *Stem cell reports* 10.1 (2018), pp. 101–119. URL: http://www.ncbi.nlm.nih.gov/pubmed/29249664%20http://www.pubmedcentral.nih.gov/articlerender.fcgi?artid=PMC5770275.

[329] Margit Bleijs et al. "Xenograft and organoid model systems in cancer research." In: *The EMBO journal* 38.15 (2019), e101654. URL: http://www.ncbi.nlm.nih.gov/pubmed/31282586%20http://www.pubmedcentral.nih.gov/articlerender.fcgi?artid=PMC6670015.

[330] Paula G Miller and Michael L Shuler. "Design and demonstration of a pumpless 14 compartment microphysiological system." In: *Biotechnology and bioengineering* 113.10 (2016), pp. 2213–27. URL: http://www.ncbi.nlm.nih.gov/pubmed/27070809.

[331] Boyang Zhang et al. "Advances in organ-on-a-chip engineering". In: *Nature Reviews Materials* 3.8 (Aug. 2018), pp. 257–278. URL: http://www.nature.com/articles/s41578-018-0034-7.

[332] *emulatebio*. 2019. URL: www.emulatebio.com.

[333] Joshua A Bagley et al. "Fused cerebral organoids model interactions between brain regions." In: *Nature methods* 14.7 (July 2017), pp. 743–751. URL: http://www.ncbi.nlm.nih.gov/pubmed/28504681%20http://www.pubmedcentral.nih.gov/articlerender.fcgi?artid=PMC5540177.

[334] Fikri Birey et al. "Assembly of functionally integrated human forebrain spheroids." In: *Nature* 545.7652 (2017), pp. 54–59. URL: http://www.ncbi.nlm.nih.gov/pubmed/28445465%20http://www.pubmedcentral.nih.gov/articlerender.fcgi?artid=PMC5805137.

[335] Hiroyuki Koike et al. "Modelling human hepato-biliary-pancreatic organogenesis from the foregut-midgut boundary." In: *Nature* 574.7776 (2019), pp. 112–116. URL: http://www.ncbi.nlm.nih.gov/pubmed/31554966.

[336] Fernando Martin-Belmonte and Mirna Perez-Moreno. "Epithelial cell polarity, stem cells and cancer." In: *Nature reviews. Cancer* 12.1 (Dec. 2011), pp. 23–38. URL: http://www.ncbi.nlm.nih.gov/pubmed/22169974.

[337] Lorenzo Moroni et al. "Biofabrication strategies for 3D in vitro models and regenerative medicine." In: *Nature reviews. Materials* 3.5 (May 2018), pp. 21–37. URL: http://www.ncbi.nlm.nih.gov/pubmed/31223488%20http://www.pubmedcentral.nih.gov/articlerender.fcgi?artid=PMC6586020.

[338] Tyler K Merceron et al. "A 3D bioprinted complex structure for engineering the muscle-tendon unit." In: *Biofabrication* 7.3 (June 2015), p. 035003. URL: http://www.ncbi.nlm.nih.gov/pubmed/26081669.

[339] Thomas J Hinton et al. "Three-dimensional printing of complex biological structures by freeform reversible embedding of suspended hydrogels." In: *Science advances* 1.9 (Oct. 2015), e1500758. URL: http://www.ncbi.nlm.nih.gov/pubmed/26601312%20http://www.pubmedcentral.nih.gov/articlerender.fcgi?artid=PMC4646826.

[340] Daejin Min et al. "Bioprinting of biomimetic skin containing melanocytes." In: *Experimental dermatology* 27.5 (2018), pp. 453–459. URL: http://www.ncbi.nlm.nih.gov/pubmed/28453913.

[341] NASA. *Three-dimensional Bioprinting in Space*. 2019. URL: https://www.nasa.gov/mission_pages/station/research/news/b4h-3rd/it-3d-bioprinting-in-space/.

[342] Vladimir Mironov et al. "Organ printing: tissue spheroids as building blocks." In: *Biomaterials* 30.12 (Apr. 2009), pp. 2164–74. URL: http://www.ncbi.nlm.nih.gov/pubmed/19176247%20http://www.pubmedcentral.nih.gov/articlerender.fcgi?artid=PMC3773699.

[343] Nupura S Bhise et al. "A liver-on-a-chip platform with bioprinted hepatic spheroids." In: *Biofabrication* 8.1 (Jan. 2016), p. 014101. URL: http://www.ncbi.nlm.nih.gov/pubmed/26756674.

[344] Michael J. Kratochvil et al. "Engineered materials for organoid systems". In: *Nature Reviews Materials* 4.9 (Sept. 2019), pp. 606–622. URL: http://www.nature.com/articles/s41578-019-0129-9.

[345] Mark A Skylar-Scott et al. "Biomanufacturing of organ-specific tissues with high cellular density and embedded vascular channels." In: *Science advances* 5.9 (2019), eaaw2459. URL: http://www.ncbi.nlm.nih.gov/pubmed/31523707%20http://www.pubmedcentral.nih.gov/articlerender.fcgi?artid=PMC6731072.

[346] Norman Sachs et al. "Intestinal epithelial organoids fuse to form self-organizing tubes in floating collagen gels." In: *Development (Cambridge, England)* 144.6 (2017), pp. 1107–1112. URL: http://www.ncbi.nlm.nih.gov/pubmed/28292848.

[347] John A Reid et al. In: *Scientific reports* 1 (May 2019), p. 7466.

[348] John A Reid et al. "Consistent and reproducible cultures of large-scale 3D mammary epithelial structures using an accessible bioprinting platform." In: *Breast cancer research : BCR* 20.1 (2018), p. 122. URL: http://www.ncbi.nlm.nih.gov/pubmed/30305139%20http://www.pubmedcentral.nih.gov/articlerender.fcgi?artid=PMC6180647.

[349] Hagan Bayley et al. “Droplet interface bilayers.” In: *Molecular bioSystems* 4.12 (Dec. 2008), pp. 1191–208. URL: http://www.ncbi.nlm.nih.gov/pubmed/19396383%20http://www.pubmedcentral.nih.gov/articlerender.fcgi?artid=PMC2763081.

[350] Gabriel Villar, Alexander D Graham, and Hagan Bayley. “A tissue-like printed material.” In: *Science (New York, N.Y.)* 340.6128 (Apr. 2013), pp. 48–52. URL: http://www.ncbi.nlm.nih.gov/pubmed/23559243%20http://www.pubmedcentral.nih.gov/articlerender.fcgi?artid=PMC3750497.

[351] Xiaoying Zhang and Yangde Zhang. “Tissue Engineering Applications of Three-Dimensional Bioprinting.” In: *Cell biochemistry and biophysics* 72.3 (July 2015), pp. 777–82. URL: http://www.ncbi.nlm.nih.gov/pubmed/25663505.

[352] Robert T. Abraham and Arthur Weiss. “Jurkat T cells and development of the T-cell receptor signalling paradigm”. In: *Nature Reviews Immunology* 4.4 (Apr. 2004), pp. 301–308. URL: http://www.nature.com/articles/nri1330.

[353] AMBIO. *Reinnervate Perfusion Plate Dynamic Circulation and Perfusion of Culture Medium Within a Multi-welled Plate*. 2019. URL: http://www.amsbio.com/brochures/Perfusion-AppNote-9.pdf.

[354] Nicolas Broguiere et al. “Growth of Epithelial Organoids in a Defined Hydrogel”. In: *Advanced Materials* 30.43 (Oct. 2018), p. 1801621. URL: http://doi.wiley.com/10.1002/adma.201801621.

[355] E Gentleman et al. “Short collagen fibers provide control of contraction and permeability in fibroblast-seeded collagen gels.” In: *Tissue engineering* 10.3-4 (), pp. 421–7. URL: http://www.ncbi.nlm.nih.gov/pubmed/15165459.

[356] Jacob Bear. “Dynamics of Fluids in Porous Media”. In: *Soil Science* 120.2 (Aug. 1975), pp. 162–163. URL: https://insights.ovid.com/crossref?an=00010694-197508000-00022.

[357] M Pruniéras, M Régnier, and D Woodley. “Methods for cultivation of keratinocytes with an air-liquid interface.” In: *The Journal of investigative dermatology* 81.1 Suppl (July 1983), 28s–33s. URL: http://www.ncbi.nlm.nih.gov/pubmed/6190962.

[358] B L Weusten et al. “Spatiotemporal characteristics of physiological gastroesophageal reflux.” In: *The American journal of physiology* 266.3 Pt 1 (Mar. 1994), G357–62. URL: http://www.ncbi.nlm.nih.gov/pubmed/8166276.

[359] Masahiro Asaka et al. “What Role Does Helicobacter pylori Play in Gastric Cancer?” In: *Gastroenterology* 113.6 (Dec. 1997), S56–S60. URL: https://doi.org/10.1016/S0016-5085(97)80013-3.

[360] Ludovico Buti et al. “CagAâ€“ASPP2 complex mediates loss of cell polarity and favors H. Pylori colonization of human gastric organoids”. In: *Proceedings of the National Academy of Sciences of the United States of America* (2020).

[361] Thorsten Doede et al. “Unsuccessful alloplastic esophageal replacement with porcine small intestinal submucosa.” In: *Artificial organs* 33.4 (Apr. 2009), pp. 328–33. URL: http://www.ncbi.nlm.nih.gov/pubmed/19335409.

[362] John W Briel et al. "Prevalence and risk factors for ischemia, leak, and stricture of esophageal anastomosis: gastric pull-up versus colon interposition." In: *Journal of the American College of Surgeons* 198.4 (Apr. 2004), 536–41, discussion 541–2. URL: http://www.ncbi.nlm.nih.gov/pubmed/15051003.

[363] Aazam Dabirian et al. "Quality of life in ostomy patients: a qualitative study." In: *Patient preference and adherence* 5 (Dec. 2010), pp. 1–5. URL: http://www.ncbi.nlm.nih.gov/pubmed/21311696%20http://www.pubmedcentral.nih.gov/articlerender.fcgi?artid=PMC3034300.

[364] Stephen F Badylak et al. "Esophageal preservation in five male patients after endoscopic inner-layer circumferential resection in the setting of superficial cancer: a regenerative medicine approach with a biologic scaffold." In: *Tissue engineering. Part A* 17.11-12 (June 2011), pp. 1643–50. URL: http://www.ncbi.nlm.nih.gov/pubmed/21306292%20http://www.pubmedcentral.nih.gov/articlerender.fcgi?artid=PMC3098955.

[365] Alejandro Nieponice et al. "Patch esophagoplasty: esophageal reconstruction using biologic scaffolds." In: *The Annals of thoracic surgery* 97.1 (Jan. 2014), pp. 283–8. URL: http://www.ncbi.nlm.nih.gov/pubmed/24266951.

[366] Takeshi Ohki et al. "Prevention of esophageal stricture after endoscopic submucosal dissection using tissue-engineered cell sheets." In: *Gastroenterology* 143.3 (Sept. 2012), 582–588.e2. URL: http://www.ncbi.nlm.nih.gov/pubmed/22561054.

[367] Mahboubeh Jafarkhani et al. "Bioprinting in Vascularization Strategies". In: *Iranian biomedical journal* 23.1 (2019), pp. 9–20. URL: http://www.ncbi.nlm.nih.gov/pubmed/30458600%20http://www.pubmedcentral.nih.gov/articlerender.fcgi?artid=PMC6305822.

[368] Khalil N Bitar and Elie Zakhem. "Bioengineering the gut: future prospects of regenerative medicine." In: *Nature reviews. Gastroenterology & hepatology* 13.9 (2016), pp. 543–56. URL: http://www.ncbi.nlm.nih.gov/pubmed/27507104.

[369] Miltenyi Biotec. *Dead cell removal kit*. 2020. URL: https://www.miltenyibiotec.com/ES-en/products/macs-sample-preparation/removal-reagents/dead-cell-removal-kit.html#130-090-101.

[370] Cyrille Norotte et al. "Scaffold-free vascular tissue engineering using bioprinting." In: *Biomaterials* 30.30 (Oct. 2009), pp. 5910–7. URL: http://www.ncbi.nlm.nih.gov/pubmed/19664819%20http://www.pubmedcentral.nih.gov/articlerender.fcgi?artid=PMC2748110.

[371] Cecilia Ximenez and Javier Torres. "Development of Microbiota in Infants and its Role in Maturation of Gut Mucosa and Immune System." In: *Archives of medical research* 48.8 (2017), pp. 666–680. URL: http://www.ncbi.nlm.nih.gov/pubmed/29198451.

[372] Daniel Sprockett, Tadashi Fukami, and David A Relman. "Role of priority effects in the early-life assembly of the gut microbiota." In: *Nature reviews. Gastroenterology & hepatology* 15.4 (2018), pp. 197–205. URL: http://www.ncbi.nlm.nih.gov/pubmed/29362469%20http://www.pubmedcentral.nih.gov/articlerender.fcgi?artid=PMC6813786.

[373] Herbert Tilg et al. "The Intestinal Microbiota in Colorectal Cancer." In: *Cancer cell* 33.6 (2018), pp. 954–964. URL: http://www.ncbi.nlm.nih.gov/pubmed/29657127.

[374] Rui M Ferreira et al. "Gastric microbial community profiling reveals a dysbiotic cancer-associated microbiota." In: *Gut* 67.2 (2018), pp. 226–236. URL: http://www.ncbi.nlm.nih.gov/pubmed/29102920%20http://www.pubmedcentral.nih.gov/articlerender.fcgi?artid=PMC5868293.

[375] Allison Cabinian et al. "Gut symbiotic microbes imprint intestinal immune cells with the innate receptor SLAMF4 which contributes to gut immune protection against enteric pathogens." In: *Gut* 67.5 (2018), pp. 847–859. URL: http://www.ncbi.nlm.nih.gov/pubmed/28341747%20http://www.pubmedcentral.nih.gov/articlerender.fcgi?artid=PMC5890651.

[376] Julian R Marchesi et al. "The gut microbiota and host health: a new clinical frontier." In: *Gut* 65.2 (Feb. 2016), pp. 330–9. URL: http://www.ncbi.nlm.nih.gov/pubmed/26338727%20http://www.pubmedcentral.nih.gov/articlerender.fcgi?artid=PMC4752653.

[377] Ting-Ting Huang et al. "Current Understanding of Gut Microbiota in Mood Disorders: An Update of Human Studies." In: *Frontiers in genetics* 10 (2019), p. 98. URL: http://www.ncbi.nlm.nih.gov/pubmed/30838027%20http://www.pubmedcentral.nih.gov/articlerender.fcgi?artid=PMC6389720.

[378] Jeremy Appleton. "The Gut-Brain Axis: Influence of Microbiota on Mood and Mental Health." In: *Integrative medicine (Encinitas, Calif.)* 17.4 (Aug. 2018), pp. 28–32. URL: http://www.ncbi.nlm.nih.gov/pubmed/31043907%20http://www.pubmedcentral.nih.gov/articlerender.fcgi?artid=PMC6469458.

[379] Mireia Valles-Colomer et al. "The neuroactive potential of the human gut microbiota in quality of life and depression". In: *Nature Microbiology* 4.4 (Apr. 2019), pp. 623–632. URL: http://www.nature.com/articles/s41564-018-0337-x.

[380] Marie-Claire Arrieta, Jens Walter, and B Brett Finlay. "Human Microbiota-Associated Mice: A Model with Challenges." In: *Cell host & microbe* 19.5 (May 2016), pp. 575–8. URL: http://www.ncbi.nlm.nih.gov/pubmed/27173924.

[381] Devanjali Dutta and Hans Clevers. "Organoid culture systems to study host-pathogen interactions." In: *Current opinion in immunology* 48 (Oct. 2017), pp. 15–22. URL: http://www.ncbi.nlm.nih.gov/pubmed/28756233.

[382] Mehdi Sadaghian Sadabad et al. "A simple coculture system shows mutualism between anaerobic faecalibacteria and epithelial Caco-2 cells." In: *Scientific reports* 5 (Dec. 2015), p. 17906. URL: http://www.ncbi.nlm.nih.gov/pubmed/26667159%20http://www.pubmedcentral.nih.gov/articlerender.fcgi?artid=PMC4678368.

[383] Manuela Teresa Raimondi, Diego Albani, and Carmen Giordano. "An Organ-On-A-Chip Engineered Platform to Study the Microbiota-Gut-Brain Axis in Neurodegeneration." In: *Trends in molecular medicine* 25.9 (Sept. 2019), pp. 737–740. URL: http://www.ncbi.nlm.nih.gov/pubmed/31422037.

[384] Hyeongsun Moon et al. "Krt5+/Krt15+ foregut basal progenitors give rise to cyclooxygenase-2-dependent tumours in response to gastric acid stress." In: *Nature communications* 10.1 (2019), p. 2225. URL: http://www.ncbi.nlm.nih.gov/pubmed/31110179%20http://www.pubmedcentral.nih.gov/articlerender.fcgi?artid=PMC6527614.

[385] Alexandra Lind et al. "The immune cell composition in Barrett's metaplastic tissue resembles that in normal duodenal tissue." In: *PloS one* 7.4 (2012), e33899. URL: http://www.ncbi.nlm.nih.gov/pubmed/22509265%20http://www.pubmedcentral.nih.gov/articlerender.fcgi?artid=PMC3317926.

[386] Alexandra Lind et al. "The Microenvironment in Barrett's Esophagus Tissue Is Characterized by High FOXP3 and RALDH2 Levels." In: *Frontiers in immunology* 9 (2018), p. 1375. URL: http://www.ncbi.nlm.nih.gov/pubmed/29967615%20http://www.pubmedcentral.nih.gov/articlerender.fcgi?artid=PMC6015910.

[387] Fergus Noble et al. "Tumour infiltrating lymphocytes correlate with improved survival in patients with oesophageal adenocarcinoma." In: *Cancer immunology, immunotherapy : CII* 65.6 (2016), pp. 651–62. URL: http://www.ncbi.nlm.nih.gov/pubmed/27020682%20http://www.pubmedcentral.nih.gov/articlerender.fcgi?artid=PMC4880639.

[388] Alexandra V Stein et al. "High intratumoural but not peritumoural inflammatory host response is associated with better prognosis in primary resected oesophageal adenocarcinomas." In: *Pathology* 49.1 (Jan. 2017), pp. 30–37. URL: http://www.ncbi.nlm.nih.gov/pubmed/27916317.

[389] Alberto Mantovani et al. "Tumour-associated macrophages as treatment targets in oncology." In: *Nature reviews. Clinical oncology* 14.7 (July 2017), pp. 399–416. URL: http://www.ncbi.nlm.nih.gov/pubmed/28117416%20http://www.pubmedcentral.nih.gov/articlerender.fcgi?artid=PMC5480600.

[390] Amir Sharabi et al. "Regulatory T cells in the treatment of disease." In: *Nature reviews. Drug discovery* 17.11 (2018), pp. 823–844. URL: http://www.ncbi.nlm.nih.gov/pubmed/30310234.

[391] Gianmarco Contino et al. "The Evolving Genomic Landscape of Barrett's Esophagus and Esophageal Adenocarcinoma". In: *Gastroenterology* 153.3 (Sept. 2017), 657–673.e1. URL: https://linkinghub.elsevier.com/retrieve/pii/S0016508517359085.

[392] Alice L Givan. "Flow cytometry: an introduction." In: *Methods in molecular biology (Clifton, N.J.)* 699 (2011), pp. 1–29. URL: http://www.ncbi.nlm.nih.gov/pubmed/21116976.

[393] B Schmitz et al. "Magnetic activated cell sorting (MACS)–a new immunomagnetic method for megakaryocytic cell isolation: comparison of different separation techniques." In: *European journal of haematology* 52.5 (May 1994), pp. 267–75. URL: http://www.ncbi.nlm.nih.gov/pubmed/8020626.

[394] Matthew H Spitzer and Garry P Nolan. "Mass Cytometry: Single Cells, Many Features." In: *Cell* 165.4 (May 2016), pp. 780–91. URL: http://www.ncbi.nlm.nih.gov/pubmed/27153492%20http://www.pubmedcentral.nih.gov/articlerender.fcgi?artid=PMC4860251.

[395] Byungjin Hwang, Ji Hyun Lee, and Duhee Bang. "Single-cell RNA sequencing technologies and bioinformatics pipelines". In: *Experimental & Molecular Medicine* 50.8 (Aug. 2018), p. 96. URL: http://www.nature.com/articles/s12276-018-0071-8.

[396] Aleksandra A. Kolodziejczyk et al. "The Technology and Biology of Single-Cell RNA Sequencing". In: *Molecular Cell* 58.4 (May 2015), pp. 610–620. URL: https://linkinghub.elsevier.com/retrieve/pii/S1097276515002610.

[397] Byungjin Hwang, Ji Hyun Lee, and Duhee Bang. "Single-cell RNA sequencing technologies and bioinformatics pipelines." In: *Experimental & molecular medicine* 50.8 (2018), p. 96. URL: http://www.ncbi.nlm.nih.gov/pubmed/30089861%20http://www.pubmedcentral.nih.gov/articlerender.fcgi?artid=PMC6082860.

[398] Aaron M Newman et al. "Robust enumeration of cell subsets from tissue expression profiles." In: *Nature methods* 12.5 (May 2015), pp. 453–7. URL: http://www.ncbi.nlm.nih.gov/pubmed/25822800%20http://www.pubmedcentral.nih.gov/articlerender.fcgi?artid=PMC4739640.

[399] Binbin Chen et al. "Profiling Tumor Infiltrating Immune Cells with CIBERSORT." In: *Methods in molecular biology (Clifton, N.J.)* 1711 (2018), pp. 243–259. URL: http://www.ncbi.nlm.nih.gov/pubmed/29344893%20http://www.pubmedcentral.nih.gov/articlerender.fcgi?artid=PMC5895181.

[400] Maayan Baron et al. "A Single-Cell Transcriptomic Map of the Human and Mouse Pancreas Reveals Inter- and Intra-cell Population Structure." In: *Cell systems* 3.4 (2016), 346–360.e4. URL: http://www.ncbi.nlm.nih.gov/pubmed/27667365%20http://www.pubmedcentral.nih.gov/articlerender.fcgi?artid=PMC5228327.

[401] Xuran Wang et al. "Bulk tissue cell type deconvolution with multi-subject single-cell expression reference." In: *Nature communications* 10.1 (2019), p. 380. URL: http://www.ncbi.nlm.nih.gov/pubmed/30670690%20http://www.pubmedcentral.nih.gov/articlerender.fcgi?artid=PMC6342984.

[402] Samuel G Rodriques et al. "Slide-seq: A scalable technology for measuring genome-wide expression at high spatial resolution." In: *Science (New York, N.Y.)* 363.6434 (2019), pp. 1463–1467. URL: http://www.ncbi.nlm.nih.gov/pubmed/30923225%20http://www.pubmedcentral.nih.gov/articlerender.fcgi?artid=PMC6927209.

[403] Peggi M Angel et al. "Advances in MALDI imaging mass spectrometry of proteins in cardiac tissue, including the heart valve." In: *Biochimica et biophysica acta. Proteins and proteomics* 1865.7 (July 2017), pp. 927–935. URL: http://www.ncbi.nlm.nih.gov/pubmed/28341601%20http://www.pubmedcentral.nih.gov/articlerender.fcgi?artid=PMC5527275.

[404] Michaela Aichler and Axel Walch. "MALDI Imaging mass spectrometry: current frontiers and perspectives in pathology research and practice." In: *Laboratory investigation; a journal of technical methods and pathology* 95.4 (Apr. 2015), pp. 422–31. URL: http://www.ncbi.nlm.nih.gov/pubmed/25621874.

[405] Eric J Yang et al. "Microanatomy of the cervical and anorectal squamocolumnar junctions: a proposed model for anatomical differences in HPV-related cancer risk". In: *Modern Pathology* 28.7 (July 2015), pp. 994–1000. URL: http://www.nature.com/articles/modpathol201554.

[406] Isabella Wimmer et al. "Systematic evaluation of RNA quality, microarray data reliability and pathway analysis in fresh, fresh frozen and formalin-fixed paraffin-embedded tissue samples". In: *Scientific Reports* 8.1 (Dec. 2018), p. 6351. URL: http://www.nature.com/articles/s41598-018-24781-6.

[407] André M N Silva et al. "Post-translational modifications and mass spectrometry detection." In: *Free radical biology & medicine* 65 (Dec. 2013), pp. 925–941. URL: http://www.ncbi.nlm.nih.gov/pubmed/24002012.

[408] E W Lin et al. "The tumor microenvironment in esophageal cancer." In: *Oncogene* 35.41 (2016), pp. 5337–5349. URL: http://www.ncbi.nlm.nih.gov/pubmed/26923327%20http://www.pubmedcentral.nih.gov/articlerender.fcgi?artid=PMC5003768.

[409] Abel Jacobus Bronkhorst, Vida Ungerer, and Stefan Holdenrieder. "The emerging role of cell-free DNA as a molecular marker for cancer management". In: *Biomolecular Detection and Quantification* 17 (Mar. 2019), p. 100087. URL: https://linkinghub.elsevier.com/retrieve/pii/S221475351830024X.

[410] Joshua D Cohen et al. "Combined circulating tumor DNA and protein biomarker-based liquid biopsy for the earlier detection of pancreatic cancers." In: *Proceedings of the National Academy of Sciences of the United States of America* 114.38 (2017), pp. 10202–10207. URL: http://www.ncbi.nlm.nih.gov/pubmed/28874546%20http://www.pubmedcentral.nih.gov/articlerender.fcgi?artid=PMC5617273.

[411] Biljana Jovov et al. "Role of E-cadherin in the pathogenesis of gastroesophageal reflux disease." In: *The American journal of gastroenterology* 106.6 (June 2011), pp. 1039–47. URL: http://www.ncbi.nlm.nih.gov/pubmed/21448147%20http://www.pubmedcentral.nih.gov/articlerender.fcgi?artid=PMC3568513.

[412] Ian Holland et al. "3D biofabrication for tubular tissue engineering". In: *Bio-Design and Manufacturing* 1.2 (June 2018), pp. 89–100. URL: http://link.springer.com/10.1007/s42242-018-0013-2.

[413] Maria Victoria Tuttolomondo et al. "Dye–collagen interactions. Mechanism, kinetic and thermodynamic analysis". In: *RSC Advances* 5.71 (2015), pp. 57395–57405. URL: http://xlink.rsc.org/?DOI=C5RA08611F.

[414] William A. Cooper and Joseph I. Miller. "Jejunal Interposition for Esophageal Replacement". In: *Operative Techniques in Thoracic and Cardiovascular Surgery* 4.3 (Aug. 1999), pp. 239–251. URL: https://linkinghub.elsevier.com/retrieve/pii/S1522294207701204.